eCAM
Evidence-Based Complementary and Alternative Medicine

Complementary and Alternative Medicine in Cancer Stem Cells

Guest Editors: Hui-Fen Liao, K. S. Clifford Chao, Yu-Jen Chen, and Min Shen Chang

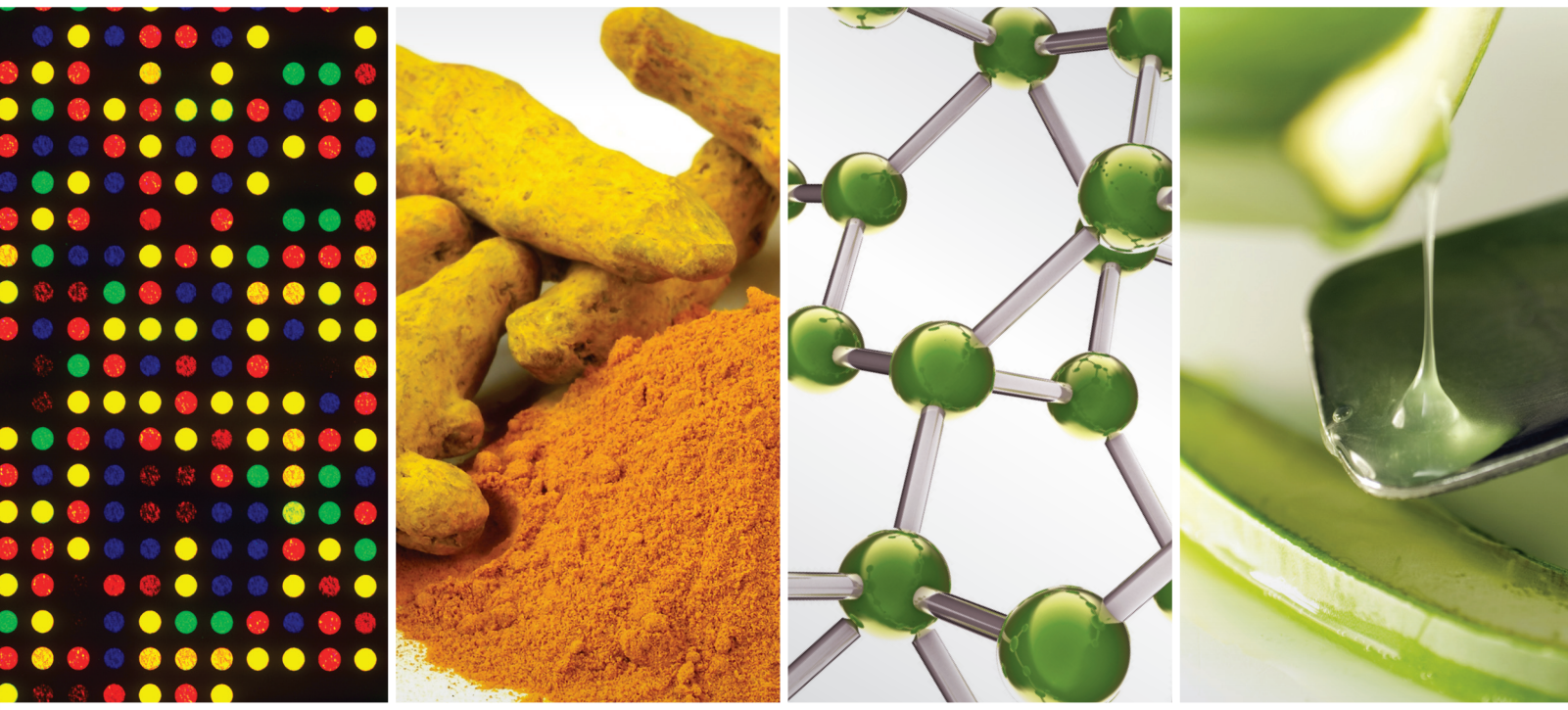

Complementary and Alternative Medicine in Cancer Stem Cells

Evidence-Based Complementary and Alternative Medicine

Complementary and Alternative Medicine in Cancer Stem Cells

Guest Editors: Hui-Fen Liao, K. S. Clifford Chao, Yu-Jen Chen, and Min Shen Chang

Editorial Board

Contents

Hindawi Publishing Corporation
Evidence-Based Complementary and Alternative Medicine
Volume 2013, Article ID 560274, 2 pages
http://dx.doi.org/10.1155/2013/560274

Editorial

Complementary and Alternative Medicine in Cancer Stem Cells

Hui-Fen Liao,[1] K. S. Clifford Chao,[2] Yu-Jen Chen,[3] and Min Shen Chang[4]

[1] *Department of Biochemical Science and Technology, National Chiayi University, Chiayi 600, Taiwan*
[2] *Department of Radiation Oncology, Columbia University, New York, NY 10032, USA*
[3] *Department of Medical Research and Department of Radiation Oncology, Mackay Memorial Hospital, Taipei 104, Taiwan*
[4] *Department of Ophthalmology and Visual Sciences, Vanderbilt University, Nashville, TN 37232, USA*

Correspondence should be addressed to Hui-Fen Liao; liao.huifen@gmail.com

Received 11 June 2013; Accepted 11 June 2013

Cancer stem cells (CSCs), a small subpopulation of cancer cells prone to form tumorigenesis, resemble normal stem cells with self-renewal and differentiation characteristics. CSCs have recently been identified in leukemia and various types of solid tumors. There is growing evidence indicating that CSCs might be the principal cause for the development of resistance to cancer treatments, recurrence, and metastasis. Emerging data indicates that CSCs and normal stem cells may share cellular pathways regulating proliferation and differentiation. These pathways include, but not limited to, polycomb group transcriptional repressor Bmi-1, Notch, Sonic hedgehog, and Wnt pathways. Therefore, identification of CSC markers, selection and development of unique therapeutics targeting CSCs and related signaling pathways have been extensively investigated. In this special issue, we publish articles that explore aspects of complementary and alternative medicine (CAM) associated with CSCs in basic research, in translational medicine, and in clinical application for cancer treatment. The topic will highlight current research, encourage additional research, draw attention to the subject, and ultimately help advance the field of CAM application in CSCs.

Considering the widespread research on the role of CAM in CSCs, 1 review and 12 research articles have been included in the current special issue. Among the papers, Y. C. Huang et al. contributed with an excellent review about naturally occurring compounds and derivatives targeting Sonic hedgehog signaling. C. W. Chang et al. and Y. M. Liu et al. reported the effect of *Antrodia cinnamomea* against CSCs of head and neck cancer and hepatoma, respectively. Q. A. Jia et al. contributed a research on chemosensitization of hepatoma by using herbal compound "Songyou Yin." Y. A. Shen et al. published data for resveratrol on stemness, epithelial-mesenchymal transition, and metabolic reprogramming of CSCs in nasopharyngeal carcinoma through p53 activation. Y. J. Chen et al. provided another bioactivity of resveratrol against alpha-melanocyte-stimulating hormone signaling, viability, and invasiveness in melanoma cells. Y. C. Su et al. further demonstrated the effect of resveratrol on downregulating interleukin 6-stimulated Sonic hedgehog signaling in human acute myeloid leukemia. W. Y. Liao et al. found that cyclohexylmethyl flavonoids could suppress propagation of breast CSCs via downregulation of NANOG. B. Yan et al. reported β-elemene as an antiangiogenesis agent targeting Notch-1 in gastric cancer stem-like cells. C. M. Lee et al. presented results of pterostilbene, a blue berry isolate, on suppressing irradiation-mediated enrichment of hepatoma $CD133^+$ stem cells. For lung cancer, C. T. Yeh et al. demonstrated antimycin A as a potential anti-CSCs agent.

The aforementioned papers published in this special issue represent quite attractive and promising results about CAM in management of CSCs. In most of these papers, the mechanisms underlying their anti-CSCs properties have been well addressed.

Acknowledgments

As the guest editorial team, we would like to express our deep appreciation to the article contributors, our reviewers, and the Editorial Board of ECAM.

Hui-Fen Liao
K. S. Clifford Chao
Yu-Jen Chen
Min Shen Chang

Hindawi Publishing Corporation
Evidence-Based Complementary and Alternative Medicine
Volume 2013, Article ID 258425, 9 pages
http://dx.doi.org/10.1155/2013/258425

Research Article

BlueBerry Isolate, Pterostilbene, Functions as a Potential Anticancer Stem Cell Agent in Suppressing Irradiation-Mediated Enrichment of Hepatoma Stem Cells

Chi-Ming Lee,[1,2,3] Yen-Hao Su,[4] Thanh-Tuan Huynh,[5] Wei-Hwa Lee,[6] Jeng-Fong Chiou,[1,2,3] Yen-Kuang Lin,[7] Michael Hsiao,[8] Chih-Hsiung Wu,[4] Yuh-Feng Lin,[5] Alexander T. H. Wu,[9,10,11] and Chi-Tai Yeh[4,5,12]

[1] *Department of Diagnostic Radiology, Taipei Medical University Hospital, Taipei 11031, Taiwan*
[2] *Department of Radiology, School of Medicine, College of Medicine, Taipei Medical University, Taipei 11031, Taiwan*
[3] *Department of Radiation Oncology, Taipei Medical University Hospital, Taipei 11031, Taiwan*
[4] *Departments of Surgery, Taipei Medical University-Shuang Ho Hospital, Taipei 23561, Taiwan*
[5] *Graduate Institute of Clinical Medicine, Taipei Medical University, Taipei 11031, Taiwan*
[6] *Department of Pathology, Taipei Medical University-Shuang Ho Hospital, Taipei 23561, Taiwan*
[7] *Biostatistics and Research Consultation Center, Taipei Medical University, Taipei 11031, Taiwan*
[8] *Genomics Research Center, Academia Sinica, Taipei 115, Taiwan*
[9] *School of Medical Laboratory Science and Biotechnology, Taipei Medical University, Taipei 11031, Taiwan*
[10] *Ph.D. Program for Translational Medicine, College of Medical Science and Technology, Taipei Medical University, Taipei 11031, Taiwan*
[11] *Translational Research Laboratory, Cancer Center, Taipei Medical University Hospital, Taipei 11031, Taiwan*
[12] *Graduate Institute of Medical Sciences, National Defense Medical Center, Graduate Institute of Medical Sciences, National Defense Medical Center, Taipei 11490, Taiwan*

Correspondence should be addressed to Alexander T. H. Wu; chaw1211@yahoo.com and Chi-Tai Yeh; ctyeh@tmu.edu.tw

Received 9 March 2013; Accepted 8 April 2013

Academic Editor: Yu-Jen Chen

For many malignancies, radiation therapy remains the second option only to surgery in terms of its curative potential. However, radiation-induced tumor cell death is limited by a number of factors, including the adverse response of the tumor microenvironment to the treatment and either intrinsic or acquired mechanisms of evasive resistance, and the existence of cancer stem cells (CSCs). In this study, we demonstrated that using different doses of irradiation led to the enrichment of $CD133^+$ Mahlavu cells using flow cytometric method. Subsequently, $CD133^+$ Mahlavu cells enriched by irradiation were characterized for their stemness gene expression, self-renewal, migration/invasion abilities, and radiation resistance. Having established irradiation-enriched $CD133^+$ Mahlavu cells with CSC properties, we evaluated a phytochemical, pterostilbene (PT), found abundantly in blueberries, against irradiation-enriched CSCs. It was shown that PT treatment dose-dependently reduced the enrichment of $CD133^+$ Mahlavu cells upon irradiation; PT treatment also prevented tumor sphere formation, reduced stemness gene expression, and suppressed invasion and migration abilities as well as increasing apoptosis of $CD133^+$ Mahlavu CSCs. Based on our experimental data, pterostilbene could be used to prevent the enrichment of $CD133^+$ hepatoma CSCs and should be considered for future clinical testing as a combined agent for HCC patients.

1. Introduction

Hepatocelluar carcinoma (HCC) represents one of the most common cancer types in the world. The standard treatment options for HCC often involve radiation- and chemotherapy. Despite advances in the detection and treatment of the disease, mortality rate remains high because current therapies are limited by the emergence of radiation- and

chemo-therapy-resistant cancer cells. Existing radiation-therapies against HCC are usually developed against the bulk of the tumor mass, where although they are able to initially shrink the size of the tumor, they fail to eradicate the lesion in full, thus resulting in disease relapse. Recently, HCC progression has been thought to be driven by cancer stem cells (CSC) through their capacity for self-renewal, production of heterogeneous progeny, and resistance to radiation-therapy and to limitlessly divide. The process of re-population has been suggested as the result of accelerated division of stem-cells during treatment (radiation) and/or the enrichment of the CSCs [1]. Therefore, clarification of the radioresistance mechanism is essential for developing novel therapeutic modalities to sensitize hepatoma cells to radiation and improve patient survival.

CSCs are a subpopulation of tumors that are responsible for tumor maintenance and spreading. These cells are characterized to possess unlimited proliferation potential, self-renewal ability, and differentiation capability to generate progenies that constitute the major tumor population [2]. The existence of CSCs has been described in a variety of hematologic and solid tumors including those of the breast, brain, colon, pancreas, lung, liver, and esophagus. CSCs are resistant to many current cancer treatments, including chemo- and radiation therapy [3]. In addition to driving tumorigenesis, CSCs might contribute to distant metastasis and disease relapse [4]. This suggests that the standard interventions, while killing the bulk of tumor cells, may ultimately fail because they do not eliminate CSCs but represent a selection pressure for CSCs.

Since CSCs share similarities with stem cells, stem cell-associated surface markers have been used to identify and isolate CSCs in vitro. For example, leukemia stem cells are enriched in the $CD34^+/CD38^-$ subset of cells and $CD133^+$ cells have been implicated as CSCs in many different cancer types including liver [5, 6]. In addition, CSCs can form spherical colonies in suspension cultures characterized and termed tumorspheres. Importantly, isolated CSCs exhibit increased resistance to chemotherapeutic agent and ionizing radiation [2]. Therefore, CSCs have become an important target for drug development.

Pterostilbene (*trans*-3,5-dimethoxy-4′-hydroxystilbene) was first isolated from red sandalwood (*Pterocarpus santalinus*) and subsequently identified in the grape berries of *Vitis vinifera*. Pterostilbene has attracted much attention because it has been demonstrated to have both chemopreventive activity and tumor-killing effects similar to those of resveratrol. For instance, pterostilbene was indicated to induce cell cycle arrest and apoptosis in a variety of cancer cell lines including lung, liver, breast, and pancreas [7]. Recently, it has been reported that pterostilbene prevents azoxymethane- (AOM-) induced colon tumorigenesis in mice via suppressing cancer cell proliferation and the induction of apoptotic pathways [8]. In addition, several pharmacological properties of pterostilbene make it an ideal anticancer agent for development. Structurally, pterostilbene contains two methoxy groups and one hydroxyl group as compared to those of resveratrol which has three hydroxyl groups. The two methoxy groups substantially increase the lipophilicity and oral absorption of pterostilbene leading to a higher potential for cellular uptake. In addition, when administered orally, pterostilbene shows 95% bioavailability while only 20% in the case of resveratrol [9]. Furthermore, pterostilbene's half-life is also seven times longer than resveratrol, 105 min versus 14 min [10].

Collectively, pterostilbene possesses many desired anti-cancer properties for the development as potential clinical agent. In this study, we evaluated and provided evidence for the use of pterostilbene for targeting and eliminating radiation-enriched $CD133^+$ HCC CSCs.

2. Materials and Methods

2.1. Materials. Pterostilbene (3,5-dimethoxy-4-hydroxystilbene, 99.7% purity) was generously provided by Professor Chi-Tang Ho (Rutgers University, NJ, USA). MTT dye (tetrazolium dye (thiazolyl blue tetrazolium bromide)) was purchased from Sigma-Aldrich (St. Louis, MO, USA). Primary antibodies c-Myc, CXCR4, COX-2, NF-κB (p65), Twist1, vimentin, E-cadherin, and β-actin were purchased from Cell Signaling Technology (Boston, MA, USA). Pterostilbene was dissolved in DMSO and further diluted in sterile culture medium immediately prior to use. A TRIzol RNA isolation kit was obtained from Life Technologies (Rockville, MD, USA); and primers for RT-PCR, dNTP, reverse transcriptase, and Taq polymerase were obtained from Gibco BRL (Cergy Pontoise, France).

2.2. Cell Line and Cell Culture. Human hepatoma cell line Mahlavu cells were grown in Dulbecco's modified Eagle's medium (DMEM, Life Technologies, Grand Island, NY, USA) supplemented with 10% (v/v) fetal bovine serum in 5% CO_2, 37°C humidified incubator. Cell culture and subsequent experiments were used and carried out according to the guidelines established by Environmental and Experimental Safety Committee, Taipei Medical University, Taiwan.

2.3. Irradiation. Human HCC cell line, Mahlavu cells were cultured until 80% confluency was reached and subjected to different doses of gamma irradiation (Department of Radiation Oncology, Taipei Medical University Hospital, Taiwan). Briefly, the culture media was replaced with HESS buffer prior to irradiation using a linear accelerator (Varian Medical System, Palo Alto, CA, USA) using 6 megavolts of energy with a source-to-target distance of 100 cm. The cells were placed on a 1 cm bolus and treated with a posterior-anterior direction portal to allow a 1 cm radiation buildup. A radiation absorption doses from 1, 5, and 10 Gy per single fraction were delivered to Mahlavu cells. Surviving cells were subsequently cultured and subjected to flow cytometric analysis.

2.4. Isolation of $CD133^+$ Cancer Stem Cells Using Fluorescence Activated Cell Sorting (FACS). $CD133^+$ cells were labeled and sorted using magnetic microbeads (Miltenyi Biotec, Auburn, CA, USA) and labeled with or isotype control antibodies (all from Coulter-Immunotech Co., Miami, FL, USA). Cells were analyzed and sorted on a FACSAria Cell Sorter unit

(Becton Dickinson), using propidium iodide (PI) as a viable stain. Cells were gated on low side scatter, low-to-moderate forward scatter, and low PI. For data acquisition, at least 10,000 events were analyzed. The purity and viability of isolated cells were routinely >98%.

2.5. Cell Invasion and Migration Assay. The metastatic ability of $CD133^+$ and parental Mahlavu cells was measured using Boyden chamber invasion assay. Briefly, cells were trypsinized, washed with PBS buffer, and resuspended in a serum-free DMEM medium (5×10^4 cells/200 uL) in the presence or absence of pterostilbene. The cells were then seeded into the upper chambers of matrigel coated filter inserts. A serum-containing DMEM medium (500 μL) was added to the lower chambers. After incubating for 24 h at 37°C, filter inserts were removed from the wells, the cells that invaded or migrated through the membrane were stained with propidium iodide and fluorescence images were taken. The invasive cells were then counted using the Analytical Imaging Station software package (Imaging Research, ON, Canada). To measure the migratory ability, cells were seeded into a Boyden chamber with 8 mm pore polycarbonate filters, which were not coated with matrigel. Different concentrations of pterostilbene were used for the evaluation. The migration assay was measured as described in the invasion assay.

2.6. Western Blotting. Total cell lysates were prepared using the protein extraction Kit (Panomics, Fremont, CA, USA). Samples (10 mg) of total cell lysates were separated electrophoretically by a 10% SDS-PAGE gel and transferred onto a polyvinylidene fluoride membrane using the BioRad Mini Protean electrotransfer system. The blots were subsequently blocked with 5% skim milk in PBST for 30 min and were probed with primary antibodies, namely, CD133, c-Myc, and COX2 overnight at 4°C. The membranes were sequentially detected with an appropriate peroxidase-conjugated secondary antibody. The blots were washed in PBST, signals were developed using the ECL (enhanced chemiluminescence) detection kit, and images were obtained using UVP BioDoc-It system (Upland, CA, USA).

2.7. Statistical Analysis. Statistical Package of Social Sciences software (version 13.0) (SPSS, Inc., Chicago, IL, USA) was used for statistical analysis. Student's t-test was used to determine the statistical significance of the differences between experimental groups; P values less than 0.05 were considered statistically significant. The level of statistical significance was set at 0.05 for all tests.

3. Results

3.1. Irradiation-Enriched $CD133^+$ Subpopulation of Mahlavu HCC Cells. Human hepatoma cell line Mahlavu was used as a cell model in this study. Mahlavu cells were irradiated with increasing dose of γ-radiation (from 1 to 10 Gy) and subjected to flow cytometric analysis for CD133 expression. We found that the percentage of $CD133^+$ subpopulation cells increased as the dose of irradiation increased (Figure 1(a)). This observation supported our hypothesis that irradiation posted a selection pressure for the $CD133^+$ subpopulation cancer cells. Subsequently, we characterized the expression profiles between parental and $CD133^+$ Mahlavu cells, a significant elevation in the stemness genes including CD133 and c-Myc as well as proinflammatory marker COX-2, and Bcl-2 and survivin (prosurvival gene) were observed (Figure 1(b)). These observations suggested that enrichment of $CD133^+$ Mahlavu cells with the characteristics of cancer-stem-like cells.

3.2. $CD133^+$ Mahlavu Cells Exhibited Cancer-Stem-Like Cell Properties. $CD133^+$ Mahlavu cells enriched by irradiation were examined for their CSC properties. $CD133^+$ Mahlavu cells were found to form a higher number (approximately 4-fold higher) of tumor aggregates and/or spheres as compared to that of parental cells (Figure 2(a)). In addition, $CD133^+$ Mahlavu cells were approximately 3 times more resistant towards irradiation comparing to parental Mahlavu counterparts (at 5 Gy, Figure 2(b)). Finally, we also examined the invasive ability of $CD133^+$ and parental Mahlavu cells. $CD133^+$ Mahlavu cells exhibited an approximately 8-fold increase in their invasive ability when compared to their parental counterparts (Figure 2(c)). Therefore, our data suggested that irradiation could enrich $CD133^+$ HCC CSCs characterized by a significantly enhanced malignant properties (as in self-renewal, irradiation-resistant, and invasive abilities).

3.3. Pterostilbene Treatment Suppressed the Percentage of $CD133^+$ Mahlavu Cells Enriched by Irradiation and Cancer Stem Cell Properties. Pterostilbene, a stilbenoid chemically related to resveratrol and found in blueberries and grapes, has been implicated for its chemopreventive and anticancer activities. However, the potential anti-CSCs effect of pterostilbene has not been fully examined. In this study, Mahlavu cells were pretreated with an increasing concentrations of pterostilbene (PT, 5, 10 and 20 μM) prior to irradiation. The enrichment of $CD133^+$ cells by irradiation (5 Gy) was dose-dependently suppressed by this pretreatment of pterostilbene (Figure 3(a)). For instance, at the highest PT concentration (20 μM), the percentage of $CD133^+$ Mahlavu cells was down to approximately 0.7% as compared to 16.5% in the control group. Our data suggested that PT could be specific against $CD133^+$ Mahlavu cells so that at high concentrations, $CD133^+$ Mahlavu cells were eliminated by its presence. On subsequent observations, pterostilbene dose-dependently suppressed the tumor aggregate/sphere formation ability of $CD133^+$ Mahlavu cells (Figure 3(b)). It was evident that the tumor aggregates were significantly disrupted in the presence of PT (insert Figure 3(b)). PT-treated tumor aggregates were harvested for western blot analysis and revealed that PT treatment indeed suppressed stemness gene expression including CD133, c-Myc, and proinflammatory molecule COX-2 (Figure 3(c)). Note that the expression of one of the key proapoptotic molecules, PARP (poly(ADP-ribose) polymerase) was elevated under PT treatment, suggesting that PT also triggered apoptosis in $CD133^+$ Mahlavu cells. Furthermore, we have

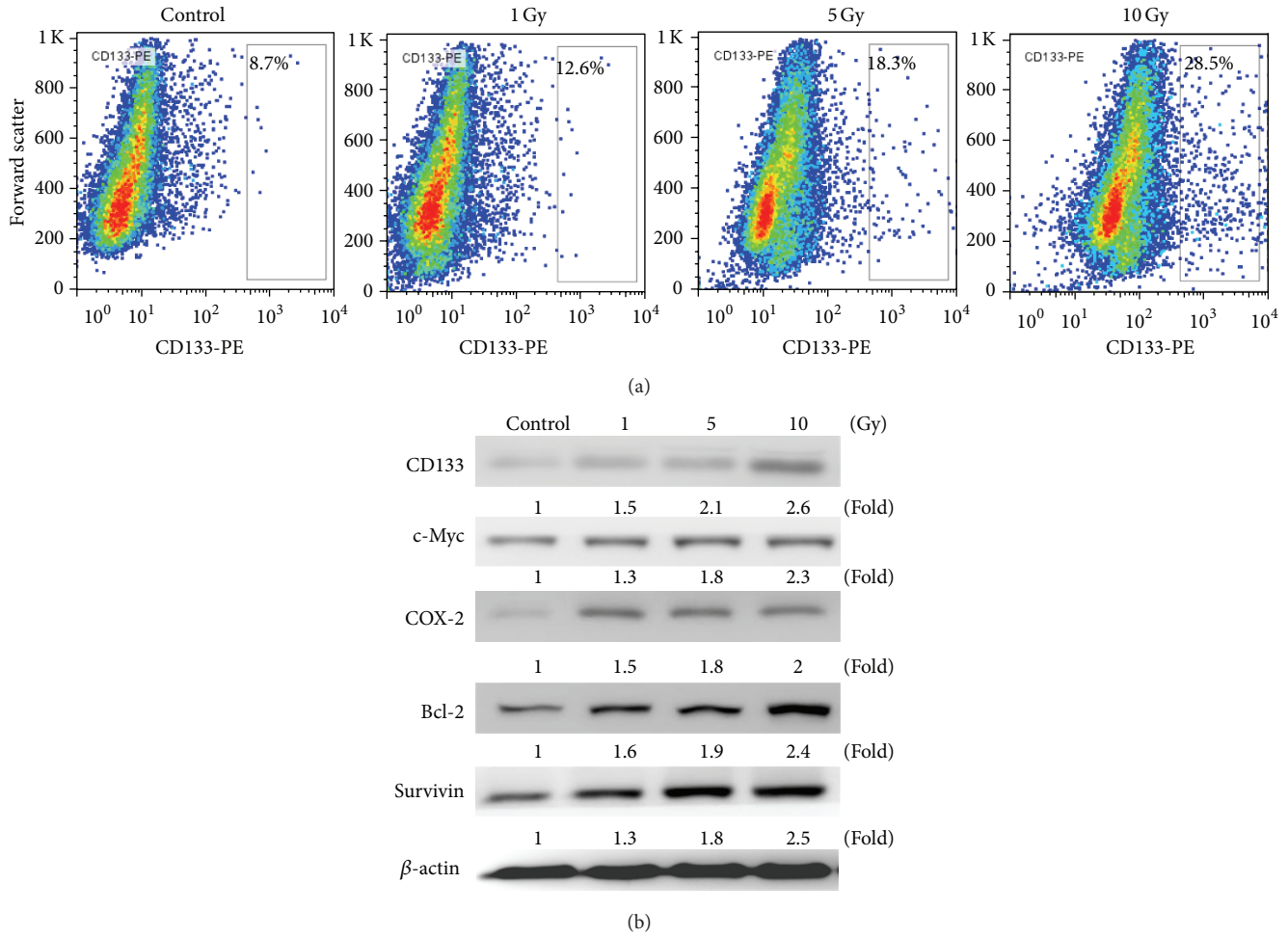

Figure 1: Irradiation increased $CD133^+$ subpopulations in HCC cells. (a) Mahlavu cells, subjected to irradiation (1, 5, and 10 Gy), were analyzed using flowcytometric method. (a) Parental Mahlavu cells were found to contain approximately 8.7% $CD133^+$ cells, but this subpopulation increased as the dose of irradiation increased that is, 5 Gy to 18.3%. (b) Western blot analysis indicated that $CD133^+$ Mahlavu cells were enriched by irradiation and showed an increased expression level of c-Myc (stemness gene) and COX-2 (proinflammatory gene) and Bcl-2 and survivin (prosurvival gene) as compared to their parental counterparts.

included another cell line SK-Hep-1 to demonstrate that this is not Mahlavu-specific occurrence. Irradiation also enriched $CD133^+$ cancer stem-like Sk-Hep-1 HCC cells and pterostilbene treatment suppressed the enrichment of $CD133^+$ SK-Hep-1 cells and its stemness (see Supplementary Figures 1 and 2 available online at http://dx.doi.org/10.1155/2013/258425). Taken together, pterostilbene appeared to prevent the generation or enrichment of HCC CSCs by irradiation and suppressed the CSC properties in Mahlavu and SK-Hep-1 cells.

3.4. Pterostilbene Treatment Decreased Metastatic Potential in $CD133^+$ Mahlavu Cells. Finally, we evaluated if the addition of PT could affect the metastatic potential of $CD133^+$ Mahlavu cells. In the presence of PT (5, 10, and 20 μM), the migration and invasion abilities of $CD133^+$ Mahlavu cells were both severely hindered (Figures 4(a) and 4(b), resp.). For instance, at 20 μM, PT reduced the migration ability of $CD133^+$ Mahlavu cells down to approximately 20% and invasion ability down to 30% (Figures 4(a) and 4(b), resp.). Mechanistically, PT was found to negatively modulate key molecules associated with metastasis. For instance, the major EMT marker vimentin was reduced in $CD133^+$ Mahlavu cells treated with PT in a dose-dependent manner (Figure 4(c)). Mice which received pterostilbene demonstrated significantly lower tumor burden, as evident by gross tumor volume (Supplementary Figure 3). In addition, chemotactic associated molecule CXCR4 was downregulated in the presence of PT. Importantly, one of the key transcription factors associated with epithelial-to-mesenchymal transition (EMT), Twist1, was also downregulated by pterostilbene treatment.

4. Discussion and Conclusions

One of the most challenging tasks in managing liver cancer is the high incidence of treatment resistance. The presence of cancer stem cells was been suggested to play important role in treatment resistance and disease progression. However,

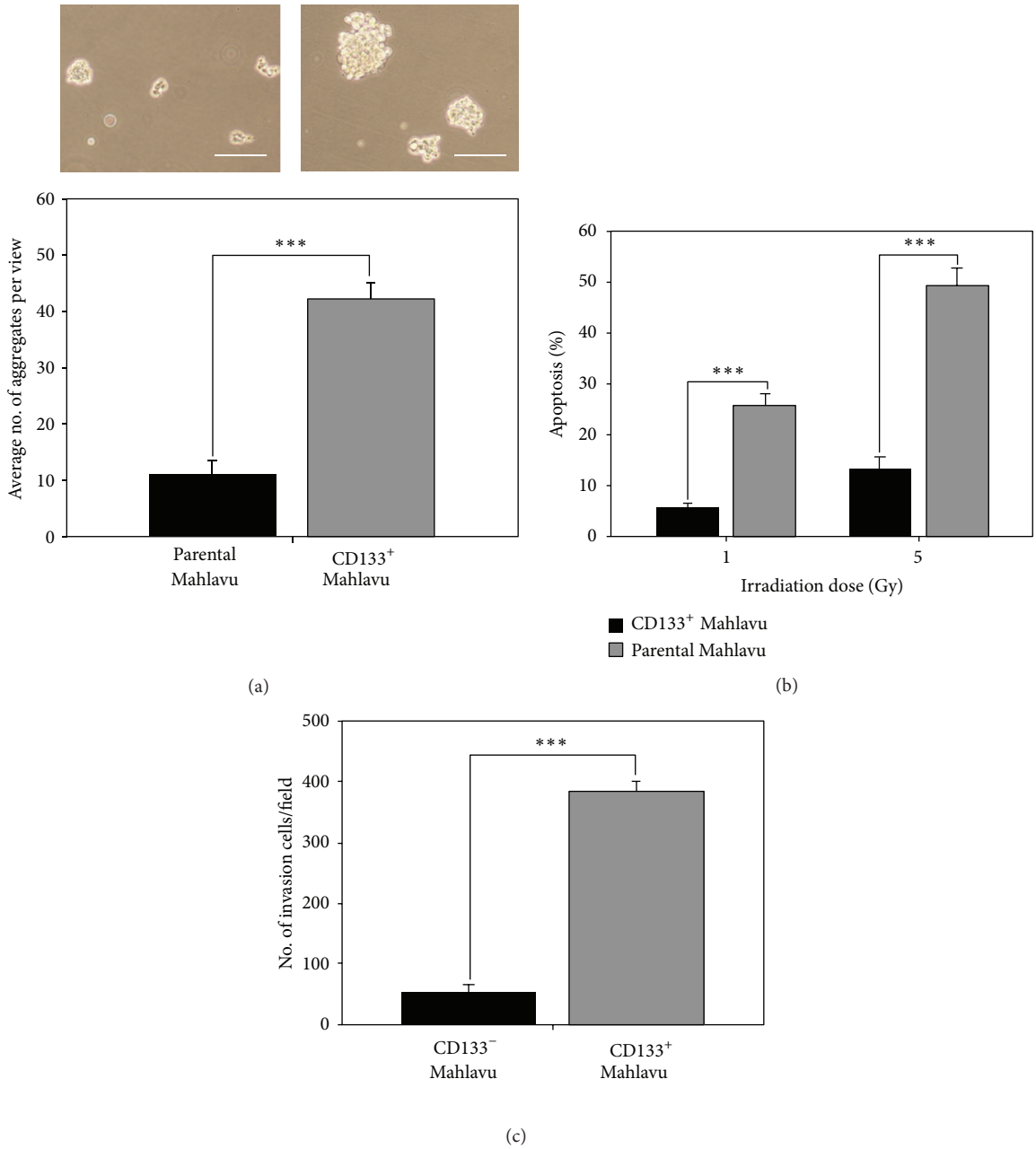

Figure 2: CD133$^+$ Mahlavu cells exhibited cancer-stem like cell properties. (a) CD133$^+$ Mahlavu cells exhibited a higher ability to form cell aggregates and/or tumor spheroids. (b) CD133$^+$ and parental Mahlavu cells were irradiated with 2 different doses (1 and 5 Gy). CD133$^+$ Mahlavu cells demonstrated increased resistance against irradiation as compared to CD133-counterparts. (c) CD133$^+$ Mahlavu cells were also significantly more invasive than their CD133-counterparts. Bars: 50 μm.

as how the CSCs are generated remains poorly understood. Emerging evidence has implicated that current therapeutic strategies may actually help enrich and select for treatment-resistant CSCs [1, 3]. In the present study, we demonstrated that in the wake of irradiation, the surviving Mahlavu cells represented a subpopulation of cells which were not only CD133$^+$ but also treatment-resistant. In addition, under serum-deprived culture condition, these CD133$^+$ Mahlavu cells demonstrated enhanced ability to form tumor aggregates and/or spheres, a key characteristic of cancer stem cells [4]. Similarly, it has been reported that irradiation increased the number of CD133$^+$ glioma stem cells and CD24 (-/low) breast cancer stem cells [11, 12], and these cancer stem cells played a major role in radiation resistance. Taken together, these observations provide an important rationale for developing alternative treatment strategies for HCC management.

The natural occurring pterostilbene (*trans*-3,5-dimethoxy-4-hydroxystilbene) is an antioxidant predominantly found in blueberries, grapes, and tree wood [9, 13]. Pterostilbene and resveratrol have similar pharmacologic

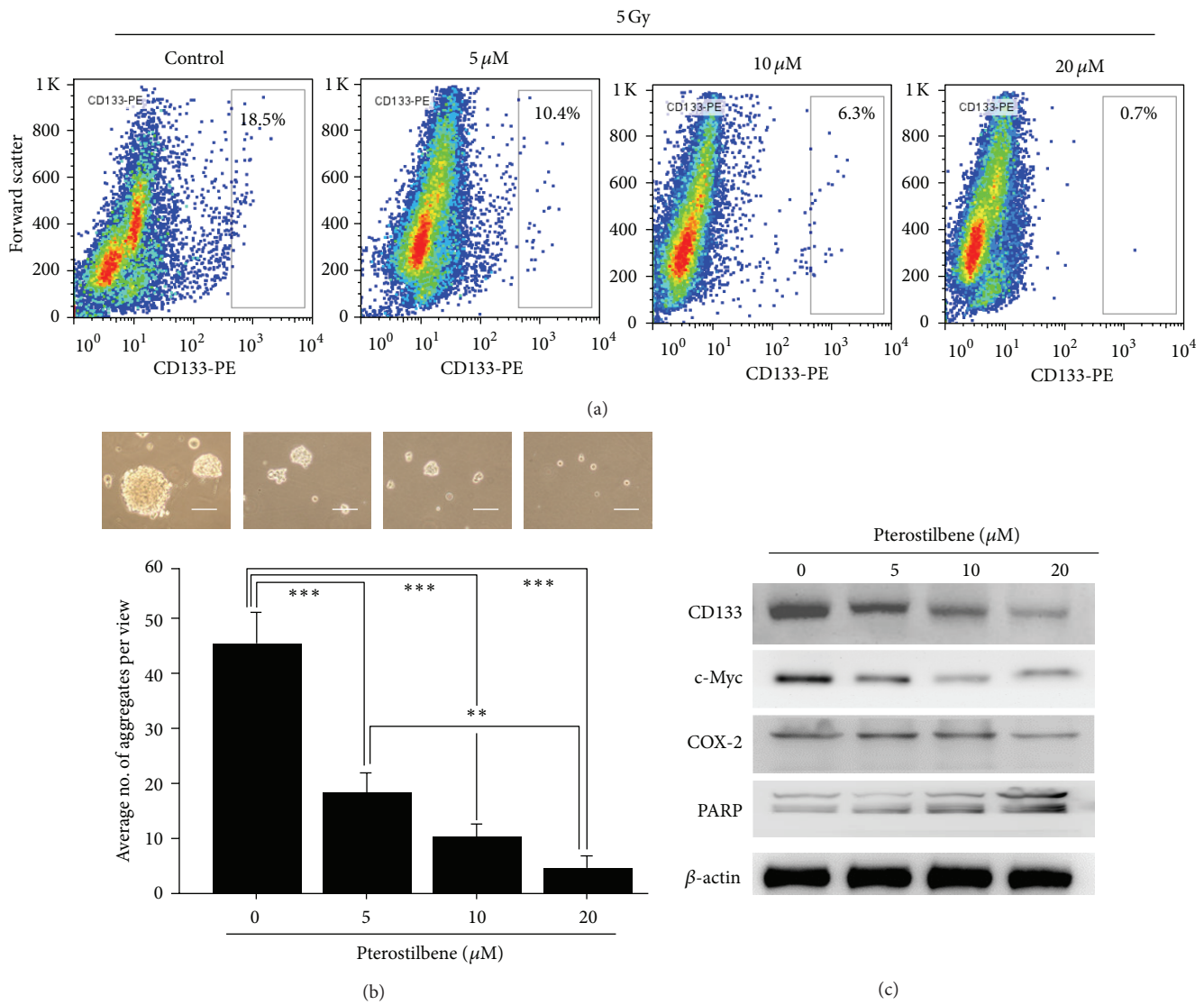

Figure 3: Pterostilbene treatment decreased the percentage of CD133$^+$ Mahlavu cells. (a) Irradiated Mahlavu cells were treated with different concentrations of pterostilbene and analyzed for the abundance of CD133$^+$ cells. Dose-dependently, pterostilbene decreased the CD133$^+$ subpopulation cells. (b) Pterostilbene disrupted the tumor sphere-forming ability of CD133$^+$ Mahlavu cells. When pterostilbene was added into the culture medium of CD133$^+$ Mahlavu cells, pterostilbene dose-dependently prevented Mahlavu tumor sphere formation. (c) Total protein lysates were obtained from pterostilbene-treated Mahlavu tumor spheres for western blot analysis. The expression levels of stemness markers such as CD133, c-Myc, and proinflammation marker COX-2 were suppressed by the addition of pterostilbene in a dose-dependent manner, while proapoptosis marker PARP was increased under pterostilbene treatment.

properties; however, pterostilbene has several advantages. For instance, pterostilbene contains two methoxy groups and one hydroxyl group whereas resveratrol has three hydroxyl groups. The two methoxy groups have been suggested to substantially increase pterostilbene's lipophilicity and oral absorption, resulting in a higher potential for cellular uptake. In addition, when administered orally, pterostilbene shows 95% bioavailability while resveratrol only has 20% bioavailability [13]. More importantly, Pterostilbene's half-life has been estimated approximately seven times longer than that of resveratrol [10]. Taken together, pterostilbene represents a more superior candidate for anticancer agent over resveratrol. Based on these premises, pterostilbene was selected and evaluated for its potential in targeting and eliminating HCC CSCs. In the present study, we provided in vitro evidence that pterostilbene treatment prevented the enrichment of CD133$^+$ Mahlavu cells generated by irradiation and/or promoted apoptosis of these CD133$^+$ cells. Importantly, pterostilbene treatment significantly suppressed the cancer stem cell properties of CD133$^+$ Mahlavu cells, namely, tumor aggregate/sphere formation as well as inhibited migration/invasion abilities of CD133$^+$ Mahlavu cells. Although the precise mechanism as how PT treatment contributed to the prevention of CSC generation by irradiation is not

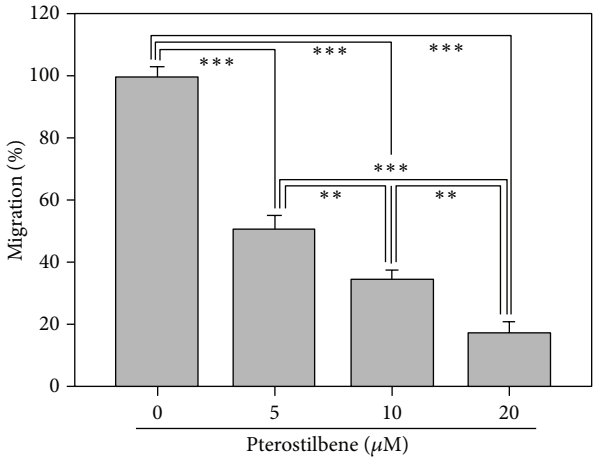

(a)

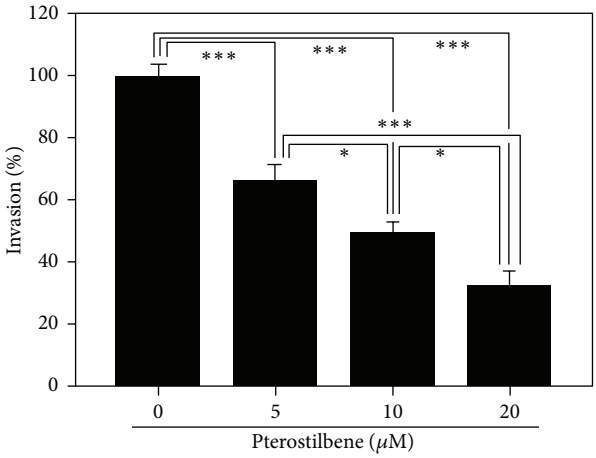

(b)

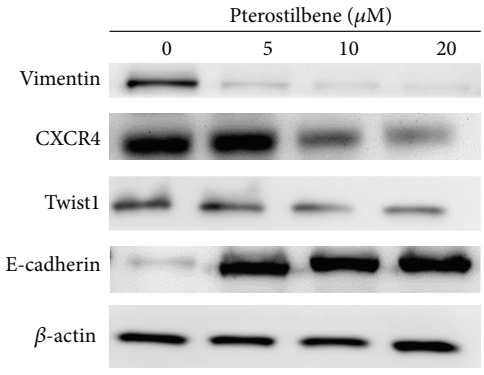

(c)

Figure 4: Pterostilbene treatment suppressed the migration and invasion of CD133$^+$ Mahlavu cells. (a) CD133$^+$ Mahlavu cells were treated with an increasing concentration of pterostilbene (5–15 μM). Pterostilbene treatment led to a dose-dependent suppression in the migration. (b) Similarly, the invasiveness of CD133$^+$ Mahlavu cells was decreased as the concentration of pterostilbene increased. (c) Western blot analysis of pterostilbene-treated CD133$^+$ Mahlavu cells. Pterostilbene-mediated suppression on migration and invasiveness were correlated to the decreased expression level of prometastasis molecules including vimentin, CXCR4 and Twist1 while the level of epithelial marker E-cadherin increased.

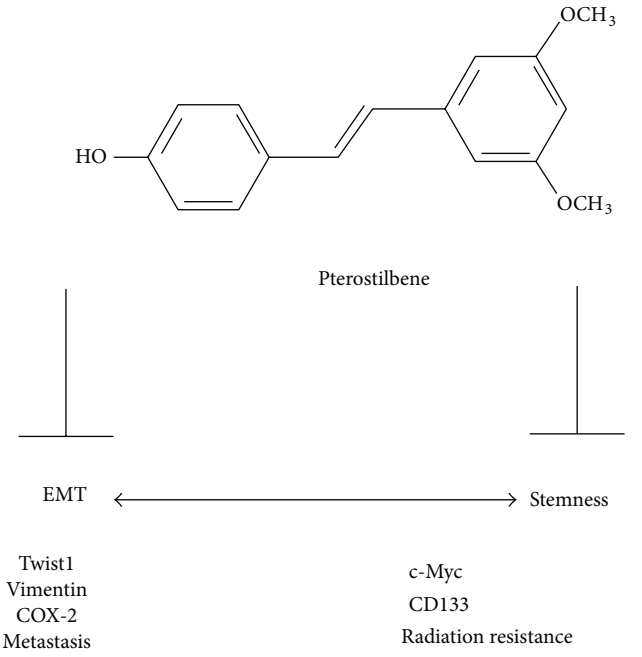

Figure 5: Proposed mechanism for pterostilbene-mediated anti-CSC effects. Pterostilbene suppresses CSC generation by negatively regulating the expression levels of c-Myc and CD133 and inhibiting EMT by downregulating Twist1, vimentin, and COX-2 expressions. The double arrow implies that EMT is associated with the increasing stemness of cancer stem cells. Blunt arrow represents suppression.

clear, it is likely that PT as a potent antioxidant fended off irradiation-induced oxidative stress and inflammation by suppressing the expression level of COX-2 [7]. Importantly, COX-2 has been indicated as a key molecule in cancer-associated inflammation as well as the promoter of epithelial-to-mesenchymal transition (EMT) in liver cancer [14]. This is in agreement with our observations that PT treatment negatively regulated major EMT markers including CXCR4, vimentin, and Twist1, all of which have been associated with cancer metastasis and poor prognosis [15]. Studies have indicated that the propensity of EMT is associated with the generation of breast CSCs [16, 17]. Thus, we proposed that PT suppressed the generation of irradiation-induced CD133$^+$ HCC CSCs by targeting key EMT molecules (Figure 5).

Notably, PT treatment also reduced the expression of c-Myc, a potent stemness and oncogene [18]. The suppression of c-Myc expression by PT might have a direct impact on several oncogenic properties. First, the disruption of tumor aggregates/spheres in the presence of PT could be the result of PT-mediated c-Myc downregulation, which led to cellular differentiation. Second, the suppression of c-Myc might also contribute to the decreased radiation resistance in CD133$^+$ Mahlavu CSCs. It has been shown that the modulation of c-Myc leads to radiation sensitization of hepatoma cells [19, 20]. Furthermore, our unpublished data showed that PT treatment could suppress another major molecule, survivin, which has been implicated for radiation resistance in glioma [21].

Interestingly, according to our in vitro data, pterostilbene (at low concentrations ranging from 2.5 to 10 μM) posed inhibitory activity against Mahlavu tumor spheres. In agreement, pterostilbene was also shown to exert potent antiproliferative ability against MCF7 breast cancer cells [22]. In our in vivo study, 5 mg/Kg daily intraperitoneal injection of pterostilbene could significantly delay and suppress the onset of M2 TAM cocultured MDA-MB-231 tumorigenesis [23]. Our in vitro and in vivo data suggests that pterostilbene could reduce the enrichment of $CD133^+$ Mahlavu cells upon irradiation and target the liver cancer stem cells. This low concentration of pterostilbene may be achievable in vivo. According to a previous study [24], pterostilbene has an estimated bioavailability of 12.4%, a half-life of 2.38 ± 0.84 h, and a glucuronidated pterostilbene metabolite with half-life of ~8 hours excreted in urine.

In conclusion, our current study demonstrated that irradiation could enrich $CD133^+$ subpopulation of Mahlavu cells. These cells possess cancer stem cell characteristics such as increased tumor sphere forming ability, enhanced resistance towards irradiation, and elevated metastatic potential. In the presence of pterostilbene, these aforementioned phenomenea could be suppressed via the downregulation of c-Myc, COX-2, and EMT markers such as vimentin, CXCR4, and Twist1. Therefore, pterostilbene could be used in combination with radiation therapy to prevent the generation of CSCs and possibly leads to an improved outcome in HCC patients.

Conflict of Interests

The authors declare no conflict of interests.

Authors' Contribution

C.-M. Lee, Y.-H. Su, and T.-T. Huynh contributed equally to this work.

Acknowledgments

This research was supported by Grants from the National Science Council (NSC101-2325-B-038-005 and NSC100-2313-B-038-001-MY3 to C.-T. Yeh). This study was also supported by Grants from Center of Excellence for Cancer Research at Taipei Medical University (DOH101-TD-C-111-008) to C.-T. Yeh and grants from Taipei Medical University (TMU 100-AE3-Y02 and 100TMU-TMUH-09 to A. T. H. Wu and TMU100-AE3-Y04 and 101TMU-SHH-04 and to C.-T. Yeh).

References

[1] L. G. Marcu and E. Bezak, "Influence of stem-cell cycle time on accelerated re-population during radiotherapy in head and neck cancer," *Cell Proliferation*, vol. 45, pp. 404–412, 2012.

[2] J. A. Magee, E. Piskounova, and S. J. Morrison, "Cancer stem cells: impact, heterogeneity, and uncertainty," *Cancer Cell*, vol. 21, pp. 283–296, 2012.

[3] L. V. Nguyen, R. Vanner, P. Dirks, and C. J. Eaves, "Cancer stem cells: an evolving concept. Nature reviews," *Cancer*, vol. 12, pp. 133–143, 2012.

[4] J. E. Visvader and G. J. Lindeman, "Cancer stem cells: current status and evolving complexities," *Cell Stem Cell*, vol. 10, pp. 717–728, 2012.

[5] V. Catalano, S. Di Franco, F. Iovino, F. Dieli, G. Stassi, and M. Todaro, "CD133 as a target for colon cancer," *Expert Opinion on Therapeutic Targets*, vol. 16, no. 3, pp. 259–267, 2012.

[6] V. Madka and C. V. Rao, "Cancer stem cell markers as potential targets for epithelial cancers," *Indian Journal of Experimental Biology*, vol. 49, pp. 826–835, 2011.

[7] D. McCormack and D. McFadden, "Pterostilbene and cancer: current review," *Journal of Surgical Research*, vol. 173, pp. e53–e61, 2012.

[8] Y. S. Chiou, M. L. Tsai, K. Nagabhushanam et al., "Pterostilbene is more potent than resveratrol in preventing azoxymethane (AOM)-induced colon tumorigenesis via activation of the NF-E2-related factor 2 (Nrf2)-mediated antioxidant signaling pathway," *Journal of Agricultural and Food Chemistry*, vol. 59, no. 6, pp. 2725–2733, 2011.

[9] K. A. Roupe, C. M. Remsberg, J. A. Yáñez, and N. M. Davies, "Pharmacometrics of stilbenes: seguing towards the clinic," *Current Clinical Pharmacology*, vol. 1, no. 1, pp. 81–101, 2006.

[10] C. M. Remsberg, J. A. Yáñez, Y. Ohgami, K. R. Vega-Villa, A. M. Rimando, and N. M. Davies, "Pharmacometrics of pterostilbene: preclinical pharmacokinetics and metabolism, anticancer, antiinflammatory, antioxidant and analgesic activity," *Phytotherapy Research*, vol. 22, no. 2, pp. 169–179, 2008.

[11] S. Bao, Q. Wu, R. E. McLendon et al., "Glioma stem cells promote radioresistance by preferential activation of the DNA damage response," *Nature*, vol. 444, no. 7120, pp. 756–760, 2006.

[12] C. Lagadec, E. Vlashi, L. Della Donna et al., "Survival and self-renewing capacity of breast cancer initiating cells during fractionated radiation treatment," *Breast Cancer Research*, vol. 12, no. 1, article R13, 2010.

[13] H. S. Lin, B. D. Yue, and P. C. Ho, "Determination of pterostilbene in rat plasma by a simple HPLC-UV method and its application in pre-clinical pharmacokinetic study," *Biomedical Chromatography*, vol. 23, no. 12, pp. 1308–1315, 2009.

[14] O. O. Ogunwobi, T. Wang, L. Zhang, and C. Liu, "Cyclooxygenase-2 and Akt mediate multiple growth-factor-induced epithelial-mesenchymal transition in human hepatocellular carcinoma," *Journal of Gastroenterology and Hepatology*, vol. 27, pp. 566–578, 2012.

[15] C. Raimondi, W. Gianni, E. Cortesi, and P. Gazzaniga, "Cancer stem cells and epithelial-mesenchymal transition: revisiting minimal residual disease," *Current Cancer Drug Targets*, vol. 10, no. 5, pp. 496–508, 2010.

[16] T. Blick, H. Hugo, E. Widodo et al., "Epithelial mesenchymal transition traits in human breast cancer cell lines parallel the $CD^{hi/}_{44}CD^{lO/-}_{24}$ stem cell phenotype in human breast cancer," *Journal of Mammary Gland Biology and Neoplasia*, vol. 15, no. 2, pp. 235–252, 2010.

[17] S. A. Mani, W. Guo, M. J. Liao et al., "The epithelial-mesenchymal transition generates cells with properties of stem cells," *Cell*, vol. 133, no. 4, pp. 704–715, 2008.

[18] C. V. Dang, "MYC on the path to cancer," *Cell*, vol. 149, pp. 22–35, 2012.

[19] Y. Xie, J. Zhang, Y. Xu, and C. Shao, "SirT1 confers hypoxia-induced radioresistance via the modulation of c-Myc stabilization on hepatoma cells," *Journal of Radiation Research*, vol. 53, pp. 44–50, 2012.

[20] B. Y. Kim, S. Y. Kwak, J. S. Yang, and Y. H. Han, "Phosphorylation and stabilization of c-Myc by NEMO renders cells resistant to ionizing radiation through up-regulation of gamma-GCS," *Oncology Reports*, vol. 26, pp. 1587–1593, 2011.

[21] S. Reichert, C. Rödel, J. Mirsch et al., "Survivin inhibition and DNA double-strand break repair: a molecular mechanism to overcome radioresistance in glioblastoma," *Radiotherapy and Oncology*, vol. 101, pp. 51–58, 2011.

[22] S. Mena, M. L. Rodríguez, X. Ponsoda, J. M. Estrela, M. Jäättela, and A. L. Ortega, "Pterostilbene-induced tumor cytotoxicity: a lysosomal membrane permeabilization-dependent mechanism," *PLoS ONE*, vol. 7, no. 9, Article ID e44524, 2012.

[23] K. K. Mak, A. T. Wu, W. H. Lee et al., "Pterostilbene, a bioactive component of blueberries, suppresses the generation of breast cancer stem cells within tumor microenvironment and metastasis via modulating NF-κB/microRNA 448 circuit," *Molecular Nutrition & Food Research*, 2013.

[24] M. H. Pan, Y. S. Chiou, W. J. Chen, J. M. Wang, V. Badmaev, and C. T. Ho, "Pterostilbene inhibited tumor invasion via suppressing multiple signal transduction pathways in human hepatocellular carcinoma cells," *Carcinogenesis*, vol. 30, no. 7, pp. 1234–1242, 2009.

Hindawi Publishing Corporation
Evidence-Based Complementary and Alternative Medicine
Volume 2013, Article ID 910451, 13 pages
http://dx.doi.org/10.1155/2013/910451

Research Article

A Preclinical Evaluation of Antimycin A as a Potential Antilung Cancer Stem Cell Agent

Chi-Tai Yeh,[1,2,3] Chun-Li Su,[4] Chi-Ying F. Huang,[5,6,7] Justin Kung-Yi Lin,[8] Wei-Hwa Lee,[9] Peter M.-H. Chang,[5,10] Yu-Lun Kuo,[11] Yu-Wen Liu,[6] Liang-Shun Wang,[1,12] Chih-Hsiung Wu,[13] Yi-Shing Shieh,[14] Yi-Hua Jan,[15,16] Yung-Jen Chuang,[15] Michael Hsiao,[16] and Alexander T. H. Wu[17,18]

[1] *Graduate Institute of Clinical Medicine, Taipei Medical University, Taipei 11031, Taiwan*
[2] *Cancer Center, Taipei Medical University-Shuang Ho Hospital, Taipei 23561, Taiwan*
[3] *Graduate Institute of Medical Sciences, National Defense Medical Center, Taipei 11490, Taiwan*
[4] *Department of Human Development and Family Studies, National Taiwan Normal University, Taipei 10610, Taiwan*
[5] *Institute of Clinical Medicine, National Yang-Ming University, Taipei 11272, Taiwan*
[6] *Institute of Biopharmaceutical Sciences, National Yang-Ming University, Taipei 11272, Taiwan*
[7] *Cancer Research Center and Genome Research Center, National Yang-Ming University, Taipei 11272, Taiwan*
[8] *Department of Chinese Medicine, Taipei Medical University Hospital, Taipei 11031, Taiwan*
[9] *Department of Pathology, Shuang Ho Hospital, Taipei Medical University, Taipei 23561, Taiwan*
[10] *Division of Hematology and Oncology, Department of Medicine, Taipei Veterans General Hospital, Taipei 11271, Taiwan*
[11] *Department of Computer Science and Information Engineering, National Taiwan University, Taipei 10617, Taiwan*
[12] *Division of Thoracic Surgery, Department of Surgery, Taipei Medical University-Shuang Ho Hospital, Taipei 23561, Taiwan*
[13] *Department of Surgery, Taipei Medical University-Shuang Ho Hospital, Taipei 23561, Taiwan*
[14] *Department of Oral Diagnosis, Tri-Service General Hospital, National Defense Medical Center, Taipei 114, Taiwan*
[15] *Institute of Bioinformatics and Structural Biology, National Tsing Hua University, Hsinchu 30013, Taiwan*
[16] *Genomics Research Center, Academia Sinica, Taipei 115, Taiwan*
[17] *The Ph.D. Program for Translational Medicine, College of Medical Science and Technology, Taipei Medical University, 250 Wu-Hsing Street, Taipei 11031, Taiwan*
[18] *Translational Research Laboratory, Cancer Center, Taipei Medical University Hospital, Taipei 11031, Taiwan*

Correspondence should be addressed to Alexander T. H. Wu; chaw1211@tmu.edu.tw

Received 10 March 2013; Accepted 12 April 2013

Academic Editor: Yu-Jen Chen

Drug resistance and tumor recurrence are major obstacles in treating lung cancer patients. Accumulating evidence considers lung cancer stem cells (CSCs) as the major contributor to these clinical challenges. Agents that can target lung CSCs could potentially provide a more effective treatment than traditional chemotherapy. Here, we utilized the side-population (SP) method to isolate lung CSCs from A549 and PC-9 cell lines. Subsequently, a high throughput platform, connectivity maps (CMAPs), was used to identify potential anti-CSC agents. An antibiotic, antimycin A (AMA), was identified as a top candidate. SP A549 cells exhibited an elevated stemness profile, including Nanog, β-catenin, Sox2, and CD133, and increased self-renewal ability. AMA treatment was found to suppress β-catenin signaling components and tumor sphere formation. Furthermore, AMA treatment decreased the proliferation of gefitinib-resistant PC-9/GR cells and percentage of SP population. AMA demonstrated synergistic suppression of PC-9/GR cell viability when combined with gefitinib. Finally, AMA treatment suppressed tumorigenesis in mice inoculated with A549 SP cells. Collectively, we have identified AMA using CMAP as a novel antilung CSC agent, which acts to downregulate β-catenin signaling. The combination of AMA and targeted therapeutic agents could be considered for overcoming drug resistance and relapse in lung cancer patients.

1. Introduction

Lung cancer ranks as one of the most deadly malignancies globally and accounts for approximately 0.16 million deaths in the United States alone [1]. Although targeted therapeutic agents such as gefitinib and erlotinib have been shown to be effective in patients with specific mutations in the epidermal growth factor receptor (EGFR) [2, 3], they do not work successfully in EGFR wild-type patients, and even in the patients who are initially sensitive towards these drugs will eventually acquire resistance. For instance, the median progression-free survival after first-line treatment of gefitinib in sensitive EGFR mutated patients is only 10 months [4, 5]. Currently, no alternative and/or effective treatment options can be offered to patients once drug resistance has emerged. Therefore, there is an urgent need to discover and develop alternative agents that can overcome drug resistance in lung cancer patients. Although the mechanism(s) responsible for the development of drug resistance remains elusive, the existence of cancer stem cells (CSCs) provides a rational potential target for investigation.

CSCs have emerged as one of the hallmarks of cancer and a key contributor to drug resistance and disease relapse. CSCs residing in the heterogenous tumor population are defined based on their ability to seed tumors at limiting dilutions *in vivo*. In addition, CSC-enriched cancer cell populations also exhibit certain properties *in vitro*; thus, CSC-enriched subpopulations can be isolated by utilizing cell-surface marker profiles. For example, leukemia stem cells are enriched for a subset of cells that are $CD34^+/CD38^-$ [6]. Importantly, isolated CSCs can form spherical colonies in suspension cultures that are known as tumor spheroids [7]. Furthermore, CSC-enriched populations exhibit increased resistance to chemotherapeutic agents and ionizing radiation [8]. Collectively, these stem cell-like features define and characterize CSCs. The existence of CSCs has been described in a variety of hematologic and solid malignancies including those of the breast, brain, colon, pancreas, lung, liver, and esophagus [9]. In addition to driving tumorigenesis, CSCs have also been shown to contribute to tumor metastasis and recurrence after treatment. This suggests that current interventions, while killing the bulk of tumor cells, may ultimately fail because they do not eliminate CSCs, which survive to regenerate new tumors. Thus, understanding the underlying mechanisms responsible for the generation of CSCs is essential for developing drugs that may improve treatment efficacy and prevent carcinogenesis of all types of cancer [10].

The connectivity maps (CMAP) is a collection of genome-wide transcriptional expression data from cultured human cancer cells that were treated with bioactive small molecules, along with pattern-matching algorithms that collectively facilitate the discovery of connections between queries by the transitory feature of common gene-expression changes. CMAP allow the user to screen compounds against various disease signatures. Drugs are paired with diseases using pattern-matching methods with a high level of resolution and specificity [11]. A strong positive connectivity score (similarity) indicates that a particular drug induces the gene expression of its corresponding query; in contrast, a strong negative connectivity score (dissimilarity) denotes that the agent reverses the expression of the query. Therefore, agents with strong negative connectivity scores could theoretically reverse a particular biological state by modulating the gene signatures. This unique feature of CMAP offers a high throughput platform for pairing potential therapeutic drugs and specific diseases. Taking advantage of this signature pattern-matching feature of CMAP, we hypothesized that if a drug could modulate a set of gene signatures (partially or globally) in CSCs so that the resulting gene pattern resembles the control (parental cell) gene pattern, this particular drug may be effective in controlling or treating CSCs. Using a collection of established gene expression signatures obtained from embryonic stem cells (ESCs) and CSCs as the input for the CMAP database, we have identified antimycin A (AMA), one of the antibiotics in CMAP database, as a potential anti-CSC agent.

AMA is a potent antifungal agent identified in symbiotic Streptomyces bacteria which reside within the nests of fungal cultivating ants to help confer protection against a range of microfungal weeds [12]. It is also the active component in Fintrol, a chemical piscicide used in fisheries management. AMA functions as a mitochondrial electron transport inhibitor; it has been used to examine the sites of reactive oxygen species generation in mitochondria isolated from chronic obstructive pulmonary disease patients and its relationship with local oxidative stress induced by exercise [13]. Based on its ability to disrupt mitochondrial function, AMA was tested for its potential as an alternative anticancer agent. Recently, AMA has been show to suppress lung cancer cell proliferation by inducing oxidative stress [14]. Interestingly, AMA was identified by CMAP as one of the top-ranking anti-CSC candidates. Here, we intended to examine AMA's potential in suppressing lung CSC generation. First, we isolated and characterized lung CSCs using the side-population method and subsequently examined the effects of AMA on lung CSCs. We found that AMA decreased the self-renewal ability by decreasing their expression of β-catenin signaling components. Furthermore, we showed that AMA decreased the percentage of side-population cells in lung cancer cell lines; in combination with gefitinib, AMA effectively eliminated gefitinib-resistant lung cancer cells by negatively modulating β-catenin signaling. Finally, AMA was shown to suppress lung tumorigenesis *in vivo*. In summary, we provide evidence that AMA, an antibiotic identified using CMAP, is a potential new agent that can target and eliminate lung CSCs.

2. Materials and Methods

2.1. Chemicals. Gefitinib was purchased from LC Laboratories (Woburn, MA, USA) and dissolved in dimethyl sulfoxide (DMSO) as a 10 mM stock solution. Antimycin A, Verapamil, Hoechst 33342 and MTT dye (tetrazolium dye (thiazolyl Blue tetrazolium bromide)) was purchased from Sigma-Aldrich (St. Louis, MO, USA). Primary antibodies to β-catenin, NF-κB (p65), cyclin D1, TCF-4, Vimentin, and β-actin were purchased from Cell Signaling Technology (Boston, MA, USA). CD133/1 (AC133)-PE, human was purchased from

Miltenyi Biotec (Cambridge, MA, USA). Antimycin A was dissolved in dimethyl sulfoxide (DMSO) and further diluted in sterile culture medium immediately before use. A TRIzol RNA isolation kit was obtained from Life Technologies (Rockville, MD, USA), and primers for RT-PCR, dNTP, reverse transcriptase, and Taq polymerase were obtained from Gibco BRL (Cergy Pontoise, France).

2.2. Cell Lines and Culture. Lung cancer cell lines A549 and PC-9 were obtained from the ATCC. PC-9 is derived from a patient with adenocarcinoma and harbors an EGFR exon 19 in-frame deletion that is highly sensitive to EGFR-TKIs. PC-9/GR is a cell line resistant to gefitinib that was established by chronic exposure of PC-9 cells to medium containing increasing concentrations of the drug [15]. Briefly, PC-9 cells were first exposed to 10 nmol/L of gefitinib in medium containing 10% fetal bovine serum, and the concentration of gefitinib was then increased in a stepwise manner. Cells that were able to grow in 1 μmol/L gefitinib were obtained 6 months after initial expose. The decreased sensitivity did not reverse even after the cells were kept in culture for >4 months without gefitinib. These cells were grown in RPMI 1640 culture medium or Dulbecco's modified Eagle's medium (GIBCO-Life Technologies, Inc., Gaithersburg, MD) supplemented with 10% fetal bovine serum (FBS), penicillin (100 UI/mL), and streptomycin (100 μg/mL) at 37°C in a humidified atmosphere with 5% CO_2 and harvested with trypsin-EDTA when the cells were in exponential growth.

2.3. Isolation of A549 Side Population Cells by Cell Sorting. To examine the existence of CSCs in an established A549 carcinoma cell line, side population (SP) cells were isolated by flow cytometry and cell sorting techniques. SP cells that expressed ATP-binding cassette (ABC) transporters (ABCG2) and Hoechst 33342 efflux activity were sorted by FACSaria flow cytometry. Lung cancer cells were labeled with 2.5 μg/mL Hoechst 33342 (Sigma-Aldrich) for 30 min at 37°C. The control cells were incubated in the presence of 25 μM verapamil (Sigma-Aldrich), a broad spectrum ABC transporter inhibitor. Propidium iodine (PI) (1 μg/mL) was added to discriminate dead cells. Analysis and sorting were performed on FACSaria flow cytometers (Becton Dickinson, San Jose, CA). After sorting, A549 SP sphere cells were plated at a density of 1000 cells/mL under stem cell conditions by resuspending them in tumor sphere medium consisting of serum-free HEScGRO medium, N2 supplement (Invitrogen, Carlsbad, CA), 10 ng/mL human recombinant bFGF (Invitrogen, Calsbad, CA), and 10 ng/mL EGF; subsequently, they were cultured in ultralow attachment plates (Corning, NY, USA) for approximately 1 week.

2.4. Assessment of the Growth of A549 SP and NSP Cells following Antimycin A Treatment. Sulforhodamine B (SRB) dye (Sigma-Aldrich, Munich, Germany) was used to test the effects of selective inhibitors on cell growth and viability of SP cells. Antimycin A was dissolved in DMSO before diluting with growth medium to a final DMSO concentration of <0.05%. The A549 SP cells were seeded into 96-well plates in growth medium at 500 cells/well. After 24 h, the medium was replaced with fresh growth medium containing antimycin A, and the cells were incubated for another 48 h. The cells were then fixed by gently adding 50 μL TCA (50%) to each well for a final TCA concentration of 10%, with subsequent incubation for 1 h at 4°C. The plates were then washed 5 times with tap water and air dried. The dried plates were stained with 100 μL of 0.4% (w/v) SRB prepared in 1% (v/v) acetic acid for 10 min at room temperature. The plates were rinsed quickly 4 times with 1% acetic acid to remove unbound dye and then air dried until no moisture was visible. The bound dye was solubilized in 20 mmol/L Tris base (100 μL/well) for 5 min on a shaker. Optical densities were read on a microplate reader (Molecular Devices, Sunnyvale, CA) at 562 nm.

2.5. β-Catenin/TCF Transcription Reporter Assay. A549 SP cells were plated in 6-well plates, grown to 80%–90% confluence, and transiently transfected with TOPflash and FOPflash plasmids, respectively. TOPflash has 3 copies of the Tcf/Lef binding sites upstream of a thymidine kinase (TK) promoter and the firefly luciferase gene. FOPflash is used as control for measuring nonspecific activation of the reporter. All transfections were performed with Lipofectamine and 0.3 μg of TOPflash or FOPflash plasmids. To normalize transfection efficiency, cells were cotransfected with 0.2 μg of the internal control reporter encoding Renilla reniformis luciferase driven under the TK promoter. After transfection, cells were incubated in medium with or without antimycin A (0–10 μM) for 48 hours and then lysed with reporter lysis buffer. Luciferase activity was determined by Dual-Luciferase Assay System kit according to vendor's protocol. The experiments were performed in triplicate, and the results were reported as folds of induction compared with control group after normalization to transfection efficiency.

2.6. RT-PCR. Total RNA was purified from the SP cells using Trizol reagent (Invitrogen, Carlsbad, CA) according to the manufacturer's protocol. RNA (2 μg) was added to RT-PCR reactions (final primer concentration of 0.5 μM). After a 42°C/60 min reverse transcription step, 30 cycles of amplification were performed at 94°C for 30 sec, 58°C for 50 sec, and 72°C for 50 sec. PCR products were run on 1.5% agarose gels for identification. Primers used were 5′-CAG AGT ACA ACG CCA AAC CA-3′ and 5′-AAA TCA CGA TGA GGG TCA GC-3′ for CD133, and 5′-GAA GGT GAA GGT CGG AGT C-3′ and 5′-CAA AGT TGT CAT GGA TGA CC-3′ for GAPDH. The Q-PCR primers used for detecting gene expression of CD133, Sox2, β-catenin, and Nanog were as follows: CD133-specific primers (sense primer 5′-TCTTGACCGACTGAGACCCAAC-3′ and antisense primer 5′-ACTTGATGGATGCACCAAGCAC-3′), Sox2-specific primers (sense primer 5′-GACAGTTACGCGCACATGAA-3′ and antisense primer 5′-TAGGTCTGCGAGCTGGTCAT-3′), β-catenin-specific primers (sense primer 5′-GCGTGGACAATGGCTACTCAAG-3′ and antisense primer 5′-TATTAACTACCACCTGGTCCTC-3′), and Nanog-specific primers (sense primer 5′-GTGATTTGTGGGCCTGAAGA-3′ and antisense primer 5′-ACACAGCTGGGTGGAAGAGA-3′).

2.7. Western Blotting. Cell lysates were prepared using a ReadyPrep Protein Extraction Kit (Bio-Rad, Hercules, CA) according to instructions provided. Total cell lysates (50 μg) were separated using 10% SDS-PAGE and transferred onto a polyvinylidene fluoride membrane using the BioRad Mini Protean transfer system. The blots were then blocked with 5% skim milk in PBST for 1 h and probed with primary antibodies overnight at 4°C. The membrane was further incubated overnight at 4°C with respective specific antibodies against active β-catenin (1 : 1000), TCF-4 (1 : 1000), cyclin D1 (1 : 1000), NF-κB/p65 (1 : 1000), and β-actin (1 : 5000). After incubation with primary antibodies, the membrane was washed with TBST 3 times. The membrane was then incubated with horseradish peroxidase-labeled secondary antibody for 45 minutes at room temperature and washed with TBST 3 times. Final detection was performed with enhanced chemiluminescence (ECL) Western blotting reagents and the BioSpectrum Imaging System (UVP, Upland, CA).

2.8. In Vivo Evaluation of the Effects of Antimycin A on Cancer Stem Cells. All animal studies were performed strictly under the animal experimentation protocols approved by Taipei Medical University. A549 side-population cells were first modified to express the dual reporter system FUW-Luc-mCherry-Puro (a generous gift from Dr. Andrew Kung, Lurie family Imaging Center, Dana Farber Cancer Institute, MA). Imaging-ready A549 side-population cells were harvested and injected via the tail vein of NOD/SCID mice (5.5×10^5 cells). Tumor-bearing mice were then subdivided into control and Antimycin A-treated groups (10 mg/kg i.p. injection, 3 times a week). Tumor burden was noninvasively assessed based on bioluminescence intensity for 4-5 weeks using the IVIS200 system (Caliper life sciences Inc., Hopkinton, MA). Tumor biopsies were obtained at the end of the experiment by humanely sacrificed the animals.

2.9. Histology and Immunohistochemical Staining. Tumor tissues were fixed in 10% formalin and embedded in paraffin. Serial sections of the embedded specimens were deparaffinized and then rehydrated in a graduated fashion and stained with hematoxylin and eosin (H&E). For immunohistochemical staining, the deparaffinized slides were subjected to antigen retrieval and probed with anti-beta-catenin (1 : 100), anti-NF-κB-p65 (1 : 200), anti-Vimentin (1 : 100), or anti-E-cadherin (1 : 100) antibodies, or isotype IgG control. Slides were washed and incubated with biotinylated link universal antiserum, followed by horseradish peroxidase-streptavidin conjugate (LSAB 1 kit). The slides were rinsed, and color was developed using 3,3-diaminobenzidine hydrochloride as a chromogen. Finally, sections were rinsed in distilled water, counterstained with Mayer's hematoxylin, and mounted with DPX mounting medium for evaluation. Pictures were captured with a Photometrics CoolSnap CF color camera (Nikon, Lewisville, TX).

2.10. Statistical Analysis. Each experiment was performed in triplicate. The results were expressed as the means ± SEM. The comparisons of means between two groups were analyzed with independent sample t-tests. For comparison of more than two groups, Analysis of Variance (ANOVA) was conducted to examine the equality of means. A Bonferroni post hoc analysis was executed following a significant ANOVA to detect differences. The threshold of significance was set at $P = 0.05$ throughout the study.

3. Results

3.1. Identification of Antimycin A (AMA) as a Potential Anti-CSC Agent Using the Connectivity Map Database. Using a CMAP algorithm in combination with gene signatures from ESCs and CSCs, we were able to identify a group of antibiotics from the CMAP database that have the potential to reverse the CSC-associated gene signatures (see Supplementary Table 1 in Supplementary Material available online at http://dx.doi.org/10.1155/2013/910451). One of the top-ranking candidates was AMA. A previous study showed the ESC transcription program used by Wong and coworkers [16] as similar to the Myc module [17]. Therefore, AMA signatures obtained from CMAP were subsequently subjected to Gene Set Enrichment Analysis (GSEA), which is a computational method that determines whether an a priori defined set of genes shows statistically significant, concordant differences between two biological states. The concordant gene expression behavior of the AMA signature was found to reverse both ESC and Myc modules, which are very close to each other and correlate well with CSC-like phenotypes (Figure 1). This analysis raised the possibility that targeting these specific cancer-associated ESC-like gene signatures could result in the inhibition of CSCs. In addition, treatment of lung cancer stem cells (CL141) with AMA resulted in downregulation of c-Myc (data not shown), suggesting that AMA has the potential to reverse lung CSC-like gene signatures.

3.2. Identification and Characterization of Side-Population Cells from the Lung Cancer Cell Line A549. To validate the potential anti-CSC function of AMA, a consistent and reliable cell model of lung CSCs was required. Based on this premise, we first identified and isolated SP cells from the A549 lung cancer cell line by flow cytometry based on the SP's ability to exclude Hoechst 33342 DNA binding dye (Figure 2(a)). The isolated SP cells demonstrated a marked elevation of stem cell-associated mRNA transcripts, including Nanog, β-catenin, Sox2, and CD133, compared to the non-SP counterparts (Figure 2(b)). In addition, the transcriptional activity of β-catenin-TCF/LEF was markedly increased in SP cells compared to non-SP counterparts (Figure 2(c)). More importantly, when cultured in serum-deprived stem cell medium, SP cells demonstrated an enhanced ability to form tumor aggregates or spheroids, while non-SP cells showed a significantly lower ability to form tumor spheroids (Figure 2(d)). Collectively, SP cells isolated from the A549 lung cancer cell line demonstrated a spectrum of stem cell-like characteristics.

3.3. Antimycin A Suppresses the Ability of A549 SP Cells to Form Tumor Spheroids by Disrupting β-Catenin/TCF-4 Signaling. Once establishing A549 SP cells as tumor cancer stem-like cells, we subsequently used this platform to

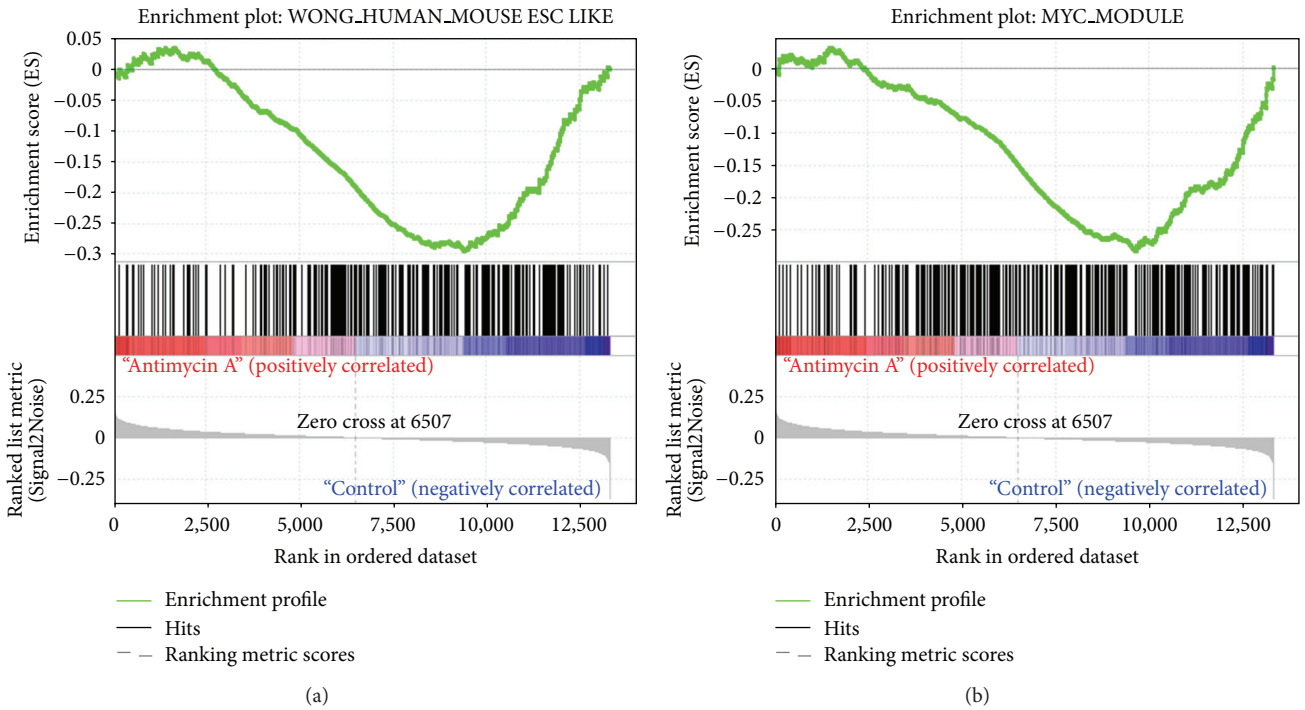

Figure 1: Identification of antimycin A as a potential anti-CSC agent using the connectivity maps database. Gene set enrichment analysis (GSEA) demonstrated that the AMA drug signature reverses Wong's ESC module (a) and the Myc module from Kim's study (b). Both modules have been correlated with CSC-like phenotypes, suggesting antimycin A have the potential to reverse lung CSC signature.

examine AMA's ability to suppress the stemness of A549 SP cells. AMA treatment suppressed the tumor spheroid-forming ability of A549 SP cells in a dose-dependent manner (Figure 3(a)). Because β-catenin/TCF-4 signalling plays a pivotal role in stem cell development [18, 19], we examined whether AMA's ability to suppress the formation of tumor spheroids was through this pathway. AMA treatment significantly downregulated the expression of β-catenin/TCF-4 and cyclin D1 in A549 SP cells at a low concentration (2.5 μM). At higher concentrations (5–10 μM), AMA suppressed the expression of two major signalling pathways that are often dysregulated in cancer cells, namely, Wnt/β-catenin and NF-κB (Figure 3(b)). Additionally, AMA inhibited β-catenin transcription in A549 SP cells (Figure 3(c)). Of equal importance, AMA-treated A549 SP cells exhibited decreased CD133 expression (from 45.6% in control cells to 3.2% in treated cells) as demonstrated by flow cytometry (upper panels, Figure 3(d)) and RT-PCR analysis (lower panels, Figure 3(d)).

3.4. Antimycin A Targets the Gefitinib-Resistant Lung Cancer Cell Line PC-9/GR. Acquired resistance towards targeted therapeutic agents represents one of the major properties of cancer stem cells. Thus, we intended to test if AMA could target gefitinib-resistant lung cancer cells. PC-9/GR cells were grown in the presence of gefitinib, AMA, or both drugs (Figure 4(a)). AMA treatment (5 μM) inhibited the proliferation of PC-9/GR cells to the smallest extent (35%), followed by gefitinib treatment (42%). Importantly, the combination of both drugs eradicated approximately 80% of PC-9/GR cells. Isobologram analysis indicated that AMA and gefitinib worked synergistically to eliminate PC-9/GR lung cancer cells (Figure 4(b)).

One of the key features of side-population cells is their high expression of ABCG2 pumps and the ability to exclude Hoechst dye (reflecting their ability to exclude drugs). Thus, to demonstrate AMA's ability to overcome drug resistance, PC-9/GR (gefitinib-resistant PC-9) cells were subjected to SP analysis. When treated with AMA (5 and 10 μM), the percentage of A549 SP cells (1.81% in control samples) decreased to 0.85% and 0.11%, respectively (upper panels, Figure 4(c)). Similarly, SP cells from PC-9 (wild-type) and PC-9/GR cells were also examined. We found that the initial percentage of SP cells in each cell line was approximately 2.6% and 3.8%, respectively (lower panels, Figure 4(c)). Again, AMA treatment eliminated SP cells in a dose-dependent fashion. To explore the molecular mechanisms mediated by AMA, total protein lysates were harvested from A549 SP cells. The expression levels of stemness molecules including β-catenin and TCF4 were decreased. NF-κB/p65 and cyclin D1 expression was also suppressed by AMA and the combined treatment (Figure 4(d)). These data demonstrate that AMA possesses the ability to eliminate cancer stem-like SP cells in drug resistant lung cancer cells, both alone and in combination with other treatments.

3.5. Antimycin A Inhibits Tumorigenesis In Vivo . Tumor-initiating ability is one of the most important hallmarks of cancer stem cells. Therefore, we further explored the anticancer stem cell ability of AMA using an immune compromised mouse xenograft model. Firefly luciferase-expressing A549

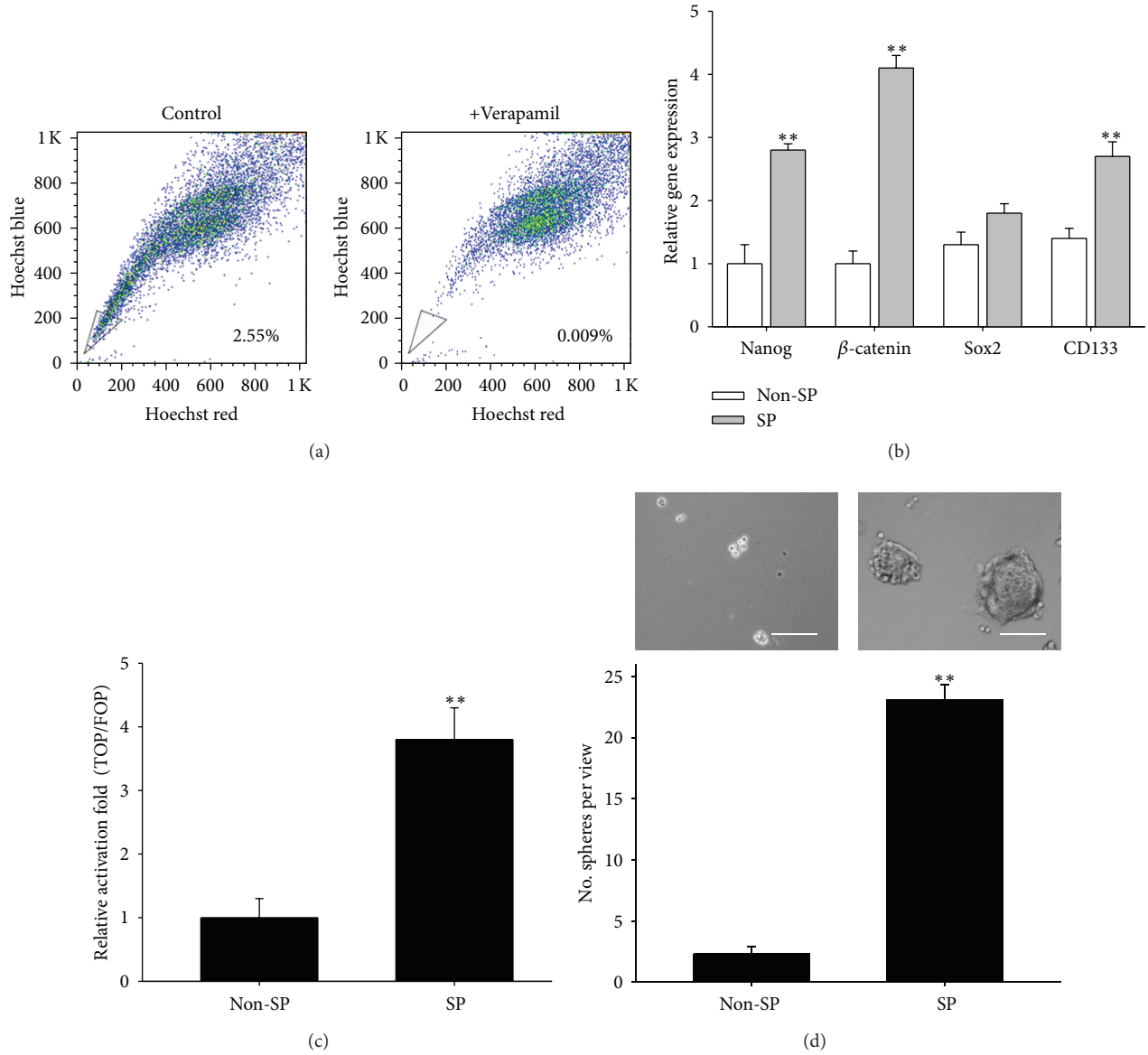

Figure 2: Characterization of lung cancer stem cell properties via side population assays. (a) Side-population flow cytometric analysis of A549 lung cancer cells. Approximately 2.55% of cells were identified as SP. (b) Real-time PCR analysis showed that A549 SP cells contained higher levels of Nanog, β-catenin, Sox2, and CD133 mRNA transcripts compared to their non-SP counterparts. (c) A549 SP cells showed higher β-catenin-TCF/LEF transcriptional activity than their non-SP counterparts. TOPFLASH (TOP) or FOPFLASH (FOP) plasmids (0.3 μg) were used for the reporter assay. (d) A549 SP cells showed a higher ability (approximately 8-fold) to form tumor spheroids in serum-deprived medium culture than non-SP cells. Scale bar, 50 μm. *denotes $P < 0.05$ while **represents $P < 0.01$ as compared to their respective controls.

SP cells were subcutaneously injected into NOD/SCID mice; mice were then divided into two groups: one receiving AMA treatment (i.p. injection, 10 mg/kg, 3 times/week) and one receiving vehicle. Tumorigenesis was monitored using a noninvasive molecular system. Three weeks after inoculation, AMA-treated mice exhibited a lower ability to initiate lung tumors (lower panel, Figure 5(a)) when compared to the vehicle-treated group (upper panel, Figure 5(a)) as reflected by the bioluminescence images. The tumor burden was monitored using the change in bioluminescence over a period of 5 weeks (after tumor inoculation), and the AMA-treated group demonstrated a significantly lower increase in bioluminescence as compared to the vehicle-treated counterpart. The data from bioluminescence imaging was supported by immunohistochemical analysis of the tumor biopsies obtained from both groups. Tumor sections from AMA-treated mice demonstrated a decreased expression of β-catenin, NF-κB/p65, and Vimentin, and an increased expression of E-cadherin (lower panels, Figure 5(c)), compared to samples from the control mice (upper panels,

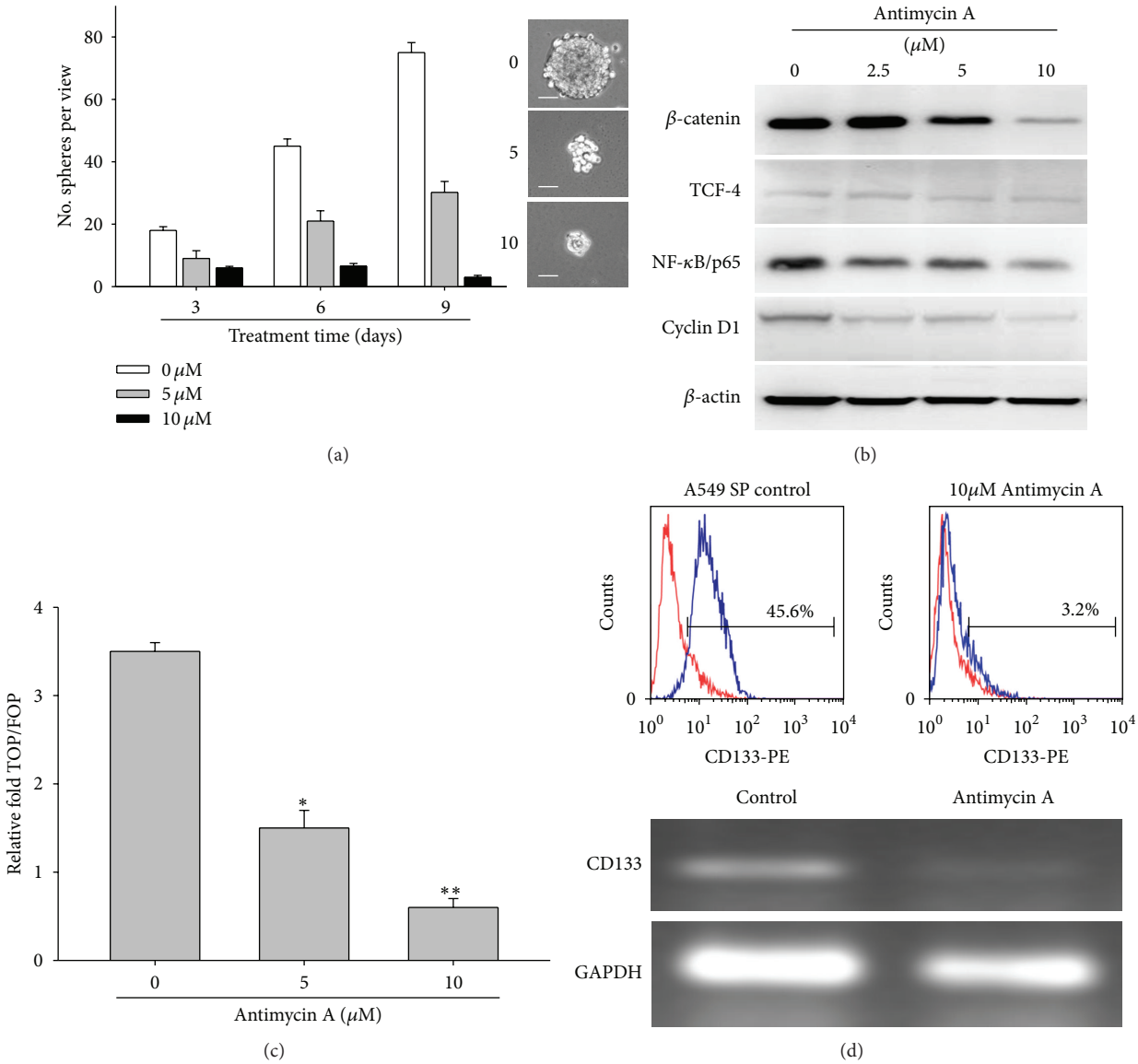

Figure 3: Antimycin A dose dependently suppresses the self-renewing ability of lung cancer stem cells. (a) Different concentrations of AMA (0, 5, and 10 μM) were used to treat A549 tumor spheroids. AMA exhibited a dose-dependent ability to inhibit tumor sphere formation. Inserts depict the morphology of AMA-treated tumor spheroids. Scale bar, 50 μm. (b) Western blot analysis of AMA-treated A549 tumor spheroids. AMA dose dependently suppressed the expression of components of the β-catenin signaling cascade. (c) TOP/FOP luciferase assay was used to examine AMA's ability to suppress β-catenin-TCF/LEF transcriptional activity in A549 SP cells. AMA treatment significantly suppressed the transcriptional activity of the β-catenin pathway as indicated by decreased luciferase activity as the concentration of AMA increased. (d) Flow cytometric and RT-PCR analyses of AMA-mediated downregulation of CD133 expression. By flow cytometric analysis, AMA treatment suppressed the percentage of A549 SP cells that expressed CD133 by approximately 40%. Consistently, RT-PCR analysis demonstrated a significantly downregulated CD133 transcript in AMA-treated A549 SP cells. GAPDH served as internal control. *denotes $P < 0.05$ while **represents $P < 0.01$ as compared to their respective controls.

Figure 5(c)). Collectively, these findings suggested that AMA treatment efficiently suppressed tumorigenesis *in vivo* by negatively modulating β-catenin (stemness marker), NF-κB (inflammatory marker), and Vimentin (mesenchymal marker).

4. Discussion

Drug resistance, metastasis, and disease recurrence have been the major obstacles encountered in the management of cancer patients. Lung cancer remains a major cause of cancer-related lethality due to high incidence and recurrence in spite of significant advances in staging and therapies [20, 21]. Studies have demonstrated that stem cells present in the airways may be the initiators of lung tumorigenesis. These putative stem cells exhibit tumorigenic characteristics, including a high proliferative ability, multipotent differentiation, drug resistance, and increased metastatic potential compared to other cells [22, 23]. Therefore, these so-called lung CSCs represent

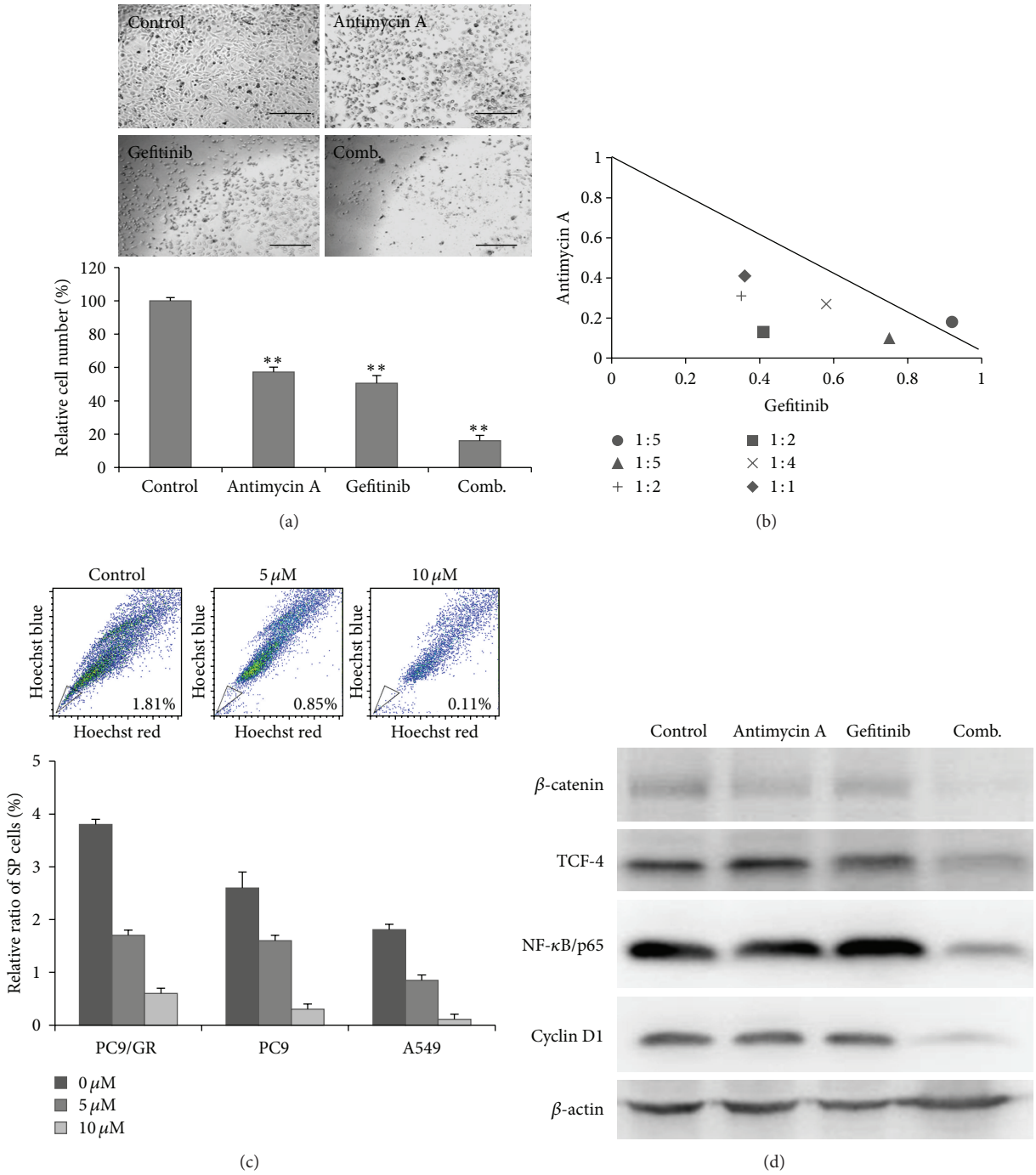

Figure 4: Antimycin A overcomes gefitinib resistance in lung cancer cells. (a) Gefitinib-resistant PC-9 lung cancer cells (PC-9/GR) were treated with gefitinib (5 μM), AMA (5 μM), and the two agents combined. AMA or gefitinib alone could only suppress PC-9/GR proliferation by approximately 35% and 42%, respectively. Gefitinib and AMA combined synergistically suppressed PC-9/GR proliferation by approximately 80%. Scale bar, 100 μm. (b) Isobologram analysis showed that the combination of gefitinib and AMA suppressed PC-9/GR proliferation synergistically. Normalized isobolograms are shown where PC-9/GR were exposed for 48 h to different combinations of AMA (0.5, 2.5, and 5 μM) and gefitinib (2.5, 5, and 10 μM). Symbols designate the combination index value for each fraction affected. The curves were generated by Calcusyn software to fit the experimental points. The data are representative of three independent experiments. Values below the line are synergistic, whereas those close to the line are additive and those above the line antagonistic. (c) AMA dose dependently decreased the percentage of side-population cells in lung cancer cells. A representative flow cytometric analysis showed that AMA decreased the percentage of SP cells in the A549 cell line (upper panel); AMA also suppressed the SP cell populations in PC-9 and PC-9/GR cell lines (bottom panel). (d) Western blot analysis demonstrated that gefitinib (5 μM) and AMA (5 μM) combination treatment significantly inhibited β-catenin-associated signaling components in A549 SP cells. *denotes $P < 0.05$ while **represents $P < 0.01$ as compared to their respective controls.

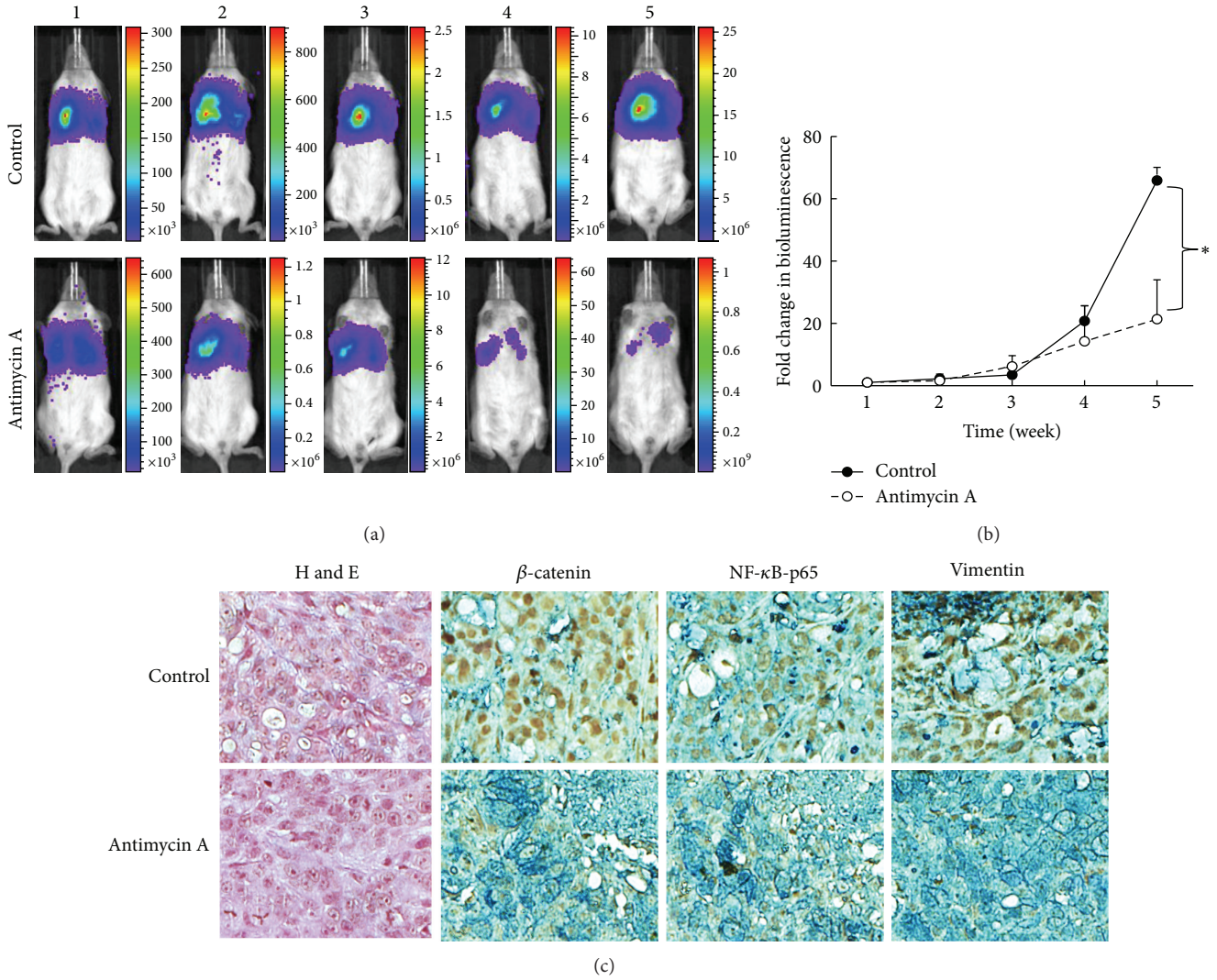

Figure 5: Antimycin A suppresses lung tumorigenesis *in vivo*. (a) Noninvasive bioluminescence imaging was used to monitor the tumor inhibitory effects of AMA *in vivo*. Mice bearing A549 SP cells were divided into control and AMA groups ($N = 5$ each group). Over time, AMA-treated mice demonstrated suppressed lung tumorigenesis, as demonstrated by lower bioluminescence signals. (b) Quantitative bioluminescence data demonstrate the fold changes in bioluminescence signal over time from both control and AMA groups. (c) Immunohistochemical analysis of tumor biopsies. AMA-treated sections demonstrated weaker staining of β-catenin and NF-κB-p65 compared to those in the sections from control animals. Analysis of EMT markers indicates that AMA-treated sections showed decreased Vimentin and increased E-cadherin as compared to the sections obtained from control mice. *refers to the significant difference observed in the fold change in bioluminescence between control and antimycin A groups. $^*P < 0.05$.

a target for drug development. To test our hypothesis, we used a CMAP database in combination with gene signatures from ESCs or CSCs and identified AMA as a potential anti-CSC agent. Of equal importance, we utilized flow cytometry (side-population) to identify and isolate lung CSCs for evaluating the anti-CSC functionality of AMA. AMA was shown to significantly suppress the self-renewing ability of A549 CSCs by negatively modulating the β-catenin signaling cascade. More importantly, using the gefitinib-resistant lung cancer cell line PC-9/GR, we showed that AMA overcame gefitinib resistance. Finally, AMA's antitumor ability was validated *in vivo*.

The CMAP system was originally developed to generate a detailed map that links gene patterns associated with disease to corresponding patterns produced by drug candidates and a variety of genetic manipulations. We took advantage of this system by incorporating ESC or CSC signatures into the algorithm. The reason for evaluating the ESC signatures is that certain phenotypes are found to be crossover between ESCs and CSCs [16, 17]. Specifically, we searched for drugs in the database which were capable of "reversing" the ESC signature to one which resembles to a normal non-CSC signature. From the GSEA analysis, it is interesting to find that AMA reverses both ESC modules from the Wong et al. and Kim et al. studies [16, 17], which have correlated well with CSC-like phenotypes such as relapse and progression.

Using flow cytometry, we identified and isolated a small numbers of SP cells, which are characterized by their ability

to exclude Hoechst 33342 by ABC transporters. These SP cells have been shown to possess stem-cell characteristics [24]. We demonstrated an increased expression of stemness genes, including Nanog, β-catenin, Sox2, and CD133, all of which have been implicated and used in the identification and characterization of CSCs [25–27]. Although aberrant β-catenin activation has been prominently indicated for colorectal carcinogenesis and progression [15, 19, 28], its role in lung cancer and the generation of lung CSCs has not been well described. We observed that isolated A549 SP cells exhibited an elevated level of β-catenin activity and higher ability to form tumor spheroids. The ability to form tumor spheroids not only marks the self-renewal ability of these SP cells, but also represents an operational measure of the number of cancer-initiating cells within a tumor population [29]. Thus, the increased ability of A549 SP cells to form tumor spheroids strongly suggested that these cells resemble CSCs. More importantly, the correlation between high tumor spheroid-forming ability and increased β-catenin activity in A549 SP cells indicated that the β-catenin pathway could play an important role in the generation and maintenance of lung CSCs. Our data were further supported by studies where increased β-catenin signaling was implicated in cell fate determination of upper airway progenitor cells and the acceleration of lung cancer progression [18, 30–32].

Using high throughput platforms, different groups have been able to identify an antibiotic, Salinomycin, as an anticancer stem cell agent [33–35]. These studies provided an important precedent for the rapid identification of effective agents against CSCs. In this study, using CMAP, we identified another antibiotic, AMA, as a potential anti-CSC compound. AMA is an antifungal agent, that is, derived from *Streptomyces kitazawensis* [36] and is a potent inhibitor of succinate oxidase, NADH oxidase, and mitochondrial electron transport between cytochromes b and c [14, 37]. In addition, previous studies indicated that AMA induced apoptosis in lung cancer cells via the generation of reactive oxygen species and negative modulation of the MAPK signaling pathways [38, 39]. After establishing A549 SP cells as a representative CSC model, we tested AMA's ability to eliminate CSCs. Tumor spheroids from A549 SP cells appeared to be sensitive to AMA in a dose-dependent fashion, evident from the number of spheroids decreased as AMA concentration increased. AMA-treated tumor spheroids demonstrated suppressed expression levels of β-catenin and its signaling components including TCF-4, NF-κB, and cyclin D1, which provides a partial explanation of how AMA was able to inhibit tumor spheroid formation. Therefore, the observation that AMA suppressed the formation of A549 tumor spheroids and downregulated the β-catenin signaling cascade suggests that it could be a potential anti-CSC agent.

One of the major obstacles in treating lung cancer patients is drug resistance. Patients who originally were responsive towards targeted therapeutic agents such as the EGFR inhibitors gefitinib and erlotinib inevitably develop resistance. In this study, we used the gefitinib-resistant lung cancer cell line PC-9/GR to demonstrate that under the presence of AMA, PC-9/GR cells became sensitive towards gefitinib. In addition, AMA and gefitinib were shown to synergistically suppress PC-9/GR SP cells. Another gefitinib-resistant NSCLC cell line H1975 (bearing T790 M mutation) was shown to be sensitive towards AMA treatment (Supplementary Figure 1), suggesting that AMA could target lung CSCs regardless of its EGFR genotype. Furthermore, the combination of AMA and gefitinib suppressed the expression of components of the β-catenin cascade. This observation is important since lung basal cell-specific β-catenin activation leads to increased cell proliferation, enhanced self-renewal ability, and induction of early components of early epithelial-mesenchymal transition (EMT), including increased Snail transcription and reduced E-cadherin expression [18].

Equally important, it has been suggested that cross-talk between signaling pathways may contribute to the cellular diversity associated with stem cells during embryogenesis and tissue maintenance and may have a key role in the generation/maintenance of CSCs. For instance, cross-talk was identified between the β-catenin and EGFR signaling cascades [40]. It is plausible that AMA sensitized PC-9/GR cells by suppressing β-catenin cascades, which led to the inhibition of EGFR signaling, thereby achieving dual inhibition of both signaling cascades (Supplementary Figure 2). As precisely how AMA affects EGFR signaling is not clear at the moment and is under our investigation.

Of interest, our hypothesis and data were echoed and supported by recent studies in which various compounds that selectively target CSCs have been discovered. These agents include microbial-derived and plant-derived molecules that target key signaling pathways of CSCs [41, 42] or antibodies against CSC-specific cell surface markers [43]. Salinomycin, another antibiotic discovered using high throughput screening methodology, was shown to selectively kill human breast CSCs [33]. In that study, $CD44^+$ $CD24^-$ $ALDH1^+$ breast CSCs treated with salinomycin alone demonstrated reduced colony forming efficiency and increased apoptosis; these effects were greater when salinomycin was combined with doxorubicin. Similar results were observed in our study, where gefitinib-resistant lung cancer cells (PC-9/GR) were more effectively killed by the combination of AMA and gefitinib than by AMA or gefitinib alone, providing evidence that AMA alone and/or in combination with targeted anticancer drugs effectively eliminate CSCs. In addition, both AMA (Figure 5) and salinomycin [33] promote the differentiation of cells. Notably, CSCs have been shown to contain lower ROS levels and are associated with increased expression of free radical scavenging systems [44]. Thus, pharmacological depletion of ROS scavengers could decrease their clonogenicity and resensitization towards pharmacological agents or radiation. Because AMA is a potent mitochondrial inhibitor [14, 37], the addition of AMA may decrease the ability of CSCs to combat treatment-induced oxidative stress and lead to their eradication. In support, AMA has been demonstrated to cause the loss of mitochondrial membrane potential in Calu-6 lung cancer cells. Interestingly, the intracellular ROS level was decreased in AMA-treated Calu-6 cells while $O_2^{\bullet -}$ among ROS was increased. More importantly, AMA treatment induced GSH depletion in Calu-6 cells rendering the cells more susceptible to chemotherapeutic agents [39]. It is interesting to note that β-catenin signaling has been shown to

activate ROS-defending enzymes such as GST1 (glutathione S transferase 1), which plays an important role in combating drug-induced ROS in the liver [45]. The observation where AMA treatment reduced β-catenin signaling provides additional explanation why AMA functioned synergistically with gefitinib and overcame gefitinib resistance in PC-9/GR cells.

Our data and others suggest a possible link between dysfunctional mitochondrial activity and decreased self-renewal capacity by AMA treatment; this could be due to the decreased expression of β-catenin. We previously showed that β-catenin silencing led to the decreased expression of glutathione S-transferase pi 1 (GSTP1) and intracellular GSH level [46]. We believe that AMA suppresses the self-renewal ability of lung CSCs via multiple pathways including ROS modulation and more importantly decreased β-catenin signaling components (cyclin D1) as well as other stemness genes such as Sox2, Nanog, and CD133. Therefore, AMA (or other mitochondrial modulators) could be used in combination with currently available chemotherapeutic agents to eliminate CSCs and reduce the chance of recurrence.

In conclusion, using CMAP, we were able to rapidly identify AMA as an antilung CSC agent. We provided evidence that AMA suppressed the self-renewal ability of lung CSCs through negative modulation of the β-catenin signaling cascade. More importantly, AMA in combination with gefitinib decreased the percentage of gefitinib-resistant PC-9/GR SP cells. Therefore, AMA could be used in combination with gefitinib to combat drug resistance in lung cancer patients.

Conflict of Interests

All authors declare no conflict of interests.

Authors' Contribution

Alexander T. H. Wu, Chi-Ying F. Huang, Chun-Li Su, and Chi-Tai Yeh designed the experiments and wrote the paper; Justin Kung-Yi Lin, Wei-Hwa Lee, Peter M.-H. Chang, Liang-Shun Wang, Chih-Hsiung Wu, Yi-Shing Shieh, Yung-Jen Chuang, and Michael Hsiao performed the experiments and analyzed data; Yu-Lun Kuo, Yi-Hua Jan, and Yu-Wen Liu performed CMAP inquires and analysis. Chi-Tai Yeh, Chun-Li Su, and Chi-Ying F. Huang contributed equally.

Acknowledgments

The authors appreciate the excellent technical assistance on tumor xenograft experiments and noninvasive imaging from Mr. Bo-Yang Huang. This research was funded by the National Science Council of Taiwan: NSC102-2325-B-010-011 to Chi-Ying F. Huang, NSC100-2313-B-038-001-MY3 to Chi-Tai Yeh, NSC101-2313-B-003-002-MY3 to Chun-Li Su, NSC101-2314-B-075-042 to Peter M.-H. Chang, NSC101-2321-B-001-042 to Michael Hsiao, and NSC99-2628-B-038-010-MY3 to Alexander T. H. Wu. This study was also supported by grants from the Ministry of Education, Aim for the Top University Plan (National Yang Ming University), the Ministry of Economic Affairs (Taiwan) (102-EC-17-A-17-S1-152), and Center of Excellence for Cancer Research at Taipei Veterans General Hospital (DOH102-TD-C-111-007) to Chi-Ying F. Huang, Center of Excellence for Cancer Research at Taipei Medical University (DOH102-TD-C-111-008) to Chi-Tai Yeh, National Taiwan Normal University, Taiwan (100NTNU-D-06), to Chun-Li Su and Chi-Ying F. Huang, and Taipei Medical University (101-TMU-SHH-05 and TMU100-AE3-Y02 to Alexander T. H. Wu and 100-TMU-SHH-07 to Chi-Tai Yeh).

References

[1] A. Jemal, R. Siegel, E. Ward, T. Murray, J. Xu, and M. J. Thun, "Cancer statistics, 2007," *CA: A Cancer Journal for Clinicians*, vol. 57, no. 1, pp. 43–66, 2007.

[2] W. Pao and J. Chmielecki, "Rational, biologically based treatment of *EGFR*-mutant non-small-cell lung cancer," *Nature Reviews Cancer*, vol. 10, no. 11, pp. 760–774, 2010.

[3] P. A. Nguewa, A. Calvo, S. S. Pullamsetti, G. A. Banat, F. Grimminger, and R. Savai, "Tyrosine kinase inhibitors with antiangiogenic properties for the treatment of non-small cell lung cancer," *Expert Opinion on Investigational Drugs*, vol. 20, no. 1, pp. 61–74, 2011.

[4] M. Maemondo, A. Inoue, K. Kobayashi et al., "Gefitinib or chemotherapy for non-small-cell lung cancer with mutated *EGFR*," *The New England Journal of Medicine*, vol. 362, no. 25, pp. 2380–2388, 2010.

[5] T. S. Mok, Y. L. Wu, S. Thongprasert et al., "Gefitinib or carboplatin-paclitaxel in pulmonary adenocarcinoma," *The New England Journal of Medicine*, vol. 361, no. 10, pp. 947–957, 2009.

[6] D. S. Krause and R. A. van Etten, "Right on target: eradicating leukemic stem cells," *Trends in Molecular Medicine*, vol. 13, no. 11, pp. 470–481, 2007.

[7] J. C. Liu, T. Deng, R. S. Lehal, J. Kim, and E. Zacksenhaus, "Identification of tumorsphere- and tumor-initiating cells in HER2/Neu-induced mammary tumors," *Cancer Research*, vol. 67, no. 18, pp. 8671–8681, 2007.

[8] H. Ishii, M. Iwatsuki, K. Ieta et al., "Cancer stem cells and chemoradiation resistance," *Cancer Science*, vol. 99, no. 10, pp. 1871–1877, 2008.

[9] Y. M. Yang and J. W. Chang, "Current status and issues in cancer stem cell study," *Cancer Investigation*, vol. 26, no. 7, pp. 741–755, 2008.

[10] A. Chang, "Chemotherapy, chemoresistance and the changing treatment landscape for NSCLC," *Lung Cancer*, vol. 71, no. 1, pp. 3–10, 2011.

[11] W. L. Yang, Y. E. Lee, M. H. Chen, K. M. Chao, and C. Y. Huang, "*In-silico* drug screening and potential target identification for hepatocellular carcinoma using support vector machines based on drug screening result," *Gene*, vol. 6, no. 12, pp. 01451–01455, 2012.

[12] R. F. Seipke, J. Barke, C. Brearley et al., "A single *Streptomyces* symbiont makes multiple antifungals to support the fungus farming ant *Acromyrmex octospinosus*," *PLoS ONE*, vol. 6, no. 8, Article ID e22028, 2011.

[13] O. Shaham, N. G. Slate, O. Goldberger et al., "A plasma signature of human mitochondrial disease revealed through metabolic profiling of spent media from cultured muscle cells," *Proceedings of the National Academy of Sciences of the United States of America*, vol. 107, no. 4, pp. 1571–1575, 2010.

[14] Y. H. Han, S. H. Kim, S. Z. Kim, and W. H. Park, "Antimycin A as a mitochondrial electron transport inhibitor prevents the growth of human lung cancer A549 cells," *Oncology Reports*, vol. 20, no. 3, pp. 689–693, 2008.

[15] H. Siemens, J. Neumann, R. Jackstadt et al., "Detection of *miR-34a* promoter methylation in combination with elevated expression of c-Met and beta-catenin predicts distant metastasis of colon cancer," *Clinical Cancer Research*, vol. 19, no. 3, pp. 710–720, 2013.

[16] D. J. Wong, H. Liu, T. W. Ridky, D. Cassarino, E. Segal, and H. Y. Chang, "Module map of stem cell genes guides creation of epithelial cancer stem cells," *Cell Stem Cell*, vol. 2, no. 4, pp. 333–344, 2008.

[17] J. Kim, A. J. Woo, J. Chu et al., "A Myc network accounts for similarities between embryonic stem and cancer cell transcription programs," *Cell*, vol. 143, no. 2, pp. 313–324, 2010.

[18] A. Giangreco, L. Lu, C. Vickers et al., "β-catenin determines upper airway progenitor cell fate and preinvasive squamous lung cancer progression by modulating epithelial-mesenchymal transition," *Journal of Pathology*, vol. 226, no. 4, pp. 575–587, 2012.

[19] J. Han, P. Sridevi, M. Ramirez, K. J. Ludwig, and J. Y. Wang, "β-catenin-dependent lysosomal targeting of internalized tumor necrosis factor-α suppresses caspase-8 activation in apoptosis-resistant colon cancer cells," *Molecular Biology of the Cell*, vol. 24, no. 4, pp. 465–473, 2013.

[20] T. M. Kim, S. H. Yim, J. S. Lee et al., "Genome-wide screening of genomic alterations and their clinicopathologic implications in non-small cell lung cancers," *Clinical Cancer Research*, vol. 11, no. 23, pp. 8235–8242, 2005.

[21] R. D. Petty, M. C. Nicolson, K. M. Kerr, E. Collie-Duguid, and G. I. Murray, "Gene expression profiling in non-small cell lung cancer: from molecular mechanisms to clinical application," *Clinical Cancer Research*, vol. 10, no. 10, pp. 3237–3248, 2004.

[22] C. Lin, H. Song, C. Huang et al., "Alveolar type II cells possess the capability of initiating lung tumor development," *PLoS ONE*, vol. 7, no. 12, Article ID e53817, 2012.

[23] S. Wang, Z. Y. Xu, L. F. Wang, and W. Su, "CD133+ cancer stem cells in lung cancer," *Frontiers in Bioscience*, vol. 18, pp. 447–453, 2013.

[24] M. A. Goodell, K. Brose, G. Paradis, A. S. Conner, and R. C. Mulligan, "Isolation and functional properties of murine hematopoietic stem cells that are replicating *in vivo*," *Journal of Experimental Medicine*, vol. 183, no. 4, pp. 1797–1806, 1996.

[25] S. H. Chiou, M. L. Wang, Y. T. Chou et al., "Coexpression of *Oct4* and *Nanog* enhances malignancy in lung adenocarcinoma by inducing cancer stem cell-like properties and epithelial-mesenchymal transdifferentiation," *Cancer Research*, vol. 70, no. 24, pp. 10433–10444, 2010.

[26] A. He, W. Qi, Y. Huang et al., "CD133 expression predicts lung metastasis and poor prognosis in osteosarcoma patients: a clinical and experimental study," *Experimental and Therapeutic Medicine*, vol. 4, no. 3, pp. 435–441, 2012.

[27] S. Singh, J. Trevino, N. Bora-Singhal et al., "EGFR/Src/Akt signaling modulates Sox2 expression and self-renewal of stem-like side-population cells in non-small cell lung cancer," *Molecular Cancer*, vol. 11, article 73, 2012.

[28] J. Rosenbluh, D. Nijhawan, A. G. Cox et al., "β-catenin-driven cancers require a YAP1 transcriptional complex for survival and tumorigenesis," *Cell*, vol. 151, no. 7, pp. 1457–1473, 2012.

[29] C. M. Fillmore and C. Kuperwasser, "Human breast cancer cell lines contain stem-like cells that self-renew, give rise to phenotypically diverse progeny and survive chemotherapy," *Breast Cancer Research*, vol. 10, no. 2, article R25, 2008.

[30] E. C. Pacheco-Pinedo, A. C. Durham, K. M. Stewart et al., "Wnt/β-catenin signaling accelerates mouse lung tumorigenesis by imposing an embryonic distal progenitor phenotype on lung epithelium," *Journal of Clinical Investigation*, vol. 121, no. 5, pp. 1935–1945, 2011.

[31] S. S. Sidhu, R. Nawroth, M. Retz, H. Lemjabbar-Alaoui, V. Dasari, and C. Basbaum, "EMMPRIN regulates the canonical Wnt/β-catenin signaling pathway, a potential role in accelerating lung tumorigenesis," *Oncogene*, vol. 29, no. 29, pp. 4145–4156, 2010.

[32] C. T. Yeh, A. T. Wu, P. M. Chang et al., "Trifluoperazine, an antipsychotic agent, inhibits cancer stem cell growth and overcomes drug resistance of lung cancer," *The American Journal of Respiratory and Critical Care Medicine*, vol. 186, no. 11, pp. 1180–1188, 2012.

[33] P. B. Gupta, T. T. Onder, G. Jiang et al., "Identification of selective inhibitors of cancer stem cells by high-throughput screening," *Cell*, vol. 138, no. 4, pp. 645–659, 2009.

[34] D. Lu, M. Y. Choi, J. Yu, J. E. Castro, T. J. Kipps, and D. A. Carson, "Salinomycin inhibits Wnt signaling and selectively induces apoptosis in chronic lymphocytic leukemia cells," *Proceedings of the National Academy of Sciences of the United States of America*, vol. 108, no. 32, pp. 13253–13257, 2011.

[35] K. Rowan, "High-throughput screening finds potential killer of cancer stem cells," *Journal of the National Cancer Institute*, vol. 101, no. 21, pp. 1438–1439, 2009.

[36] K. Nakayama, F. Okamoto, and Y. Harada, "Antimycin A: isolation from a new *Streptomyces* and activity against rice plant blast fungi," *Journal of Antibiotics*, vol. 9, no. 2, pp. 63–66, 1956.

[37] Y. W. Han, S. Z. Kim, S. H. Kim, and W. H. Park, "The changes of intracellular H_2O_2 are an important factor maintaining mitochondria membrane potential of antimycin A-treated As4.1 juxtaglomerular cells," *Biochemical Pharmacology*, vol. 73, no. 6, pp. 863–872, 2007.

[38] Y. H. Han, H. J. Moon, B. R. You, S. Z. Kim, S. H. Kim, and W. H. Park, "p38 inhibitor intensified cell death in antimycin A-treated As4.1 juxtaglomerular cells via the enhancement of GSH depletion," *Anticancer Research*, vol. 29, no. 11, pp. 4423–4431, 2009.

[39] Y. H. Han and W. H. Park, "The effects of MAPK inhibitors on antimycin A-treated Calu-6 lung cancer cells in relation to cell growth, reactive oxygen species, and glutathione," *Molecular and Cellular Biochemistry*, vol. 333, no. 1-2, pp. 211–219, 2010.

[40] M. U. Latasa, F. Salis, R. Urtasun et al., "Regulation of amphiregulin gene expression by β-catenin signaling in human hepatocellular carcinoma cells: a novel crosstalk between FGF19 and the EGFR system," *PLoS ONE*, vol. 7, no. 12, Article ID e52711, 2012.

[41] B. T. Kawasaki, E. M. Hurt, T. Mistree, and W. L. Farrar, "Targeting cancer stem cells with phytochemicals," *Molecular Interventions*, vol. 8, no. 4, pp. 174–184, 2008.

[42] Y. Li, M. S. Wicha, S. J. Schwartz, and D. Sun, "Implications of cancer stem cell theory for cancer chemoprevention by natural dietary compounds," *Journal of Nutritional Biochemistry*, vol. 22, no. 9, pp. 799–806, 2011.

[43] C. Ginestier, S. Liu, M. E. Diebel et al., "CXCR1 blockade selectively targets human breast cancer stem cells in vitro and in xenografts," *Journal of Clinical Investigation*, vol. 120, no. 2, pp. 485–497, 2010.

[44] M. Diehn, R. W. Cho, N. A. Lobo et al., "Association of reactive oxygen species levels and radioresistance in cancer stem cells," *Nature*, vol. 458, no. 7239, pp. 780–783, 2009.

[45] S. Giera, A. Braeuning, C. Köhle et al., "Wnt/β-catenin signaling activates and determines hepatic zonal expression of glutathione S-transferases in mouse liver," *Toxicological Sciences*, vol. 115, no. 1, pp. 22–33, 2010.

[46] L. C. Lin, C. T. Yeh, C. C. Kuo et al., "Sulforaphane potentiates the efficacy of imatinib against chronic leukemia cancer stem cells through enhanced abrogation of Wnt/β-catenin function," *Journal of Agricultural and Food Chemistry*, vol. 60, no. 28, pp. 7031–7039, 2012.

Hindawi Publishing Corporation
Evidence-Based Complementary and Alternative Medicine
Volume 2013, Article ID 946451, 15 pages
http://dx.doi.org/10.1155/2013/946451

Research Article

Active Component of *Antrodia cinnamomea* Mycelia Targeting Head and Neck Cancer Initiating Cells through Exaggerated Autophagic Cell Death

Ching-Wen Chang,[1] Chien-Chih Chen,[2] Meng-Ju Wu,[1] Yu-Syuan Chen,[1] Chin-Chu Chen,[3] Sen-Je Sheu,[3] Ting-Wei Lin,[3] Shiu-Huey Chou,[4] Shu-Chun Lin,[1] Chung-Ji Liu,[5] Te-Chang Lee,[6] Chih-Yang Huang,[7,8,9] and Jeng-Fan Lo[1,7,10,11,12]

[1] *Institute of Oral Biology, National Yang-Ming University, No. 155, Section 2, Li-Nong Street, Taipei 11221, Taiwan*
[2] *Department of Biotechnology, Hungkuang University, Taichung, Taiwan*
[3] *Grape King Inc., Taoyuan County, Taiwan*
[4] *Department of Life Science, Fu-Jen University, New Taipei City, Taiwan*
[5] *Department of Oral and Maxillofacial Surgery, Mackay Memorial Hospital, Taipei, Taiwan*
[6] *Institute of Biomedical Sciences, Academia Sinica, Taipei, Taiwan*
[7] *Graduate Institute of Chinese Medical Science and Institute of Medical Science, China Medical University, No. 91, Hsueh-Shih Road, Taichung 40402, Taiwan*
[8] *Institute of Basic Medical Science, China Medical University, Taichung, Taiwan*
[9] *Department of Health and Nutrition Biotechnology, Asia University, Taichung, Taiwan*
[10] *Cancer Research Center & Genome Research Center, National Yang-Ming University, Taipei, Taiwan*
[11] *Department of Dentistry, Taipei Veterans General Hospital, Taipei, Taiwan*
[12] *National Yang-Ming University, VGH Genome Research Center, Taipei, Taiwan*

Correspondence should be addressed to Chih-Yang Huang; cyhuang@asia.edu.tw and Jeng-Fan Lo; jflo@ym.edu.tw

Received 20 March 2013; Accepted 8 May 2013

Academic Editor: Yu-Jen Chen

Head and neck squamous cell carcinoma (HNSCC) is a highly lethal cancer. Previously, we identify head and neck cancer initiating cells (HN-CICs), which are highly tumorigenic and resistant to conventional therapy. Therefore, development of drug candidates that effectively target HN-CICs would benefit future head and neck cancer therapy. In this study, we first successfully screened for an active component, named YMGKI-1, from natural products of *Antrodia cinnamomea* Mycelia (ACM), which can target the stemness properties of HNSCC. Treatment of YMGKI-1 significantly downregulated the aldehyde dehydrogenase (ALDH) activity, one of the characteristics of CIC in HNSCC cells. Additionally, the tumorigenic properties of HNSCC cells were attenuated by YMGKI-1 treatment *in vivo*. Further, the stemness properties of HN-CICs, which are responsible for the malignancy of HNSCC, were also diminished by YMGKI-1 treatment. Strikingly, YMGKI-1 also effectively suppressed the cell viability of HN-CICs but not normal stem cells. Finally, YMGKI-1 induces the cell death of HN-CICs by dysregulating the exaggerated autophagic signaling pathways. Together, our results indicate that YMGKI-1 successfully lessens stemness properties and tumorigenicity of HN-CICs. These findings provide a new drug candidate from purified components of ACM as an alternative therapy for head and neck cancer in the future.

1. Introduction

Head and neck squamous cell carcinoma (HNSCC) represents the sixth most common cancer worldwide and the third most common cancer in developing nations [1]. Despite the recent advancements in the multidisciplinary treatment of HNSCC, prognosis of patients with locally advanced diseases and long-term survival rates remains unsatisfactory [2].

Over the past decade, increasing evidence suggests that the hierarchical model of cancer initiating cells (CICs) or cancer stem cells (CSCs) in that each tumor formation is governed by a rare subpopulation of cells with self-renewal capacity [3]. CICs have been demonstrated to have capacities of promoting tumor growth, tumor regeneration, metastatic progression, and tumor recurrence [4, 5]. It is imperative to uncover new therapeutic drug on targeting cancer stem cells [6].

Previously, we have verified a subpopulation of HNSCC cells (HNSCCs) displaying the characteristics of CICs [5]. In addition, we have identified molecular markers such as CD133 [8] and ^{mem}GRP78 (membrane anchoring GRP78) [9] for targeting CICs. Others have found that Aldehyde dehydrogenase (ALDH), which has been demonstrated as a breast cancer CIC marker [10], could also be the CIC marker of head and neck cancer and other cancers [11, 12]. More recently, we have successfully verified an epithelial-mesenchymal transition (EMT) related gene expression, S100A4, which is upregulated in HN-CICs. Consequently, we have shown that significant downregulation of ALDH activity comes along with loss of stemness properties in S100A4 knockdown HNSCCs and HN-CICs [13]. Therefore, the cell-based ALDH activity assay is useful as a screening system for drug candidates, which would target the stemness properties of cells. With the assay system, we would be able to screen for active components of natural products from Chinese medicinal herbals on target cellular ALDH activity *in vitro*.

It has been reported that CICs, bearing highly malignant stem cell traits acquired through processes such as the EMT, would survive during metabolic stress only if they adopt adaptive mechanisms such as autophagy [14]. However, autophagy has a dual role in CICs [15]. Autophagy has been linked to the maintenance of breast cancer stem-like phenotype [16]. In contrast, some studies demonstrate that autophagy plays an essential role in differentiation of glioma-initiating cells [17] and in inhibition of colon cancer stem cell [18]. Thus, the role of autophagy in CICs remains elusive.

Antrodia cinnamomea, a rare mushroom of the family Polyporaceae, only grows naturally in Taiwan [19]. For Taiwanese traditional medicinal treatment, *Antrodia cinnamomea* has been applied for diarrhea, intoxication, hypertension, abdominal pain, itchy skin [20], and cancers therapy [21]. The biological or physiological functions of the crude extracts or purified active components of fruiting bodies or submerged cultured mycelia of *Antrodia cinnamomea* have been examined. Empirically, these active components of natural products from *Antrodia cinnamomea* showed antioxidant [20], anti-inflammatory [22], hepatoprotective [23], and antitumor activities. Further, the antitumor activities of *Antrodia cinnamomea* have recently become popular as an alternative therapeutic agent for several types of human cancer [21, 24].

Several pure compounds in the fruiting body of *Antrodia cinnamomea* have been isolated and identified with antitumor activity [25]. Compounds of maleic and succinic acid derivatives from the mycelium of *Antrodia cinnamomea* exhibit significant cytotoxic effects on Lewis lung carcinoma (LLC) tumor cell [26]. However, the inhibitory effect of *Antrodia cinnamomea* on the cancer initiating cells has never been studied. Therefore, we are interested in screening and evaluating the effects of active components from *Antrodia cinnamomea* on targeting CICs and in elucidating the possible biological mechanisms mediating the antitumor activity *in vitro* and *in vivo*.

Herein, we exploited the perivous *in vitro* cell-based ALDH activity assay system to screen for the active components from *Antrodia cinnamomea* Mycelia extracts (ACMEs) with effective cytotoxicity toward to CICs. We used both *in vitro* assays and *in vivo* xenograft mouse models to examine the cytotoxic effects of a purified component of ACME, YMGKI-1 (a derivative of maleic and succinic acid), on the HN-CICs. Strikingly, YMGKI-1 treatment diminished stemness properties and tumorigenicity of HN-CICs both *in vitro* and *in vivo*. Finally, we demonstrated that the induction of cell death in YMGKI-1-treated HN-CICs is through dysregulatory autophagic signaling, which is regulated mainly by mTOR molecular pathway. Thus, our study indicates that we have successfully isolated active compounds from natural products of *Antrodia cinnamomea* Mycelia (ACM) with selective and effective cytotoxicity on HN-CICs. Further, our findings provide a new drug candidate as an alternative therapy for head and neck cancer in the future.

2. Materials and Methods

2.1. Extraction, Isolation, Purification, and Structure Determination of Single Compounds from the ACM. YMGKI-1 (3-[4-(3-Methylbut-2-enyloxy)phenyl]-4-isobutyl-N-hydroxypyrrole-2,5-dione; Mw: 329 Da) from ACMs and the chemical structure of the purified chemicals were performed and determined by Dr. Chien-Chih Chen (Hungkuang University, Taichung, Taiwan). The purification procedure of YMGKI-I from ACMs was described in Supplementary Materials and Methods available online at http://dx.doi.org/10.1155/2013/946451. Dimethyl sulfoxide (DMSO) (Sigma-Aldrich D2650, Saint Louis, MO) is used as a drug solvent.

2.2. Cell Lines. Human tongue carcinoma cells (SAS) were obtained from the Japanese Collection of Research Bioresources (Tokyo, Japan) [27]. Human gingival squamous carcinoma cells (OECM-1) were provided from Dr. C. L. Meng (National Defense Medical College, Taipei, Taiwan). Primary culture of normal human oral keratinocytes (NHOKs) was as described [5]. Additionally, the amniotic fluid stem cells-2 (AFSC-2) and hematopoietic stem cell (HSC) were isolated by Dr. Shiu-Huey Chou at Fu-Jen University. The isolation protocols of AFSC-2 and HSC were described in Supplementary Materials and Methods.

2.3. Antibodies and Reagents. Anti-Oct-4 (MAB430), anti-Nanog (AB9220), anti-CD133 (MAB4310), and anti-GAPDH (MAB374) were obtained from Millipore Corporation (Billerica, MA). Anti-GRP78 (610978) and anti-E-cadherin (610182) were obtained from BD Bioscience (San Jose, CA). Anti-Notch2 (sc-5545) and anti-PI3K (sc-1637) were obtained from Santa Cruz Biotechnology, Inc. (Santa Cruz, CA). Anti-LC3

(no. 81631), anti-phosphor mTOR (Ser2448) (no. 2971), anti-phosphor p44/p42 MAPK (Thr202/Tyr204) (no. 9101), anti-phosphor p38 MAPK (Thr180/Tyr182) (no. 9211), anti-HER2 (no. 2165), and anti-phosphor EGFR (Tyr1068) (no. 2234) were obtained from Cell Signaling Technology, Inc. (Danvers, MA). 3-Methyladenine (3-MA) (M9281), Metformin (Mf) (D150959) was obtained from Sigma-Aldrich (Saint Louis, MO).

2.4. Cell Lines Cultivation and Enrichment of HN-CICs. In brief, SAS and OECM1 were grown in DMEM or in RPMI supplemented with 10% FBS (Grand Island, NY), respectively. The SAS cells were then cultured in tumor sphere medium consisting of serum-free DMEM/F12 medium (GIBCO), N2 supplement (GIBCO), 10 ng/mL human recombinant basic fibroblast growth factor-basic (FGF), and 10 ng/mL Epidermal Growth Factor (EGF) (R&D Systems, Minneapolis, MN). Cells were plated at a density of 7.5×10^4 live cells/10 mm dish, and the medium was changed every other day until the tumor sphere formation was achieved to enrich the SAS-HN-CICs or OECM1-HN-CICs in about 4 weeks [5].

2.5. ALDH Activity Assay. The ALDEFLUOR kit (Stem Cell Technologies, Durham, NC, USA) was used to examine the ALDH enzymatic activity [13]. Single cell suspension obtained from cancer cells with or without treatment was suspended in ALDEFLUOR assay buffer containing ALDH substrate (BAAA, 1 μmol/L per 1×10^6 cells) and incubated during 40 minutes at 37°C. As negative control, for each sample of cells an aliquot was treated with 50 mmol/L diethylaminobenzaldehyde (DEAB), a specific ALDH inhibitor. This resulted in a significant decrease in the fluorescence intensity of ALDH-positive cells and was used to identify the ALDH-positive cells. The amount of intracellular fluorescence was measured by FACS Calibur apparatus (Becton Dickinson, San Diego, CA).

2.6. Side Population Analysis. Cells were resuspended at 1×10^6/mL in prewarmed DMEM with 2% FCS. Hoechst 33342 dye was added at a final concentration of 5 μg/mL in the presence or absence of fumitremorgin C (FTC) (10 μM; Sigma, St Louis, MO, USA) and was incubated at 37°C for 90 min with intermittent shaking. At the end of the incubation, the cells were washed with ice-cold HBSS with 2% FCS and centrifuged down at 4°C and resuspended in ice-cold HBSS containing 2% FCS. Propidium iodide at a final concentration of 2 μg/mL was added to the cells to gate viable cells. The cells were filtered through a 40 μm cell strainer to obtain single cell suspension before analysis. The Hoechst 33342 dye was excited at 357 nm and its fluorescence was dual-wavelength analyzed (blue, 402–446 nm; red, 650–670 nm). Analyses were done on FACS Aria (Becton Dickinson, San Diego, CA).

2.7. Cell Viability Assay. Cell viability was measured by MTT assay based on the ability of live cells to convert tetrazolium salt into purple formazan. Cells were seeded onto 24-well dishes with medium containing YMGKI-1 at concentrations ranging from 0 to 35 μg/mL for 24 hr. After treatment for the indicated times, 5 μL of MTT solution (4 mg MTT/mL PBS) was added to each well and the plate was incubated at 37°C for 3 h. After the removal of medium, 100 μL of DMSO was added to each well and the plate was gently shaken for 30 min. The absorbance was determined at 560 nm. The cell viability was calculated as OD of experimental groups/OD of control groups × 100%.

2.8. Apoptotic Assay. Apoptotic cells were detected with an Annexin V-APC kit (Calbiochem, Darmstadt, Germany) according to manufacturer's guidelines. After staining, the cells were incubated with 20 μg/mL propidium iodide (PI) to gate the dead cells. Consequently, the fluorescent signals from Annexin V or PI were analyzed by FACS Canto apparatus (Becton Dickinson, San Diego, CA, USA).

2.9. Matrigel Invasion Assay. For transwell migration assays, 2×10^5 cells were plated into the top chamber of a transwell (Corning, Acton, MA) with a porous transparent polyethylene terephthalate membrane (8.0 μm pore size). Cells were plated in medium with lower serum (0.5% FBS), and medium supplemented with higher serum (10% FBS) was used as a chemoattractant in the lower chamber. The cells were incubated for 24 h and cells that did not migrate through the pores were removed by a cotton swab. Cells on the lower surface of the membrane were stained with Hoechst 33258 (Sigma-Aldrich) to show the nuclei; fluorescence was detected at a magnification of 100x using a fluorescence microscope (Carl Zeiss, Oberkochen, Germany). The number of fluorescent cells in a total of five randomly selected fields was counted.

2.10. Anchorage Independent Growth Assay. Each well (35 mm) of a six-well culture dish was coated with 2 mL bottom agar (Sigma-Aldrich) mixture (DMEM, 10% (v/v) FBS, 0.6% (w/v) agar). After the bottom layer was solidified, 2 mL top agar-medium mixture (DMEM, 10% (v/v) FBS, 0.3% (w/v) agar) containing 2×10^4 cells was added, and the dishes were incubated at 37°C for 2 weeks. Plates were stained with 0.005% Crystal Violet and then the colonies were counted. The number of total colonies was counted over five fields per well for a total of 15 fields in triplicate experiments.

2.11. Acridine Orange (AO) Staining Assay. Cells were washed with Hank's buffered salt solution (HBSS) twice, followed by staining with 1 μg/mL acridine orange (Sigma, A 6014), and diluted in HBSS containing 5% FBS for 15 min at 37°C. After staining, cells were washed ice-cold HBSS with 5% FBS and centrifuged down at 4°C and resuspended in ice-cold HBSS containing 5% FBS. The stained cells were observed under a red filter fluorescence microscope. To quantify the AVO formation, the acridine orange stained cells were resuspended in HBSS containing 5% FBS and analyzed by FACS Canto apparatus (Becton Dickinson, San Diego, CA, USA) [28].

2.12. In Vivo Tumorigenic Assay. All the animal practices in this study were approved and in accordance with the Institutional Animal Care and Use Committee (IACUC) of National

Yang-Ming University, Taipei, Taiwan (IACUC approval nos. 1001223 and 991235). The effect of YMGKI-1 on antitumorigenic activity was examined in 8-week-old nude BALB/c nu/nu mice ($n = 3$ per group). SAS cells exposed to YMGKI-1 (1×10^6) were subcutaneously injected into the subcutaneous of nude mice. Tumors were generally palpable at 5 to 7 days after inoculation and tumor volumes were measured (using a caliper and calculated as length $\times$ width^2 $\times$ 0.5) twice weekly until 28 days after injection. To determine the therapeutic effect of YMGKI-1 on regression, SAS cells (5×10^5 cells in 0.1 mL DMEM) were inoculated subcutaneously into the back of nude BALB/c nu/nu mice ($n = 3$ per group). Tumors were allowed to develop to be palpable. Then, the YMGKI-1 was administered intraperitoneally at days 11, 13, and 17 after SAS cell inoculation, and tumor volumes were determined twice weekly. The tumor volume was calculated according to the formula: (Length $\times$ Width^2)/2 [5].

2.13. Statistics. An unpaired t-test was used for the statistical analysis. The results were considered to be statistically different when the P value was <0.05.

3. Results

3.1. Effective Targeting of HN-CICs by YMGKI-1 Treatment. Cancer-initiating cells (CICs) are a rare subpopulation of cancer cells, which are responsible for tumor growth and cancer recurrence during conventional chemotherapy or radiotherapy [3, 4]. High ALDH activity has been used as a selection marker to isolated breast cancer CICs or head and neck CICs (HN-CICs) [29]. Therefore, we first utilized the *in vitro* cell-based aldehyde dehydrogenase (ALDH) activity assay system to screen for the active components from *Antrodia cinnamomea* mycelia extract (ACME) with effective reduction on ALDH activity of cells. Of the tested compounds purified from ACME, YMGKI-1 (a malic and succinic acid derivative (Figure 1(a))) significantly reduced the ALDH enzymatic activity of YMGKI-1-treated SAS cells in a dose-dependent manner (Figure 1(b)). We also found that YMGKI-1 diminished the ALDH enzyme activity in other human cancer cell lines (Supplementary Table 1). Next, treatment with YMGKI-1 also reduced the percentage of ^{mem}GRP78$^+$ cells in HNSCC cells, where ^{mem}GRP78 has been used as a cell surface marker for isolation of HN-CICs (Figure 1(c)) [9]. In Figure 1(d), we showed that treatment of YMGKI-1 in OECM1 cells caused the decreasing of the side population (SP) cells, which is also one of the characteristics of CICs [30]. To further evaluate the inhibitory effect of YMGKI-1 treatment on different cell lines including normal human oral keratinocytes (NHOKs), amniotic fluid stem cells-2 (AFSC-2), hematopoietic stem cell (HSC), parental SAS, and SAS-HN-CICs, the MTT cell proliferation assay was applied. Interestingly, we observed a massive decrease in viability of the SAS-HN-CICs but no significant inhibition on the other cells (Figure 1(e); $^{**}P < 0.01$; $^{***}P < 0.001$). Hence, the previous findings suggest that YMGKI-1 might effectively and selectively target HN-CICs.

3.2. Reduction of Xenograft Tumor Growth on YMGKI-1-Treated HNSCC Cells. Existence of HN-CICs is critical for the tumor growth of HNSCC *in vivo* [5, 8, 9, 13]. In Figure 1, we showed that YMGKI-1 treatment effectively diminished the stemness properties of HN-CICs in HNSCCs. Therefore, we wanted to determine if YMGKI-1 treatment could attenuate the tumor initiating activity of HNSCC *in vivo*. As shown in Figure 2(a), nude mice injected with YMGKI-1 pretreated SAS cells, a tumorigenic cell line, displayed significant reduction of the tumor growth as compared to those mice injected with untreated SAS cells ($^{*}P < 0.05$; $^{**}P < 0.01$). Next, whether YMGKI-1 could function as a therapeutic reagent on attenuating the tumor growth was examined as follow. We first subcutaneously implanted parental SAS cells into nude mice and allowed the tumors to be established. Mice bearing palpable tumor were then intraperitoneally injected with YMGKI-1 or DMSO (as control). Effectively, tumor-bearing mice receiving YMGKI-1 treatment afterward displayed reduced tumor size and the tumor growth curves in comparison with the control mice (Figure 2(b)) ($^{*}P < 0.05$; $^{**}P < 0.01$). In the meantime, we did not observe severe side effect but with little body weight loss from mice with YMGKI-1 treatment (data not shown).

3.3. Diminished Stemness Properties and Enhanced Differentiation Ability in YMGKI-1-Treated HN-CICs. To further evaluate whether treatment of YMGKI-1 would hinder the stemness properties of HN-CICs, we examined the following stemness properties of YMGKI-1-treated HN-CICs. We first observed that YMGKI-1 treatment significantly decreased the percentage of ^{mem}GRP78$^+$ or CD133$^+$ cells in enriched SAS-HN-CICs (Figures 3(a) and 3(b)), where ^{mem}GRP78$^+$ or CD133$^+$ cells have been demonstrated as CICs with higher stemness properties [5, 9]. Inversely, SAS-HN-CICs with the YMGKI-1 treatment displayed enhanced expression of epithelial differentiation marker, cytokeratin 18 (CK-18) (Figure 3(c)). Immunoblot analyses also showed that the expression of "cancer stemness" proteins (Oct-4, Nanog and Notch2) and GRP78 was diminished in YMGKI-1-treated SAS-HN-CICs (Figure 3(d)). In contrast, the YMGKI-1-treated SAS-HN-CICs displayed increased expression of epithelial-like protein (E-Cadherin) (Figure 3(d)). Together, YMGKI-1 treatment diminished the stemness properties but enhanced the differentiation ability of HN-CICs.

3.4. Reduction of Cell Survival and Malignancy of HN-CICs by YMGKI-1 Treatment In Vitro. Herein, we wanted to determine whether YMGKI-1 treatment affects cell survival and malignancy of HN-CICs or HNSCCs *in vitro*. Cells were first treated with YMGKI-1 and analyzed by flow cytometry, and the cells stained positively with propidium iodide (PI) were accounted as "dead" cells. Interestingly, YMGKI-1 treatment significantly induced cell death in SAS-HN-CICs whereas no significant cytotoxicity or morphological change was observed in YMGKI-1-treated parental SAS cells (Supplementary Figures S1A and S1B). Collectively, these results suggest that YMGKI-1 effectively suppresses the growth of SAS-HN-CICs but not parental SAS cells. Further, the *in vitro*

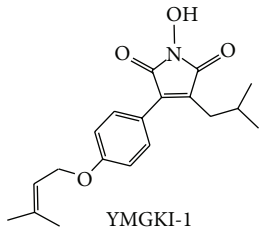

(a)

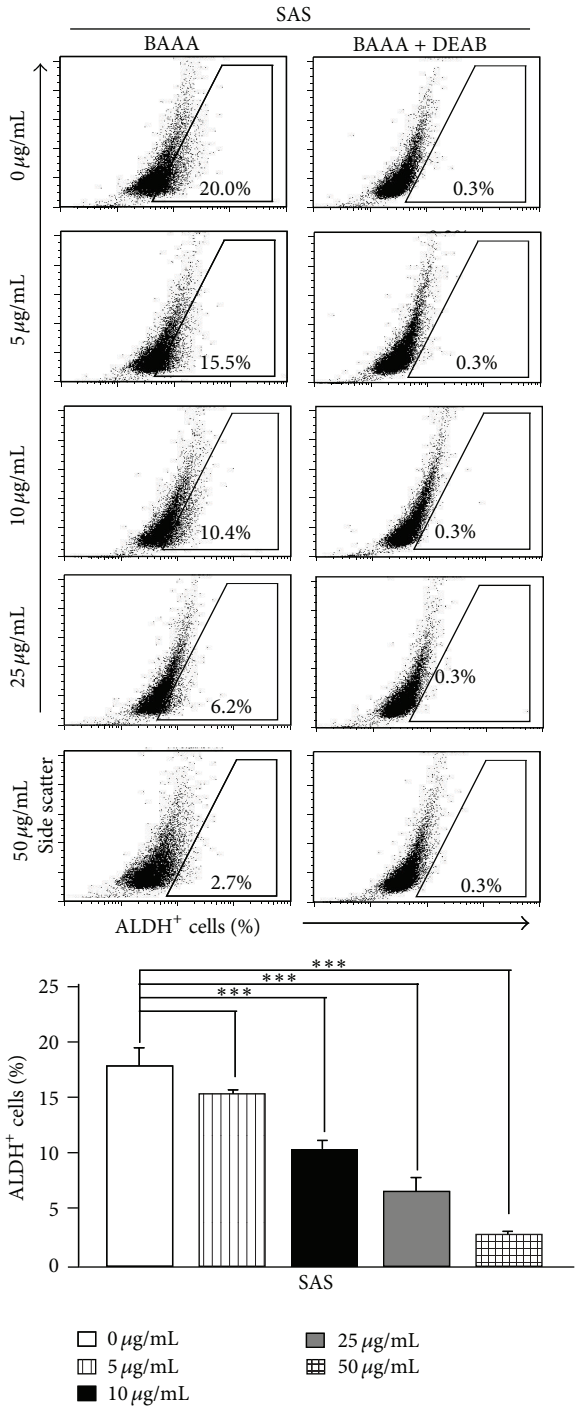

(b)

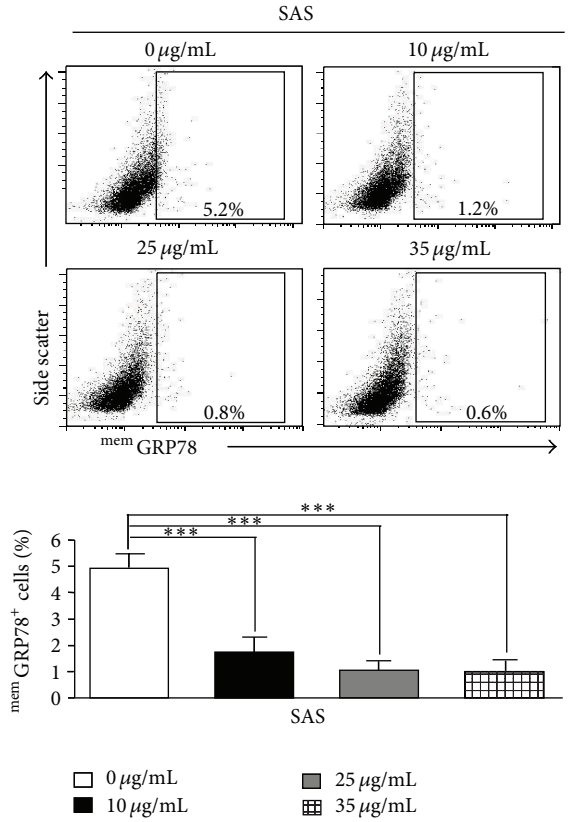

(c)

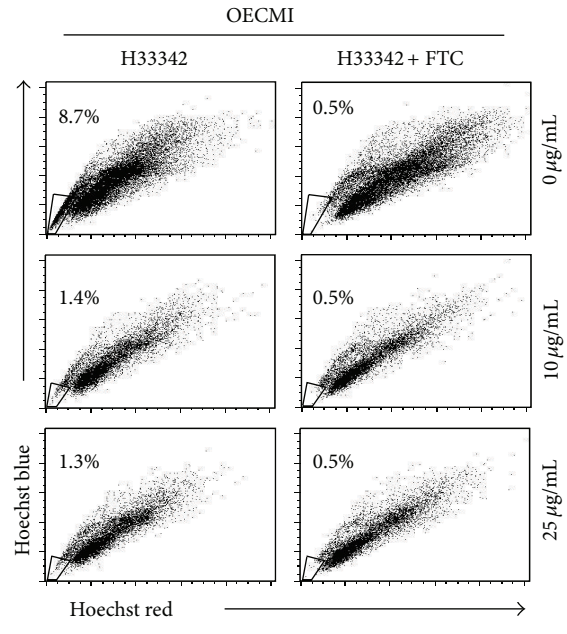

(d)

Figure 1: Continued.

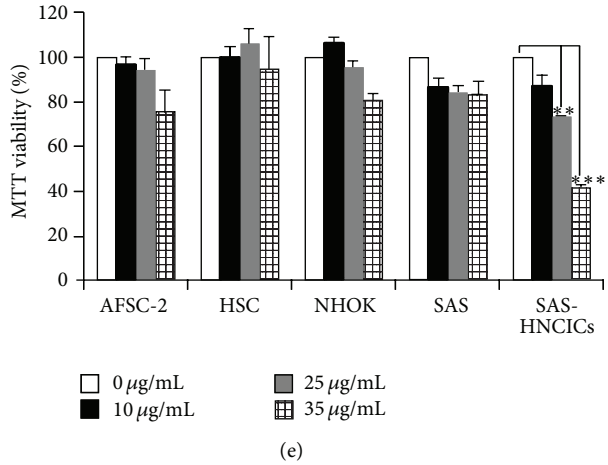

(e)

Figure 1: YMGKI-1 treatment effectively affects CIC subpopulation of HNSCC cells but not normal stem cells. (a) Chemical structure of YMGKI-1 isolated from the mycelium of *Antrodia cinnamomea*. (b) SAS cells were treated with 0, 10, 25, and 50 μg/mL of YMGKI-1 for 24 hr, afterward; the ALDH activity of YMGKI-1 treated cells was examined by flow cytometry. DEAB, the inhibitor of ALDH1 enzyme, was used to verify the ALDH-positive cells. The $^{mem}GRP78^{+}$ cells (c) or side population (d) of YMGKI-1-treated SAS or OECM1 cells were stained by anti-GRP78 antibody or Hoechst 33342 (see Section 2), respectively, and analyzed by flow cytometry. (e) The cell viability of YMGKI-1-treated parental SAS cells, normal human oral keratinocytes (NHOKs), amniotic fluid stem cells-2 (AFSC-2), and hematopoietic stem cell (HSC) and SAS-HN-CICs was measured by MTT assay, respectively. The data are means ± SD of triplicate samples from three experiments ($^{**}P < 0.01$; $^{***}P < 0.001$). The same concentration (0.03%) of vehicle (DMSO) was added to all control groups.

malignancy of YMGKI-1-treated SAS-HN-CICs including matrigel invasion ability and anchorage independent growth was evaluated. As shown in Figures 3(b) and 3(c), the invasiveness and soft agar colony formation abilities of YMGKI-1 treated SAS-HN-CICs were significantly reduced.

3.5. Induction of Autophagic Cell Death in YMGKI-1-Treated HN-CICs. Due to the observation of induced cell death in YMGKI-1-treated HN-CICs (Supplementary Figures S1A and S1B), next, we wanted to examine whether the dying cells of YMGKI-1-treated HN-CICs were undergoing apoptosis. Apoptosis is designated as type I programmed cell death, and the apoptotic cells are determined by costaining with Annexin-V (AV) and propidium iodide (PI) [31]. When SAS-HN-CICs were cultivated with YMGKI-1 of 35 μg/mL, there was a slight decrease in early apoptotic cells (AV^{+}/PI^{-}) (Figure 5(a); untreated: 2.1% versus treated: 1.8%) but a significant increase in later apoptotic cell death (AV^{+}/PI^{+}) (Figure 5(a); untreated: 3.7% versus treated: 23.6%). Nevertheless, many YMGKI-1 treated cells could die from the other programmed cell death such as autophagy (untreated: (AV^{-}/PI^{+}: 6.7%) versus treated: (AV^{-}/PI^{+}: 40.8%)) (Figure 5(a)).

To further understand the molecular mechanism by which to cause the YMGKI-1 induced cell death in HN-CICs, we wanted to determine whether YMGKI-1 treatment induced autophagy in HN-CICs. Acidification of autolysosomes caused by lysosomes fusion with autophagosomes is regarded as an indication of cell autophagy, and autophagy is characterized by AVO formation, which can be detected and measured by acridine orange staining [32]. Using acridine orange staining, we showed progressive increasing in formation of AVO in a dose-dependent manner of YMGKI-1 treated HN-CICs (Figure 5(b)). Further, under the treatment with 10, 25, or 35 μg/mL concentrations of YMGKI-1, we detected that around 12%, 20%, or 43% of HN-CICs underwent autophagy by flow cytometry analyses, respectively (Figure 5(c)).

Autophagy is defined as type II programmed cell death and could be also determined by the induction of LC3-II [33]. Thus, we wanted to utilize the amount of LC3-II or the LC3-II/LC3-I ratio, which is positively correlated with the number of autophagosomes, to identify whether the YMGKI-1-induced dying cells were undergoing autophagy. As shown in Figure 5(d), an increase of LC3-II/LC3-I ratio in YMGKI-1 treated cells was observed in a dose-dependent manner. To further confirm that autophagic cell death was responsible for the cell death of YMGKI-1-treated HN-CICs, we evaluated the protective effect of 3-methyladenine (3-MA; a prototypic autophagy inhibitor [33]) in HN-CICs with combined treatment with YMGKI-1 and 3-MA. As expected, 3-MA cotreatment attenuated the cell death and the LC3-II accumulation induced by YMGKI-1 treatment in HN-CICs (Figures 5(e) and 5(f)).

We also examined the effects of YMGKI-1 treatment on the expression of apoptosis-related proteins in HN-CICs (Supplementary Figure S2A). HN-CICs treated with YMGKI-1 resulted in cleavage of caspase-3 and poly (ADP-ribose) polymerase (PARP) at 35 μg/mL but not at 10 or 25 μg/mL. Recent data support that the execution of apoptosis could be dependent on the occurrence of autophagy [33, 34]. In summary, our results suggest that YMGKI-1-treated HN-CICs were undergoing the activation of autophagic cell death by which to cause apoptosis.

3.6. Affected Signaling Pathways in YMGKI-1-Treated HN-CICs. The activation of mTOR-mediated signaling pathway

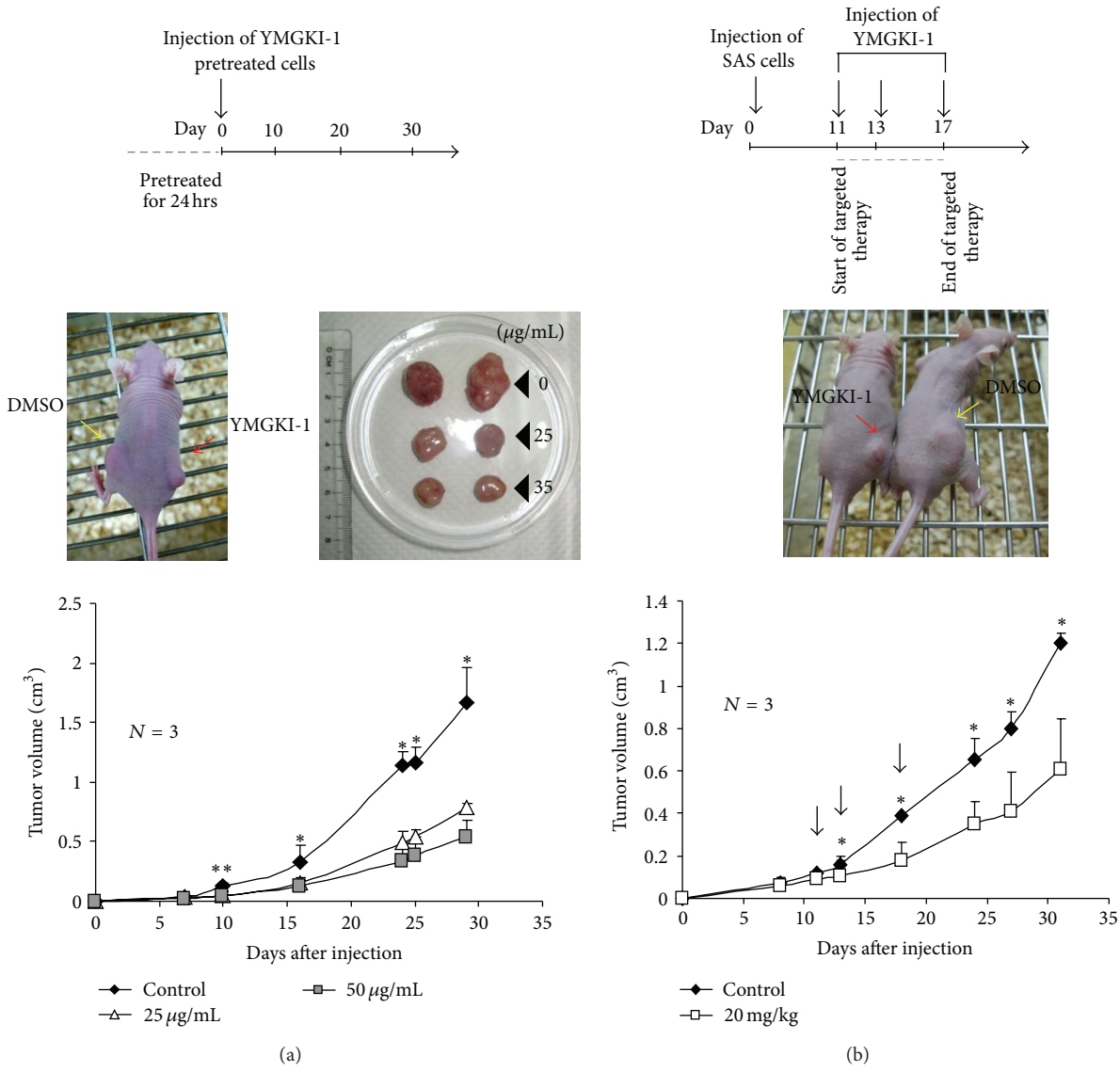

Figure 2: YMGKI-1 treatment suppresses xenograft tumor growth *in vivo*. (a) SAS cells pretreated with YMGKI-1 (0, 25, 50 μg/mL) for 24 hr were injected into the subcutaneous space of nude mice. Representative image of nude mice displaying tumor growth caused by either control SAS cells (DMSO) injected into the left subcutaneous space or SAS cells with pretreatment of YMGKI-1 (25 μg/mL) injected into the right subcutaneous space on day 20 (middle left panel). Image of dissected tumors collected on day 30 (left column: DMSO (control), middle column: treated with 25 μg/mL, and right column: treated with 50 μg/mL) (middle right panel). The tumor growth curves on nude mice inoculated with YMGKI-1 pretreated SAS cells were recorded (lower panel). (b) Therapeutic model to demonstrate the effect of YMGKI-1 treatment on inhibiting tumor growth. Parental SAS cells (1×10^6 cells) were subcutaneously implanted into the right back of nude mice and allowed to develop tumors to a size around 0.1 cm^3. On days 11, 13, and 17 after cells implantation, nude mice bearing SAS-derived tumors were intraperitoneally injected with YMGKI-1 (20 mg/kg) or DMSO (as control). On day 24, the image of mice, including control mouse (DMSO) on the right side plus experimental mouse (YMGKI-1 treatment) on the left side, was collected (middle panel). Additionally, the tumor growth curves were recorded (bottom panel). Error bars correspond to SD ($n = 3$; $^*P < 0.05$; $^{**}P < 0.01$).

is known to inhibit autophagy. In addition, the mTOR pathway is activated for self-renewal, cell survival, and malignancy of CICs [35]. In addition, HER2 overexpression is reported to be able to increase the stem/progenitor cell population in malignant mammary cells. Increased levels of HER2 can activate the PI3K/Akt pathway which is related to self-renewal ability in stem cells [36]. Further, activation of phosphor-AMPK can inactivate the mTOR complex-1, inversely, to cause the activation of autophagy [37].

Herein, we examined the effect of YMGKI-1 on these signaling molecules by immunoblot analyses. As shown in Figures 6(a) and 6(b), YMGKI-1 treatment in HN-CICs effectively decreased the expression level of phosphor-mTOR, HER2, phosphor-EGFR, Phosphatidylinositol 3-kinases (PI3K), phosphor-p44/42 MAPK (Thr202/Tyr204), and phosphor-AMPK but not phosphor-p38 MAPK in a dose-dependent manner. Additionally, cotreatment of 3-MA attenuated the expression of phospho-AMPK, which is

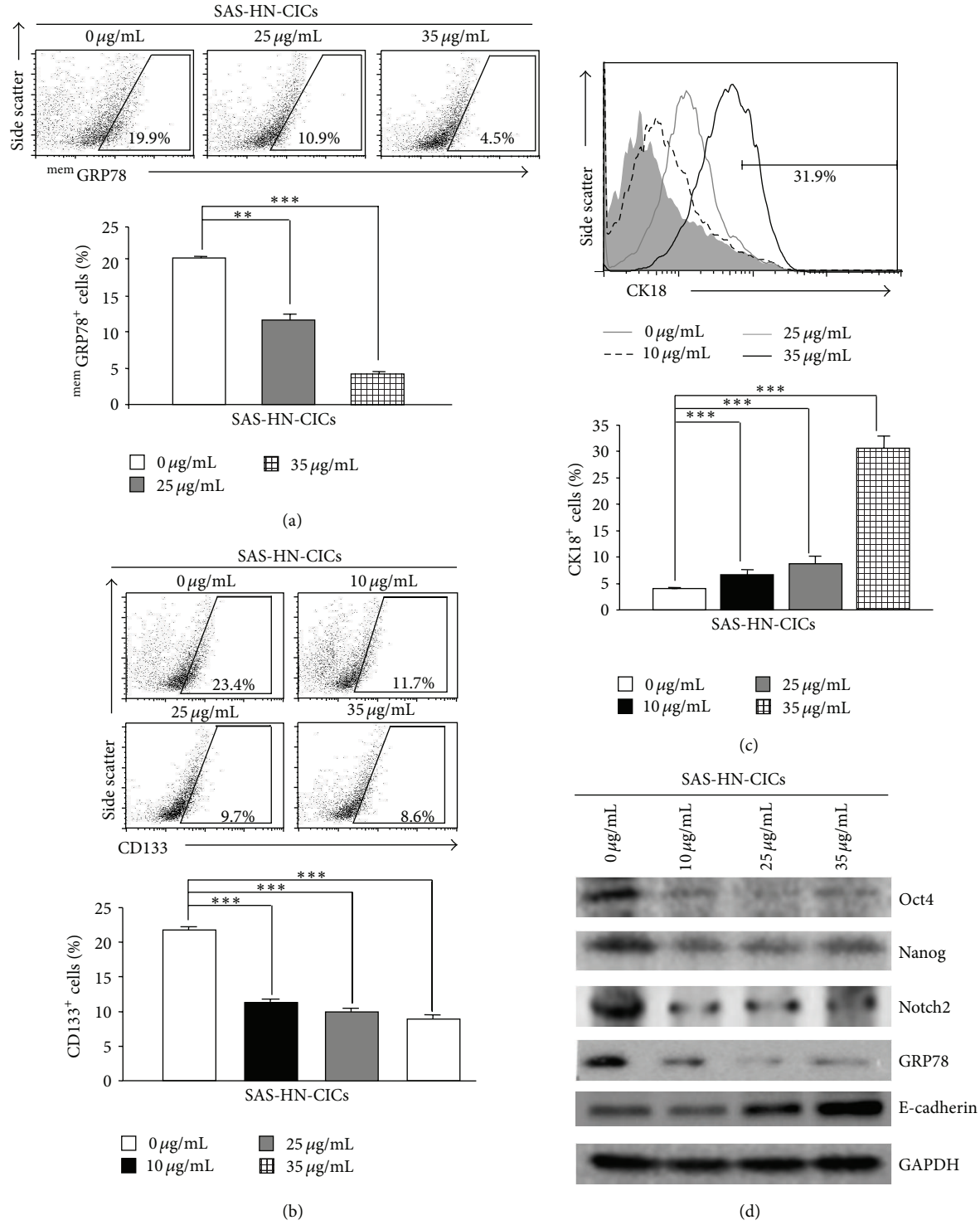

Figure 3: YMGKI-1 treatment diminishes stemness properties and enhances differentiation capability in HN-CICs. SAS-HN-CICs were treated with YMGKI-1 at different concentration for 24 hr, then stained with anti-GRP78 (a), anti-CD133 (b), or anti-CK18 (c) antibodies, respectively, and quantitated by flow cytometry. Data are means ± SD of triplicate samples from three experiments ($^{**}P < 0.01$; $^{***}P < 0.005$). Dead cells were excluded by gating on the propidium-iodide- (PI-) positive cell fraction. (d) Crude cell extract proteins of YMGKI-1-treated-SAS-HN-CICs were collected, electrophores, and analyzed by immunoblotting against anti-Oct-4, anti-Nanog, anti-Notch2, anti-GRP78, anti-E-cadherin, or anti-GAPDH antibodies as indicated. The immunoactive signal of GAPDH protein of different crude cell extracts was referred as loading control. The same concentration (0.03%) of vehicle (DMSO) was added to all control groups.

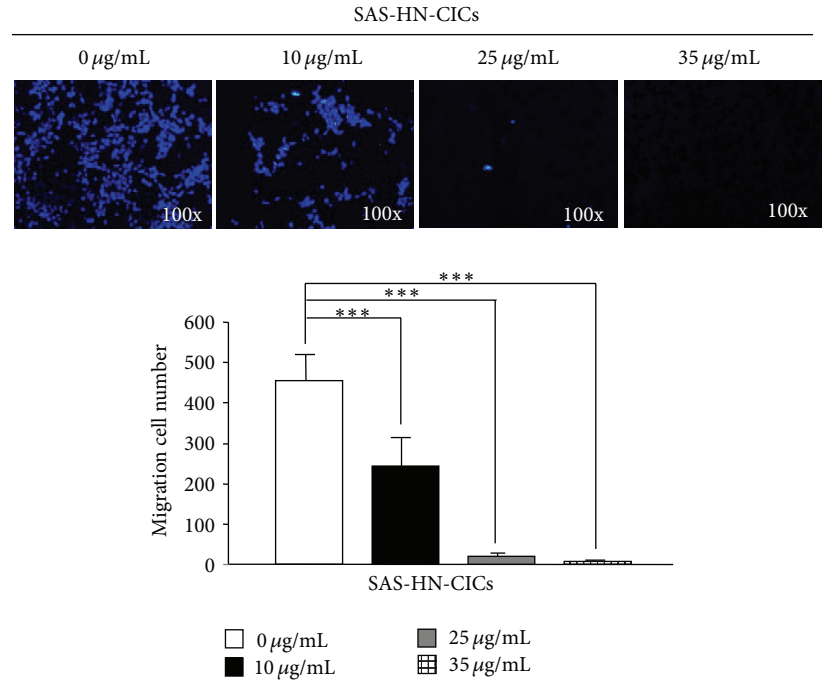

(a)

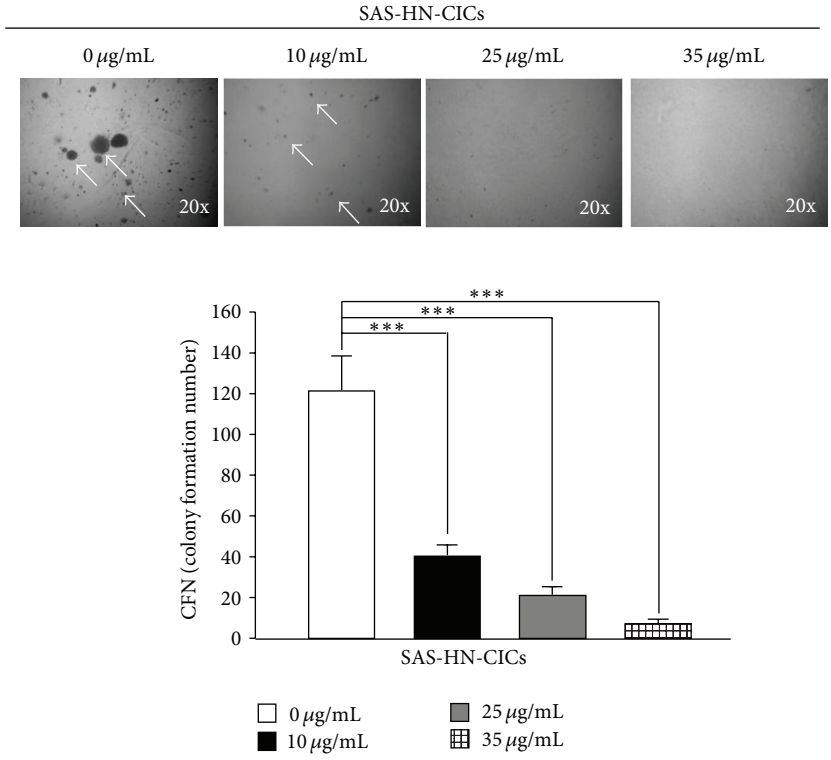

(b)

Figure 4: YMGKI-1 treatment reduces cell malignancy of HN-CICs *in vitro*. (a) SAS-HN-CICs were treated with 0, 10, 25, and 35 μg/mL of YMGKI-1 for 24 hr, afterward, plated onto transwell, and analyzed as Materials and Methods. Dead cells were excluded by trypan blue dye. (b) SAS-HN-CICs were treated with 0, 10, 25, and 35 μg/mL of YMGKI-1 for 24 hr, afterward, plated onto soft agar for 12 day. The colony formation ability of previous cells was examined (see Section 2). Data are means ± SD of triplicate samples from three experiments ($^{***}P < 0.005$). The same concentration (0.03%) of vehicle (DMSO) was added to all control groups.

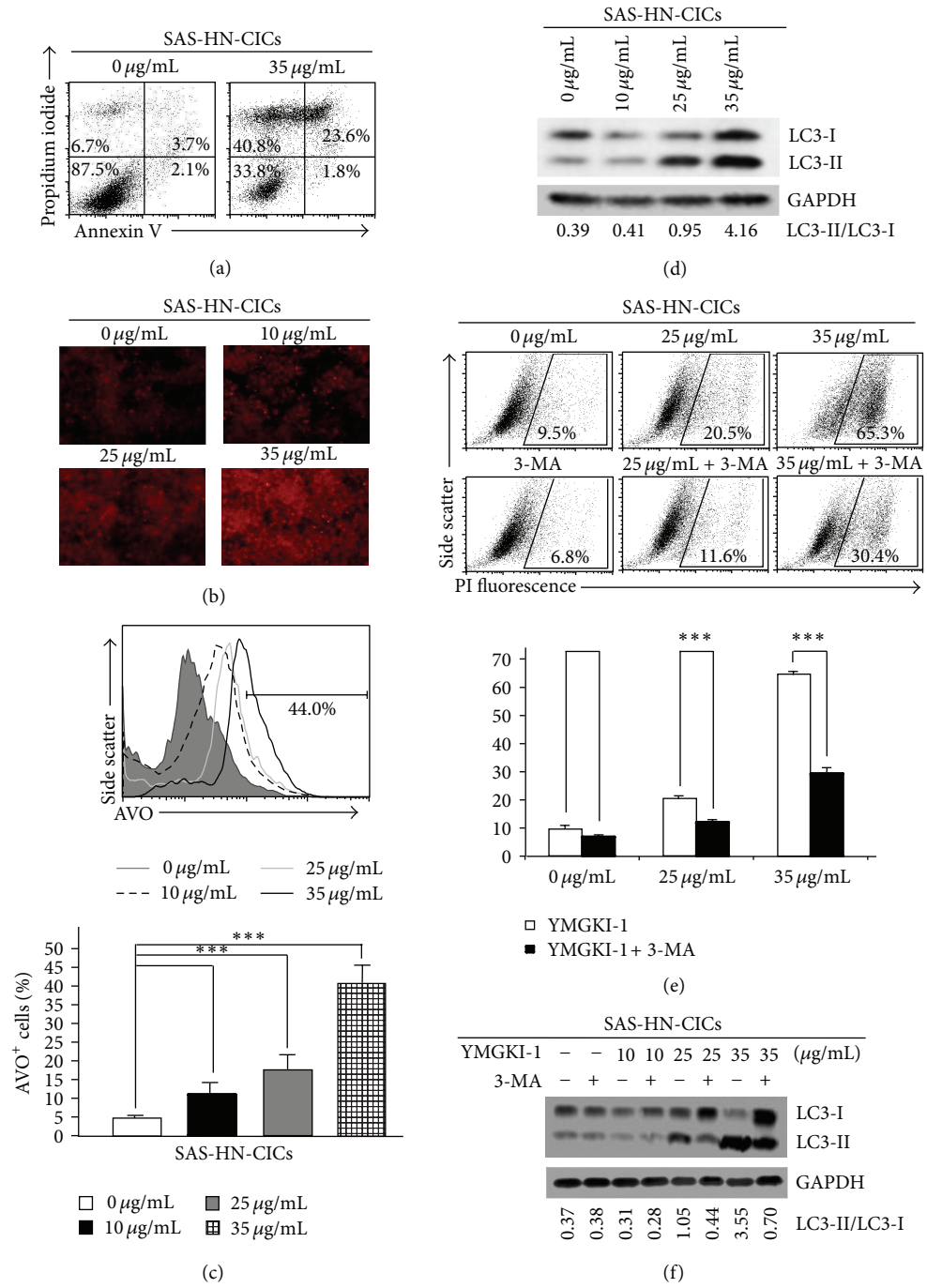

Figure 5: YMGKI-1 treatment induces autophagic cell death in HN-CICs. (a) SAS-HN-CICs treated with 35 μg/mL of YMGKI-1 were costained with Annexin V and Propidium iodide (PI) and examined by flow cytometry. (b) SAS-HN-CICs were treated with YMGKI-1 at different concentration for 24 hr, afterward, stained with acridine orange, and observed under a red filter fluorescence microscope. (c) Acridine orange (AO) positively stained cells of SAS-HN-CICs in (b) were quantitated by flow cytometric analysis (upper panel). The mean fluorescence intensity of AO stained cells was calculated (lower panel). Data are means ± SD of triplicate samples from three experiments ($^{***}P < 0.005$). (d) Crude cell extract proteins of YMGKI-1-treated SAS-HN-CICs were collected, electrophorized, and further analyzed by immunoblotting against anti-LC3 or anti-GAPDH serum as indicated. (e) SAS-HN-CICs cells were either singly treated with 0, 25, or 35 μg/mL of YMGKI-1, or cotreated with 3-Methylamphetamine (3-MA), an autophagy inhibitor, for 24 hr, afterward, stained with propidium iodide (PI), and then examined by flow cytometry. Data are means ± SD of triplicate samples from three experiments ($^{***}P < 0.005$). (f) Crude cell extract proteins of SAS-HN-CICs singly treated with YMGKI-1 or cotreated with 3-MA were isolated and analyzed by immunoblotting against anti-LC3 or anti-GAPDH serum as indicated. The immunoactive signal of GAPDH protein of different crude cell extracts was referred as loading control. The same concentration (0.03%) of vehicle (DMSO) was added to all control groups.

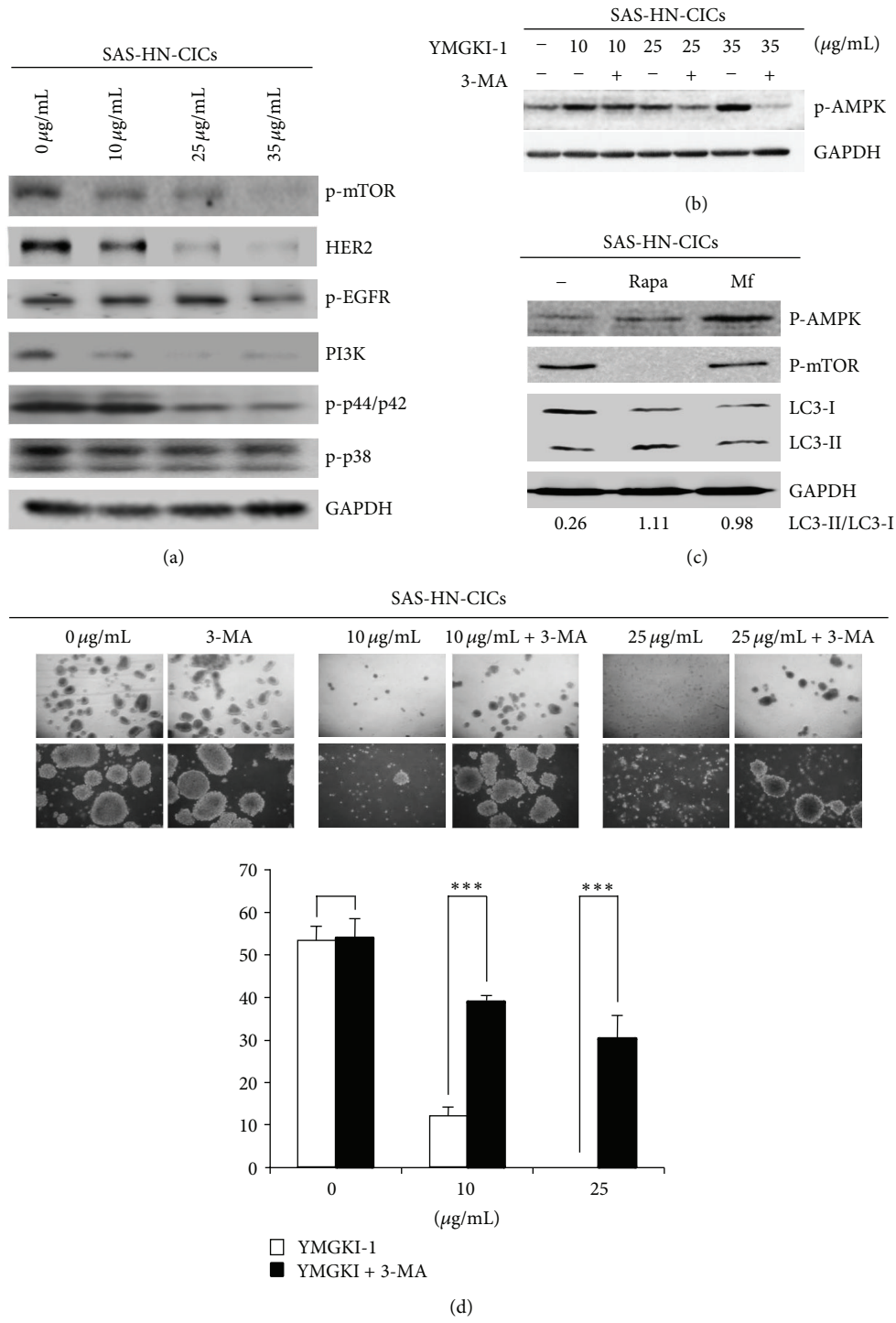

Figure 6: YMGKI-1 treatment dysregulates the autophagy and diminishes the sphere formation ability in HN-CICs. (a) Crude cell extract proteins of YMGKI-1-treated SAS-HN-CICs were collected, electrophorized, and analyzed by immunoblotting against anti-LC3, anti-phosphor-mTOR, anti-HER2, PI3K, anti-phosphor-p44/42 MAPK, anti-phosphor-p38, or anti-GAPDH serum as indicated. (b) Crude cell extract proteins of SAS-HN-CICs singly treated with YMGKI-1 or cotreated with 3-MA were isolated and analyzed by immunoblotting against anti-phosphor AMPK or anti-GAPDH serum as indicated. (c) SAS-HN-CICs were treated with metformin (10 mM) or rapamycin (100 nM) for 96 hr. Consequently, immunoblotting analysis was performed by against anti-phosphor-AMPK, anti-phosphor-mTOR, and anti-LC3 or anti-GAPDH serum as indicated. The immunoactive signal of GAPDH protein of different crude cell extracts was referred as loading control. (d) Single cell suspension of SAS-HN-CICs was treated with YMGKI-1 or cotreated with 3-MA for 24 hr, and the sphere formation ability of YMGKI-1 or cotreated with 3-MA-treated HNCICs cells was examined. Arrows indicated the sphere cells. Data are means ± SD of triplicate samples from three experiments ($^{***}P < 0.005$). The same concentration (0.03%) of vehicle (DMSO) was added to all control groups.

induced by YMGKI-1 treatment in HN-CICs (Figure 6(b)). It has been reported that AMPK activator like metformin or EGCG selectively kills cancer stem cells [38, 39]. To address the role of AMPK and mTOR on mediating HN-CICs through autophagy, we treated HN-CICs with AMPK activators metformin (Mf) or mTOR inhibitors rapamycin (Rapa), respectively. As shown in Figure 6(c), HN-CICs treated with metformin or rapamycin displayed slight induction of LC3-II along with upregulation of phosphor-AMPK or downregulation of phosphor-mTOR, respectively (Figure 6(c)). In the meantime, we did not observe significant cell death from HN-CICs under metformin or rapamycin treatment (Supplementary Figure S3B). These data suggest that YMGKI-1 treatment in HN-CICs simultaneously induced dysregulatory autophagic cell death through multiple mechanisms.

3.7. Attenuation of Inhibitory Effect of YMGKI-1 by Autophagy Repressor on Sphere Formation Ability of HN-CICs. To further investigate whether the "antistemness" properties of YMGKI-1 are autophagy dependent, the sphere formation ability of YMGKI-1-treated HN-CICs was analyzed. As shown in Figure 6(d), YMGKI-1 treatment significantly inhibited the sphere formation ability of HN-CICs. Further, cotreatment of 3-MA lessened the inhibitory effect of YMGKI-1 on sphere formation ability. The results indicated that YMGKI-1 treatment inhibited the stemness properties through autophagy activation in HN-CICs.

3.8. Autophagic Pathway and Putative Molecules Regulated by YMGKI-1. It has been known that cells undergoing epithelial-mesenchymal transition (EMT) can gain stem cell properties [40]. We also observed that YMGKI-1 treatment not only increased the expression of CK-18, an epithelial differentiation marker, but also reduced the expression of "cancer stemness" genes and markers in HN-CICs (Figures 1(b)–1(d), Figures 3(a)–3(d)). Intriguingly, Tseng et al. predict that Himanimide-C, a YMGKI-1 analogue, might be a potential inhibitor of cyclooxygenase-2 (COX-2) and 5-lipoxygenase (5-LOX) [7], which play important roles in EMT [40, 41]. Collectively, we hypothesize that YMGKI-1 might suppress EMT and stemness properties of HN-CICs by inhibiting 5-LOX or COX-2. Therefore, we proposed a molecular signaling pathway in HN-CICs responding to YMGKI-1 treatment (Figure 7). Overall, YMGKI-1 would directly or indirectly regulate the autophagic pathway mediated by mTOR and AMPK, in addition to the aforementioned putative COX-2 or 5-LOX molecules, by which YMGKI-1 regulates the stemness, tumorigenicity, differentiation ability, and cell death of HN-CICs. The future research to delineate the function of YMGKI-1 or YMGKI-1 derivatives on HN-CICs will benefit future cancer therapeutics.

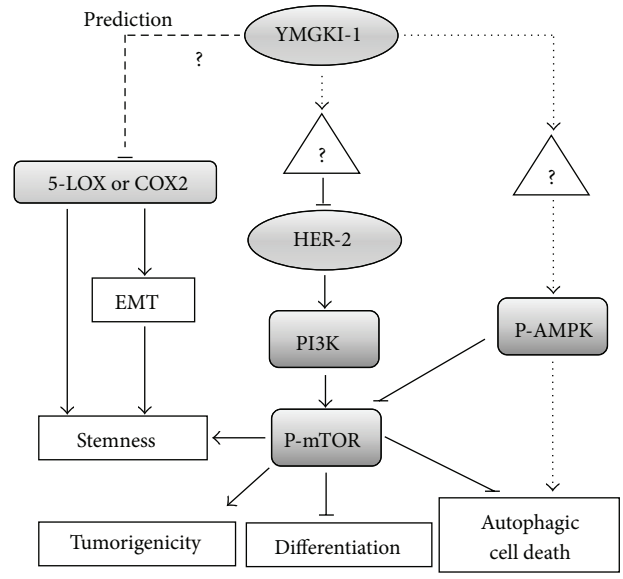

Figure 7: Schematic of the possible signaling pathways regulated by YMGKI-1, through which to inhibit the EMT, stemness properties, and tumorigenicity of head and neck cancer initiating cells (HN-CICs). The HER2/PI3K/MAPK/mTOR signaling pathway plays an important role in self-renewal, survival, and malignancy of CICs. YMGKI-1 would directly or indirectly inhibit the HER2/PI3K/MAPK/mTOR pathway. Further, an YMGKI-1 analogue is predicted to be a potential inhibitor of cyclooxygenase-2 (COX-2) and 5-lipoxygenase (5-LOX) which are related to epithelial-mesenchymal transition (EMT) [7]. YMGKI-1 might also prevent cells from undergoing EMT to gain stem cell properties via inhibiting COX-2 or 5-LOX. (—) refers to known pathway; (- - -) refers to unknown relationship; (. . . . . .) refers to prediction.

4. Discussion

In this study, we utilized the *in vitro* cell-based ALDH activity assay system to screen drugs on targeting cancer initiating cells. YMGKI-1, a purified component of natural product, *Antrodia cinnamomea* mycelia extract, decreased ALDH activity in oral cancer and other cancer cell lines (Figure 1 and Supplementary Table 1). We also showed that YMGKI-1 treatment reduced the stemness properties of parental SAS cells (Figures 1(c) and 1(d)). In addition, we demonstrated that YMGKI-1 suppressed tumor growth in preventive and therapeutic model *in vivo* (Figure 2). Moreover, YMGKI-1 treatment in SAS-HN-CICs abrogated the *in vitro* malignancy and downregulated the stemness properties (Figures 3 and 4). Finally, YMGKI-1 was able to inhibit the growth of HN-CICs by dysregulatory autophagic cell death (Figure 5). Of note, coaddition of YMGKI-1 and autophagy inhibitor (3-MA) to HN-CICs attenuated the cell death, LC3-II accumulation, AMPK activation, and the morphological change of spheroid cells induced by YMGKI-1 treatment (Figure 6). All of these suggest that YMGKI-1 can function as a prospective drug for targeting CICs, and the future research to delineate the function of other YMGKI-1 analogues on HN-CICs will be of benefit for future cancer therapeutics.

Recently, the role of autophagy in the biology of stem cell and cancer initiating cell has been controversial. Cufí and colleagues report that autophagy is positively linked to the maintenance of breast cancer stem-like phenotype [42]. Conversely, others demonstrate that autophagy promotes the differentiation of glioma-initiating cells [17]. Herein, our results indicated that YMGKI-1 can not only induce autophagy but also downregulate the stemness properties and malignancy

of HN-CICs (Figures 3 and 5). Although basal autophagic activity in some cells contributes to cytoprotective process against environmental stress [15], our findings suggest that the dysregulatory autophagy induced by YMGKI-1 treatment may effectively contribute to the enhanced cell death in HN-CICs but not in majority HNSCC cells (Figures 3(a) and 5 and Supplementary Figures S1 and S3). Further, we showed that YMGKI-1 induced autophagic cell death in HN-CICs through multiple molecular mechanisms including activation of AMPK and downregulation of PI3K-mTOR pathway (Figure 6). Of note, the aforementioned two signaling pathways center the regulation of autophagy. In addition, there are various signaling cascades that regulate mTOR including the HER2/PI3K (class I) pathway; inhibition of HER2/PI3K (class I) pathway has been shown to induce autophagy in cancer [43].

Under sufficient supply of growth factors and nutrients, the active mTORC1 stimulates growth-related processes such as protein translation, for example, by phosphorylation of S6K1 and 4E-BP, while simultaneously inhibiting self-consuming processes such as autophagy [44]. In opposite, the AMPK activity is enhanced when the intracellular ATP/AMP ratio is decreased. Further, AMPK activation induces autophagy through inhibition of mTORC1 [37]. Therefore, both AMPK and mTOR pathways play the crucial roles simultaneously in YMGKI-1-mediated autophagic HNSCC cell death. To further address the role of AMPK and mTOR on mediating HN-CICs through autophagy, we treated HN-CICs with AMPK activators metformin (Mf) or mTOR inhibitors rapamycin, respectively. As shown in Figure 6(c), HN-CICs treated with metformin or rapamycin displayed induction of autophagy. Nevertheless, we did not observe cell death from HN-CICs under single treatment with either metformin or rapamycin (Supplementary Figure S3B). Because of lack of induced cell death in HN-CICs by single treatment with metformin or rapamycin, it is worth note that YMGKI-1 induces dysregulatory autophagic cell death through multiple mechanisms. It will be of interest to determine how multiple mechanisms regulate autophagic cell death in HN-CICs.

Charafe-Jauffret et al. and Todaro et al. demonstrate that cancer stem cells highly express tumorigenic and metastatic activity [45, 46]. Although cancer stem cells may vary among different types of cancer, YMGKI-1 might have common effect on them. Other than HNSCC, here, we had tested the cytotoxic effect of YMGKI-1 treatment on colon, breast, and lung cancer cell lines. As shown in Supplementary Table 1, the more tumorigenic or metastatic cancer cell lines displayed higher reduction of $ALDH^+$ cells under the YMGKI-1 treatment. Together, our data evidences that YMGKI-1 can significantly affect CICs population without discrepancy on different types of tumor.

Conventional anticancer treatments can often transiently shrink tumor volume instead of targeting or killing CICs, which lead to treatment failure, tumor recurrence, and patient death. Cancer initiating cells model suggests that tumors consist of CICs and differentiated cancer cells [3]. In the future, the main treatment strategy will be based on depletion of both the CICs pool and the residual majority cancer cells with combinatorial treatment including CIC-targeted anticancer drugs and conventional cancer therapeutic drugs [47]. Furthermore, in Figure 5(b), we observed that YMGKI-1 effectively inhibited the activation of HER2 but inversely enhanced the expression of phosphor-Src activity (data not shown). The Src kinase activity is closely related to cancerous malignancy [48]. Additionally, Zhang et al. discover that increased Src activation confers considerable Herceptin resistance in breast cancer cells and correlated with Herceptin resistance in breast cancer patients [49]. It is plausible that a combination with YMGKI-1 and Src kinase inhibitor will be a highly effective therapeutic protocol for head and neck cancer treatment. Further research effort with regard to the aforementioned phenomenon is needed in this area.

Together, our present research showed that YMGKI-1, a natural compound from ACME, can specifically and effectively target HN-CICs and diminish the CICs properties and activate dysregulatory autophagic cell death. Therefore, YMGKI-1 treatment might be a potential therapeutic target for HNSCC by eliminating CICs.

Conflict of Interests

No potential conflict of interests was disclosed.

Authors' Contribution

Ching-Wen Chang, Chien-Chih Chen, and Meng-Ju Wu have equal contribution for the first authorship.

Acknowledgments

The authors thank Dr. K-W Chang (Department of Dentistry, National Yang-Ming University) for providing critical comment. This study was supported by research Grants from National Science Council (NSC99N024, NSC100-2314-B-040-001, NSC100N446, and NSC101N050), Taipei Veterans General Hospital (V99ER2-006 and VGHUST99-P6-39), National Yang-Ming University (Ministry of Education, Aim for the Top University Plan: 99ACT303-2, 100ACT513, 100ACT807, 101ACT513, and 102ACTC14), MacKay Hospital (Mackay 10187), and Grape King Inc. (YM99C021 and 101J041) in Taiwan.

References

[1] R. I. Haddad and D. M. Shin, "Recent advances in head and neck cancer," *The New England Journal of Medicine*, vol. 359, pp. 1143–1154, 2008.

[2] R. Siegel, D. Naishadham, and A. Jemal, "Cancer statistics, 2013," *A Cancer Journal for Clinicians*, vol. 63, no. 1, pp. 11–30, 2013.

[3] H. Clevers, "The cancer stem cell: premises, promises and challenges," *Nature Medicine*, vol. 17, no. 3, pp. 313–319, 2011.

[4] Y. Li and J. Laterra, "Cancer stem cells: distinct entities or dynamically regulated phenotypes?" *Cancer Research*, vol. 72, no. 3, pp. 576–580, 2012.

[5] S. H. Chiou, C. C. Yu, C. Y. Huang et al., "Positive correlations of Oct-4 and Nanog in oral cancer stem-like cells and high-grade oral squamous cell carcinoma," *Clinical Cancer Research*, vol. 14, pp. 4085–4095, 2008.

[6] R. Morrison, S. M. Schleicher, Y. Sun et al., "Targeting the mechanisms of resistance to chemotherapy and radiotherapy with the cancer stem cell hypothesis," *Journal of Oncology*, vol. 2011, Article ID :941876, 2011.

[7] T. H. Tseng, S. K. Chuang, C. Hu et al., "The synthesis of morusin as a potent antitumor agent," *Tetrahedron*, vol. 66, pp. 1335–1340, 2010.

[8] Y. S. Chen, M. J. Wu, C. Y. Huang et al., "CD133/Src axis mediates tumor initiating property and epithelial-mesenchymal transition of head and neck cancer," *PloS ONE*, vol. 6, no. 11, Article ID e28053, 2011.

[9] M. J. Wu, C. I. Jan, Y. G. Tsay et al., "Elimination of head and neck cancer initiating cells through targeting glucose regulated protein78 signaling," *Molecular Cancer*, vol. 9, p. 283, 2010.

[10] A. K. Croker, D. Goodale, J. Chu et al., "High aldehyde dehydrogenase and expression of cancer stem cell markers selects for breast cancer cells with enhanced malignant and metastatic ability," *Journal of Cellular and Molecular Medicine*, vol. 13, no. 8, pp. 2236–2252, 2009.

[11] L. Wang, P. Park, H. Zhang, F. La Marca, and C. Lin, "Prospective identification of tumorigenic osteosarcoma cancer stem cells in OS99-1 cells based on high aldehyde dehydrogenase activity," *International Journal of Cancer*, vol. 128, no. 2, pp. 294–303, 2011.

[12] Z. G. Chen, "The cancer stem cell concept in progression of head and neck cancer," *Journal of Oncology*, vol. 2009, Article ID 894064, 2009.

[13] J. F. Lo, C. C. Yu, S. H. Chiou et al., "The epithelial-mesenchymal transition mediator S100A4 maintains cancer-initiating cells in head and neck cancers," *Cancer Research*, vol. 71, no. 5, pp. 1912–1923, 2011.

[14] F. Janku, D. J. McConkey, D. S. Hong, and R. Kurzrock, "Autophagy as a target for anticancer therapy," *Nature Reviews Clinical Oncology*, vol. 8, pp. 528–539, 2011.

[15] A. Apel, H. Zentgraf, M. W. Büchler, and I. Herr, "Autophagy—a double-edged sword in oncology," *International Journal of Cancer*, vol. 125, no. 5, pp. 991–995, 2009.

[16] M. Chaterjee and K. L. van Golen, "Breast cancer stem cells survive periods of farnesyl-transferase inhibitor-induced dormancy by undergoing autophagy," *Bone Marrow Research*, vol. 2011, Article ID 362938, 2011.

[17] W. Zhuang, B. Li, L. Long, L. Chen, Q. Huang, and Z. Liang, "Induction of autophagy promotes differentiation of glioma-initiating cells and their radiosensitivity," *International Journal of Cancer*, vol. 129, no. 11, pp. 2720–2731, 2011.

[18] D. Kwatra, D. Subramaniam, P. Ramamoorthy et al., "Methanolic extracts of bitter melon inhibit colon cancer stem cells by affecting energy homeostasis and autophagy," *Evidence-Based Complementary and Alternative Medicine*, vol. 2013, Article ID 702869, p. 14, 2013.

[19] Y. Shen, S. Yang, C. Lin, C. Chen, Y. Kuo, and C. Chen, "Zhankuic acid F: a new metabolite from a formosan fungus *Antrodia cinnamomea*," *Planta Medica*, vol. 63, no. 1, pp. 86–88, 1997.

[20] M. D. Wu, M. J. Cheng, W. Y. Wang et al., "Antioxidant activities of extracts and metabolites isolated from the fungus *Antrodia cinnamomea*," *Natural Product Research*, vol. 25, no. 16, pp. 1488–1496, 2011.

[21] C. C. Lee, H. L. Yang, T. D. Way et al., "Inhibition of cell growth and induction of apoptosis by *Antrodia camphorata* in HER-2/neu-overexpressing breast cancer cells through the induction of ROS, depletion of HER-2/neu, and disruption of the PI3K/Akt signaling pathway," *Evidence-Based Complementary and Alternative Medicine*, vol. 2012, Article ID 702857, 2012.

[22] C. Wen, C. Chang, S. Huang et al., "Anti-inflammatory effects of methanol extract of *Antrodia cinnamomea* mycelia both in vitro and in vivo," *Journal of Ethnopharmacology*, vol. 137, no. 1, pp. 575–584, 2011.

[23] Y. Ho, M. Lin, K. Duan, and Y. Chen, "The hepatoprotective activity against ethanol-induced cytotoxicity by aqueous extract of *Antrodia cinnamomea*," *Journal of the Chinese Institute of Chemical Engineers*, vol. 39, no. 5, pp. 441–447, 2008.

[24] Y. C. Hseu, H. T. Tsou, K. J. Kumar, K. Y. Lin, H. W. Chang, and H. L. Yang, "The antitumor activity of *Antrodia camphorata* in melanoma cells: modulation of wnt/β-catenin signaling pathways," *Evidence-Based Complementary and Alternative Medicine*, vol. 2012, Article ID 197309, 2012.

[25] Y. Tzeng and M. Geethangili, "Review of pharmacological effects of *Antrodia camphorata* and its bioactive compounds," *Evidence-based Complementary and Alternative Medicine*, vol. 2011, Article ID 212641, 2011.

[26] N. Nakamura, A. Hirakawa, J. Gao et al., "Five new maleic and succinic acid derivatives from the mycelium of *Antrodia camphorata* and their cytotoxic effects on LLC tumor cell line," *Journal of Natural Products*, vol. 67, no. 1, pp. 46–48, 2004.

[27] K. Okumura, A. Konishi, M. Tanaka, M. Kanazawa, K. Kogawa, and Y. Niitsu, "Establishment of high- and low-invasion clones derived for a human tongue squamous-cell carcinoma cell line SAS," *Journal of Cancer Research and Clinical Oncology*, vol. 122, no. 4, pp. 243–248, 1996.

[28] I. L. Hsin, C. Ou, T. Wu et al., "GMI, an immunomodulatory protein from Ganoderma microsporum, induces autophagy in non-small cell lung cancer cells," *Autophagy*, vol. 7, no. 8, pp. 873–882, 2011.

[29] M. R. Clay, M. Tabor, J. H. Owen et al., "Single-marker identification of head and neck squamous cell carcinoma cancer stem cells with aldehyde dehydrogenase," *Head and Neck*, vol. 32, no. 9, pp. 1195–1201, 2010.

[30] S. B. Keysar and A. Jimeno, "More than markers: biological significance of cancer stem cell-defining molecules," *Molecular Cancer Therapeutics*, vol. 9, no. 9, pp. 2450–2457, 2010.

[31] Z. Bacsó, R. B. Everson, and J. F. Eliason, "The DNA of annexin V-binding apoptotic cells is highly fragmented," *Cancer Research*, vol. 60, no. 16, pp. 4623–4628, 2000.

[32] H. Takeuchi, Y. Kondo, K. Fujiwara et al., "Synergistic augmentation of rapamycin-induced autophagy in malignant glioma cells by phosphatidylinositol 3-kinase/protein kinase B inhibitors," *Cancer Research*, vol. 65, no. 8, pp. 3336–3346, 2005.

[33] Y. Kondo, T. Kanzawa, R. Sawaya, and S. Kondo, "The role of autophagy in cancer development and response to therapy," *Nature Reviews Cancer*, vol. 5, no. 9, pp. 726–734, 2005.

[34] R. Mathew, V. Karantza-Wadsworth, and E. White, "Role of autophagy in cancer," *Nature Reviews Cancer*, vol. 7, no. 12, pp. 961–967, 2007.

[35] A. M. Martelli, C. Evangelisti, F. Chiarini et al., "The emerging role of the phosphatidylinositol 3-kinase/Akt/mammalian target of rapamycin signaling network in normal myelopoiesis and leukemogenesis," *Biochimica et Biophysica Acta*, vol. 1803, no. 9, pp. 991–1002, 2010.

[36] H. Korkaya, A. Paulson, F. Iovino, and M. S. Wicha, "HER2 regulates the mammary stem/progenitor cell population driving tumorigenesis and invasion," *Oncogene*, vol. 27, no. 47, pp. 6120–6130, 2008.

[37] A. J. Meijer and P. Codogno, "AMP-activated protein kinase and autophagy," *Autophagy*, vol. 3, no. 3, pp. 238–240, 2007.

[38] A. Sato, J. Sunayama, M. Okada et al., "Glioma-initiating cell elimination by metformin activation of FOXO3 via AMPK," *Stem Cells Translational Medicine*, vol. 1, no. 11, pp. 811–824, 2012.

[39] D. Chen, S. Pamu, Q. Cui, T. H. Chan, and Q. P. Dou, "Novel epigallocatechin gallate (EGCG) analogs activate AMP-activated protein kinase pathway and target cancer stem cells," *Bioorganic and Medicinal Chemistry*, vol. 20, no. 9, pp. 3031–3037, 2012.

[40] H. J. Li, F. Reinhardt, H. R. Herschman, and R. A. Weinberg, "Cancer-stimulated mesenchymal stem cells create a carcinoma stem cell niche via prostaglandin E2 signaling," *Cancer Discovery*, vol. 2, no. 9, pp. 840–855, 2012.

[41] V. Y. Shin, H. C. Jin, E. K. O. Ng, J. J. Y. Sung, K. M. Chu, and C. H. Cho, "Activation of 5-lipoxygenase is required for nicotine mediated epithelial-mesenchymal transition and tumor cell growth," *Cancer Letters*, vol. 292, no. 2, pp. 237–245, 2010.

[42] S. Cufí, A. Vazquez-Martin, C. Oliveras-Ferraros, B. Martin-Castillo, L. Vellon, and J. A. Menendez, "Autophagy positively regulates the $CD44^{+}CD24^{-}$/low breast cancer stem-like phenotype," *Cell Cycle*, vol. 10, no. 22, pp. 3871–3885, 2011.

[43] Y. Kondo and S. Kondo, "Autophagy and cancer therapy," *Autophagy*, vol. 2, no. 2, pp. 85–90, 2006.

[44] S. Wullschleger, R. Loewith, and M. N. Hall, "TOR signaling in growth and metabolism," *Cell*, vol. 124, no. 3, pp. 471–484, 2006.

[45] E. Charafe-Jauffret, C. Ginestier, F. Iovino et al., "Breast cancer cell lines contain functional cancer stem sells with metastatic capacity and a distinct molecular signature," *Cancer Research*, vol. 69, no. 4, pp. 1302–1313, 2009.

[46] M. Todaro, F. Iovino, V. Eterno et al., "Tumorigenic and metastatic activity of human thyroid cancer stem cells," *Cancer Research*, vol. 70, no. 21, pp. 8874–8885, 2010.

[47] L. M. Howells, S. Sale, S. N. Sriramareddy et al., "Curcumin ameliorates oxaliplatin-induced chemoresistance in HCT116 colorectal cancer cells in vitro and in vivo," *International Journal of Cancer*, vol. 129, no. 2, pp. 476–486, 2011.

[48] L. C. Kim, L. Song, and E. B. Haura, "Src kinases as therapeutic targets for cancer," *Nature Reviews Clinical Oncology*, vol. 6, pp. 587–595, 2009.

[49] S. Zhang, W. Huang, P. Li et al., "Combating trastuzumab resistance by targeting SRC, a common node downstream of multiple resistance pathways," *Nature Medicine*, vol. 17, no. 4, pp. 461–469, 2011.

Hindawi Publishing Corporation
Evidence-Based Complementary and Alternative Medicine
Volume 2013, Article ID 632121, 8 pages
http://dx.doi.org/10.1155/2013/632121

Research Article

Resveratrol Inhibits Alpha-Melanocyte-Stimulating Hormone Signaling, Viability, and Invasiveness in Melanoma Cells

Yu-Jen Chen,[1,2,3] Ying-Yin Chen,[4] Yi-Feng Lin,[4] Hsuan-Yun Hu,[4] and Hui-Fen Liao[4]

[1] *Department of Radiation Oncology, Mackay Memorial Hospital, Taipei 104, Taiwan*
[2] *Institute of Traditional Medicine, National Yang Ming University, Taipei 112, Taiwan*
[3] *Department & Graduate Institute of Pharmacology, College of Medicine, Taipei Medical University, Taipei 110, Taiwan*
[4] *Department of Biochemical Science and Technology, National Chiayi University, 300 University Road, Chiayi 600, Taiwan*

Correspondence should be addressed to Hui-Fen Liao; liao.huifen@gmail.com

Received 9 March 2013; Accepted 7 May 2013

Academic Editor: K. S. Clifford Chao

Melanoma is a malignancy with high potential to invasion and treatment resistance. The α-melanocyte-stimulating hormone (α-MSH) signal transduction involving Wnt/β-catenin, c-Kit, and microphthalmia-associated transcription factor (MITF), a known pathway to produce melanin, has been demonstrated as one of cancer stem cell characteristics. This study was aimed to examine the effect of resveratrol, an abundant ingredient of grape and medicinal plants, on α-MSH signaling, viability, and invasiveness in melanoma cells. By α-MSH treatment, the melanin production in B16 melanoma cells was augmented as a validation for activation of α-MSH signaling. The upregulated expression of α-MSH signaling-related molecules β-catenin, c-Kit, and MITF was suppressed by resveratrol and/or STI571 treatment. Nuclear translocation of MITF, a hallmark of α-MSH signaling activation, was inhibited by combined treatment of resveratrol and STI571. At effective concentration, resveratrol and/or STI571 inhibited cell viability and α-MSH-activated matrix metalloproteinase- (MMP-)9 expression and invasion capacity of B16 melanoma cells. In conclusion, resveratrol enhances STI571 effect on suppressing the α-MSH signaling, viability, and invasiveness in melanoma cells. It implicates that resveratrol may have potential to modulate the cancer stem cell characteristics of melanoma.

1. Introduction

Melanoma is the most frequent cause of mortality in skin cancer with highly potential for widespread metastasis [1]. The UV-induced damage having distinct mutational signatures including C to T transitions may increase the risk of melanoma [2]. The α-melanocyte-stimulating hormone (α-MSH) is required for the development of melanin in human skin and hair [3, 4]. α-MSH binds to its specific receptor (MC1R) and increases cAMP, which activates melanogenesis by activating a melanocyte specific transcription factor, microphthalmia-associated transcription factor (MITF) [5]. MITF is a transcription factor contained in several cell types and is involved in the regulation of melanocyte differentiation, pigmentation, proliferation, and survival of cells [6].

Isoform MITF-M acts as dual roles in the Wnt signaling pathway and functions as both a nuclear target and a nuclear mediator of Wnt/β-catenin signaling [7]. The binding of Wnt to its receptor Frizzled leads to inactivation of glycogen synthase kinase-3β, followed by the accumulation of β-catenin and its translocation to nucleus. Wnt/β-catenin signaling upregulates MITF-M expression through the interaction with a member of the lymphoid enhancing factor-1 (LEF-1) [7].

c-Kit (CD117), a receptor tyrosine kinase of stem cell factor (SCF), is a proto-oncogene that can serve as a potential target for molecular therapy of metastatic melanoma [8]. The expression of c-Kit in the majority of mucosal melanomas suggests that it may be useful in the assessment of these tumors for potential treatment with tyrosine kinase inhibitors, such as Imatinib [9]. Imatinib (STI571), a selective inhibitor targeting Abl as well as c-Kit and the platelet-derived growth factor receptor, has been tested for the efficacy and toxicities in metastatic melanoma patients, suggesting

that c-Kit might be a drugging target for treatment of melanoma [8].

Cancer stem cells (CSCs) or cancer initiating cells are a subset of tumor cells able to show self-renewal and differentiation. CSCs, which express stemness properties, are hypothesized to be responsible for tumorigenesis, metastasis, and resistance to cancer treatment [10]. Growing number of research groups isolated and identified CSCs, by appropriate selection markers, in various malignancies, such as leukemia, melanoma, breast, brain, colon, pancreas, and liver cancers [11]. In melanoma, CSCs tend to express developmental genes and stem cell markers including Notch receptors, Wnt proteins, CD133, c-Kit/CD117, and nestin antigens [12]. Recent articles have described that $CD133^+$ melanoma stem cells expressed certain ABC transporters to efflux drugs, such as ABCB5 protein, and may cause the chemotherapeutic resistance [13]. Additionally, MITF, regulating melanocytes and melanoma development, has also been reported as a factor supporting melanoma stem cell properties [14, 15].

Conventional cytotoxic agents are designed to eliminate proliferation of cancer cells. However, this strategy is not sufficient to inhibit the CSCs and, by contrast, may increase tumor relapse, metastasis, and resistance to further chemotherapy. Complementary and alternative medicine (CAM) has been demonstrated that may be effective in CSC inhibition. For examples, salinomycin inhibited the proliferation, migration, and invasion of human endometrial cancer stem-like cells [16]. Resveratrol, a natural polyphenolic polyphenol isolated from red wine and traditional Chinese medicine *Polygonum cuspidatum*, possesses several biological activities including antitumor, anti-inflammation, and anti-aging effects [17]. Resveratrol combined with conventional chemotherapy treatment eliminated tumor-initiating stem-like and epithelial-mesenchymal transition (EMT) properties in malignant head and neck cancers [17]. However, the effect and possible pathways of resveratrol in regulating growth of melanoma are still unclear.

The present study are aimed to further examine the role of α-melanocyte-stimulating hormone (α-MSH) signal transduction involving Wnt/β-catenin, c-Kit, and MITF, known pathways to produce melanin and have been considered as CSC-associated markers in melanoma. The effects of resveratrol, an abundant ingredient of foods and medicinal plants, with and without STI571 (imatinib mesylate) treatment on α-MSH signaling, viability, and invasiveness in melanoma cells were examined.

2. Materials and Methods

2.1. Materials and Cells. STI571 (also named imatinib mesylate) was kindly provided from Novartis Pharmaceutical Co. (Basel, Switzerland). Resveratrol, α-MSH, and reagents used in this study were purchased from Sigma-Aldrich (St. Louis, MO, USA). Murine melanoma B16 cells were purchased from the American Type Culture Collection (ATCC, Manassas, VA, USA) and were maintained in medium containing Dulbecco's modified Eagle's medium (DMEM; Gibco, Invitrogen Corporation, NY, USA) supplemented with 10% fetal bovine serum (Gibco, Grand Island, NY, USA) and 2 mM L-glutamine (Sigma) and incubated in an incubator (5% CO_2, 37°C).

2.2. Melanin Content Assay. The treated cells were collected, washed with phosphate-buffered saline (PBS, 137 mM NaCl, 12 mM Phosphate, 2.7 mM KCl, pH 7.4), and centrifuged at 12,000 rpm for 10 min. The supernatant was removed and the pellet was added with NaOH (1 M) and reacted at 60°C for 3 h. Then, the aliquots of cell lysates were placed in 96-well plates, and the amount of melanin was determined by measuring the absorbance at 400 nm using an enzyme-linked immune-sorbent assay (ELISA) reader. Melanin contents were expressed as percentages of those of untreated controls.

2.3. Western Blot Analysis. The treated cells were collected, lysed, and isolated the total proteins. Protein samples were quantified using a bicinchoninic acid (BCA) protein assay kit (Bio-Rad, Hercules, CA, USA), and the same amount of protein (100 μg per well) was disrupted with 2x concentrated electrophoresis sample buffer (1 M Tris, pH 6.8, 5% SDS, 40% glycerol, 0.005% bromophenol blue, and 8% β-mercaptoethanol). After analyzing the samples by subjecting to 10% sodium dodecyl sulfate (SDS) polyacrylamide gel electrophoresis, the protein gel was transferred to a polyvinylidene difluoride (PVDF) membrane, blotted with primary antibodies, including anti-Wnt-1 (1 : 200 dilution, BioSource, Bethesda, MD, USA), anti-β-catenin (1 : 200 dilution, Santa Cruz Biotechnology, Dallas, TX, USA), anti-MITF (1 : 200 dilution, Santa Cruz), anti-MMP-9 (1 : 1000 dilution, Santa Cruz), anti-histone H3 (1 : 500 dilution, Epitomic, Burlingame, CA, USA), and anti-glyceraldehyde-3-phosphate dehydrogenase (GAPDH, 1 : 1000 dilution, Santa Cruz), and then incubated at 4°C for overnight. The membrane was further hybridized with horseradish peroxidase (HRP) conjugated secondary antibody (1 : 1000 dilution, Santa Cruz) for 1.5 h followed by exposing with enhanced chemiluminescence (Perkin Elmer, Waltham, MA, USA). Relative protein levels were determined by densitometry using ImageJ software (Version 1.36b, NIH, Bethesda, MD, USA) with normalization to the internal control.

2.4. Immunofluorescence Staining of c-Kit. The treated cells were collected, washed with PBS (contain 5% Bovine serum albumin, BSA), and reacted with anti-c-Kit/CD117/SCFR primary antibody (1 : 200 dilution, Bioss Inc., Woburn, MA, USA) and immunofluorescence FITC-conjugated anti-IgG-TR antibody (1 : 500 dilution, Bioss Inc.) in order to determine the distribution of c-Kit in cells. The percentage of c-Kit-positive cells was analyzed by a NucleoCounter NC-3000 system (ChemoMetec A/S, Allerød, Denmark), and the cell morphology was then photographed under a fluorescence microscope at a magnification of 200x.

2.5. Preparation of Nuclear and Cytosolic Extracts from Cells. To prepare the cytosolic and nuclear proteins, the nuclear extraction buffer (500 mM NaCl, 1.5 mM $MgCl_2$, 0.2 mM EDTA, 1 mM DTT, 20% Glycerol, 0.1% Triton X-100, and

20 mM HEPES, pH 7.4) was used to separate the cell nuclei from the cytosolic extract. Then, the nuclei were resuspended in lysis buffer (150 mM NaCl, 0.1% SDS, 1% Triton X-100, and 100 mM Tris, pH 8.0) and centrifuged at 400 g for 10 min. The nuclear proteins were collected and stored at −80°C. The protein concentrations were determined using a BCA protein assay kit, and the expression of cytosolic and nuclear MITF was assayed by Western blotting.

2.6. Cell Viability Assay. B16 melanoma cells (2×10^5 cells/mL) were cultured for 12 h and then incubated with α-MSH (10 nM), STI571 (20 μM), and/or Resveratrol (15 μM) for a further 72 h. Then, the treated cells were collected and cell viability was measured by trypan blue dye exclusion test and observed under a microscope at a magnification of 100x.

2.7. Cell Invasion Assay. Assays of cell invasion properties were performed using a modified Boyden chamber with polyethylene terephthalate filter inserts coated with a Matrigel matrix (BD Biosciences, NJ, USA) in 24-well plates containing 8 mm pores. In brief, 10^5 cells were suspended in a serum-free medium with 0.5% BSA. Then, cells were plated into the upper chamber followed by filling the lower chamber with the same medium with or without α-MSH (10 nM), STI571 (20 μM), and/or resveratrol (15 μM). Cells were incubated for 24 h, the noninvading cells were gently removed, and the cells invading the lower side were stained with Liu's stain (Sigma) and counted by microscopic examination.

2.8. Statistical Analysis. Data were obtained from three independent experiments and expressed as the mean ± standard error (SE). Statistical comparisons were based on Student's t-test or analysis of variance. Differences were considered significant at $P < 0.05$. All statistical analyses were carried out using SigmaStat and Sigma Plot software (Jandel Scientific, San Rafael, CA).

3. Results

3.1. Effect of α-MSH on Melanoma B16 Cells. α-MSH stimulated the melanin expression in B16 cells in a concentration-dependent manner. In Figure 1(a), B16 cells treated with α-MSH (0–10 nM) markedly increased the melanin content. In Figure 1(b), melanin was determined by measuring the absorbance at 400 nm using an ELISA reader. We further tested the signaling molecule expression, cells viability, and invasiveness in melanoma cells with and without the treatment of 10 nM α-MSH.

3.2. Expression of Wnt/β-Catenin in B16 Cells. α-MSH upregulated Wnt-1 and β-catenin expression in B16 cells. In Figure 2, the expression of Wnt-1 was not changed when the cells treated with STI571 or resveratrol. STI571 treatment significantly increased the β-catenin level in cells, but resveratrol did not have such effect.

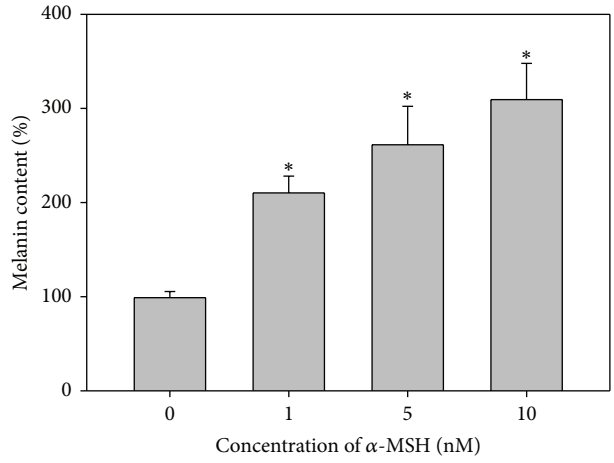

(a)

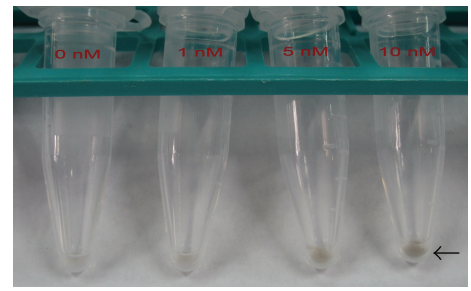

(b)

Figure 1: Effect of α-MSH on melanin synthesis in melanoma B16 cells. (a) Melanin content in α-MSH (0–10 nM) treated cells. (b) Melanin expression in the treated cell pellet. $^*P < 0.05$ as compared to the control group. The results were calculated from three independent experiments and expressed as mean ± standard error (SE).

3.3. Expression of c-Kit in B16 Cells. By immunofluorescence staining, the expression of surface marker c-Kit was upregulated by α-MSH treatment in B16 cells, with both the percent of c-Kit-positive cells (Figure 3(a)) and fluorescence intensity (Figure 3(b)). STI571 and/or resveratrol significantly decreased the c-Kit level that increased by α-MSH (Figures 3(a) and 3(b)).

3.4. Expression of Cytosolic and Nuclear MITF in B16 Cells. In Figure 4, the cytosolic and nuclear proteins were isolated from the treated cells and assayed the expression of MITF. α-MSH-treated B16 cells significantly increased MITF expression in both cytosolic and nuclear fractions. STI571 combined treatment with resveratrol markedly decreased both cytosolic and nuclear MITF levels that increased by α-MSH.

3.5. Effect of Resveratrol on α-MSH Signaling, Viability, and Invasiveness. In Figure 5(a), resveratrol and combined treatment with STI571 significantly decreased the viability of B16 cells with and without α-MSH treatment. In Figure 5(b), α-MSH treatment increased MMP-9 expression in B16 cells.

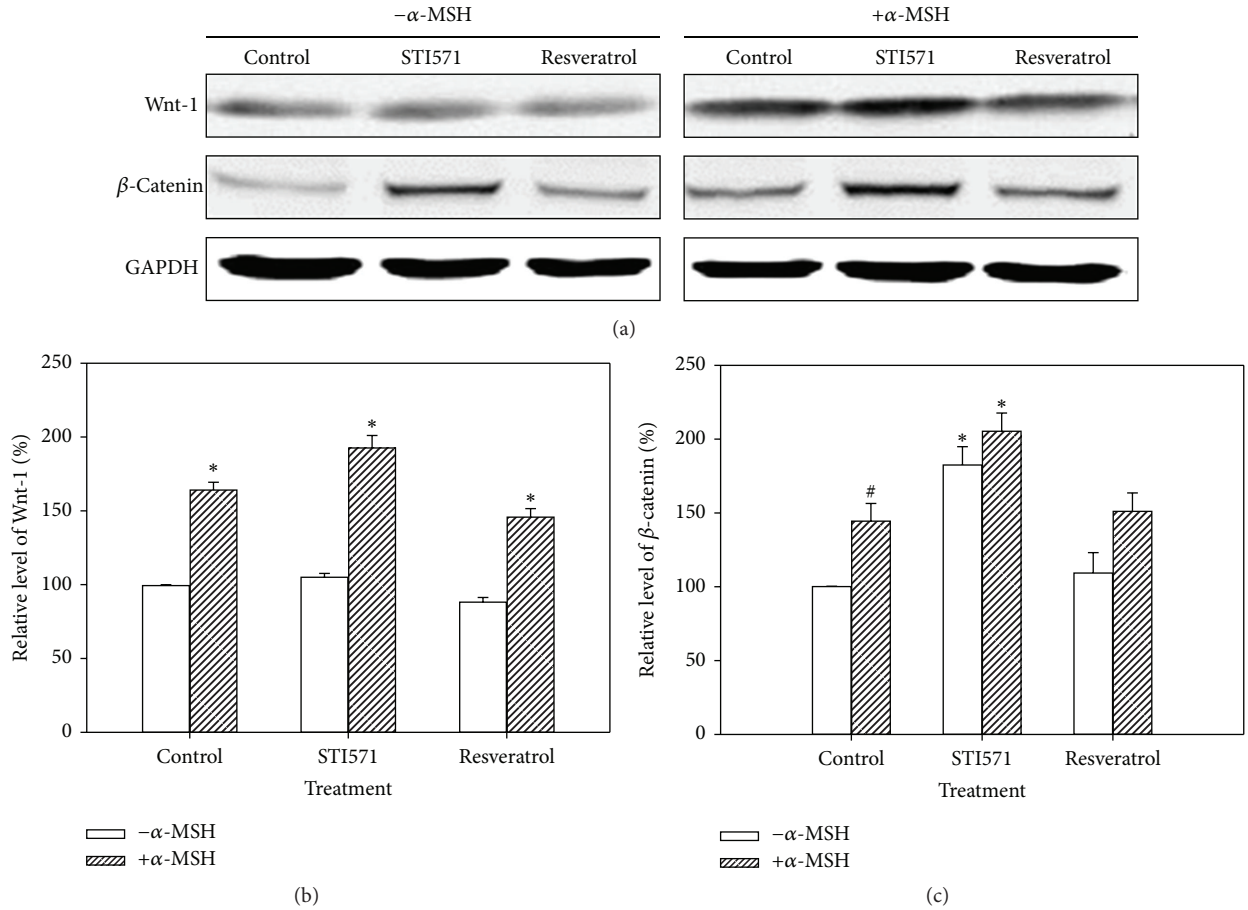

Figure 2: Expression of Wnt-1 and β-catenin in B16 cells with α-MSH (10 nM), STI571 (20 μM), and/or resveratrol (15 μM) treatment by using the Western blot analysis. The relative values were normalized to the internal control GAPDH and the data were expressed as mean ± SE. $^{*}P < 0.05$ as compared to the control group. $^{\#}P < 0.05$ as compared between α-MSH treatment and untreated group.

Resveratrol, but not STI571, significantly decreased MMP-9 level in cells with and without α-MSH treatment. Additionally, B16 cells with α-MSH treatment markedly increased invasion capacity. As shown in Figure 5(c), resveratrol and combined treatment with STI571 significantly inhibited the invasion of cells stimulated by α-MSH.

4. Discussion

The incidence of melanoma has been rising at an alarming rate in both men and women causing mortality and resistance to current therapies [18]. The present study stimulated melanoma B16 cells with α-MSH and demonstrated the increased expression of melanin production to be accompanied with the upregulation of CSC-associated molecules (Wnt-1/β-catenin, c-Kit, MITF, and MMP-9) and invasion ability. Resveratrol, a natural product isolated from traditional Chinese medicine (*Rheum officinale* Baill. and *Polygonum cuspidatum*) and foods (grape skin, red wine, cranberries, blueberries, and peanuts) [19, 20], alone or combined treatment with drug STI571 was effective in inhibiting the abovementioned molecule expression, decreasing the cell viability, as well as suppressing the invasion of melanoma B16 cells. For further development of a new treatment strategy in the future, the pharmacological kinetic profiles of oral administration of resveratrol and STI571 are necessary to clarify the possible mechanism of combination *in vivo*.

Epidermal keratinocytes and melanocytes have been the subject of many skin biology studies because they respond to a rich variety of inflammatory and immunomodulating cytokines, hormones, vitamins, UV light, toxins, and physical injury [21]. Melanin is produced in melanocytes and melanomas through metabolism of melanogenic enzymes, such as tyrosinase. Certain pathways, including α-MSH, Wnt/β-catenin, c-Kit, and their downstream modulation of MITF signaling, receive signals from receptors and initiate melanogenesis process [22]. Articles reported that resveratrol exhibited the inhibitory activity against tyrosinase and MITF may have potential in melanogenesis inhibition [23, 24]. This study treated melanoma B16 cells with α-MSH and demonstrated that the melanin level was increased in a concentration-dependent manner (Figure 1). The α-MSH-mediated activation also stimulated Wnt/β-catenin and c-Kit up-regulation, an experimental model resembling clinical melanoma development. In embryonic and adult cells,

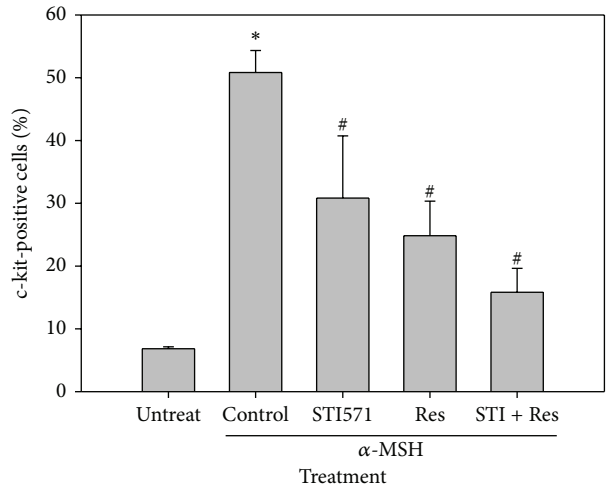

(a)

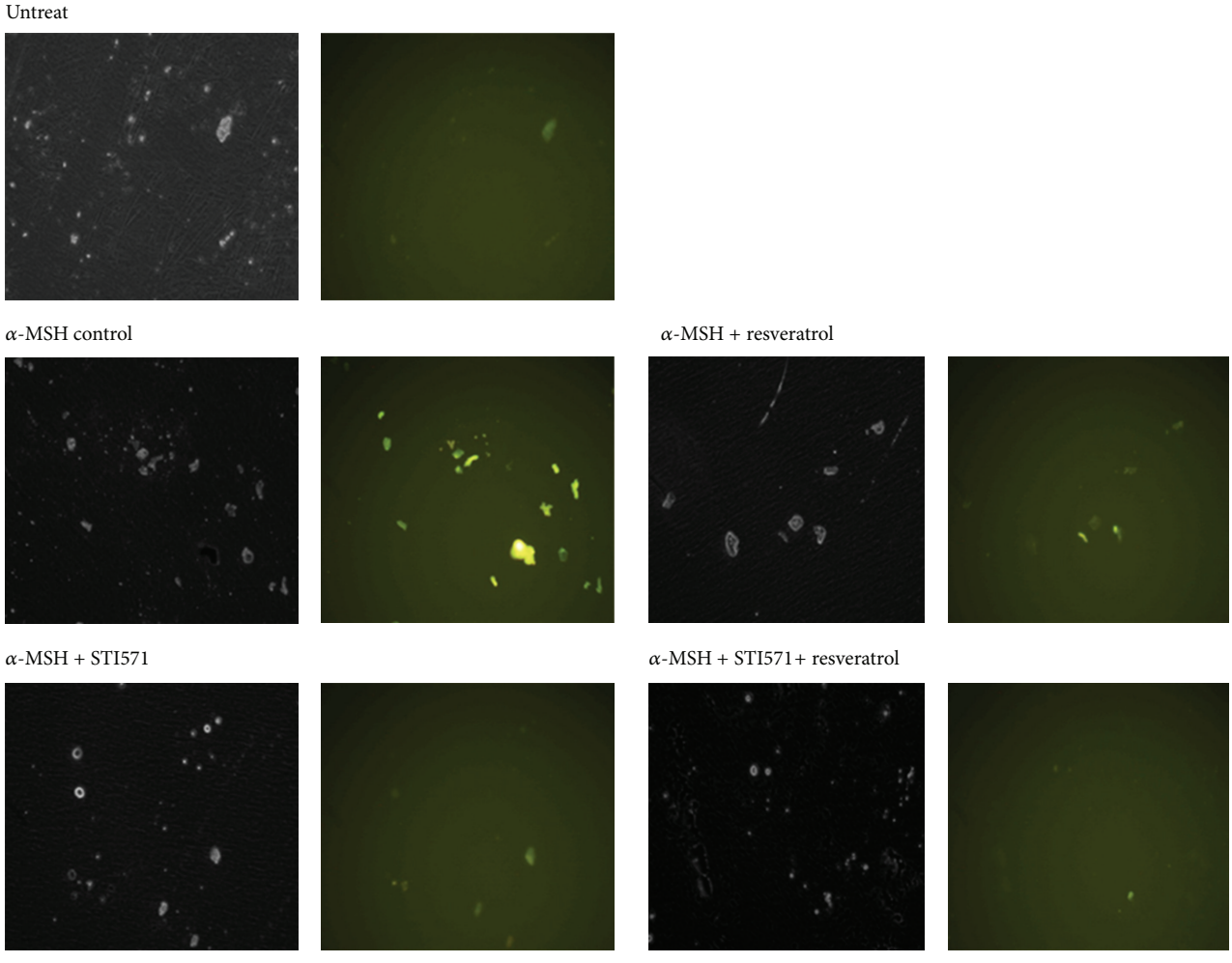

(b)

Figure 3: Expression of c-Kit on cell surface. (a) Percentage of c-Kit-positive cells. (b) Immunofluorescence staining of c-Kit. These cells were stained with FITC-conjugated anti-c-Kit antibody (green) and observed under a microscope (200x). $^{*}P < 0.05$ as compared to the untreated group. $^{\#}P < 0.05$ as compared to the α-MSH alone group. Res: resveratrol; STI: STI571.

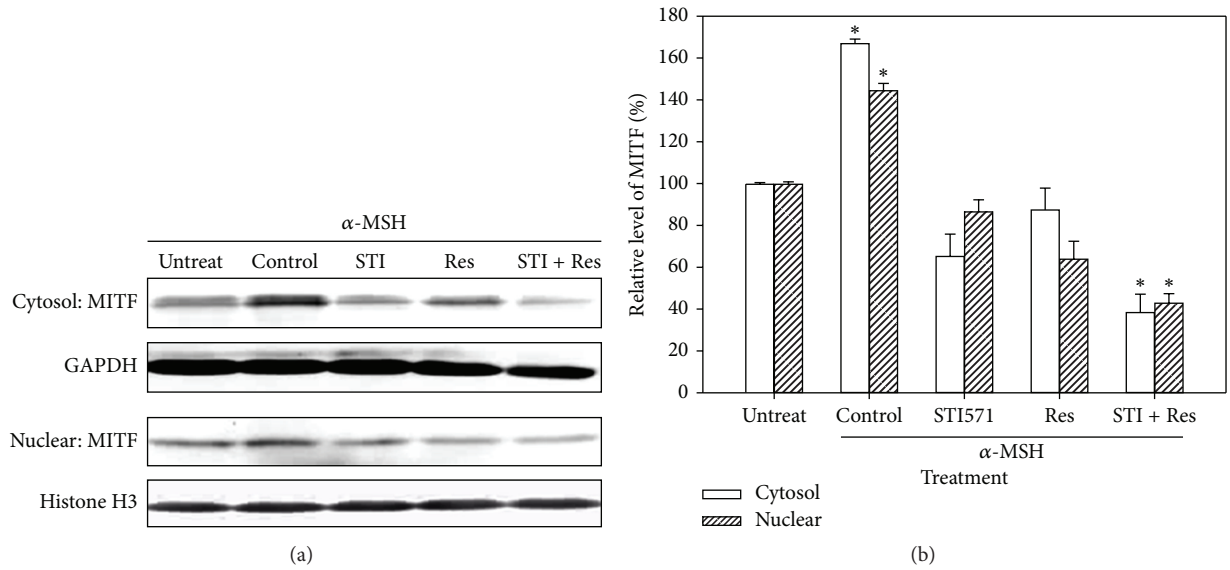

Figure 4: Expression of nuclear and cytosolic MITF in B16 cells with α-MSH (10 nM), STI571 (20 μM), and/or resveratrol (15 μM) treatment by using the Western blot analysis. The relative values normalized to the internal control GAPDH (cytosol) and histone H3 (nuclear) were calculated from three independent experiments. Data were expressed as mean ± SE. $^*P < 0.05$ as compared to the control group. Res: resveratrol; STI: STI571.

the Wnt/β-catenin pathway involved several cellular activities, such as cell proliferation, migration, and differentiation [25]. β-catenin, an important intermediate in Wnt signaling pathway, has been identified as a key point for melanocyte development [26]. c-Kit (CD117), the receptor for the stem cell factor (SCFR), is a growth factor for melanocyte migration and proliferation and has been shown differential expression in various malignant melanocytic lesions with dermis invasion and to differentiate metastatic melanoma from primary melanoma [27]. Additionally, α-MSH is a physiological ligand that binds to melanocortin-1 receptor, initiates signal transduction to induce transcription factor MITF expression, and then leads to increase in melanin synthesis [5].

Among skin cancers, melanoma responds poorly to chemotherapy. For examples, melanoma B16/PDGF-BB cells have reported not being sensitive to paclitaxel, but that combination of tyrosine kinase inhibitors (such as imatinib and vatalanib) could increase the inhibitory effects, suggesting a novel target for the treatment of melanomas expressing c-Kit [28]. MITF and P27 are the key molecules that switch the transition between melanoma-initiating cells and their differentiated progeny. Therefore, the CDK inhibitor P27 is increased in MITF-depleted cells and is required for exacerbation of the tumorigenic properties of melanoma cells [29]. Like CSCs, the expression of melanogenic molecules, such as Wnt/β-catenin, c-Kit, and MITF, in melanoma exhibits strong morphological, functional, and molecular heterogeneity that might reflect the existence of different cancer cell populations. In melanoma B16 cells, the present study demonstrated that the CSC-associated molecules Wnt/β-catenin, c-Kit, and MITF were up-regulated by the stimulation of α-MSH. The expression of MMP-9 and the invasion capacity were also increased in α-MSH-treated B16 cell. It was suggested that α-MSH might induced the melanoma cell populations toward stem-like properties, causing the cells to be more resistant to chemotherapy and more prone to metastasis.

Resveratrol, a phytochemical widely found in foods and in traditional Chinese medicines, has been reported that possesses various bioactivities in cancer cells [30–32]. For examples, resveratrol prevents injury of endothelial cells in high-dose interleukin-2 therapy against melanoma [30]. In chronic myeloid leukemic K562 cells, resveratrol acts as a Bcr-Abl inhibitor and suppresses Sonic hedgehog (Shh) signaling, another CSC signaling pathway, in both STI571-sensitive and -resistant cells [31]. Resveratrol also reduces IL-6-mediated Shh signal expression in acute myeloid leukemia [32]. Although articles reported that resveratrol inhibits tumor-initiating stem-like cells properties in head and neck cancer [17], breast cancer [33], glioblastoma [34], and pancreatic cancer [35], there is no research indicating the effect of resveratrol on CSCs of melanoma. In this study, we first demonstrated that resveratrol alone or combined with STI571 was effective on inhibiting the expression of CSC-associated molecules and the CSC characteristics of melanoma B16 cells.

5. Conclusions

Resveratrol could suppress the α-MSH signaling and CSC characteristics in melanoma cells. It implicates that resveratrol may have potential to be developed as a novel therapeutic agent against CSCs of melanoma.

Conflict of Interests

The authors declare that they have no conflict of interests.

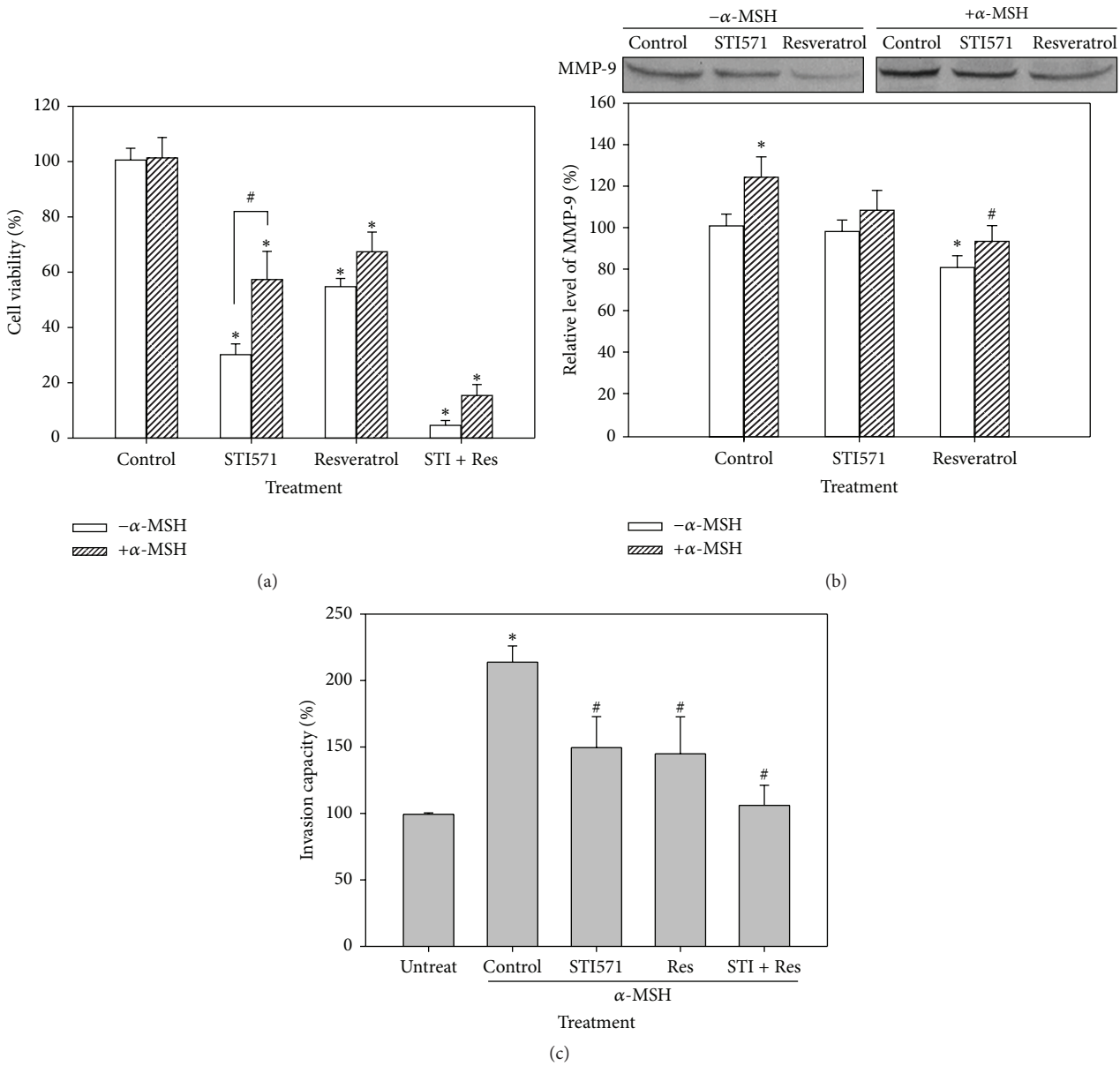

Figure 5: Effect of resveratrol on cell viability, MMP-9 expression, and invasion capacity in B16 cells with α-MSH (10 nM), STI571 (20 μM), and/or resveratrol (15 μM) treatment. (a) Viability assay by using a trypan blue dye exclusion test. (b) MMP-9 expression by Western blotting. (c) Cell invasion assay. $^{*}P < 0.05$ as compared to the control group. $^{\#}P < 0.05$ as compared between α-MSH treatment and untreated group. Res: resveratrol; STI: STI571.

Acknowledgment

This study was supported by Grants NSC 99–2313-B-415-002-MY3, 101-2321-B-415-001, 100-2314-B-195-007-MY3, and 98-2314-B-195-005-MY3 from the National Science Council of the Republic of China, Taipei, Taiwan.

References

[1] S. Ghattas, J. Howle, W. Wang, R. Kefford, and S. Gruenewald, "Intravascular metastatic melanoma: a difficult diagnosis," *Australasian Journal of Dermatology*, vol. 54, no. 2, pp. 141–143, 2013.

[2] J. Wangari-Talbot and S. Chen, "Genetics of melanoma," *Frontiers in Genetics*, vol. 3, p. 330, 2012.

[3] D. S. Kim, Y. M. Jeong, I. K. Park et al., "A new 2-imino-1,3-thiazoline derivative, KHG22394, inhibits melanin synthesis in mouse B16 melanoma cells," *Biological and Pharmaceutical Bulletin*, vol. 30, no. 1, pp. 180–183, 2007.

[4] G. Hunt, C. Todd, J. E. Cresswell, and A. J. Thody, "α-Melanocyte stimulating hormone and its analogue Nle4DPhe7α-MSH affect morphology, tyrosinase activity and melanogenesis in cultured human melanocytes," *Journal of Cell Science*, vol. 107, no. 1, pp. 205–211, 1994.

[5] R. Buscà and R. Ballotti, "Cyclic AMP a key messenger in the regulation of skin pigmentation," *Pigment Cell Research*, vol. 13, no. 2, pp. 60–69, 2000.

[6] K. Hasegawa, R. Furuya, H. Mizuno, K. Umishio, M. Suetsugu, and K. Sato, "Inhibitory effect of elephantopus mollis H.B. and

K. Extract on melanogenesis in B16 murine melanoma cells by downregulating microphthalmia-associated transcription factor expression," *Bioscience, Biotechnology and Biochemistry*, vol. 74, no. 9, pp. 1908–1912, 2010.

[7] H. Saito, K. Yasumoto, K. Takeda et al., "Microphthalmia-associated transcription factor in the Wnt signaling pathway," *Pigment Cell Research*, vol. 16, no. 3, pp. 261–265, 2003.

[8] L. Si and J. Guo, "C-Kit-mutated melanomas: the Chinese experience," *Current Opinion of Oncology*, vol. 25, no. 2, pp. 160–165, 2013.

[9] H. G. Liu, M. X. Kong, Q. Yao et al., "Expression of Sox10 and c-Kit in sinonasal mucosal melanomas arising in the Chinese population," *Head and Neck Pathology*, vol. 6, no. 4, pp. 401–408, 2012.

[10] M. Thill, M. J. Berna, R. Grierson et al., "Expression of CD133 and other putative stem cell markers in uveal melanoma," *Melanoma Research*, vol. 21, no. 5, pp. 405–416, 2011.

[11] E. Allegra and S. Trapasso, "Cancer stem cells in head and neck cancer," *Onco Targets and Therapy*, vol. 5, pp. 375–383, 2012.

[12] G. Pietra, C. Manzini, M. Vitale et al., "Natural killer cells kill human melanoma cells with characteristics of cancer stem cells," *International Immunology*, vol. 21, no. 7, pp. 793–801, 2009.

[13] W. M. Klein, B. P. Wu, S. Zhao et al., "Increased expression of stem cell markers in malignant melanoma," *Modern Pathology*, vol. 20, no. 1, pp. 102–107, 2007.

[14] R. E. Bell and C. Levy, "The three M's: melanoma, microphthalmia-associated transcription factor and microRNA," *Pigment Cell & MelaNoma Research*, vol. 24, no. 6, pp. 1088–1106, 2011.

[15] D. Fang, T. K. Nguyen, K. Leishear et al., "A tumorigenic subpopulation with stem cell properties in melanomas," *Cancer Research*, vol. 65, no. 20, pp. 9328–9337, 2005.

[16] S. Kusunoki, K. Kato, K. Tabu et al., "The inhibitory effect of salinomycin on the proliferation, migration and invasion of human endometrial cancer stem-like cells," *Gynecologic Oncology*, vol. 129, no. 3, pp. 598–605, 2013.

[17] F. W. Hu, L. L. Tsai, C. H. Yu, P. N. Chen, M. Y. Chou, and C. C. Yu, "Impairment of tumor-initiating stem-like property and reversal of epithelial-mesenchymal transdifferentiation in head and neck cancer by resveratrol treatment," *Molecular Nutrition & Food Research*, vol. 56, no. 8, pp. 1247–1258, 2012.

[18] M. P. Purdue, L. E. B. Freeman, W. F. Anderson, and M. A. Tucker, "Recent trends in incidence of cutaneous melanoma among US caucasian young adults," *Journal of Investigative Dermatology*, vol. 128, no. 12, pp. 2905–2908, 2008.

[19] S. K. Lee, W. Zhang, and B. J. S. Sanderson, "Selective growth inhibition of human leukemia and human lymphoblastoid cells by resveratrol via cell cycle arrest and apoptosis induction," *Journal of Agricultural and Food Chemistry*, vol. 56, no. 16, pp. 7572–7577, 2008.

[20] B. Y. Chen, C. H. Kuo, Y. C. Liu, L. Y. Ye, J. H. Chen, and C. J. Shieh, "Ultrasonic-assisted extraction of the botanical dietary supplement resveratrol and other constituents of Polygonum cuspidatum," *Journal of Natural Products*, vol. 75, no. 10, pp. 1810–1813, 2012.

[21] M. Blumenberg, "SKINOMICS: transcriptional profiling in dermatology and skin biology," *Current Genomics*, vol. 13, no. 5, pp. 363–368, 2012.

[22] T. L. Hocker, M. K. Singh, and H. Tsao, "Melanoma genetics and therapeutic approaches in the 21st century: moving from the benchside to the bedside," *Journal of Investigative Dermatology*, vol. 128, no. 11, pp. 2575–2595, 2008.

[23] H. Satooka and I. Kubo, "Resveratrol as a kcat type inhibitor for tyrosinase: potentiated melanogenesis inhibitor," *Bioorganic and Medicinal Chemistry*, vol. 20, no. 2, pp. 1090–1099, 2012.

[24] C. B. Lin, L. Babiarz, F. Liebel et al., "Modulation of microphthalmia-associated transcription factor gene expression alters skin pigmentation," *Journal of Investigative Dermatology*, vol. 119, no. 6, pp. 1330–1340, 2002.

[25] L. Larue and V. Delmas, "The WNT/beta-catenin pathway in melanoma," *Frontiers in Bioscience*, vol. 11, no. 1, pp. 733–742, 2006.

[26] R. I. Dorsky, R. T. Moon, and D. W. Raible, "Control of neural crest cell fate by the Wnt signalling pathway," *Nature*, vol. 396, no. 6709, pp. 370–72, 1998.

[27] L. Pilloni, P. Bianco, E. Difelice et al., "The usefulness of c-Kit in the immunohistochemical assessment of melanocytic lesions," *European Journal of Histochemistry*, vol. 55, no. 2, Article ID e20, 2011.

[28] A. Kłosowska-Wardęga, Y. Hasumi, A. Åhgren, C. H. Heldin, and C. Hellberg, "Combination therapy using imatinib and vatalanib improves the therapeutic efficiency of paclitaxel towards a mouse melanoma tumor," *Melanoma Research*, vol. 21, no. 1, pp. 57–65, 2011.

[29] Y. Cheli, S. Guiliano, T. Botton et al., "Mitf is the key molecular switch between mouse or human melanoma initiating cells and their differentiated progeny," *Oncogene*, vol. 30, no. 20, pp. 2307–2318, 2011.

[30] H. Guan, N. P. Singh, U. P. Singh, P. S. Nagarkatti, and M. Nagarkatti, "Resveratrol prevents endothelial cells injury in high-dose interleukin-2 therapy against melanoma," *PLoS One*, vol. 7, no. 4, Article ID e35650, 2012.

[31] H. F. Liao, Y. C. Su, Z. Y. Zheng et al., "Sonic hedgehog signaling regulates Bcr-Abl expression in human chronic myeloid leukemia cells," *Biomedicine & Pharmacotherapy*, vol. 66, no. 5, pp. 378–383, 2012.

[32] Y. C. Su, S. C. Li, Y. C. Wu et al., "Resveratrol downregulates interleukin-6-stimulated sonic hedgehog signaling in human acute myeloid leukemia," *Evidence-Based Complementary and Alternative Medicine*, vol. 2013, Article ID 547430, 11 pages, 2013.

[33] P. R. Pandey, H. Okuda, M. Watabe et al., "Resveratrol suppresses growth of cancer stem-like cells by inhibiting fatty acid synthase," *Breast Cancer Research and Treatment*, vol. 130, no. 2, pp. 387–398, 2011.

[34] Y. P. Yang, Y. L. Chang, P. I. Huang et al., "Resveratrol suppresses tumorigenicity and enhances radiosensitivity in primary glioblastoma tumor initiating cells by inhibiting the STAT3 axis," *Journal of Cellular Physiology*, vol. 227, no. 3, pp. 976–993, 2012.

[35] S. Shankar, D. Nall, S. N. Tang et al., "Resveratrol inhibits pancreatic cancer stem cell characteristics in human and KrasG12D transgenic mice by inhibiting pluripotency maintaining factors and epithelial-mesenchymal transition," *PLoS One*, vol. 6, no. 1, Article ID e16530, 2011.

Hindawi Publishing Corporation
Evidence-Based Complementary and Alternative Medicine
Volume 2013, Article ID 748587, 5 pages
http://dx.doi.org/10.1155/2013/748587

Review Article

Targeting Sonic Hedgehog Signaling by Compounds and Derivatives from Natural Products

Yu-Chuen Huang,[1,2,3] K. S. Clifford Chao,[4] Hui-Fen Liao,[5] and Yu-Jen Chen[6,7]

[1] *School of Chinese Medicine, China Medical University, Taichung 404, Taiwan*
[2] *Graduate Institute of Biostatistics, China Medical University, Taichung 404, Taiwan*
[3] *Department of Medical Research, China Medical University Hospital, Taichung 404, Taiwan*
[4] *Department of Radiation Oncology, Columbia University, New York, NY 10032, USA*
[5] *Department of Biochemical Science and Technology, National Chiayi University, Chiayi 600, Taiwan*
[6] *Institute of Traditional Medicine, National Yang-Ming University, Taipei 112, Taiwan*
[7] *Department of Radiation Oncology and Department of Medical Research, Mackay Memorial Hospital, 92 Chung-Shan North Road, Section 2, Taipei 104, Taiwan*

Correspondence should be addressed to Hui-Fen Liao; liao.huifen@gmail.com and Yu-Jen Chen; chenmdphd@gmail.com

Received 25 February 2013; Accepted 30 April 2013

Academic Editor: Min Shen Chang

Cancer stem cells (CSCs) are a major cause of cancer treatment failure, relapse, and drug resistance and are known to be responsible for cancer cell invasion and metastasis. The Sonic hedgehog (Shh) signaling pathway is crucial to embryonic development. Intriguingly, the aberrant activation of the Shh pathway plays critical roles in developing CSCs and leads to angiogenesis, migration, invasion, and metastasis. Natural compounds and chemical structure modified derivatives from complementary and alternative medicine have received increasing attention as cancer chemopreventives, and their antitumor effects have been demonstrated both *in vitro* and *in vivo*. However, reports for their bioactivity against CSCs and specifically targeting Shh signaling remain limited. In this review, we summarize investigations of the compounds cyclopamine, curcumin, epigallocatechin-3-gallate, genistein, resveratrol, zerumbone, norcantharidin, and arsenic trioxide, with a focus on Shh signaling blockade. Given that Shh signaling antagonism has been clinically proven as effective strategy against CSCs, this review may be exploitable for development of novel anticancer agents from complementary and alternative medicine.

1. Introduction

Cancer stem cells (CSCs) are a small minority of cancer cells that can proliferate extensively and form new tumors [1–4]. These properties of CSCs are thought to cause cancer treatment failure, relapse, and drug resistance [5]. As with normal stem cells, CSCs are self-renewing and can differentiate into phenotypically diverse tumor and nontumor cancer cells [2]. Several embryonic signaling pathways are known to be involved in normal stem cell maintenance, and these have recently been linked to carcinogenesis and tumor propagation. Indeed, signaling pathways that support dysregulated self-renewal and proliferation of CSCs may provide practical targets for preventing tumor regrowth and improving treatment outcomes.

Sonic hedgehog (Shh) signaling is critical to embryogenesis and is essential for the development of several tissue types and organs [6]. Aberrant activation of Shh signaling is central to CSC activities, which promotes tumor progression, angiogenesis, migration, invasion, and metastasis [7–9]. Dysregulation of Shh signaling has been involved with several malignancies, including basal cell carcinomas, medulloblastomas, leukemia, oral squamous cell carcinomas, and gastrointestinal, pancreas, lung, ovarian, breast, and

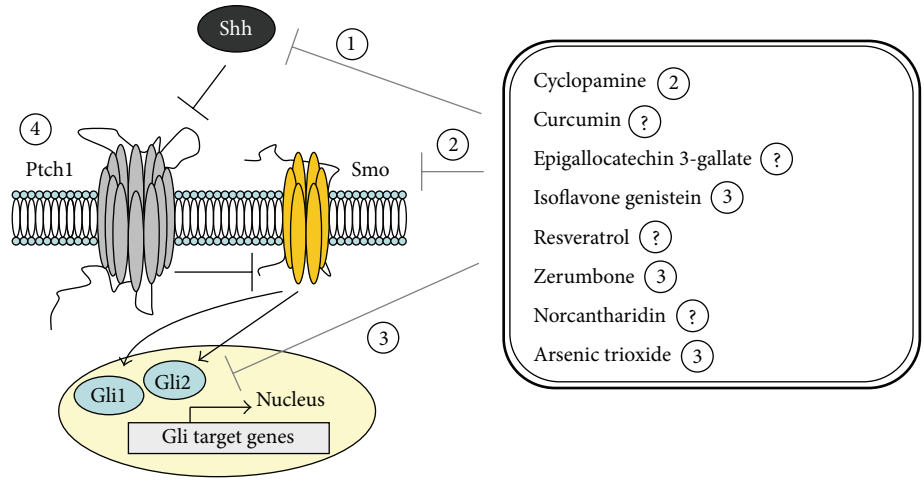

Figure 1: Targeting the Sonic hedgehog signaling pathway by compounds and derivatives from natural products. Circled numbers beside compound names indicate target Shh signaling proteins. Question marks indicate that the targeted protein is uncertain.

prostate cancers [10–14]. Shh is a secreted glycoprotein that activates signaling by binding to the transmembrane receptor patched-1 (Ptch1). Subsequently, Ptch1-mediated inactivation of Smoothened (Smo) is reversed, allowing transduction of the Shh signal, which results in nuclear translocation of cytoplasmic transcription factors of the Gli family to modulate target gene expression [15].

Since CSCs are considered as a cause of cancer treatment failure, relapse, and drug resistance, therapeutic targeting of CSCs may overcome tumor resistance, reduce relapse, and improve patient survival. The small molecule Smo inhibitor vismodegib has been demonstrated effective in reducing the basal-cell carcinoma tumor burden. However, the adverse events caused discontinuation in over half of treated patients [16]. It implicates that Shh signaling blockade is an effective strategy and remains a room to develop effective agents with more favorable safety profile. Several naturally occurring dietary compounds have shown promise as Shh signaling inhibitors. In this paper, we review the current understanding of some natural compounds that have cancer treatment potential, with a focus on targeting the Shh signaling pathway (Figure 1).

2. Compounds and Derivatives from Natural Products That Regulate Sonic Hedgehog Signaling Pathway

2.1. Cyclopamine. Cyclopamine is a naturally occurring compound from the plant *Veratrum californicum*, commonly known as corn lily, and was the first phytochemical, which demonstrated Shh pathway inhibitory activity [17, 18], and was shown to block the activation of Smo [18]. Berman et al. reported that treatment of murine medulloblastoma cells with cyclopamine inhibited proliferation, induced neuronal differentiation, and depleted CSC populations [17]. It also caused regression of murine tumor allografts and induced rapid death of cells from freshly resected human medulloblastomas [17]. Cyclopamine may inhibit development and invasiveness of human hepatocellular carcinomas (HCCs) *in vitro* and *in vivo* by inhibiting the Shh pathway. Blockade of Shh signaling may be a potential target of new therapeutic strategy for HCC [19–22]. In addition, cyclopamine effectively targeted CSCs of pancreatic cancer, breast cancer, glioblastoma, and multiple myeloma [23, 24].

2.2. Curcumin. Curcumin, the major extract of tumeric, is derived from the plant *Curcuma longa*, which is a common ingredient of mustard and curry [25, 26]. It has been widely used in traditional medicines and dietary supplements for centuries [27]. Curcumin has anti-inflammatory and antioxidant activities and has been studied as a preventive agent in several cancer models [25, 28]. After treating medulloblastoma cells with curcumin, Elamin et al. observed that curcumin caused inhibition of Shh signaling cell growth and induction of apoptotic cell death by downregulating proteins of the Shh pathway. In addition, curcumin enhanced the antitumor effects of cisplatin and γ-rays by targeting pathways that are crucial for tumor survival [29]. Moreover, curcumin inhibited prostate cancer cell growth through the Shh pathway and reduced or delayed prostate cancer growth in a transgenic adenocarcinoma mouse model [30].

2.3. Epigallocatechin-3-Gallate. Green tea is one of the most widely consumed beverages in the world [31]. Epigallocatechin-3-gallate (EGCG) acts as a potent cancer-preventive agent through various mechanisms and is the most abundant polyphenolic catechin in green tea [32]. Specifically, Tang et al. reported inhibition of the Shh pathway, induction of apoptosis, and suppression of human chondrosarcoma cell proliferation by EGCG, suggesting that EGCG could be a new therapeutic agent for patients with chondrosarcoma [33]. Moreover, EGCG was shown to inhibit prostate cancer cell growth by suppressing Gli1 mRNA expression and downregulating Gli promoter activity [30]. In transgenic prostate adenocarcinoma mice, EGCG reduced or delayed prostate tumor growth [30]. A recent report showed that

EGCG inhibited the components of Shh pathway and Gli transcriptional activity in pancreatic CSCs. It also inhibited self-renewal capacity of pancreatic CSCs, and these effects were enhanced in the presence of the flavonoid quercetin, which is present in fruits and vegetables such as onion, tea, apples, and berries [11]. These data suggest that EGCG either alone or in combination with quercetin could be used to prevent and treat pancreatic cancer [11].

2.4. Isoflavone Genistein. Soybeans are an abundant source of isoflavones. Genistein is one of the most active soy isoflavones. Numerous studies report protective effects of soy foods against breast and prostate cancers [34–37]. Indeed, soy isoflavones, particularly genistein, exert potent antiproliferative effects on breast, prostate, colon, skin, gastric, and bladder cancers [38]. In transgenic prostate adenocarcinoma mice, genistein inhibited cancer cell growth through its actions on the Shh pathway and reduced or delayed growth of prostate tumors [30]. In a study by Zhang et al., genistein not only inhibited prostate cancer cell invasion [39] but also targeted prostate CSCs and suppressed tumorigenicity [40]. This anti-CSC effect was due to inhibition of the Shh protein Gli1 [40], suggesting that genistein may be a potent chemopreventive agent against prostate CSCs.

2.5. Resveratrol. Resveratrol is a dietary polyphenol derived from plants such as grapes, berries, plums, peanuts, and *Polygonum cuspidatum* [41]. Resveratrol inhibited the proliferation of a wide variety of human cancer cells *in vitro* and slowed carcinogenesis in animal models [42, 43], suggesting therapeutic and cancer preventive effects [43]. Ślusarz et al. demonstrated involvement of Shh signaling in resveratrol-mediated inhibition of prostate cancer cell growth *in vitro* and *in vivo* [30]. Moreover, resveratrol inhibited both Shh signaling and Bcr-Abl expression in human chronic myeloid leukemia (CML) cells, indicating that resveratrol may have potential as a treatment for CML [10]. Recently, another report showed that resveratrol could effectively downregulate interleukin-6-stimulated Shh signaling in human acute myeloid leukemia [44].

2.6. Zerumbone. Zingiber zerumbet Smith is a perennial, tuberous root herb that grows mainly in southeast Asia [45]. The major extract zerumbone has been shown to increase apoptosis and inhibit cancer cell invasion and has demonstrated antitumor effects against leukemia and breast, lung, liver, and pancreatic cancers [46–49]. Hosoya et al. reported that zerumbone inhibited both Gli1- and Gli2-mediated transcription and repressed the transcription of other Shh signaling genes, including Ptch1 and BCL2, in HaCaT cells [50].

2.7. Norcantharidin. The small-molecule norcantharidin (NCTD) is a demethylated synthetic analog of naturally occurring cantharidin from blister beetles (*Mylabris phalerata* Pall.). The effects of NCTD against diverse malignancies have been investigated. It has been shown capable of inducing cell anoikis and apoptosis [51], inhibiting invasion and angiogenesis [52], and suppressing metastasis [53]. Moreover, NCTD may overcome multidrug resistance by inhibiting Shh signaling and expression of downstream multidrug resistance (MDR1) P-glycoprotein in human breast cancer cells [13].

2.8. Arsenic Trioxide. Arsenic trioxide (As_2O_3) has been used therapeutically in traditional Chinese medicine for a long time and has been shown as a highly effective treatment for relapsed acute promyelocytic leukemia [54]. In addition, arsenic trioxide can inhibit Shh signaling at the Gli protein level, although the exact mechanism remains controversial. Kim et al. demonstrated that arsenic trioxide antagonizes Shh signaling primarily through interference with Gli2 [55]. Moreover, Beauchamp and colleagues provide evidence that arsenic trioxide could inhibit the growth of Ewing sarcoma and medulloblastoma cells by targeting Gli1 [56]. These data suggest that arsenic trioxide could be used as a therapeutic agent in malignant diseases associated with Shh pathway activation.

2.9. Clinical Implications of Natural Compounds and Derivatives. Some natural compounds and their derivatives have potent antitumor effects, offering clues to the design of targeted therapeutic anticancer agents. In addition to affecting cancer related signaling pathways, natural compounds may synergize with chemotherapy and radiotherapy as antitumor agents. For example, Choi et al. showed pretreatment with zerumbone before radiation induced radiosensitization in human lung adenocarcinoma cells and in a xenograft mice model [57]. Curcumin, genistein, and EGCG have potential in the treatment of prostate cancer [30, 39, 40]. Moreover, resveratrol and NCTD are potential treatments for acute myeloid leukemia and breast cancer, respectively [13, 44]. Hence, further development of molecular tests that assess tumor tissue and DNA from patients will aid therapeutic decisions to use natural compounds. In addition, molecular markers of Shh signaling may facilitate the development of personalized cancer treatments.

3. Conclusions

In conclusion, the antitumor effects of naturally occurring compounds that target Shh signaling indicate the importance of this pathway to cancer cell invasion and metastasis. Hence, these natural compounds and related derivatives may be used as primary treatment or as adjunctive agents for combinatory treatment to improve therapeutic index against cancer. Although this review focuses only on natural compounds and related derivatives that target the Shh signaling pathway, the data summarized herein indicate that complementary and alternative medicine may comprise a multitude of compounds with potential to prevent cancer and its metastasis by targeting various signaling pathways. Further *in vitro* and *in vivo* studies, as well as clinical trials, are warranted to investigate the therapeutic potential of natural compounds against CSCs.

Conflict of Interests

The authors declare that they have no conflict of interests.

Acknowledgments

This study is supported in part by Taiwan Department of Health Clinical Trial and Research Center of Excellence (DOH102-TD-B-111-004), China Medical University, Taichung, Taiwan (CMU100-N1-08-1), and the National Science Council, Taipei, Taiwan (NSC101-2314-B-039-024, 100-2314-B-195-007-MY3, and 98–2314-B-195-005-MY3).

References

[1] H. D. Hemmati, I. Nakano, J. A. Lazareff et al., "Cancerous stem cells can arise from pediatric brain tumors," *Proceedings of the National Academy of Sciences of the United States of America*, vol. 100, no. 25, pp. 15178–15183, 2003.

[2] M. Al-Hajj and M. F. Clarke, "Self-renewal and solid tumor stem cells," *Oncogene*, vol. 23, no. 43, pp. 7274–7282, 2004.

[3] M. Al-Hajj, M. S. Wicha, A. Benito-Hernandez, S. J. Morrison, and M. F. Clarke, "Prospective identification of tumorigenic breast cancer cells," *Proceedings of the National Academy of Sciences of the United States of America*, vol. 100, no. 7, pp. 3983–3988, 2003.

[4] J. Marx, "Mutant stem cells may seed cancer," *Science*, vol. 301, no. 5638, pp. 1308–1310, 2003.

[5] R. J. Jones, W. H. Matsui, and B. D. Smith, "Cancer stem cells: are we missing the target?" *Journal of the National Cancer Institute*, vol. 96, no. 8, pp. 583–585, 2004.

[6] M. Varjosalo and J. Taipale, "Hedgehog: functions and mechanisms," *Genes and Development*, vol. 22, no. 18, pp. 2454–2472, 2008.

[7] M. Rodova, J. Fu, D. N. Watkins, R. K. Srivastava, and S. Shankar, "Sonic hedgehog signaling inhibition provides opportunities for targeted therapy by sulforaphane in regulating pancreatic cancer stem cell self-renewal," *PLoS One*, vol. 7, no. 9, Article ID e46083, 2012.

[8] Y. J. Chen, J. Sims-Mourtada, J. Izzo, and K. S. C. Chao, "Targeting the hedgehog pathway to mitigate treatment resistance," *Cell Cycle*, vol. 6, no. 15, pp. 1826–1830, 2007.

[9] R. L. Carpenter and H. W. Lo, "Hedgehog pathway and GLI1 isoforms in human cancer," *Discovery Medicine*, vol. 13, no. 69, pp. 105–113, 2012.

[10] H. F. Liao, Y. C. Su, Z. Y. Zheng et al., "Sonic hedgehog signaling regulates Bcr-Abl expression in human chronic myeloid leukemia cells," *Biomedicine and Pharmacotherapy*, vol. 66, no. 5, pp. 378–383, 2012.

[11] S. N. Tang, J. Fu, D. Nall, M. Rodova, S. Shankar, and R. K. Srivastava, "Inhibition of sonic hedgehog pathway and pluripotency maintaining factors regulate human pancreatic cancer stem cell characteristics," *International Journal of Cancer*, vol. 131, no. 1, pp. 30–40, 2012.

[12] L. Yang, G. Xie, Q. Fan, and J. Xie, "Activation of the hedgehog-signaling pathway in human cancer and the clinical implications," *Oncogene*, vol. 29, no. 4, pp. 469–481, 2010.

[13] Y. J. Chen, C. D. Kuo, S. H. Chen et al., "Small-molecule synthetic compound norcantharidin reverses multi-drug resistance by regulating Sonic hedgehog signaling in human breast cancer cells," *PLoS One*, vol. 7, no. 5, Article ID e37006, 2012.

[14] Y. F. Wang, C. J. Chang, C. P. Lin et al., "Expression of hedgehog signaling molecules as a prognostic indicator of oral squamous cell carcinoma," *Head and Neck*, vol. 34, no. 11, pp. 1556–1561, 2012.

[15] Y. Z. Feng, T. Shiozawa, T. Miyamoto et al., "Overexpression of hedgehog signaling molecules and its involvement in the proliferation of endometrial carcinoma cells," *Clinical Cancer Research*, vol. 13, no. 5, pp. 1389–1398, 2007.

[16] J. Y. Tang, J. M. kay-Wiggan, M. Aszterbaum et al., "Inhibiting the hedgehog pathway in patients with the basal-cell nevus syndrome," *The New England Journal of Medicine*, vol. 366, no. 23, pp. 2180–2188, 2012.

[17] D. M. Berman, S. S. Karhadkar, A. R. Hallahan et al., "Medulloblastoma growth inhibition by Hedgehog pathway blockade," *Science*, vol. 297, no. 5586, pp. 1559–1561, 2002.

[18] J. K. Chen, J. Taipale, M. K. Cooper, and P. A. Beachy, "Inhibition of Hedgehog signaling by direct binding of cyclopamine to Smoothened," *Genes and Development*, vol. 16, no. 21, pp. 2743–2748, 2002.

[19] K. S. Jeng, I. S. Sheen, W. J. Jeng et al., "Blockade of the sonic hedgehog pathway effectively inhibits the growth of hepatoma in mice: an in vivo study," *Oncology Letters.*, vol. 4, no. 6, pp. 1158–1162, 2012.

[20] X. L. Chen, Q. Y. Cheng, M. R. She et al., "Expression of Sonic Hedgehog signaling components in hepatocellular carcinoma and cyclopamine-induced apoptosis through Bcl-2 downregulation in vitro," *Archives of Medical Research*, vol. 41, no. 5, pp. 315–323, 2010.

[21] W. T. Cheng, K. Xu, D. Y. Tian, Z. G. Zhang, L. J. Liu, and Y. Chen, "Role of Hedgehog signaling pathway in proliferation and invasiveness of hepatocellular carcinoma cells," *International Journal of Oncology*, vol. 34, no. 3, pp. 829–836, 2009.

[22] Y. Kim, W. Y. Joon, X. Xiao, N. M. Dean, B. P. Monia, and E. G. Marcusson, "Selective down-regulation of glioma-associated oncogene 2 inhibits the proliferation of hepatocellular carcinoma cells," *Cancer Research*, vol. 67, no. 8, pp. 3583–3593, 2007.

[23] E. E. Bar, A. Chaudhry, A. Lin et al., "Cyclopamine-mediated Hedgehog pathway inhibition depletes stem-like cancer cells in glioblastoma," *Stem Cells*, vol. 25, no. 10, pp. 2524–2533, 2007.

[24] D. Subramaniam, S. Ramalingam, C. W. Houchen, and S. Anant, "Cancer stem cells: a novel paradigm for cancer prevention and treatment," *Mini Reviews in Medicinal Chemistry*, vol. 10, no. 5, pp. 359–371, 2010.

[25] Y. Li, M. S. Wicha, S. J. Schwartz, and D. Sun, "Implications of cancer stem cell theory for cancer chemoprevention by natural dietary compounds," *Journal of Nutritional Biochemistry*, vol. 22, no. 9, pp. 799–806, 2011.

[26] C.H. Park, E.R. Hahm, S. Park, H.K. Kim, and C.H. Yang, "The inhibitory mechanism of curcumin and its derivative against β-catenin/Tcf signaling," *FEBS Letters*, vol. 579, no. 13, pp. 2965–2971, 2005.

[27] B. B. Aggarwal, C. Sundaram, N. Malani, and H. Ichikawa, "Curcumin: the Indian solid gold," *Advances in Experimental Medicine and Biology*, vol. 595, pp. 1–75, 2007.

[28] Z. M. Shao, Z. Z. Shen, C. H. Liu et al., "Curcumin exerts multiple suppressive effects on human breast carcinoma cells," *International Journal of Cancer*, vol. 98, no. 2, pp. 234–240, 2002.

[29] M. H. Elamin, Z. Shinwari, S. F. Hendrayani et al., "Curcumin inhibits the sonic hedgehog signaling pathway and triggers apoptosis in medulloblastoma cells," *Molecular Carcinogenesis*, vol. 49, no. 3, pp. 302–314, 2010.

[30] A. Ślusarz, N. S. Shenouda, M. S. Sakla et al., "Common botanical compounds inhibit the hedgehog signaling pathway in prostate cancer," *Cancer Research*, vol. 70, no. 8, pp. 3382–3390, 2010.

[31] H. N. Graham, "Green tea composition, consumption, and polyphenol chemistry," *Preventive Medicine*, vol. 21, no. 3, pp. 334–350, 1992.

[32] H. Fujiki, "Two stages of cancer prevention with green tea," *Journal of Cancer Research and Clinical Oncology*, vol. 125, no. 11, pp. 589–597, 1999.

[33] G. Q. Tang, T. Q. Yan, W. Guo et al., "(-)-Epigallocatechin-3-gallate induces apoptosis and suppresses proliferation by inhibiting the human Indian Hedgehog pathway in human chondrosarcoma cells," *Journal of Cancer Research and Clinical Oncology*, vol. 136, no. 8, pp. 1179–1185, 2010.

[34] J. R. Hebert, T. G. Hurley, B. C. Olendzki, J. Teas, Y. Ma, and J. S. Hampl, "Nutritional and socioeconomic factors in relation to prostate cancer mortality: a cross-national study," *Journal of the National Cancer Institute*, vol. 90, no. 21, pp. 1637–1647, 1998.

[35] M. Verheus, C. H. van Gils, L. Keinan-Boker, P. B. Grace, S. A. Bingham, and P. H. M. Peeters, "Plasma phytoestrogens and subsequent breast cancer risk," *Journal of Clinical Oncology*, vol. 25, no. 6, pp. 648–655, 2007.

[36] H. Adlercreutz, H. Markkanen, and S. Watanabe, "Plasma concentrations of phyto-oestrogens in Japanese men," *The Lancet*, vol. 342, no. 8881, pp. 1209–1210, 1993.

[37] M. Iwasaki, M. Inoue, T. Otani et al., "Plasma isoflavone level and subsequent risk of breast cancer among japanese women: a nested case-control study from the Japan Public Health Center-based prospective study group," *Journal of Clinical Oncology*, vol. 26, no. 10, pp. 1677–1683, 2008.

[38] S. Barnes, "Effect of genistein on in vitro and in vivo models of cancer," *Journal of Nutrition*, vol. 125, no. 3, supplement, pp. 777S–783S, 1995.

[39] L. L. Zhang, L. Li, D. P. Wu et al., "A novel anti-cancer effect of genistein: reversal of epithelial mesenchymal transition in prostate cancer cells," *Acta Pharmacologica Sinica*, vol. 29, no. 9, pp. 1060–1068, 2008.

[40] L. Zhang, L. Li, M. Jiao et al., "Genistein inhibits the stemness properties of prostate cancer cells through targeting Hedgehog-Gli1 pathway," *Cancer Letters*, vol. 323, no. 1, pp. 48–57, 2012.

[41] K. B. Harikumar and B. B. Aggarwal, "Resveratrol: a multitargeted agent for age-associated chronic diseases," *Cell Cycle*, vol. 7, no. 8, pp. 1020–1037, 2008.

[42] A. Bishayee, "Cancer prevention and treatment with resveratrol: from rodent studies to clinical trials," *Cancer Prevention Research*, vol. 2, no. 5, pp. 409–418, 2009.

[43] B. B. Aggarwal, A. Bhardwaj, R. S. Aggarwal, N. P. Seeram, S. Shishodia, and Y. Takada, "Role of resveratrol in prevention and therapy of cancer: preclinical and clinical studies," *Anticancer Research*, vol. 24, no. 5 A, pp. 2783–2840, 2004.

[44] Y. C. Su, S. C. Li, Y. C. Wu, L. M. Wang, K. S. Chao, and H. F. Liao, "Resveratrol downregulates interleukin-6-stimulated sonic hedgehog signaling in human acute myeloid leukemia," *Evidence-Based Complementary and Alternative Medicine*, vol. 2013, Article ID 547430, 11 pages, 2013.

[45] S. Zhang, Q. Liu, Y. Liu, H. Qiao, and Y. Liu, "Zerumbone, a southeast Asian Ginger Sesquiterpene, induced apoptosis of pancreatic carcinoma cells through p53 signaling pathway," *Evidence-Based Complementary and Alternative Medicine*, vol. 2012, Article ID 936030, 8 pages, 2012.

[46] M. Xian, K. Ito, T. Nakazato et al., "Zerumbone, a bioactive sesquiterpene, induces G2/M cell cycle arrest and apoptosis in leukemia cells via a Fas- and mitochondria-mediated pathway," *Cancer Science*, vol. 98, no. 1, pp. 118–126, 2007.

[47] M. Kim, S. Miyamoto, Y. Yasui, T. Oyama, A. Murakami, and T. Tanaka, "Zerumbone, a tropical ginger sesquiterpene, inhibits colon and lung carcinogenesis in mice," *International Journal of Cancer*, vol. 124, no. 2, pp. 264–271, 2009.

[48] S. A. S. Sakinah, S. T. Handayani, and L. P. A. Hawariah, "Zerumbone induced apoptosis in liver cancer cells via modulation of Bax/Bcl-2 ratio," *Cancer Cell International*, vol. 7, article 4, 2007.

[49] B. Sung, S. Jhurani, S. A. Kwang et al., "Zerumbone down-regulates chemokine receptor CXCR4 expression leading to inhibition of CXCL12-induced invasion of breast and pancreatic tumor cells," *Cancer Research*, vol. 68, no. 21, pp. 8938–8944, 2008.

[50] T. Hosoya, M. A. Arai, T. Koyano, T. Kowithayakorn, and M. Ishibashi, "Naturally occurring small-molecule inhibitors of Hedgehog/GLI-mediated transcription," *ChemBioChem*, vol. 9, no. 7, pp. 1082–1092, 2008.

[51] Y. J. Chen, C. D. Kuo, Y. M. Tsai, C. C. Yu, G. S. Wang, and H. F. Liao, "Norcantharidin induces anoikis through Jun-N-terminal kinase activation in CT26 colorectal cancer cells," *Anti-Cancer Drugs*, vol. 19, no. 1, pp. 55–64, 2008.

[52] Y. J. Chen, Y. M. Tsai, C. D. Kuo, K. L. Ku, H. S. Shie, and H. F. Liao, "Norcantharidin is a small-molecule synthetic compound with anti-angiogenesis effect," *Life Sciences*, vol. 85, no. 17-18, pp. 642–651, 2009.

[53] Y. J. Chen, W. M. Chang, Y. W. Liu et al., "A small-molecule metastasis inhibitor, norcantharidin, downregulates matrix metalloproteinase-9 expression by inhibiting Sp1 transcriptional activity in colorectal cancer cells," *Chemico-Biological Interactions*, vol. 181, no. 3, pp. 440–446, 2009.

[54] B. L. Powell, "Arsenic trioxide in acute promyelocytic leukemia: potion not poison," *Expert Review of Anticancer Therapy*, vol. 11, no. 9, pp. 1317–1319, 2011.

[55] J. Kim, J. J. Lee, J. Kim, D. Gardner, and P. A. Beachy, "Arsenic antagonizes the Hedgehog pathway by preventing ciliary accumulation and reducing stability of the Gli2 transcriptional effector," *Proceedings of the National Academy of Sciences of the United States of America*, vol. 107, no. 30, pp. 13432–13437, 2010.

[56] E. M. Beauchamp, L. Ringer, G. Bulut et al., "Arsenic trioxide inhibits human cancer cell growth and tumor development in mice by blocking Hedgehog/GLI pathway," *Journal of Clinical Investigation*, vol. 121, no. 1, pp. 148–160, 2011.

[57] S. H. Choi, Y. J. Lee, W. D. Seo et al., "Altered cross-linking of HSP27 by Zerumbone as a novel strategy for overcoming HSP27-mediated radioresistance," *International Journal of Radiation Oncology Biology Physics*, vol. 79, no. 4, pp. 1196–1205, 2011.

Hindawi Publishing Corporation
Evidence-Based Complementary and Alternative Medicine
Volume 2013, Article ID 590393, 13 pages
http://dx.doi.org/10.1155/2013/590393

Research Article

Resveratrol Impedes the Stemness, Epithelial-Mesenchymal Transition, and Metabolic Reprogramming of Cancer Stem Cells in Nasopharyngeal Carcinoma through p53 Activation

Yao-An Shen,[1] Chien-Hung Lin,[2] Wei-Hsin Chi,[3] Chia-Yu Wang,[3] Yi-Tao Hsieh,[3] Yau-Huei Wei,[1,4] and Yann-Jang Chen[2,3,5]

[1] *Institute of Biochemistry and Molecular Biology, National Yang-Ming University, Taipei 112, Taiwan*
[2] *Institute of Clinical Medicine, National Yang-Ming University, Taipei 112, Taiwan*
[3] *Department of Life Sciences and Institute of Genome Sciences, National Yang-Ming University, Taipei 112, Taiwan*
[4] *Department of Medicine, Mackay Medical College, New Taipei City 252, Taiwan*
[5] *Department of Pediatrics, Taipei City Hospital, Renai Branch, Taipei 106, Taiwan*

Correspondence should be addressed to
Yau-Huei Wei; joeman@ym.edu.tw and Yann-Jang Chen; yjchen@ym.edu.tw

Received 25 January 2013; Revised 15 March 2013; Accepted 16 March 2013

Academic Editor: Hui-Fen Liao

Cancer stem cells (CSCs) are able to self-renew and are refractory to cancer treatment. To investigate the effects of resveratrol on CSCs of nasopharyngeal carcinoma (NPC), we employed a behavior selection strategy to isolate CSCs based on radioresistance, chemoresistance, and tumor sphere formation ability. These NPC CSCs displayed stem cell properties and underwent metabolic shift to predominately rely on glycolysis for energy supply. Intriguingly, we found that resveratrol turned off the metabolic switch, increased the reactive oxygen species (ROS) level, and depolarized mitochondrial membranes. These alterations in metabolism occurred concomitantly with the suppression of CSC properties including resistance to therapy, self-renewal capacity, tumor initiation capacity, and metastatic potential in NPC CSCs. We found that resveratrol impeded CSC properties through the activation of p53 and this effect could be reversed by knockdown of p53. Furthermore, resveratrol suppressed the stemness and EMT through reactivating p53 and inducing miR-145 and miR-200c, which were downregulated in NPC CSCs. In conclusion, we demonstrated that resveratrol employed the p53 pathway in regulating stemness, EMT, and metabolic reprogramming. Further investigation of the molecular mechanism of p53 activation by resveratrol may provide useful information for the development of novel therapies for cancer treatment through targeting to CSCs.

1. Introduction

Nasopharyngeal carcinoma (NPC) is a distinctive type of head and neck cancer with high prevalence rates in Southeast China and Taiwan. Unlike other head and neck cancers, most cases of NPC have high tendency to invade surrounding tissues and metastasize to regional lymph nodes at an early stage. Moreover, most mortality of NPC patients is due to local recurrence and distant metastases [1]. Although chemotherapy and radiotherapy can improve survival rate, the prognosis remains poor for patients with relapse or metastatic diseases [2]. Therefore, in order to effectively identify the target of therapy, the underlying mechanisms that lead to NPC recurrence and metastasis must be clarified.

Emerging evidence substantiated the notion that cancer stem cells (CSCs) or tumor-initiating cells are able to self-renew and regenerate tumor mass. CSCs are refractory to therapy by dint of their quiescent characteristics and expressing ATP-binding cassette transporters [3]. In addition, epithelial-mesenchymal transition (EMT) imparts not only metastasis capacity but also the CSC properties to tumor cells [4, 5]. Thereby, the discovery of potential drugs targeting at CSCs may solve the clinical curative difficulties such as therapeutic resistance, recurrence, and metastasis.

Accumulated evidence has shown that phenolic compounds, such as curcumin, epigallocathechin gallate, and resveratrol, may have potential inhibitory effects on CSCs and prevent tumor invasion and metastasis [6–9]. Among natural polyphenols, resveratrol (3,5,4′-trihydroxy-trans-stilbene) is present mostly in red wine that has pharmacological properties including antiaging, anti-inflammation, and antitumor capacity. Recent studies revealed that resveratrol induced NPC cells apoptosis through activating multiple apoptotic pathways [10]. Furthermore, resveratrol also inhibited CSC properties in pancreatic cancer, breast cancer, and glioblastoma [11–13]. Resveratrol could efficiently suppress the invasion and metastasis of tumor cells through reversing the EMT process in lung and breast cancers [14, 15]. It also reduced the self-renewal capacity and stemness gene signatures of CSCs in head and neck cancers [9].

However, the mechanisms pertaining to resveratrol mediated signaling pathways in CSCs remained unclear. In this study, we aimed to use NPC CSCs as a model to dissect the regulation of resveratrol in stemness, EMT, and metabolic signatures of CSCs and to explore the potential therapeutic targets in NPC CSCs.

2. Material and Methods

2.1. Cell Culture. Three human NPC cell lines, TW01, TW06, and HONE-1, were used in this study [16, 17]. All NPC cell lines were cultured in complete Dulbecco's Modified Eagle Medium (DMEM), supplemented with 1% sodium pyruvate, 1% nonessential amino acids, 1% of penicillin-streptomycin, and 10% fetal bovine serum (FBS) (Invitrogen, Carlsbad, CA) at 37°C with humidified 5% CO_2.

2.2. CSC Behavior Selection. To acquire high ratio of CSCs from NPC cell lines, we developed a behavior selection method according to CSC's characteristics. The parental cells would be selected through irradiation treatment, sphere formation and side population serially. Firstly, irradiation selection was performed as described previously [18]. Radioresistant clones were established after four rounds of 11 Gy irradiation at 37.9 mGy/s using Rad Source RS 2000 X-ray biological irradiator (Rad Source Technologies, Inc., Suwanee, GA). The radioresistant capacity of these cells was measured by clonogenic assay. Total of 5×10^3 cells were seeded and treated with 10 Gy irradiation. After 10 days, colonies were fixed with 3 : 1 ratio of methanol and glacial acetic acid, stained with 2% crystal violet, and counted under a phase-contrast microscope. After the radioresistant phenotype was corroborated, the selected radioresistant cells were then proceed to tumor sphere selection. Tumor sphere selection was performed as described previously [19]. Cells were seeded into 0.4% soft agar coated petri dish with serum-free DMEM. The soft surface rendered the cells unable to attach and formed tumor spheres after 10 days. Finally, CSCs were isolated with side population selection by using cells from tumor spheres. Side population assay was performed as described previously [20]. Briefly, cell concentration was adjusted to 10^6 cells/mL with DMEM medium supplemented with 2% FBS and then treated with Hoechst 33342 (5 μM, Sigma-Aldrich) and incubated in a 37°C incubator for 90 min. After twice wash with PBS, propidium iodide (PI) (2 μg/mL, Sigma-Aldrich) was added to exclude dead cells. Cells were kept at 4°C in the dark before sorting by BD FACSAria flow cytometer (BD Biosciences, San Jose, CA). The side population gating requires control experiments with the ATP-binding cassette (ABC) transporter inhibitor. As a control, cells were incubated with fumitremorgin C (FTC, 10 μM, Sigma-Aldrich) for 30 min at 37°C prior to and during Hoechst dye staining. FTC would block the ABC transporters from extruding Hoechst dye. The side population cells would exhibit high fluorescence when treated with FTC to block the efflux of Hoechst dye. We then compared the pattern with or without the treatment of FTC to define and isolate side population cells.

2.3. Survival Fraction Analysis. Survival fractions were performed by comparing the number of survival colonies of the control with the test samples under resveratrol treatment (10, 25, and 50 μM, Sigma-Aldrich) and irradiation treatment (2, 4, 6, 8, 10, and 12 Gy), respectively. Surviving fraction was calculated using the number of colonies divided by the number of cells seeded and corrected with the plating efficiency. Plating efficiency was calculated by dividing the number of colonies with the number of cancer cells seeded.

2.4. Soft Agar Assay. The plates were decoated with 1.2% soft agar as a base. After the agar solidified, 1×10^4 cells with or without 50 μM resveratrol treatment were mixed with 0.4% soft agar and seeded on the base. The colonies grown in soft agar with diameters >500 μm were counted after two weeks.

2.5. Wound Healing Migration Assay. We utilized ibidi culture inserts (ibidi GmbH, Munich, Germany) for wound healing migration assay and performed according to the manufacture's protocol. The insert contains two reservoirs separated by a 500 μm thick wall. We placed the culture insert into a 24-well culture plate and added 1×10^4 cells with or without 50 μM resveratrol treatment into each reservoir for overnight culture. A 500 μm gap was created after removing culture insert. The images of cell migration were captured by a Dino-Lite microscope eye-piece camera (Dino-Lite, Naarden, Netherlands).

2.6. Invasion Assay. For invasion assay, we placed Millicell invasion chamber (8 μm pore size, Millipore, Darmstadt, German) with Matrigel (BD Biosciences) into a 24-well plate. In the upper compartment of the invasion chamber, 1×10^4 cells were seeded and filled with 200 μL serum-free DMEM and 50 μM resveratrol. In the lower compartment of the invasion chamber, 600 μL complete DMEM with 10% FBS was added. After 24 hours incubation, the invasive cells located on the underside of the filter were fixed with 3 : 1 ratio of methanol and glacial acetic acid, stained with 2% crystal violet, and counted under a phase-contrast microscope.

2.7. Real-Time RT-PCR Analysis. Total RNA was extracted with TRIsure reagent (Bioline Reagents Ltd., London, UK). The concentration and purity of total RNA was determined by NanoDrop ND-1000 Spectrophotometer (NanoDrop Technologies, Inc., Wilmington, DE). Real-time PCR was performed using the SensiFAST SYBR Hi-ROX Kit (Bioline) on the ABI StepOnePlus Real-Time PCR machine (Applied Biosystems, Foster City, CA). The primer sequences used in this study were the same as those described previously [8, 21, 22].

2.8. Antibodies for Western Blotting and Immunofluorescence Staining. Antibodies such as anti-α-tubulin (1 : 5000, Abcam, Cambridge, MA), anti-actin (1 : 5000, Millipore, Darmstadt, German), anti-Oct3/4 (1 : 1000, Bioworld Technology, Suffolk, UK), anti-E-cadherin (1 : 5000, BD Biosciences), anti-vimentin (1 : 1000, Sigma-Aldrich), anti-p53 (1 : 1000, Millipore), and anti-phospho-p53 (Ser15) (1 : 1000, Cell Signaling, Boston, MA) were used for western blotting and immunofluorescence staining. Western blotting and immunofluorescence staining were performed as described previously [8].

2.9. Plasmids, Virus Production, and Infection. Human p53 cDNA was subcloned into pEZ-Lv201-puro lentiviral vector (GeneCopoeia, Rockville, MD, USA). p53 shRNA was cloned in pLKO.1-based lentiviral vector provided by the National RNAi Core Facility, Academia Sinica, Taiwan. We chose the p53 shRNA with the best knockdown efficiency to do further experiment from four p53 shRNAs targeted against different regions of p53. EGFP was cloned into the pAS2-puro-based lentiviral vector provided by the National RNAi Core Facility, Academia Sinica, Taiwan. Utilizing PolyJet DNA *In Vitro* Transfection Reagent (SignaGen Laboratories, Rockville, MD), 293T cells were transfected with viral vectors. The virus-containing supernatant of transfectant was filtered through a 0.45 μm pore size filter 2 days after transfection. Viral infection was achieved by adding virus-containing supernatant supplemented with 8 ng/mL polybrene. Puromycin selection (5 μg/mL) was subsequently employed 24 hours after infection. After one week of puromycin selection, stable clones were used for further analysis.

2.10. Measurement of Oxygen Consumption Rate. Oxygen consumption rate was measured by the 782 Oxygen Meter (Strathkelvin Instruments, Motherwell, UK). To measure the steady-state oxygen consumption rate of the cells, 1×10^6 cells with or without 50 μM resveratrol treatment were resuspended in 330 μL of assay buffer (125 mM sucrose, 65 mM KCl, 2 mM $MgCl_2$, and 20 mM Na^+-K^+-phosphate buffer, pH 7.2) and transferred to a closed chamber of the oxygen meter. To measure the function of the mitochondrial respiratory chain, we first permeabilized the mitochondrial outer membrane by adding 0.002% ethanol-purified digitonin (Sigma-Aldrich) to the chamber (final concentration: 0.0006%). We then injected 6 μL of succinate into the chamber (final concentration: 20 mM). To assay the efficiency of ATP synthesis, we added 1 mM ADP to the chamber to stimulate the respiration. Oxygen consumption rate was also measured with a Seahorse XF24 extracellular Flux analyzer as described by Qian and Van Houten [23]. Cells were seeded in an XF24 cell culture plate and were allowed to grow for one day. The medium was replaced with unbuffered DMEM and incubated in a 37°C incubator for 30 minutes to stabilize the pH and temperature. The oxygen consumption rate (OCR) represented mitochondrial respiration, and the rate of extracellular acidification (ECAR) indicated the lactate production rate by anaerobic glycolysis.

2.11. Lactate Production Rate. Cells with or without 50 μM resveratrol treatment were washed with PBS and replenished with fresh medium in a 37°C incubator for 5 hours. An aliquot of 10 μL of medium was then transferred to 96-well dishes and mixed with lactate reagent (Trinity Biotech Plc., Bray, Ireland). The absorbance at 540 nm was measured by an ELISA reader (PowerWave^X 340). The lactate production rate was calculated from the absorbance and was normalized by the cell number and incubation time.

2.12. Mitochondrial Membrane Potential ($\Delta\psi m$). Cells with or without resveratrol treatment were trypsinized and incubated with 0.25 μg/mL JC-1 fluorescence dye at 37°C in the dark for 15 minutes. The fluorescence intensities of FL1 and FL2 channels were analyzed with Cytomics FC500 flow cytometer (Beckman Coulter, Fullerton, CA).

2.13. Intracellular Levels of Reactive Oxygen Species (ROS). Cells with or without resveratrol treatment were washed by PBS and incubated with a medium containing 40 μM 2′,7′-dichlorofluorescin diacetate (H_2DCFDA, Invitrogen) at 37°C in the dark for 15 minutes. We then trypsinized the cells and resuspended them in PBS. H_2DCFDA was used for the determination of intracellular H_2O_2. The fluorescence intensity of FL1 channel for H_2DCFDA staining was analyzed with Cytomics FC500 flow cytometer (Beckman Coulter).

2.14. Cell Viability Assay. In the drug treatment experiment, cells were exposed to resveratrol (10, 25, 50, 75, and 100 μM), cisplatin (8 μM, Sigma-Aldrich), or 5-fluorouracil (5-FU; 10 μM, Sigma-Aldrich) for 48 hours. In the irradiation treatment experiment, cells were irradiated (5 Gy or 10 Gy) at 37.9 mGy/s using Rad Source RS 2000 X-ray biological irradiator (Rad Source Technologies, Inc.). After 2 days of culture, cells were washed with PBS, replenished with fresh medium containing 1 × Alamar Blue cell viability assay reagent (AbD Serotec, Oxford, UK), and incubated at 37°C for 2 hours. Fluorescence intensity, with the excitation wavelength at 538 nm and the emission wavelength at 590 nm, was measured using a Fluoroskan Ascent Microplate Fluorometer (Thermo Fisher Scientific, Inc., Waltham, MA).

2.15. In Vivo Analysis of the Tumor Curability by Resveratrol. To monitor the *in vivo* growth of CSCs, we first established the GFP-CSCs by transfecting a pAS2-EGFP-puro expression construct to NPC CSCs. A total of 100 GFP-CSCs were then injected into hypoglossal regions of 7-8-week-old NOD/SCID mice. In the group of resveratrol treatment, we fed mice

with 100 mg/kg resveratrol every 2 days after injecting the CSCs. The incidence of tumor growth was measured after 2 weeks. The mice were sacrificed, and the distribution of GFP-positive tumors was observed through Youlum Sky-blue II epifluorescent light (Youlum Inc., New Taipei City, Taiwan).

2.16. Statistical Analysis. All data are presented as mean ± SD. Statistical analysis was performed by using Student's t-test and a difference between groups with $P < 0.05$ is considered significant.

3. Results

3.1. NPC CSCs Exhibit Characteristics of Stemness, EMT, and Metabolic Reprogramming. The most common methods used to isolate CSCs focus on single CSC ability, such as side population or tumor sphere. To improve upon these current methods, we combined irradiation selection, tumor sphere selection, and side population selection to isolate CSCs. The three methods overlapped to form a bull's eye area where purity of CSCs may be the highest (Figure 1(a)). We started with establishing NPC radioresistant clones (Figure 1(b)) by four rounds of high-dose irradiation selection. Several radioresistant NPC clones were established. These radioresistant clones underwent tumor sphere selection and displayed higher tumor sphere formation capacity compared with parental cells (Figure 1(c)). The percentage of side population is greatly higher in tumor sphere cells than that in parental cells (Figure 1(d)). It signified that irradiation selection can increase the feasibility to obtain CSC-like cells as compared with the feasibility of isolating CSC-like cells directly from parental cells merely by tumor sphere or side population selection. Following behavior selection, the CSC clones became resistant to radiotherapy and chemotherapy and capable of forming tumor spheres. Stemness-related transcription factor Oct4 was expressed and translocated from cytoplasm to the nucleus of isolated CSCs (Figure 2(a)). This implied that nuclear Oct4 might activate its target genes and result in stem cell-like features of CSCs. CSCs also underwent an EMT with downregulation of epithelial marker E-cadherin and concomitant upregulation of mesenchymal marker vimentin (Figures 2(b) and 2(c)). CSCs manifested greater migratory capacity than did parental NPC cells (Figure 2(d)). To know the metabolic characteristics, we then investigated the organelle function of NPC CSCs. The O_2 consumption rates driven by ADP and succinate were lower in CSCs compared with those in parental NPC cells (Figure 2(e)), which implied that these CSCs might not rely on mitochondrial respiration to produce energy. Likewise, CSCs excreted higher levels of lactic acid as a by-product than did parental NPC cells (Figure 2(f)). Moreover, the level of prooxidants was relatively lower in CSCs compared with parental NPC cells through analysis of intracellular H_2O_2 with H_2DCFH-DA (Figure 2(g)). These findings revealed that CSCs displayed unique metabolic signatures similar to those of stem cells.

3.2. Resveratrol Suppresses the Stemness, EMT, and Metabolic Reprogramming in CSCs. The versatile efficacy of resveratrol on NPC CSCs was unraveled in this study. We first evaluated the sensitivity of parental cells or CSCs under different concentrations of resveratrol treatment. Cell viability was significantly affected if the concentration of resveratrol was higher than 50 μM in parental cells or CSCs (Figure 3(a)). We then mainly used 50 μM resveratrol in following assays. Resveratrol could suppress the long-term self-renewal and antianoikis capacity (Figure 3(b)) and *in vitro* tumorigenicity (Figure 3(c)). Resveratrol also significantly reduced the percentage of side population (Figure 3(d)) and migration and invasion capacity in CSCs (Figures 3(e) and 3(f)). Combining irradiation with resveratrol increased the radiosensitivity of CSCs which suggested that resveratrol could potentially serve as an irradiation sensitizer (Figure 3(g)). In addition, resveratrol diminished the expression of genes characteristic of stemness, EMT, and metabolism (Figure 3(h)). Downregulation of stemness-related genes such as Oct4, Sox2, Klf4, c-Myc, Nanog, and Lin28 depicted that resveratrol compelled the differentiation of CSCs. Under resveratrol treatment, ABCG2 suppression also increased the drug sensitivity of CSCs. In addition, resveratrol reversed the EMT phenotype of CSCs by inhibiting the expression of EMT regulators and mesenchymal markers, such as Twist, Snail, Zeb1, vimentin, and fibronectin; on the contrary, epithelial marker E-cadherin was increased. Moreover, downregulation of pyruvate dehydrogenase kinase (PDK), a negative regulator of pyruvate dehydrogenase (PDH), promoted pyruvate back to mitochondrial biosynthetic pathways in CSCs. As expected, increased O_2 consumption and decreased lactate production demonstrated that resveratrol reversed the metabolic shift in NPC CSCs (Figures 4(a) and 4(b)). Resveratrol also significantly increased the ROS level and depolarized mitochondrial membranes in CSCs especially under irradiation treatment (Figures 4(c) and 4(d)).

3.3. Resveratrol Impedes CSC Properties through p53 Activation. We found that p53 expression level was lower in CSCs than that in parental cells (Figure 5(a)). Furthermore, the mesenchymal cell shape of CSCs was reversed to epithelial type concomitant with the activation of p53 (phosphorylated at serine 15) after resveratrol treatment (Figures 5(a) and 5(b)). To confirm the idea that resveratrol could suppress the CSC properties directly through the induction of p53, we modulated the expression of p53 in CSCs by infecting a lentivirus-based full-length p53 clone and shRNAs targeting p53, respectively (Figures 5(c) and 5(d)). We then measured the oxygen consumption rate (OCR) and extracellular acid efflux rate (ECAR) of these CSCs by a Seahorse XF24 Extracellular Flux Analyzer. OCR is an indicator of mitochondrial respiration, and ECAR is predominantly a measure of lactic acid production rate during glycolysis. Similar to the effects of resveratrol, overexpression of p53 increased the OCR/ECAR ratio in CSCs; knockdown of p53 reduced the OCR/ECAR ratio during resveratrol treatment (Figure 6(a)). These data substantiated the notion that resveratrol altered the energy metabolism mainly by induction of p53. Remarkably, suppression of tumor sphere formation and soft agar colony formation achieved by resveratrol treatment could be rescued

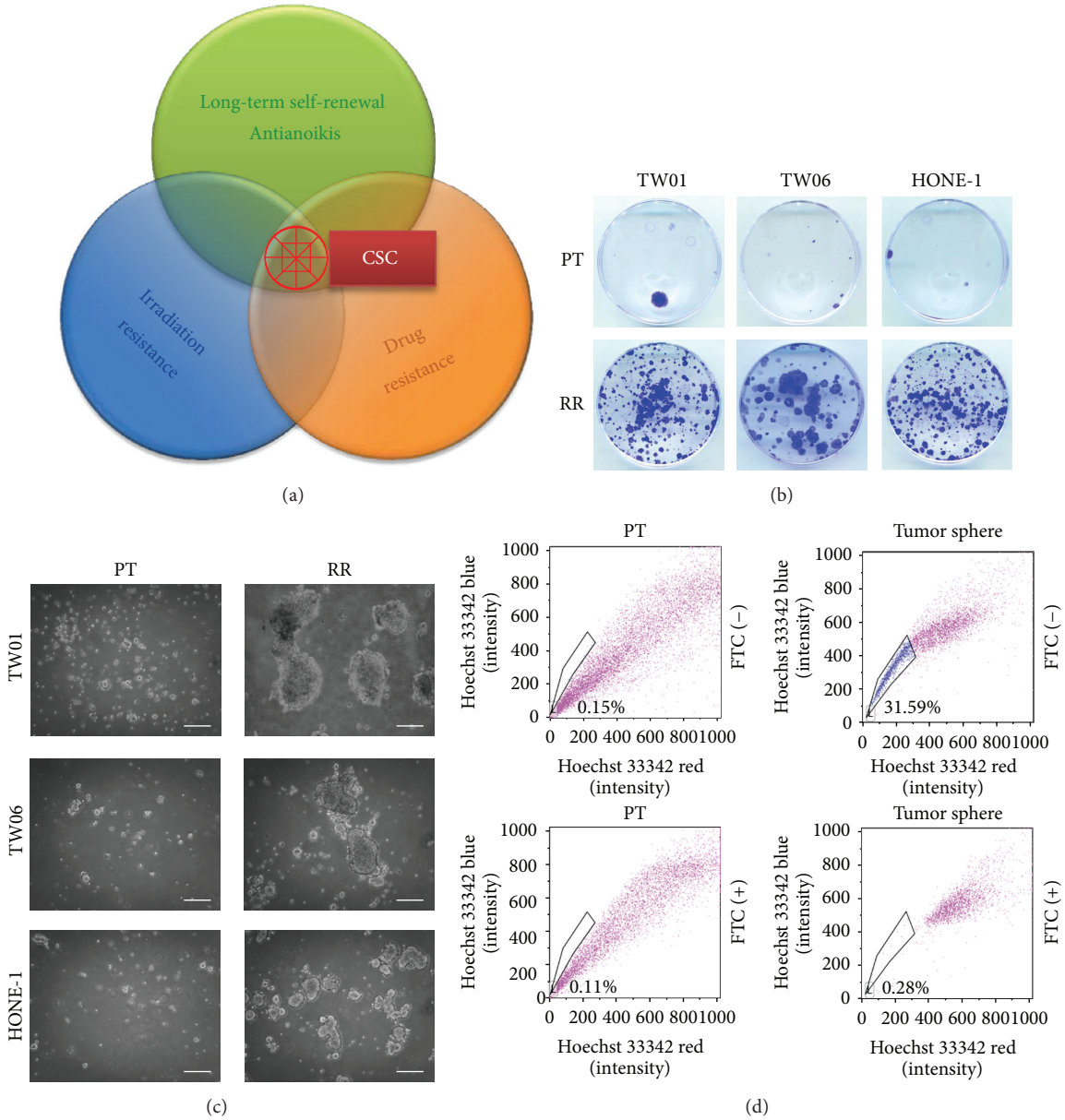

Figure 1: The concept and process validation of NPC CSC isolation achieved by behavior selection. (a) The concept of behavior selection is based on CSC properties, which are resistance to irradiation and drugs, long-term self-renewal, and antianoikis. Through the behavior selection platform, abundant and high-purity CSCs could be obtained. (b) After four rounds of 11 Gy irradiation selection, radioresistant clones (RR) of TW01, TW06, and HONE-1 were established. Further colony formation assays of these radioresistant cells and parental cells (PT) were performed with seeding 5×10^3 cells after 10 Gy irradiation. Representative images are macroscopically visible survival colonies after fixation and crystal violet staining. Radioresistant cells show distinct radioresistant phenotype. (c) After irradiation selection, tumor sphere selection was performed. Compared with parental cells, radioresistant clones could generate more and larger spheres. Scale bars indicate 100 μm. (d) Side population assay shows that TW01 parental cells (left panel) contained less side population cells compared with tumor sphere cells (right panel). The top panel represents the cells incubated with Hoechst 33342. A subset of side population cells pumped out of the Hoechst dye by ABC transporters and demonstrated low fluorescence expression. The bottom panel shows that the gating proportion is reduced from 0.15% to 0.11% in parental cells and from 31.59% to 0.28% in tumor sphere cells after fumitremorgin C (FTC) treatment. FTC can block the ABC transporters and result in full side population efflux inhibition.

by knocking down p53 (Figures 6(b) and 6(c)). Moreover, the sensitivity to irradiation and chemotherapeutic agents induced by resveratrol could be blocked by knocking down p53 (Figures 6(d) and 6(e)). Invasive capacity was also found to be derepressed after p53 knockdown in resveratrol-treated CSCs (Figure 6(f)). As anticipated, resveratrol and p53 overexpression reduced the expression of stemness and EMT, while the silencing of p53 restored the expression of

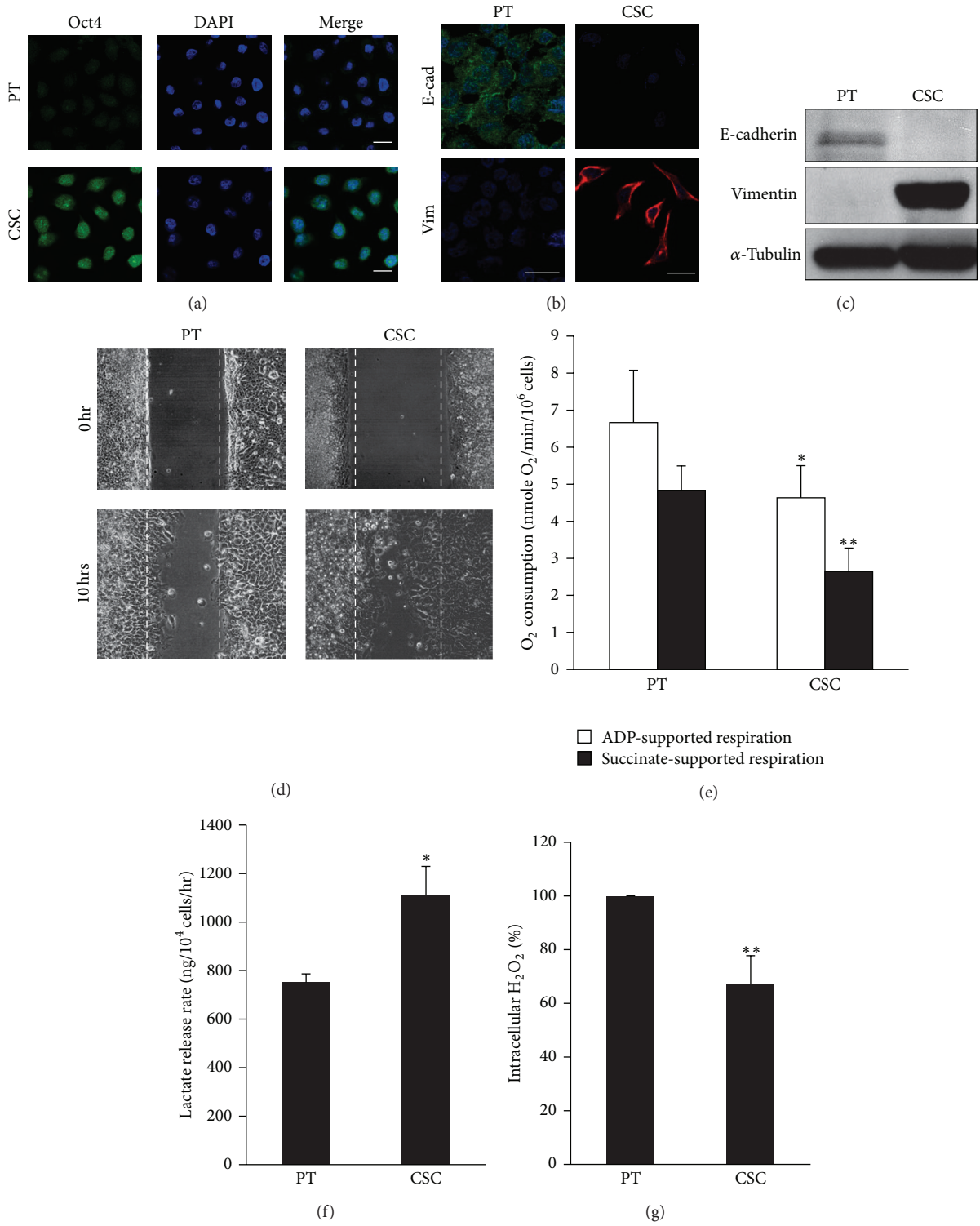

FIGURE 2: NPC CSCs manifested characteristics of stemness, EMT, and metabolic reprogramming. (a) Images of immunofluorescence staining for Oct4 expression show overexpression and nuclear translocation of Oct4 in TW01 CSCs compared with the negative control of TW01 parental cells. (b) Immunofluorescence staining indicates the transition of epithelial marker (E-cad: E-cadherin) and mesenchymal marker (Vim: Vimentin) in TW01 parental cells and CSCs. Scale bars in (a) and (b) indicate 25 μm. (c) Western blots confirm the EMT of TW01 CSCs at the protein level. (d) Wound healing assay showed higher migratory behavior of TW01 CSCs compared with TW01 parental cells. Full wound closure was observed in TW01 CSCs after 10 hours. (e) The O_2 consumption rates supported by ADP and succinate were lower in TW01 CSCs compared with TW01 parental cells. (f) TW01 CSCs had higher levels of lactate production than did TW01 parental cells. (g) Intracellular H_2O_2 level was relatively lower in TW01 CSCs compared with that in TW01 parental cells measured by H_2DCFDA staining. ($^*P < 0.05$; $^{**}P < 0.01$).

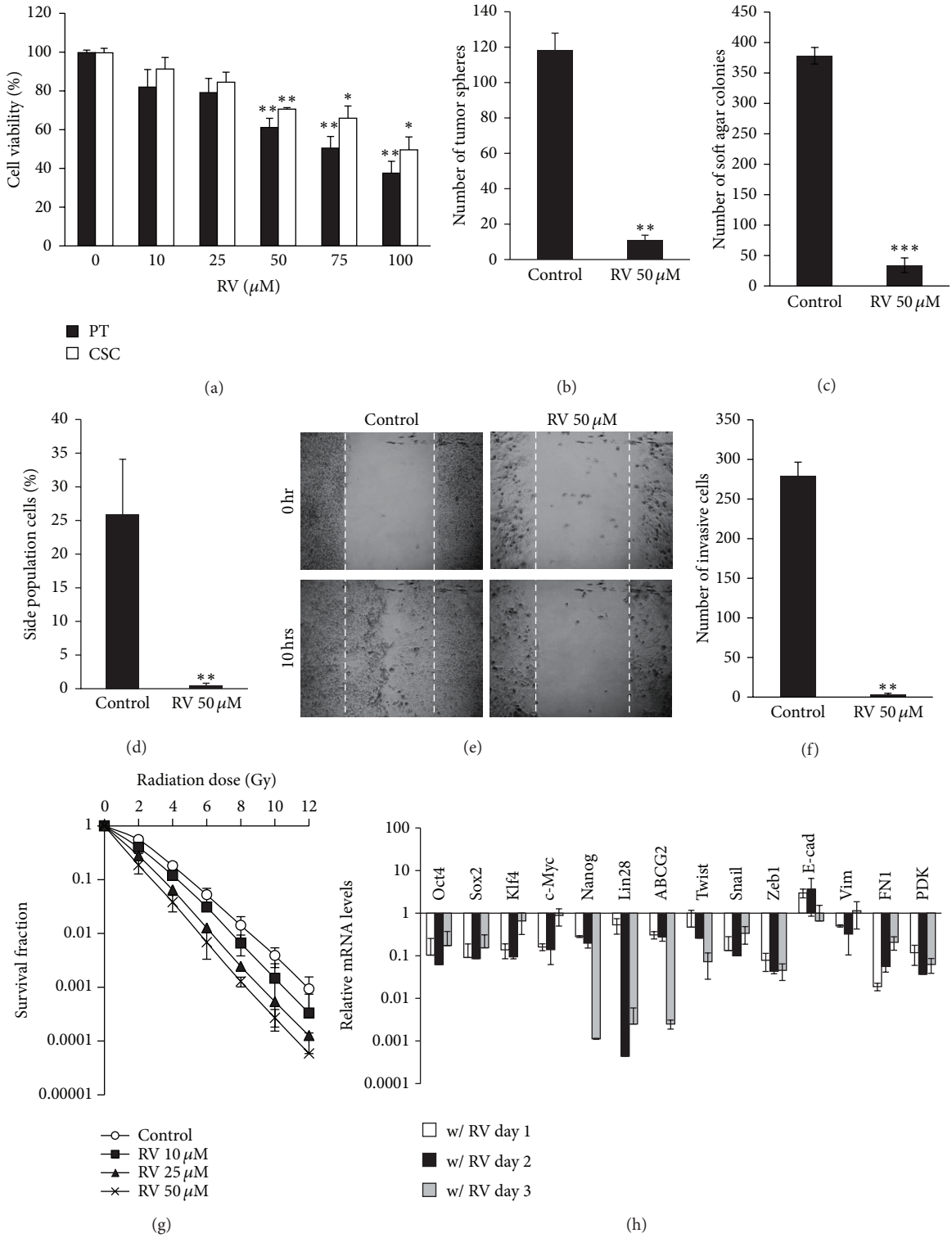

Figure 3: Resveratrol suppressed CSC properties. (a) Evaluation of cytotoxic effects of different concentration of resveratrol (RV) in TW01 parental cells and CSCs. Significant effects are shown with concentration more than 50 μM. Capacities for (b) tumor sphere formation, (c) soft agar colony formation, and (d) percentage of the side population were suppressed in TW01 CSCs after 50 μM resveratrol treatment. (e) Migration capacity analyzed by wound healing assay and (f) invasive capacity measured by transwell invasion assay were suppressed by 50 μM resveratrol in TW01 CSCs. (g) Resveratrol could increase the radiosensitivity of TW01 CSCs in a concentration-dependent manner measured by survival fraction assay. (h) Resveratrol (50 μM) altered the expression of indicated genes in TW01 CSCs. E-cad: E-cadherin; N-cad: N-cadherin; Vim: vimentin; FN1: fibronectin 1; PDK: pyruvate dehydrogenase kinase. Data were normalized with the mRNA expression level of 18*S* rRNA and compared with those of TW01 CSCs without resveratrol treatment on a log scale. ($^{*}P < 0.05$; $^{**}P < 0.01$; $^{***}P < 0.001$).

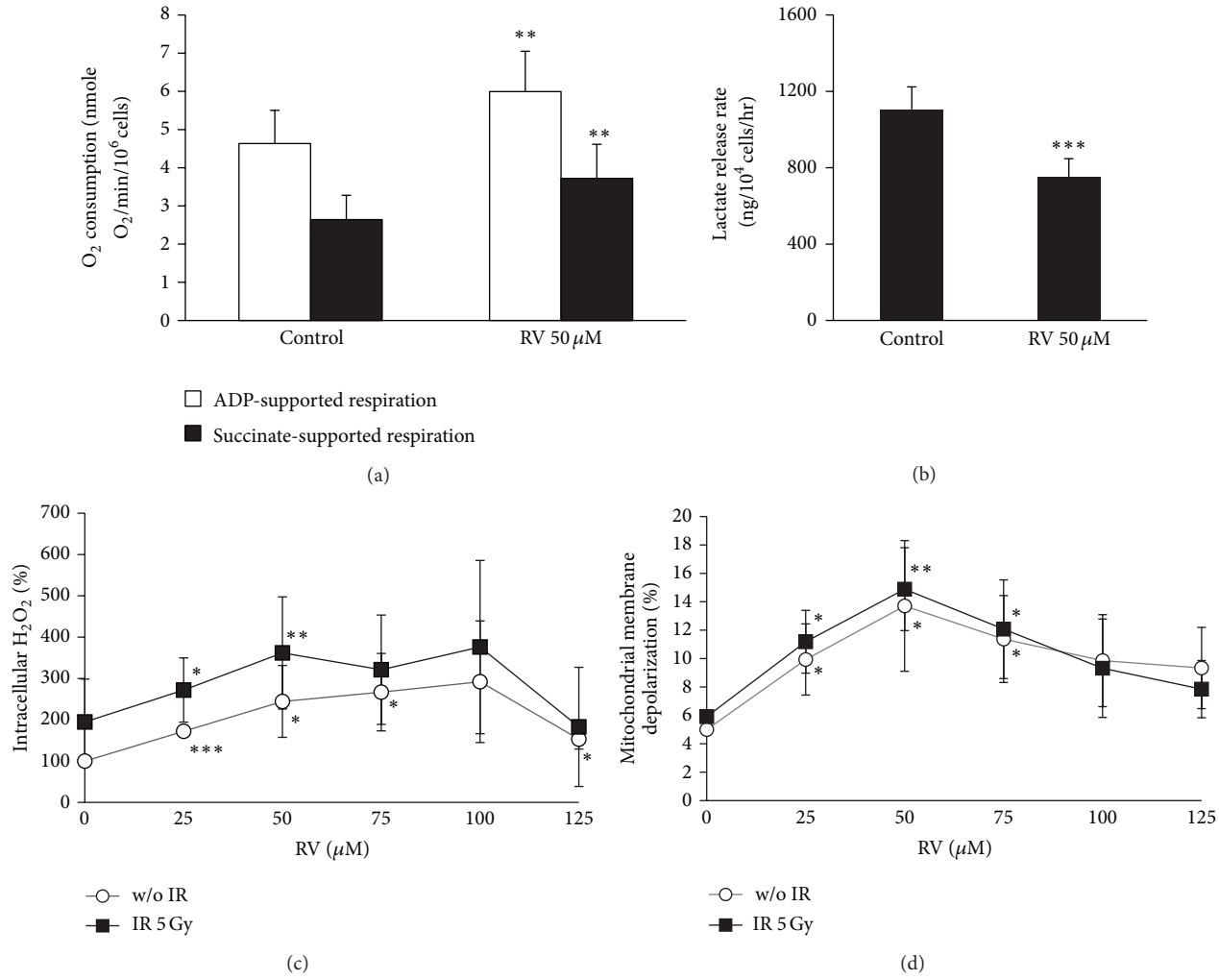

FIGURE 4: Resveratrol could reverse the metabolic reprogramming of CSCs. (a) Resveratrol (50 μM) increased O_2 consumption and (b) repressed the lactate production of TW01 CSCs. (c) Intracellular H_2O_2 was upregulated in TW01 CSCs exposed to serial doses of resveratrol and 5 Gy irradiation (IR) measured by H_2DCFDA staining. (d) Serial doses of resveratrol depolarized the mitochondrial membrane in TW01 CSCs with or without 5 Gy irradiation. The percentage of mitochondrial membrane potential depolarization was measured by the JC-1 green fluorescence shift. In (c) and (d) charts, TW01 CSCs with resveratrol treatment were compared with those of TW01 CSCs without resveratrol treatment. TW01 CSCs with both resveratrol and irradiation treatment were compared with those of TW01 CSCs with irradiation but without resveratrol treatment. ($^*P < 0.05$; $^{**}P < 0.01$; $^{***}P < 0.001$).

stemness and EMT in resveratrol-treated CSCs (Figures 6(g) and 6(h)). In addition, we noticed that miR-145 and miR-200c were downregulated in CSCs but could be upregulated by resveratrol treatment and p53 overexpression (Figure 6(i)). The upregulation of miR-145 and miR-200c could be attenuated by knockdown of p53 in resveratrol-treated CSCs (Figure 6(i)).

3.4. Resveratrol Annihilates CSCs in NOD/SCID Mice. Lastly, we examined the curative effect of resveratrol *in vivo*. We injected GFP-CSCs into the hypoglossal region of NOD/SCID mice. The mouse without resveratrol feeding was asthenic in appearance, lost their body weight gradually, and tumor lumps disseminated around the bottom of buccal mucosa (Figures 7(a) and 7(b)). By *in vivo* GFP tracking, we observed that tumor grew throughout the tongue and lower jaw of the mice without resveratrol treatment (Figure 7(c)). The CSCs were finally eradicated, and the mice stayed healthy when the mice fed with a diet supplemented with resveratrol (Figure 7(d)).

4. Discussion

Metabolism has been the focus of cancer research as early as the 1920s, when Otto Warburg observed that malignant tissues produce energy predominately by glycolysis rather than oxidative phosphorylation (OXPHOS) even when oxygen is plentiful [24]. This metabolic shift from aerobic metabolism to glycolysis also occurs in embryonic stem cells (ESCs) and induced pluripotent stem cells (iPSCs) [25]. Similar

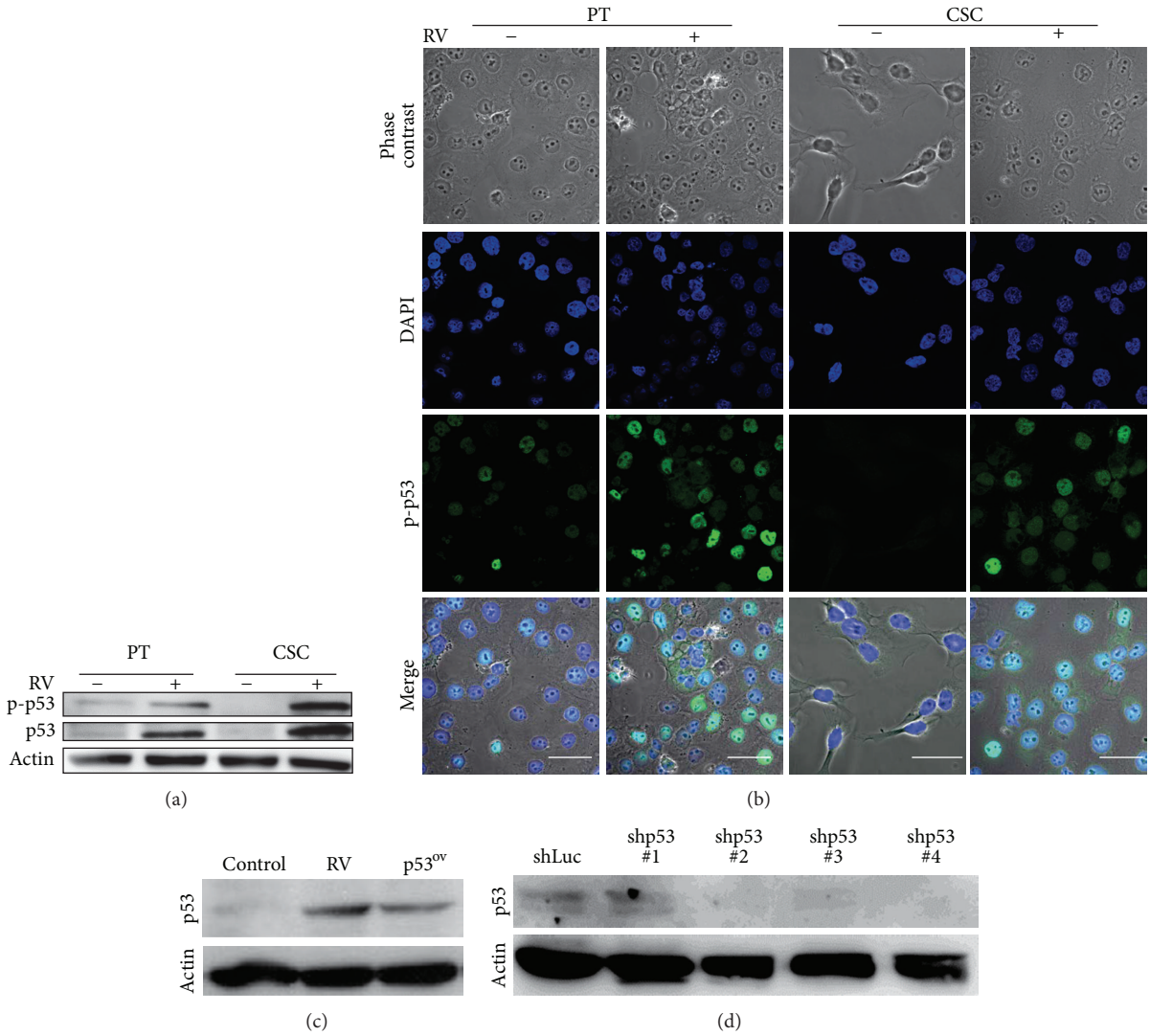

Figure 5: Resveratrol impeded EMT through p53 activation in CSCs. (a) Expressions of p53 and phosphorylated p53 (Ser15) were lower in TW01 CSC than those in TW01 parental cells. Resveratrol could increase expression of p53 and phosphorylated p53 expression both in CSC and parental cells. (b) Resveratrol (50 μM) reactivated p53, indicated by the translocation of phosphorylated p53 (Ser15) from cytoplasm to the nucleus (detected with DAPI staining), and repressed the EMT phenotype in TW01 CSCs. TW01 parental cells remained epithelial type after resveratrol treatment. Scale bars indicate 40 μm. (c) Western blot indicated the p53 expression of TW01 CSCs with 50 μM resveratrol treatment (RV) or p53 overexpression ($p53^{ov}$). (d) Western blot confirmed the p53 knockdown efficiency in TW01 CSCs. shp53#2 with the best knockdown efficiency was chose for further experiment.

to normal stem cells, breast CSCs contain a lower level of ROS compared with nontumorigenic cancer cells [26]. To date, the metabolic signatures of CSCs remain largely unknown. Our findings revealed that CSCs, like normal stem cells, underwent metabolic shift from aerobic metabolism to anaerobic glycolysis (Figures 2(e) and 2(f)). Moreover, the levels of ROS were lower in NPC CSCs that may result in radioresistance as previously reported in breast CSCs (Figures 1(b) and 2(g)).

Abundant evidence has been accumulated to substantiate the anticancer activities of resveratrol in various human cancers [27–30]. We found that resveratrol could turn off the metabolic switch, increased the ROS level, and depolarized mitochondrial membranes in NPC CSCs (Figure 4). These alterations in metabolism occurred concomitantly with the suppression of the CSC properties including the resistance to radiotherapy and chemotherapy, self-renewal capacity, tumor initiation capacity, and metastatic potential in NPC CSCs (Figure 3). Particularly worth mentioning is that resveratrol tackled the nexus of NPC CSCs which resulted in extensive suppression of stemness, EMT, and metabolism-related genes (Figure 3(h)). This extensive suppression in CSCs could also be observed after we had ectopically expressed p53, the downstream target of resveratrol (Figure 6). In addition, the suppression of CSC properties by resveratrol could be attenuated by knocking down p53 (Figure 6). These findings

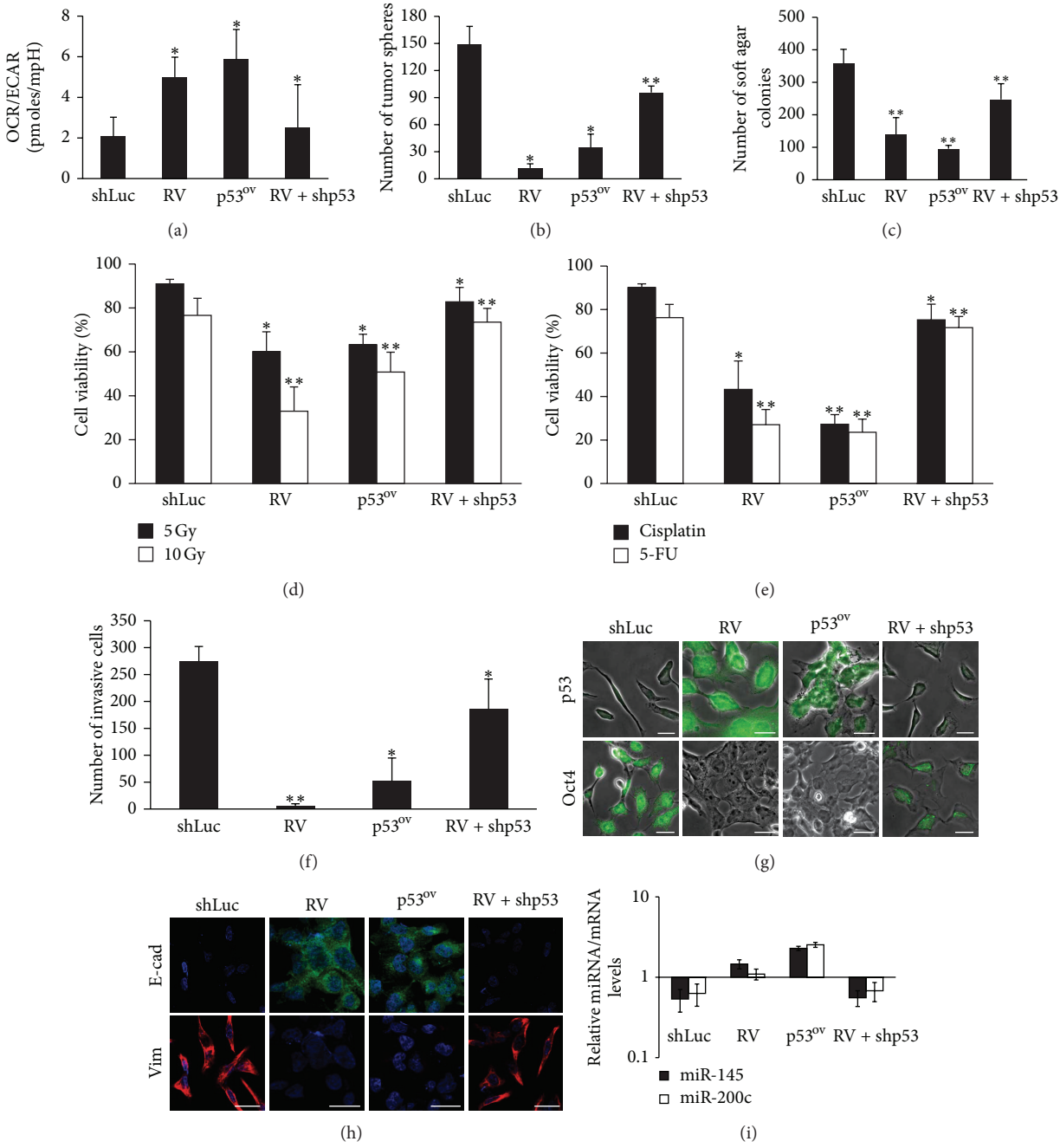

Figure 6: Loss of p53 expression reversed the effects of resveratrol on CSCs. Resveratrol and p53 overexpression had similar effects on TW01 CSCs in (a) OCR/ECAR ratio measurement, (b) tumor sphere formation assay, (c) soft agar assay, (d) cell viability assay under 5 Gy and 10 Gy irradiation, (e) cell viability assay under cisplatin (8 μM) and 5-fluorouracil (5-FU; 10 μM) treatment, and (f) invasive capacity assay. Repressing p53 expression diminished resveratrol effects. (g) Resveratrol and p53 overexpression suppressed Oct4 expression in TW01 CSCs. Loss of p53 expression reversed the effects of resveratrol. (h) Similarly, resveratrol and p53 overexpression reversed EMT process with increased E-cadherin (E-cad) and decreased vimentin (Vim) expression. Loss of p53 expression reversed the effects of resveratrol. Scale bars in (g) and (h) indicate 25 μm. (i) Upregulation of miR-145 and miR-200c was detected in resveratrol-treated and p53 overexpressed CSCs. Blocking p53 expression could reverse their expressions. Results were normalized with *RNU6B* and compared with that in TW01 parental cells. (shLuc: CSCs with shLuc as a control; RV: CSCs with resveratrol treatment; $p53^{ov}$: CSCs with p53 overexpression; RV + shp53: resveratrol-treated CSCs with p53 knockdown; RV group and $p53^{ov}$ group were compared with shLuc group; RV + shp53 group was compared with RV group; $^{*}P < 0.05$; $^{**}P < 0.01$).

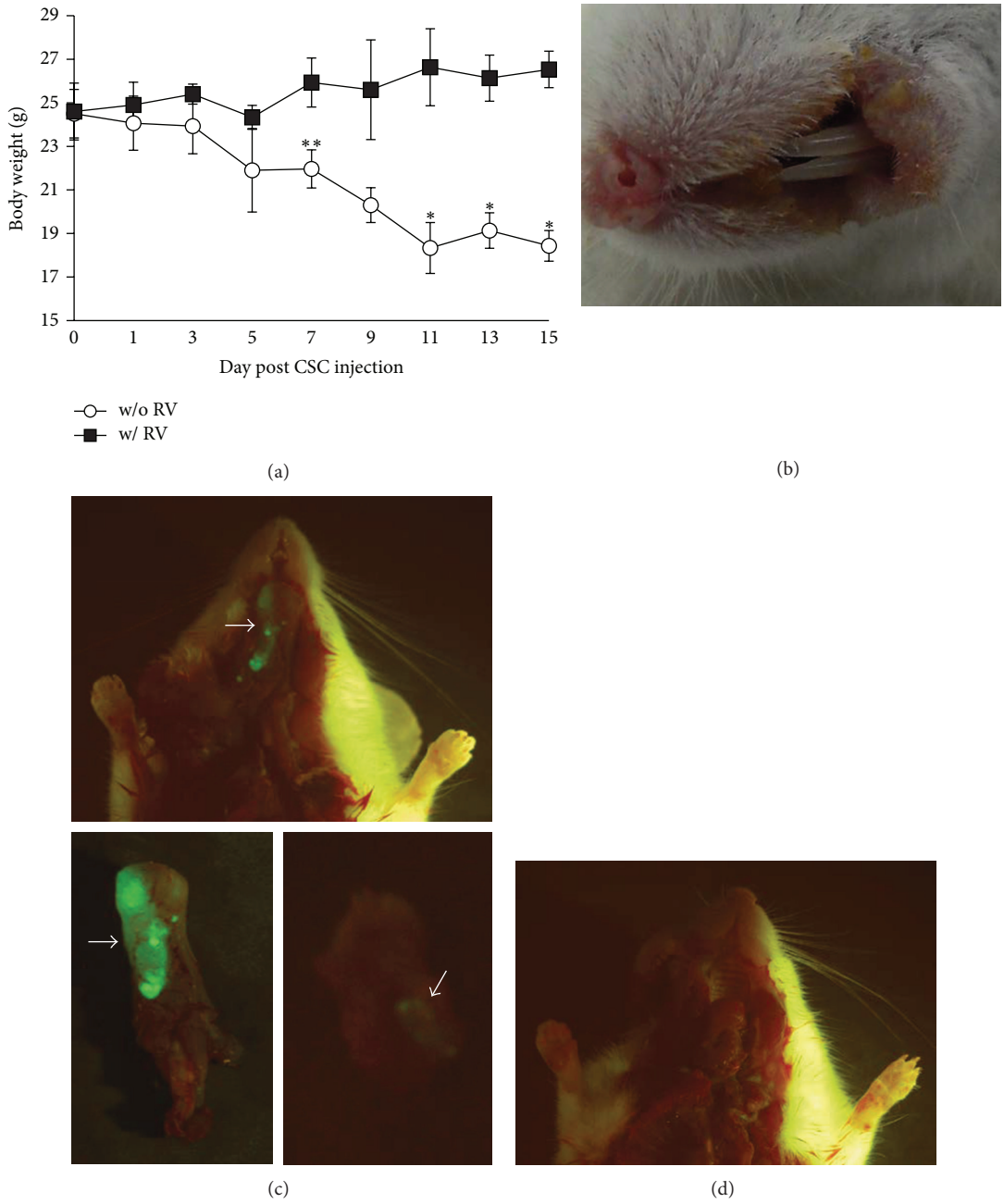

FIGURE 7: Resveratrol suppressed the *in vivo* growth of CSCs. (a) Mice without resveratrol feeding (w/o RV) were 6 g thinner in body weight as compared with the mice with resveratrol feeding (w/ RV) after 2 weeks. (b) By hypoglossal injection and without resveratrol feeding, the indurate tumor lumps disseminated around NOD/SCID mouse's buccal mucosa after two weeks. (c) By hypoglossal injection and without resveratrol feeding for two weeks, GFP-lentivirus-infected TW01 CSCs grew throughout the tongue (bottom left) and lower jaw (bottom right) of the mouse, as seen under a Sky-blue II epifluorescent light (tumor size 50–270 mm^3). (d) As seen under a Sky-blue II epifluorescent light, TW01 CSCs were eradicated in the hypoglossal region of the mouse tube-fed with resveratrol after two weeks. ($^{**}P < 0.05$; $^{**}P < 0.01$).

substantiated the notion that p53 may serve as a common link between metabolism, stemness, and EMT in CSCs.

It was reported that resveratrol can increase the p53 protein level in breast cancer cell line without altering the p53 mRNA levels, suggesting that resveratrol may still be useful to treat tumors with a loss of normal p53 function [31]. Besides, resveratrol could significantly activate intracellular Notch-1 and restore wild-type p53 expression in glioblastoma cells [32]. These findings indicate that resveratrol may be an effective drug for treatment of tumors without normal p53 function.

Recent studies have revealed a connection between p53 and stem cell biology, which signified the importance of p53 pathway in CSCs [33, 34]. Several studies indicated that

p53 pathway decreases the efficiency of reprogramming of somatic cells to iPSCs [35–39]. The absence of p53 allows the suboptimal cells to become iPSCs and also accelerates nuclear reprogramming by loss of p53-dependent cell cycle arrest. The iPSCs with functional p53 were able to form teratoma which differentiated into three germ layers. However, the absence of p53 seemed to be the tradeoff between reprogramming efficiency and tumorigenesis. The teratoma of iPSCs with p53 knockout or a mutation in p53 contained undifferentiated tissue cells which resembled tumor growth [35]. Besides, p53 could control the MDM2-mediated slug degradation [40] and suppress c-Myc through the induction of miR-145 [41]. p53 also could inhibit the expression of CD44 by modulating miR-34a in prostate CSCs [42]. Moreover, p53 was able to launch miR-200c to suppress genes that mediate EMT and stemness properties [43].

These findings suggest that p53 has a significant role in connecting reprogramming to stemness status and tumorigenesis of CSCs. In ESC studies, researchers found that miR-145 suppressed the expression of Oct4, Sox2, and Klf4 [44]. In cancer studies, researchers found that miR-145 could be considered as a tumor suppressor and was downregulated in several cancers including NPC [45]. Since resveratrol-induced p53 is able to transcriptionally activate the expression of miR-145 and miR-200c (Figure 6(i)), the role of p53 in suppressing the stemness and EMT via induction of miRNAs awaits further investigation. Through the elucidation of the p53/miRNAs mechanism, we may be able to apply this regulation in the therapy targeting at CSCs.

5. Conclusions

Thus far, the link between metabolic reprogramming, stemness, and EMT of CSCs has remained elusive. However, this link appears to be of vital importance as uncovered by the aforementioned effects of resveratrol. The regulation of p53 within stemness, EMT, and metabolic reprogramming should be further investigated with the hope that it may lead to the identification of novel therapeutic targets for future anticancer therapies in humans.

Conflict of Interests

The authors proclaim that they have no conflict of interests in conducting this study and publishing the results presented in this paper.

Authors' Contribution

Y. Shen and C. Lin contributed equally to the work.

Acknowledgments

This study was financially supported by Grants from the National Science Council, Taiwan (NSC96-2320-B-010-035-MY2, NSC99-2314-B-010-006-MY3, and NSC100-2320-B-010-024-MY3), the Department of Health, Taipei City Hospital (Grant no. 10001-62-030), the Ministry of Education for a Grant of Aim for the Top University Plan to the National Yang-Ming University. The authors thank the technical support provided by the Microarray & Gene Expression Analysis Core Facility of the National Yang-Ming University (NYMU) VGH Genome Research Center. The Gene Expression Analysis Core Facility is supported by the National Research Program for Genomic Medicine, National Science Council.

References

[1] K. W. Lo, K. F. To, and D. P. Huang, "Focus on nasopharyngeal carcinoma," *Cancer Cell*, vol. 5, no. 5, pp. 423–428, 2004.

[2] Y. Bensouda, W. Kaikani, N. Ahbeddou et al., "Treatment for metastatic nasopharyngeal carcinoma," *European Annals of Otorhinolaryngology, Head and Neck Diseases*, vol. 128, no. 2, pp. 79–85, 2011.

[3] M. T. Mueller, P. C. Hermann, and C. Heeschen, "Cancer stem cells as new therapeutic target to prevent tumour progression and metastasis," *Frontiers in Bioscience*, vol. 2, pp. 602–613, 2010.

[4] S. A. Mani, W. Guo, M. J. Liao et al., "The epithelial-mesenchymal transition generates cells with properties of stem cells," *Cell*, vol. 133, no. 4, pp. 704–715, 2008.

[5] M. Ksiazkiewicz, A. Markiewicz, and A. J. Zaczek, "Epithelial-mesenchymal transition: a hallmark in metastasis formation linking circulating tumor cells and cancer stem cells," *Pathobiology*, vol. 79, no. 4, pp. 195–208, 2012.

[6] D. Fong, A. Yeh, R. Naftalovich, T. H. Choi, and M. M. Chan, "Curcumin inhibits the side population (SP) phenotype of the rat C6 glioma cell line: towards targeting of cancer stem cells with phytochemicals," *Cancer Letters*, vol. 293, no. 1, pp. 65–72, 2010.

[7] S. N. Tang, C. Singh, D. Nall, D. Meeker, S. Shankar, and R. K. Srivastava, "The dietary bioflavonoid quercetin synergizes with epigallocathechin gallate (EGCG) to inhibit prostate cancer stem cell characteristics, invasion, migration and epithelial-mesenchymal transition," *Journal of Molecular Signaling*, vol. 5, article 14, 2012.

[8] C. H. Lin, Y. A. Shen, P. H. Hung, Y. B. Yu, and Y. J. Chen, "Epigallocathechin gallate, polyphenol present in green tea, inhibits stem-like characteristics and epithelial-mesenchymal transition in nasopharyngeal cancer cell lines," *BMC Complementary and Alternative Medicine*, vol. 12, no. 201, pp. 1–12, 2012.

[9] F. W. Hu, L. L. Tsai, C. H. Yu et al., "Impairment of tumor-initiating stem-like property and reversal of epithelial-mesenchymal transdifferentiation in head and neck cancer by resveratrol treatment," *Molecular Nutrition & Food Research*, vol. 56, no. 8, pp. 1247–1258, 2012.

[10] T. T. Huang, H. C. Lin, C. C. Chen et al., "Resveratrol induces apoptosis of human nasopharyngeal carcinoma cells via activation of multiple apoptotic pathways," *Journal of Cellular Physiology*, vol. 226, no. 3, pp. 720–728, 2011.

[11] S. Shankar, D. Nall, S. N. Tang et al., "Resveratrol inhibits pancreatic cancer stem cell characteristics in human and KrasG12D transgenic mice by inhibiting pluripotency maintaining factors and epithelial-mesenchymal transition," *PLoS ONE*, vol. 6, no. 1, Article ID e16530, 2011.

[12] P. R. Pandey, H. Okuda, M. Watabe et al., "Resveratrol suppresses growth of cancer stem-like cells by inhibiting fatty acid synthase," *Breast Cancer Research and Treatment*, vol. 130, no. 2, pp. 387–398, 2011.

[13] Y. P. Yang, Y. L. Chang, P. I. Huang et al., "Resveratrol suppresses tumorigenicity and enhances radiosensitivity in primary glioblastoma tumor initiating cells by inhibiting the STAT3 axis," *Journal of Cellular Physiology*, vol. 227, no. 3, pp. 976–993, 2011.

[14] H. Wang, H. Zhang, L. Tang et al., "Resveratrol inhibits TGF-beta1-induced epithelial-to-mesenchymal transition and suppresses lung cancer invasion and metastasis," *Toxicology*, vol. 303, pp. 139–146, 2013.

[15] D. Vergara, C. M. Valente, A. Tinelli et al., "Resveratrol inhibits the epidermal growth factor-induced epithelial mesenchymal transition in MCF-7 cells," *Cancer Letters*, vol. 310, no. 1, pp. 1–8, 2011.

[16] C. T. Lin, W. Y. Chan, W. Chen et al., "Characterization of seven newly established nasopharyngeal carcinoma cell lines," *Laboratory Investigation*, vol. 68, no. 6, pp. 716–727, 1993.

[17] R. Glaser, H. Y. Zhang, K. Yao et al., "Two epithelial tumor cell lines (HNE-1 and HONE-1) latently infected with Epstein-Barr virus that were derived from nasopharyngeal carcinomas," *Proceedings of the National Academy of Sciences of the United States of America*, vol. 86, no. 23, pp. 9524–9528, 1989.

[18] J. T. C. Chang, S. H. Chan, C. Y. Lin et al., "Differentially expressed genes in radioresistant nasopharyngeal cancer cells: gp96 and GDF15," *Molecular Cancer Therapeutics*, vol. 6, no. 8, pp. 2271–2279, 2007.

[19] S. F. Chen, Y. C. Chang, S. Nieh et al., "Nonadhesive culture system as a model of rapid sphere formation with cancer stem cell properties," *PLoS ONE*, vol. 7, no. 2, Article ID e31864, 2012.

[20] J. Wang, L. P. Guo, L. Z. Chen, Y. X. Zeng, and H. L. Shih, "Identification of cancer stem cell-like side population cells in human nasopharyngeal carcinoma cell line," *Cancer Research*, vol. 67, no. 8, pp. 3716–3724, 2007.

[21] C. S. Lin, H. T. Lee, S. Y. Lee et al., "High mitochondrial DNA copy number and bioenergetic function are associated with tumor invasion of esophageal squamous cell carcinoma cell lines," *International Journal of Molecular Sciences*, vol. 13, no. 9, pp. 11228–11246, 2012.

[22] S. Sethi, N. M. Radio, M. P. Kotlarczyk et al., "Determination of the minimal melatonin exposure required to induce osteoblast differentiation from human mesenchymal stem cells and these effects on downstream signaling pathways," *Journal of Pineal Research*, vol. 49, no. 3, pp. 222–238, 2010.

[23] W. Qian and B. Van Houten, "Alterations in bioenergetics due to changes in mitochondrial DNA copy number," *Methods*, vol. 51, no. 4, pp. 452–457, 2010.

[24] O. Warburg, "On the origin of cancer cells," *Science*, vol. 123, no. 3191, pp. 309–314, 1956.

[25] A. Prigione, B. Fauler, R. Lurz, H. Lehrach, and J. Adjaye, "The senescence-related mitochondrial/oxidative stress pathway is repressed in human induced pluripotent stem cells," *Stem Cells*, vol. 28, no. 4, pp. 721–733, 2010.

[26] M. Diehn, R. W. Cho, N. A. Lobo et al., "Association of reactive oxygen species levels and radioresistance in cancer stem cells," *Nature*, vol. 458, no. 7239, pp. 780–783, 2009.

[27] P. L. Kuo, L. C. Chiang, and C. C. Lin, "Resveratrol- induced apoptosis is mediated by p53-dependent pathway in Hep G2 cells," *Life Sciences*, vol. 72, no. 1, pp. 23–34, 2002.

[28] M. J. Atten, E. Godoy-Romero, B. M. Attar, T. Milson, M. Zopel, and O. Holian, "Resveratrol regulates cellular PKC α and δ to inhibit growth and induce apoptosis in gastric cancer cells," *Investigational New Drugs*, vol. 23, no. 2, pp. 111–119, 2005.

[29] C. L. Kao, P. I. Huang, P. H. Tsai et al., "Resveratrol-induced apoptosis and increased radiosensitivity in CD133-positive cells derived from atypical teratoid/rhabdoid tumor," *International Journal of Radiation Oncology Biology Physics*, vol. 74, no. 1, pp. 219–228, 2009.

[30] L. J. Yu, M. L. Wu, H. Li et al., "Inhibition of STAT3 expression and signaling in resveratrol-differentiated medulloblastoma cells," *Neoplasia*, vol. 10, no. 7, pp. 736–744, 2008.

[31] D. C. F. da Costa, F. A. Casanova, J. Quarti et al., "Transient transfection of a wild-type p53 gene triggers resveratrol-induced apoptosis in cancer cells," *PLoS ONE*, vol. 7, no. 11, Article ID e48746, 2012.

[32] H. Lin, W. Xiong, X. Zhang et al., "Notch-1 activation-dependent p53 restoration contributes to resveratrol-induced apoptosis in glioblastoma cells," *Oncology Reports*, vol. 26, no. 4, pp. 925–930, 2011.

[33] V. V. Prabhu, J. E. Allen, B. Hong et al., "Therapeutic targeting of the p53 pathway in cancer stem cells," *Expert Opinion Therapeutic Targets*, vol. 16, no. 12, pp. 1161–1174, 2012.

[34] C. Ginestier, E. Charafe-Jauffret, and D. Birnbaum, "p53 and cancer stem cells: the mevalonate connexion," *Cell Cycle*, vol. 11, no. 14, pp. 2583–2584, 2012.

[35] H. Hong, K. Takahashi, T. Ichisaka et al., "Suppression of induced pluripotent stem cell generation by the p53-p21 pathway," *Nature*, vol. 460, no. 7259, pp. 1132–1135, 2009.

[36] H. Li, M. Collado, A. Villasante et al., "The Ink4/Arf locus is a barrier for iPS cell reprogramming," *Nature*, vol. 460, no. 7259, pp. 1136–1139, 2009.

[37] T. Kawamura, J. Suzuki, Y. V. Wang et al., "Linking the p53 tumour suppressor pathway to somatic cell reprogramming," *Nature*, vol. 460, no. 7259, pp. 1140–1144, 2009.

[38] J. Utikal, J. M. Polo, M. Stadtfeld et al., "Immortalization eliminates a roadblock during cellular reprogramming into iPS cells," *Nature*, vol. 460, no. 7259, pp. 1145–1148, 2009.

[39] R. M. Marión, K. Strati, H. Li et al., "A p53-mediated DNA damage response limits reprogramming to ensure iPS cell genomic integrity," *Nature*, vol. 460, no. 7259, pp. 1149–1153, 2009.

[40] S. P. Wang, W. L. Wang, Y. L. Chang et al., "p53 controls cancer cell invasion by inducing the MDM2-mediated degradation of Slug," *Nature Cell Biology*, vol. 11, no. 6, pp. 694–704, 2009.

[41] M. Sachdeva, S. Zhu, F. Wu et al., "p53 represses c-Myc through induction of the tumor suppressor miR-145," *Proceedings of the National Academy of Sciences of the United States of America*, vol. 106, no. 9, pp. 3207–3212, 2009.

[42] C. Liu, K. Kelnar, B. Liu et al., "The microRNA miR-34a inhibits prostate cancer stem cells and metastasis by directly repressing CD44," *Nature Medicine*, vol. 17, no. 2, pp. 211–215, 2011.

[43] C. J. Chang, C. H. Chao, W. Xia et al., "P53 regulates epithelial-mesenchymal transition and stem cell properties through modulating miRNAs," *Nature Cell Biology*, vol. 13, no. 3, pp. 317–323, 2011.

[44] N. Xu, T. Papagiannakopoulos, G. Pan, J. A. Thomson, and K. S. Kosik, "MicroRNA-145 regulates OCT4, SOX2, and KLF4 and represses pluripotency in human embryonic stem cells," *Cell*, vol. 137, no. 4, pp. 647–658, 2009.

[45] H. C. Chen, G. H. Chen, Y. H. Chen et al., "MicroRNA deregulation and pathway alterations in nasopharyngeal carcinoma," *British Journal of Cancer*, vol. 100, no. 6, pp. 1002–1011, 2009.

Hindawi Publishing Corporation
Evidence-Based Complementary and Alternative Medicine
Volume 2013, Article ID 268468, 12 pages
http://dx.doi.org/10.1155/2013/268468

Research Article

β-Elemene-Attenuated Tumor Angiogenesis by Targeting Notch-1 in Gastric Cancer Stem-Like Cells

Bing Yan, Yuqi Zhou, Shouhan Feng, Can Lv, Lijuan Xiu, Yingcheng Zhang, Jun Shi, Yongjin Li, Pinkang Wei, and Zhifeng Qin

Department of Traditional Chinese Medicine, Changzheng Hospital, The Second Military Medical University, Shanghai 200003, China

Correspondence should be addressed to Pinkang Wei; y_bing41@163.com and Zhifeng Qin; yanbing3741@gmail.com

Received 24 January 2013; Revised 15 March 2013; Accepted 23 March 2013

Academic Editor: Yu-Jen Chen

Emerging evidence suggests that cancer stem cells are involved in tumor angiogenesis. The Notch signaling pathway is one of the most important regulators of these processes. β-Elemene, a naturally occurring compound extracted from *Curcumae Radix*, has been used as an antitumor drug for various cancers in China. However, its underlying mechanism in the treatment of gastric cancer remains largely unknown. Here, we report that CD44+ gastric cancer stem-like cells (GCSCs) showed enhanced proliferation capacity compared to their CD44− counterparts, and this proliferation was accompanied by the high expression of Notch-1 (*in vitro*). These cells were also more superior in spheroid colony formation (*in vitro*) and tumorigenicity (*in vivo*) and positively associated with microvessel density (*in vivo*). β-Elemene was demonstrated to effectively inhibit the viability of GCSCs in a dose-dependent manner, most likely by suppressing Notch-1 (*in vitro*). β-Elemene also contributed to growth suppression and attenuated the angiogenesis capacity of these cells (*in vivo*) most likely by interfering with the expression of Notch-1 but not with Dll4. Our findings indicated that GCSCs play an important role in tumor angiogenesis, and Notch-1 is one of the most likely mediators involved in these processes. β-Elemene was effective at attenuating angiogenesis by targeting the GCSCs, which could be regarded as a potential mechanism for its efficacy in gastric cancer management in the future.

1. Introduction

Tumor angiogenesis has long been known to have an essential role in tumor development and metastasis [1]. Although the underlying mechanisms of this process are not currently completely understood, they have conventionally been described as sequential activation involving endothelial sprouting from preexisting vessels, endothelial proliferation, migration, and differentiation to form tubes [2]. However, recent studies in cancer stem cells (CSCs) provided additional insight into tumor angiogenesis [3], as accumulating data have indicated that CSCs are involved in tumor angiogenesis not only by enhanced capacity of vascular endothelial growth factor (VEGF) secretion compared to its counterparts [4], but, more strikingly, they are strongly proangiogenic and can generate "CSC-derived endothelial progenitor cells" [5, 6]. CSC involvement in tumor angiogenesis has been reported in various cancers including brain tumors, skin tumors, and breast cancer [7–9]. Based on these results, some investigators have speculated that this phenomenon may not be uncommon in other CSC models [10]. Gastric cancer stem-like cells (GCSCs) have been identified in gastric cancer cell lines and primary tumors that are positive for the CD44 marker [11–14], which is a universal CSC marker that has been detected in many cancers, including head and neck squamous cell carcinoma, breast cancer, and prostate cancer [15, 16]. Although the role of GCSCs in tumor angiogenesis remains obscure, in other solid tumors, such as ovarian cancer, purified CD44 positive cells (also known as ovarian CSCs) have been demonstrated to possess a similar endothelial potential [17].

Notch signaling is an evolutionarily conserved signaling pathway that plays a fundamental role in embryonic development and adulthood. To date, four vertebrate Notch receptors (Notch 1–4) have been identified. In addition, five ligands, Dll1, Dll3, Dll4, and Jag1-2, have been found in mammals

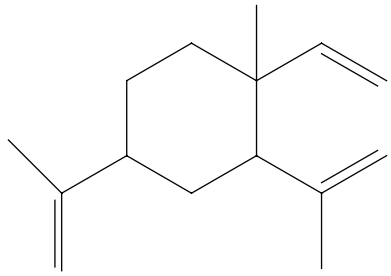

Figure 1: Chemical structure of β-Elemene.

with multiple associated target genes including Hes, Myc, and p21 [18]. It was believed that Notch signaling plays a critical role in CSCs and was regarded as a new cancer drug target [19]. Recent studies indicated that Notch signaling plays an essential role in vascular development and angiogenesis with several promising targets including Notch-1, Dll4, and Jag1 [2, 20, 21]. In gastric cancer, a previous study indicated that the activation of Notch-1 promotes disease progression [22], and the expression of Notch-1 was significantly higher in cancer cells than in normal tissues [23]. In addition, it was reported that oxaliplatin-resistant gastric cancer cell lines showed increased levels of Jag1 and Dll4, which are associated with a higher angiogenic rate [24].

β-Elemene (1-methyl-1-vinyl-2,4-diisopropenyl-cyclohexane; Figure 1), a naturally occurring compound isolated from the traditional Chinese medicinal (TCM) herb *Curcumae Radix* (Chinese Pharmacopoeia, 2010 version, http://drugs.yaojia.org/), has been approved by the State Food and Drug Administration of China to treat various solid tumors [25] and is currently under consideration for clinical studies in the United States [26]. However, the underlying mechanisms associated with its efficacy in gastric cancer are largely unknown. In this study, we investigated the role of GCSCs in tumor angiogenesis and the possible mechanism of β-Elemene for its efficacy.

2. Materials and Methods

2.1. Animals. Sixty-two 6- to 8-week-old male nude mice, weighing 20–24 g, were purchased from Shanghai Institute of Materia Medica (Chinese Academy of Science) and maintained under standard pathogen-free conditions (Laboratory Animal Center, Second Military Medical University). All mice were handled according to the recommendations of the National Institutes of Health Guidelines for the Care and Use of Laboratory Animals. The experimental protocol was approved by the Shanghai Medical Experimental Animal Care Commission.

2.2. Cell Culture and Xenografts. The human gastric cancer cell line MKN-45 was purchased from Shanghai Cells Center, the Chinese Academy of Sciences and cultured in RPMI-1640 supplemented with 10% fetal bovine serum (FBS), 10 mM HEPES, and 1% penicillin-streptomycin. Cell sorting was performed as described by Takaishi et al. [11]. In brief, confluent cells were washed once with phosphate-buffered saline (PBS) and then dissociated from plates using trypsin-EDTA and centrifuged. The cell pellets were resuspended and incubated for 30 min at 37°C with a 100-fold dilution of anti-CD44-fluorescein isothiocyanate rat monoclonal antibody (BD Biosciences, CA, USA). The samples were then stained with 4,6-diamidino-2-phenylindole (final concentration of 2 ng/mL) and then sorted with a FACSAria II flow cytometer (BD FACSAria II, CA, USA). The results were analyzed using FACSDiva version 6.1.3 software (Figure 2(a)). The purity of the sorted cells was estimated to be more than 97%. After sorting, a portion of the cells (CD44+ and CD44−) was suspended in sterile RPMI-1640 supplemented with 10% FBS, and the rest were injected subcutaneously into the axilla of the nude mice (1×10^5 cells per site) using a handmade glass micropipette. For spheroid colony formation analysis, single-cell suspension of CD44+ and CD44− cells was prepared by thoroughly dissociating with 0.25% trypsin in 0.02% EDTA (Sigma, USA). The cells were then plated in culture dishes at a density of 2×10^2 cells/dishes in RPMI-1640 containing 10% FBS and incubated for 2 weeks at 37°C; colonies containing more than 50 cells were counted after Giemsa staining.

2.3. Cell Viability and Proliferation Assay. Cell viability assays were conducted using a 3-(4,5-dimethylthiazol-2-yl)-2,5-diphenyltetrazolium bromide (MTT) kit (Beyotime, China). FACS-sorted CD44+ and CD44− cells were incubated in 96-well plates (5×10^4 cells/well). The next day, the cells were treated with various concentrations of β-elemene (0–200 μg/mL) for 48 h or for 72 h, with 6 replicates of each treatment. After incubation, 20 μL of MTT reagent was added to each well (5 mg/mL), and the cells were then incubated for another 3 h at 37°C. Cell viability was determined by measuring the optical density (OD) at 470 nm with a microplate reader (Bio-Rad Laboratories, USA). The following formula was used: cell viability = (OD of the experimental sample/OD of the control group) × 100%. Another two groups that contained CD44+ and CD44− cells were assessed for cell proliferation without any intervening measurements.

2.4. Drug Preparation and Administration. β-Elemene (97% purity) was obtained from JinGang Pharmaceuticals (Dalian, China). The mice were randomly divided into 8 groups as follows: model CD44+ group (CD44+; $N = 10$), Model CD44− group (CD44−; $N = 10$), and low-, medium- and high-dose β-elemene group (corresponding to 25 mg/kg, 50 mg/kg and 100 mg/kg, resp.). The low-, medium- and high-dose β-elemene groups included 6 mice in each of the CD44+ groups and 8 in each CD44− groups. All β-elemene-treated groups in the *in vitro* studies were CD44+; however, the cells used in the *in vivo* study contained both CD44+ and CD44− cells. Mice in the model groups were administered 0.4 mL 0.9% sodium chloride via intraperitoneal injection once every 2 days, while the experimental groups synchronously received the scheduled dose of β-elemene. Treatment was started 3 days after cell injection and continued for 8 consecutive weeks. At the end of the 8th week, the mice were euthanized, and the tumors were carefully removed and measured.

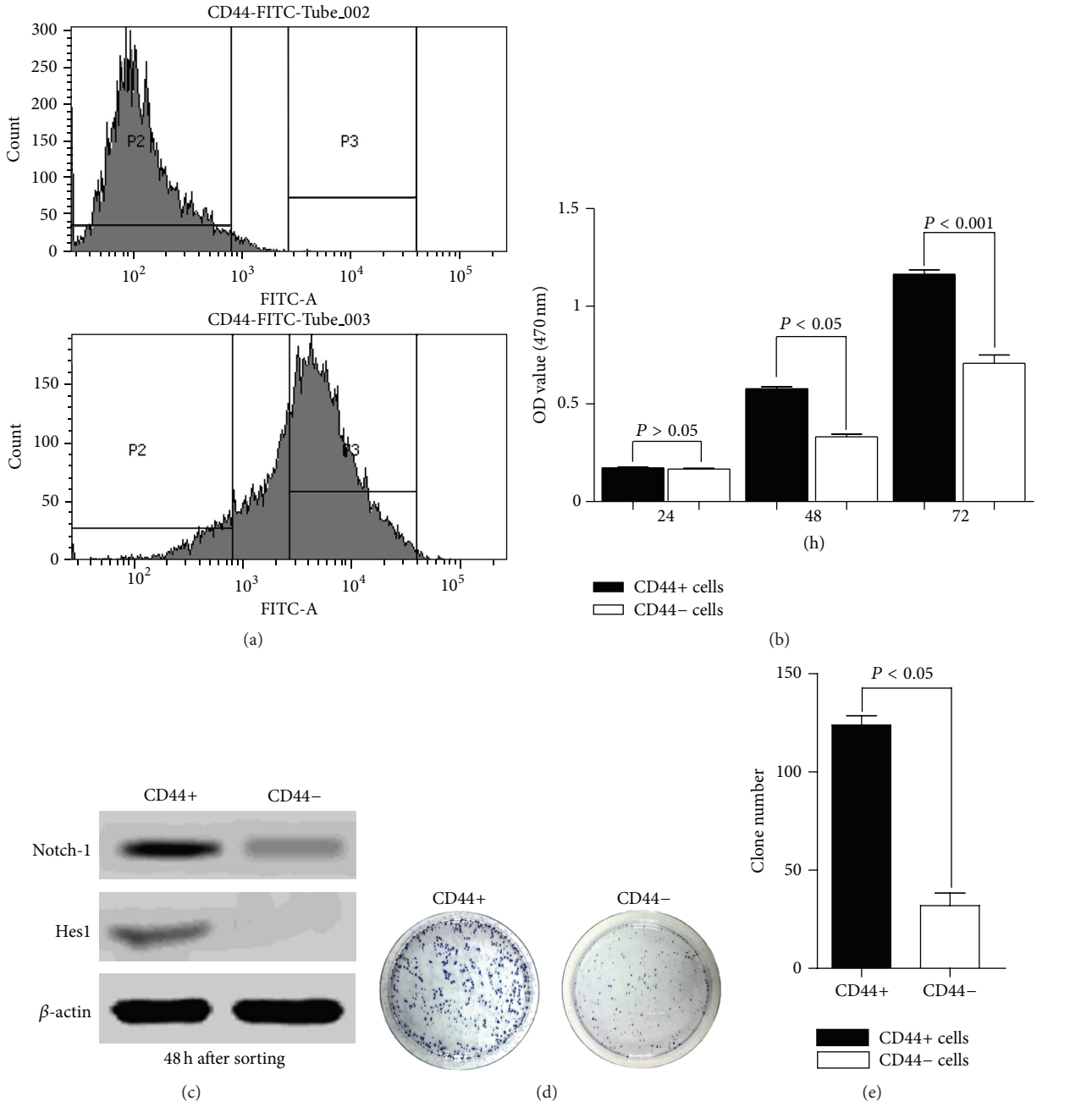

Figure 2: (a) FACS sorting results of cultured MKN-45 cells. (b) MTT assay revealed an enhanced proliferation capacity of CD44+ cells compared to CD44− cells 48 and 72 hours after sorting ($P < 0.05$ and $P < 0.001$, resp.). (c) Western blot of the cells 48 h after FACS sorting, which indicates a remarkable difference in Notch-1 and Hes1 expressions between CD44+ and CD44− cells. (d) Spheroid colony formation by CD44+ and CD44− cells. (e) Quantitive analysis of the spheroid clone formation efficacy of CD44+ and CD44− cells.

2.5. Immunohistochemical Staining (IHC) for CD34 and CD44. Tumor tissues were fixed in 10% formalin, embedded in paraffin, and processed using standard histological methods. Serial sections (5 μm) were cut from each selected paraffin block. IHC was performed with avidin-biotin-peroxidase complex kits according to the manufacturer's instructions (Invitrogen, USA). Anti-CD44 (1 : 200, Abcam, USA) and anti-CD34 (1 : 200, Abcam, USA) antibodies were used. Primary antibodies were incubated at room temperature overnight in a humidified chamber. The positive areas in the field were counted by the Image-Pro-Express system (Olympus, Japan) at a magnification of 400x (BX51, Olympus, Japan), the final value of the IHC was calculated from eight randomly selected fields of each section by following formula: total value = (positive areas × mean OD value) × 100%.

2.6. Microvessel Density (MVD). In previous studies, CD34 was demonstrated to be one of the most useful markers to

Table 1: The base sequences of primers used for quantitative real-time PCR.

Primer name	Sequence
Notch-1	
Forward	CACTGTGGGCGGGTCC
Reverse	GTTGTATTGGTTCGGCACCAT
Hes1	
Forward	AGCCAACTGAAAACACCTGATT
Reverse	GGAGTTTATGATTAGCAGTGG
Dll4	
Forward	GGTGACCTGGCGAACAGACGAGCAAAAT
Reverse	GGTGACCTGGCGAACAGACGAGCAAAAT
GAPDH	
Forward	GGCATCCTGGGCTACACT
Reverse	CCACCACCCTGTTGCTGT

identify blood vessels in gastric cancer [27–31]. To measure microvessel density (MVD) in our study, quantitative vessel counts were performed using the method described by Weidner and assessed by international consensus [32].

2.7. Western Blot Analysis of Notch-1, Hes1 (In Vitro and In Vivo) and Dll4, CD44 (In Vivo). For our *in vitro* study, cells were washed twice with ice-cold PBS, solubilized in 1% Triton lysis buffer on ice, and then quantified using the Lowry method [33]. Cell lysate proteins (40 μg) were separated by sodium dodecyl sulfate-polyacrylamide gel electrophoresis and electrophoretically transferred to nitrocellulose membranes (Millipore, USA). For our *in vivo* study, the proteins were extracted from the tissues using RIPA lysis buffer containing the protease inhibitor phenylmethanesulfonyl fluoride (PMSF, Beyotime Institute of Biotechnology, China). Proteins were separated via 10% SDS-polyacrylamide gel and transferred onto PVDF membranes (Millipore, USA). The membranes were blocked with 5% milk and then incubated with primary rabbit anti-Notch-1 (dilution 1 : 500, Abcam, USA), anti-Hes1 (dilution 1 : 200, Santa, USA), anti-Dll4 (dilution 1 : 500, Abcam, USA) and anti-CD44 (dilution 1 : 500, Abcam, USA), antibodies. Membranes were then washed and incubated with the appropriate HRP-conjugated secondary antibodies for 2 h at room temperature. Proteins were detected using an ECL detection reagent. β-actin was used as a loading control, and all images were analyzed using NIH Image J software.

2.8. Real-Time Quantitative PCR Assay for Notch-1, Hes1 (In Vitro and In Vivo) and Dll4 (In Vivo). Total RNA was extracted from 50 to 100 mg of tissue according to the protocol described for the BioEasy SYBR Green I Real-Time PCR Kit (Bo Ri Technology Co., Ltd., China). The primer sequences for specific gene amplification are listed in Table 1. Real-time PCR was performed according to the standard protocol for the SYBR Premix Ex TaqTM Perfect Real-Time system (Takara, China) using an ABI 7300 detector (Applied Biosystems, USA). Fold changes in gene expression were calculated using the $2^{-\Delta\Delta Ct}$ method. The ODs of the target genes were compared with that of GAPDH.

2.9. Statistical Analysis. All data were analyzed using SPSS 18.0 software and are presented as the mean values±standard derivation. Comparisons between different groups were evaluated using a one-way ANOVA followed by the Bonferroni test. Values of $P < 0.05$ were considered statistically significant. All the data represent the mean value determined by two experienced investigators who were blinded to the design.

3. Results

3.1. GCSCs Were More Proliferative and Tumorigenic Than the CD44− Cells In Vitro. As shown in Figure 2(b), GCSCs showed greater proliferation than their counterparts 48 h and 72 h after sorting. The expression of Notch-1 and Hes1 was also higher in CD44+ mice than in CD44− mice 48 h after sorting, which indicated that these parameters are positively associated with the proliferation of GCSCs (Figure 2(c)). In previous study, the development of tumors with defined markers in immunodeficient mice was considered as the "gold standard" for identifying CSCs [34]. In our study (*in vivo*), 10/10 mice formed tumors in model CD44+ group, and 6/10 formed tumors in model CD44− group; however, in β-elemene-treated groups, this index was 6/6 in CD44+ groups and 6-7/8 in CD44− groups. In addition, spheroid colony formation assay, which was considered as an indicative of self-renewal ability and consistent with a CSC phenotype [11], revealed that CD44+ cells were more superior than CD44− cells (Figures 2(d)-2(e)).

3.2. β-Elemene Inhibited the Viability of GCSCs as well as the Notch-1 and Hes1 Expressions In Vitro. Cell viability assays showed that β-elemene inhibited the proliferation of CD44+ cells in a dose-dependent manner (Figures 3(a)-3(b)). The IC50 values at 24, 48, and 72 h were 125.06 μg/mL, 103.75 μg/mL, and 72.43 μg/mL for CD44+ cells and 142.61 μg/mL, 117.09 μg/mL, and 97.07 μg/mL for CD44− cells, respectively. These data indicated that β-elemene has substantial antitumor effects on CD44+ MKN-45 cells. As shown in Figures 3(c)-3(d), western blotting demonstrated that β-elemene inhibits the expression of Notch-1 and Hes1 in CD44+ cells in a dose-dependent manner. At the low concentration of 50 μg/mL, the expression of Notch-1 and Hes1 showed no variation, whereas their expression significantly decreased when the cells were treated with 200 μg/mL β-elemene.

3.3. GCSCs Were Capable of Recruiting More Blood Vessels Than Were CD44− Cells, and β-Elemene Inhibited the Expression of CD44 and Reduced the MVD In Vivo. As shown in Figure 4, after 8 consecutive weeks of treatment, the tumor weight in model CD44+ mice was significantly higher than that in model CD44− mice ($P < 0.05$), in addition, a comparison between the β-elemene-treated groups and the model CD44+ group was significantly different except

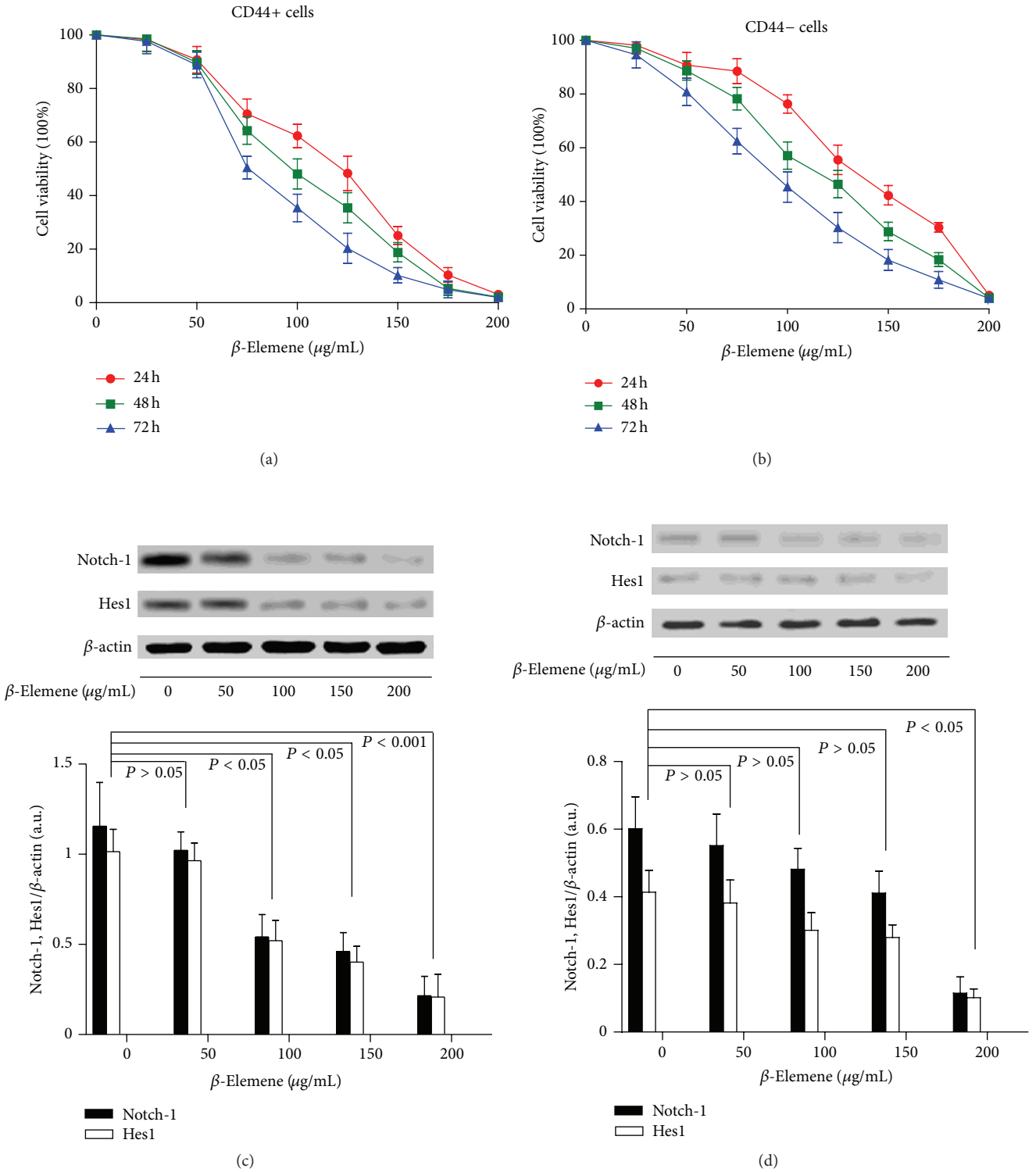

FIGURE 3: (a)-(b) Effect of β-elemene on the cell viability of CD44+ cells. CD44+ and CD44− cells were treated with 50, 100, 150, or 200 μg/mL β-elemene for 24, 48, or 72 h. The cell viability was determined using an MTT assay. Dots: mean of six independent experiments; bars: SD. (c)-(d). β-Elemene inhibited Notch-1 and Hes1 expressions *in vitro*. CD44+ and CD44− cells were seeded in 96-well plates at a density of 5×10^4 cells/well and treated with a series of β-elemene doses over 48 h. Cellular lysates were subjected to western blot analysis with antibodies against Notch-1, Hes1, and β-actin (loading control). The densitometry analysis results of the Notch-1 and Hes1 bands were normalized to β-actin using NIH Image J from six independent experiments. The data are expressed as arbitrary units.

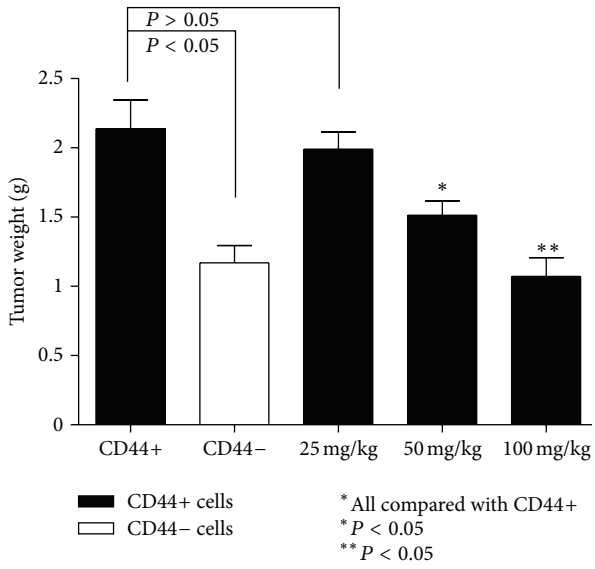

FIGURE 4: Tumor weight after 8 consecutive weeks of treatment ($N = 6$ in each groups). Model CD44+ mice had larger tumors than did model CD44− mice. β-Elemene treatment inhibited tumor growth in a dose-dependent manner.

for the 25 mg/kg group ($P > 0.05$). Based on the IHC results (Figure 5(a)), the MVD was clearly higher in the model CD44+ group than in the model CD44− group. We detected significant differences of MVD in the 50 mg/kg and 100 mg/kg groups when compared with model CD44+ group (and model CD44− group), which indicated that β-elemene can inhibit angiogenesis in a dose-dependent manner (Figure 5(b)).

In addition, as a class I transmembrane glycoprotein, CD44 was highly expressed not only in cancer cells but also in immune cells (such as leukocytes) and stromal cells (such as fibroblasts) [11]. Interestingly, despite the fact that CD44+ and all the CD44+ β-elemene-treated groups are GCSCs, the IHC results indicated that not all of the cells were CD44+ in these groups after the experiment, which suggested that CD44+ cells could give rise to CD44− cells (Figure 6(a)). We also detected a significant difference in CD44 expression between the model CD44+ and model CD44− groups ($P < 0.001$). In addition, in the CD44+ β-elemene-treated groups, the comparison of CD44+ and 50 mg/kg and CD44+ and 100 mg/kg is also significantly different in CD44 expression ($P < 0.05$) (Figure 6(b)). These results were further confirmed by western blot analysis (Figures 6(c)-6(d)).

3.4. Notch-1 and Hes1 Were Highly Expressed in GCSCs in Xenograft Mice, and β-Elemene Inhibited Their Expression in a Dose-Dependent Manner. Notch-1 and Hes1 expressions were measured by western blot and quantitative real-time PCR. As shown in Figures 7(a)-7(b), we found that Notch-1 and Hes1 expressions were significantly increased in the model CD44+ group compared with that of the model CD44− group ($P < 0.05$). In addition, the comparison between model CD44+ group and the β-elemene-treated groups (except the 25 mg/kg group) also showed an obvious significant difference ($P < 0.05$). However, we failed to detect any statistically significant differences in Dll4 expression in the model CD44+ group and CD44+ β-elemene-treated groups, although we did observe differences in expression between the model CD44+ and model CD44− groups ($P < 0.05$). Our PCR results were in agreement with our western blotting results (Figure 7(b)).

4. Discussion

Accumulating data have demonstrated the pivotal role of Notch signaling in tumor angiogenesis [2]. In the present study, we observed that GCSCs have greater Notch-1 expression than the CD44− cells (*in vitro* and *in vivo*), and we also detected a higher MVD in GCSCs in xenografted nude mice. These results, together with those of the aforementioned studies [7–9], may indicate that GCSCs play an important role in tumor angiogenesis. In addition, it has been demonstrated that the downregulation of Notch-1 contributes to cell growth inhibition in various cancers [35, 36]. In our study, we found that β-elemene could inhibit the growth of GCSCs in a dose-dependent manner accompanied by the reduced expression of Notch-1 and Hes1. Taking into consideration that CD44 is a transcriptional target of Notch-1 [37], apparently downstream of Hes1/Hey1 [38], we concluded that β-elemene could attenuate tumor angiogenesis by targeting GCSCs at least in part through Notch-1 expression. Notably, although Dll4 has been demonstrated to be a key regulator in tumor angiogenesis, β-elemene failed to influence its expression in our study. As we know, Dll4 is an endothelium-specific ligand that is expressed at sites of vascular of normal origin [39]. Its regulation is complex and may be manipulated by multiple Notch signaling [40]. Based on our current study, it is unclear whether β-elemene has a limited effect on endothelial cells or other signaling pathways involved in the regulation of Dll4.

It is worth noting that naturally occurring compounds have increasingly been demonstrated to be effective in targeting CSCs. Wang et al. demonstrated that *sulforaphane*, a dietary component of broccoli/broccoli sprouts, inhibits breast CSCs [41]; Kawahara et al. observed that *quercetin*, a major polyphenol and flavonoid commonly found in many fruits and vegetables, decreases the levels of Notch-1 protein and targets pancreatic CSCs [42]. Lin et al. indicated that the *curcumin* analogue, GO-Y030, can target colon CSCs [43]. Wang et al. further reported that *curcumin* can downregulate Notch-1 [35]. Bao et al. also demonstrated that *curcumin* can attenuate CSC markers including CD44 and EpCAM [44]. Interestingly, *curcumin* ($C_{21}H_{20}O_6$) is partially originated from the same herbal source as β-elemene in TCM (Chinese Pharmacopoeia, 2010 version, http://drugs.yaojia.org/). In addition, Zhen et al. suggested that arsenic trioxide (a drug derived from TCM) could deplete the cancer stem cell like population in gliomas [45]. Sun et al. further reported that arsenic trioxide may regulate the apoptosis of glioma stem cells via the downregulation Notch-1 and Hes1 [46]. Although the data concerning the ability of β-elemene to target CSCs

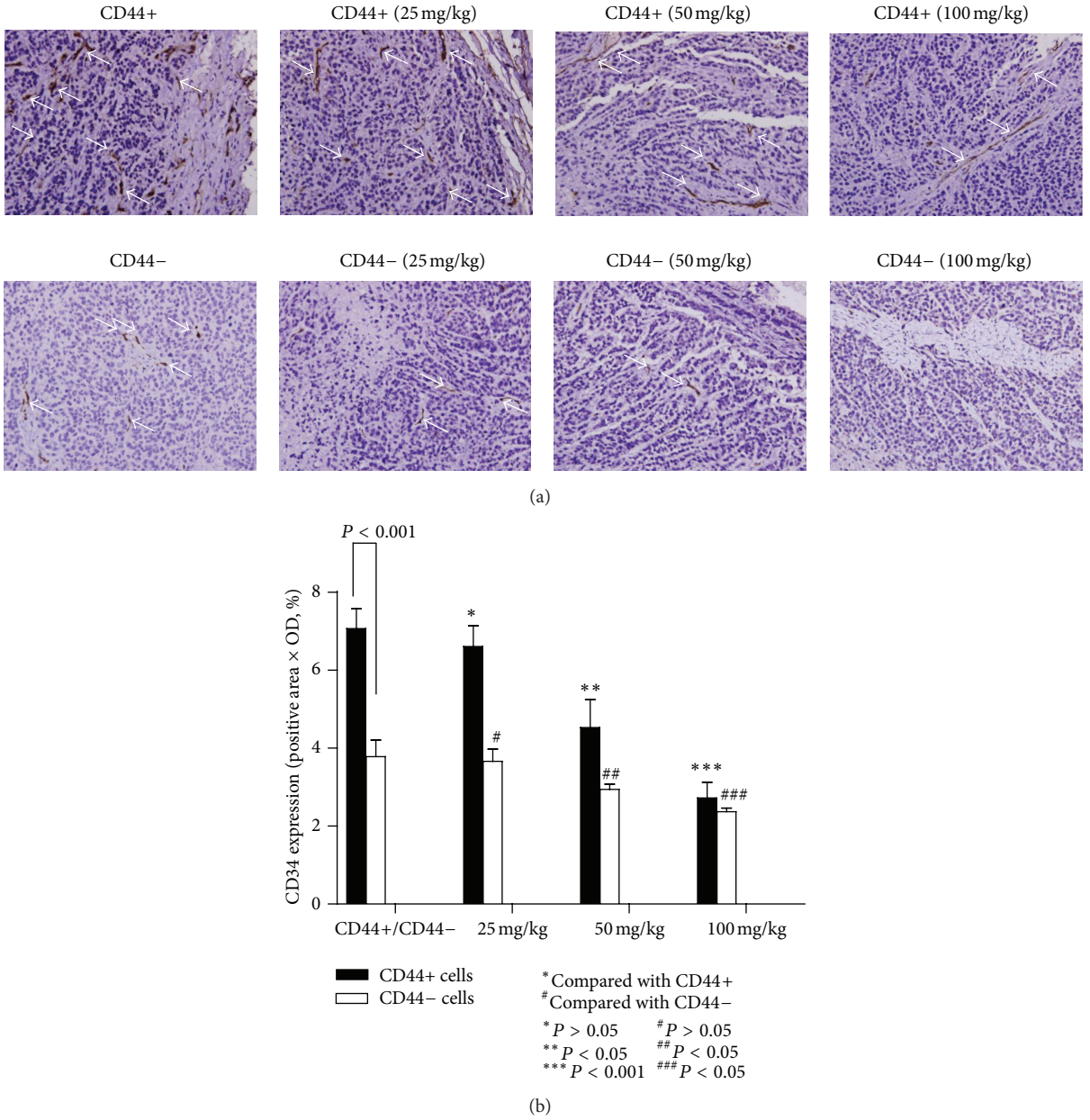

Figure 5: (a) Immunohistochemical staining results of the MVD. MVD was defined as a discrete CD34-positive endothelial cell aggregate, with or without definable lumina. Higher MVD could be detected in model CD44+ mice compared with model CD44− mice; β-elemene could inhibit the MVD in a dose-dependent manner both in the CD44+ and CD44− groups (original magnification 400x, positive areas are indicated by white arrows). (b) MVD in the different treatment groups. The model CD44+ mice showed a higher MVD than did the model CD44− mice ($N = 6$, $P < 0.05$), and β-elemene reduced MVD in a dose-dependent manner. Statistically significant differences in MVD could be detected in 50 mg/kg and 100 mg/kg in both the CD44+ or CD44− groups.

is limited, the results of our study may shed light on this possibility.

The role of CSCs in tumor angiogenesis has not been fully elucidated; however, increased VEGF secretion was one of the most studied potential mechanisms, although it has not been observed in GCSCs. For example, Beck et al. demonstrated that in CD34+ skin tumors, CSCs express higher levels of VEGF than do their daughter cells [8]. Sun et al. indicated that in breast cancer, the VEGF concentration was significantly higher in breast CD44+/CD24-cell (CSCs) conditioned medium than in CD44+/CD24+ cell-conditioned medium [9]. Bao et al. found that, in comparison with matched nonstem cell-like glioma cancer populations, stem cell-like glioma cancers consistently secreted markedly elevated levels of VEGF [4]. In our study, we observed that β-elemene could downregulate Notch-1 and Hes1, which could result in the impaired growth of GCSCs because Notch-1 and Hes1 are involved in the self-renewal and expansion of CSCs [47–49]. Although the data concerning GCSCs and VEGF secretion are currently limited, it would be reasonable

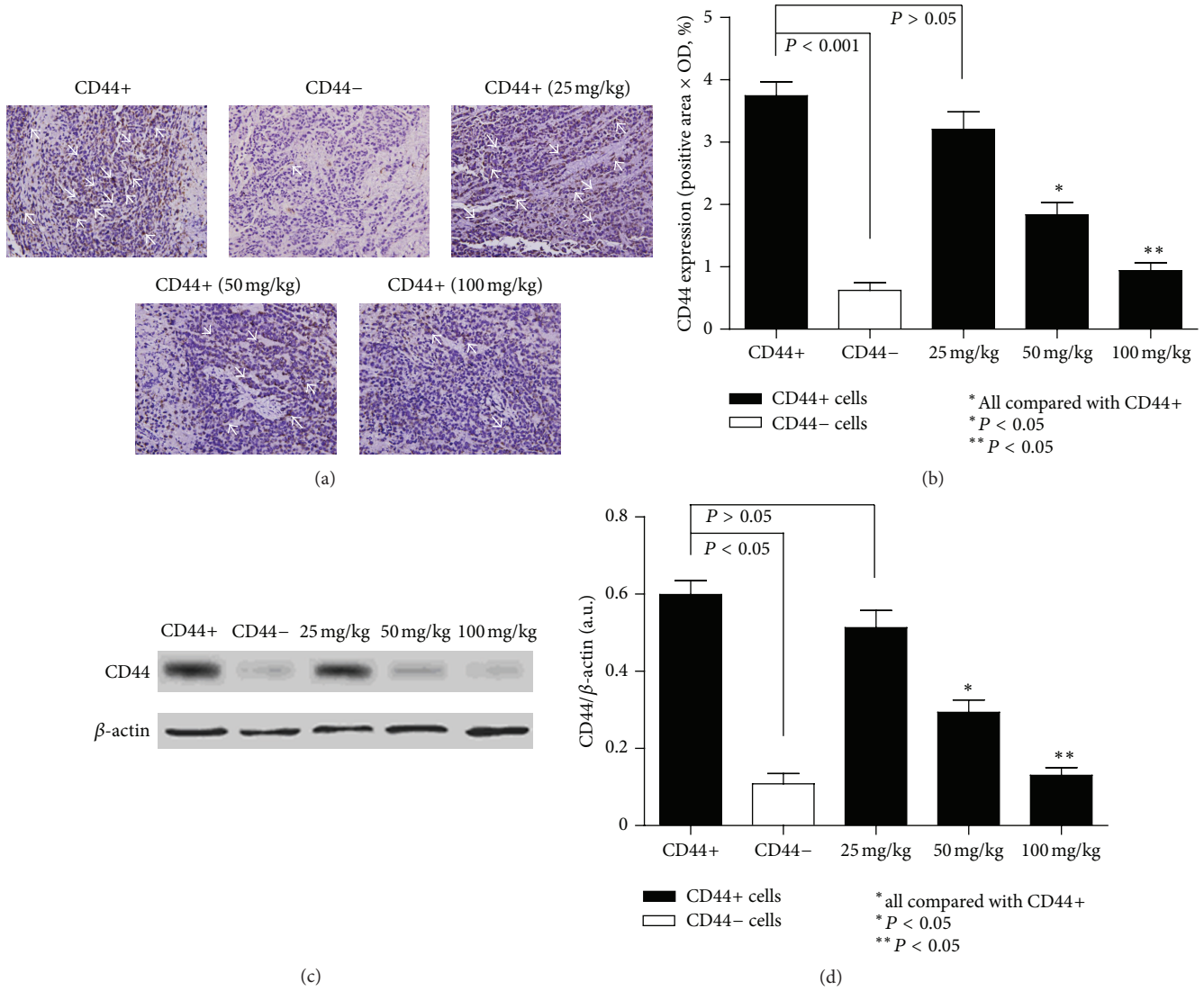

FIGURE 6: (a) Immunohistochemical staining of CD44. CD44 was highly expressed in the cancer cell membrane (original magnification 400x, positive areas are indicated by white arrows). (b) CD44 expression in each of the treatment groups ($N = 6$ in each groups). CD44 was highly expressed in model CD44+ group compared to the rest of the groups and was rarely detected in model CD44− group. The results also showed that not all of the cells in the CD44+ group were CD44 positive. β-Elemene inhibited the expression of CD44 in a dose-dependent manner. Statistically significant differences in expression of CD44 were also detected in the 50 mg/kg and 100 mg/kg groups ($P < 0.05$). (c)-(d) Western blot results of CD44 expression in model CD44+ group, model CD44− group, and all the β-elemene-treated CD44+ groups. We detected a corresponding variation of CD44 in these groups like the aforementioned IHC results of it.

to deduce the efficacy of this pharmacologic agent, as the inhibition of the self-renewal and expansion of GCSCs reduce the blood supply.

Although the VEGF pathway has been determined to be essential for developmental angiogenesis based on a number of past studies [40], a recent study has indicated the complex crosstalk between Notch and VEGF. Briefly, it was suggested that VEGF induces Dll4/Notch signaling, while Dll4/Notch signaling modulates the VEGF pathway (especially the VEGF receptor 2) [50–52]. In a previous study, β-elemene was demonstrated to be effective in cancer management by multiple mechanisms, including the inhibition of MAPK/ERK and PI3K/Akt/mTOR signaling pathways [25, 53], the activation of p38 MAPK and/or JNK [54], the downregulation of survivin and hypoxia-inducible factor-1a (HIF-1α) [55], decreasing Bcl-2 expression [56], and inducing cell cycle arrest [57] as well as cell apoptosis [58, 59]. It is notable that many of these targets are important constituents of the upstream or downstream signaling pathway of the VEGF system. For example, Nör et al. indicated that VEGF-mediated angiogenesis is associated with the induction of Bcl-2 expression [60]. Iervolino et al. also indicated that Bcl-2 overexpression in human melanoma cells increases angiogenesis [61]. Song et al. demonstrated that HIF-1α enhances the expression of VEGF in gastric cancer [62]; Yoshino et al. reported that the activation of p38 MAPK

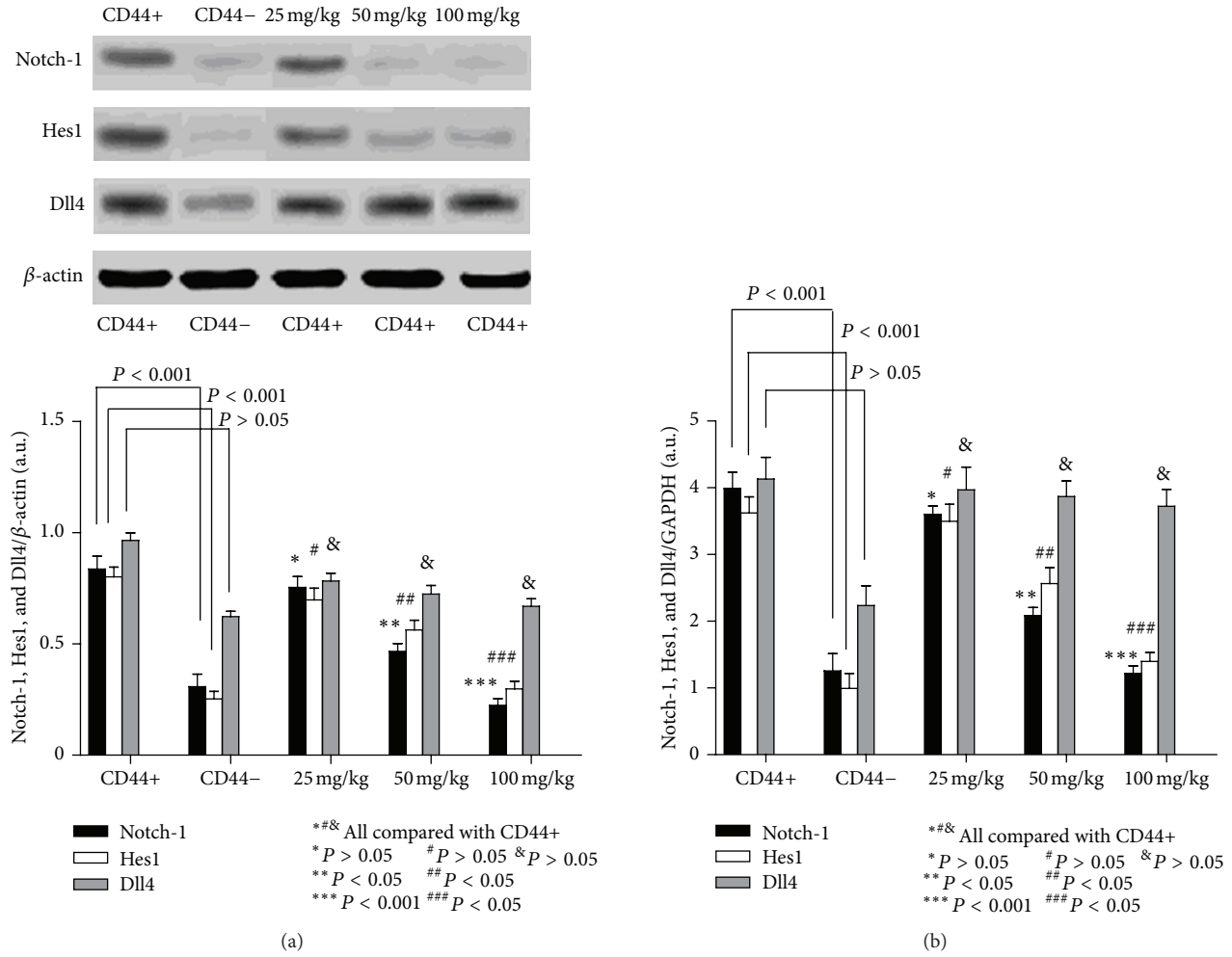

Figure 7: Western blot and real-time PCR analyses of Notch-1, Hes1, and Dll4 expressions *in vivo*. (a) Western blotting revealed that Notch-1 and Hes1 were highly expressed in the model CD44+ compared to the model CD44− group. β-Elemene inhibited the expression of Notch-1 and Hes1 in a dose-dependent manner, and statistically significant differences could be detected in the 50 mg/kg and 100 mg/kg groups. However, statistically significant differences in Dll4 expression could only be detected between the model CD44+ group and model CD44− group, and β-elemene failed to inhibit the expression of Dll4 in a dose-dependent manner. We found no statistically significant differences between any of the β-elemene-treated groups. (b) The variation of Notch-1, Hes1, and Dll4 expressions in the experimental groups was further confirmed by RT-PCR.

contributes to increased levels of VEGF secretion in human malignant glioma cells [63]. Interestingly, some of these targets that are involved in the effective mechanism of β-elemene are also associated with Notch-1. For example, Wang et al. demonstrated that the downregulation of Notch-1 could be an effective approach for inhibiting cell growth, migration, and invasion, and for inducing apoptotic cell death, which is associated with the inactivation of Akt/mTOR [36]. Qi et al. indicated that Notch-1 signaling was found to downregulate the expression of cyclin and to induce the apoptosis of cancer cells through the downregulation of Bcl-2 and the activation of JNK [64]. Chen et al. observed that Notch-1 signaling facilitates survivin expression [65]. Based on these previous studies, we speculate that there may be some crosstalk between the Notch and VEGF signaling pathways that may contribute to the efficacy of β-elemene in our study. However, additional studies are still needed to address this assumption in the future.

5. Conclusion

Our study indicated that GCSCs play an important role in tumor angiogenesis, and Notch-1 is one of the most likely mediators involved in this process. β-Elemene was effective at attenuating angiogenesis by targeting GCSCs at least in part through Notch-1 expression. This potential mechanism for β-elemene may be used to manage gastric cancer in the future.

Conflict of Interests

The authors have no conflict of interests to declare.

Acknowledgment

The authors thank Professor Jianwen Liu, Pharmacy College of East China University of Science and Technology, for technical support and constructive advice.

References

[1] R. S. Kerbel, "Tumor angiogenesis," *New England Journal of Medicine*, vol. 358, no. 19, pp. 2039–2049, 2008.

[2] J. L. Li and A. L. Harris, "Notch signaling from tumor cells: a new mechanism of angiogenesis," *Cancer Cell*, vol. 8, no. 1, pp. 1–3, 2005.

[3] Y. Zhao, Q. Bao, A. Renner et al., "Cancer stem cells and angiogenesis," *International Journal of Developmental Biology*, vol. 55, no. 4-5, pp. 477–482, 2011.

[4] S. Bao, Q. Wu, S. Sathornsumetee et al., "Stem cell-like glioma cells promote tumor angiogenesis through vascular endothelial growth factor," *Cancer Research*, vol. 66, no. 16, pp. 7843–7848, 2006.

[5] L. Ricci-Vitiani, R. Pallini, M. Biffoni et al., "Tumour vascularization via endothelial differentiation of glioblastoma stem-like cells," *Nature*, vol. 468, no. 7325, pp. 824–830, 2010.

[6] R. Wang, K. Chadalavada, J. Wilshire et al., "Glioblastoma stem-like cells give rise to tumour endothelium," *Nature*, vol. 468, no. 7325, pp. 829–835, 2010.

[7] C. Folkins, Y. Shaked, S. Man et al., "Glioma tumor stem-like cells promote tumor angiogenesis and vasculogenesis via vascular endothelial growth factor and stromal-derived factor 1," *Cancer Research*, vol. 69, no. 18, pp. 7243–7251, 2009.

[8] B. Beck, G. Driessens, S. Goossens et al., "A vascular niche and a VEGF-Nrp1 loop regulate the initiation and stemness of skin tumours," *Nature*, vol. 478, no. 7369, pp. 399–403, 2011.

[9] H. Sun, J. Jia, X. Wang et al., "CD44(+)/CD24 (-) breast cancer cells isolated from MCF-7 cultures exhibit enhanced angiogenic properties," *Clinical & Translational Oncology*, vol. 15, no. 1, pp. 46–54, 2013.

[10] V. L. Bautch, "Tumour stem cells switch sides," *Nature*, vol. 468, no. 7325, pp. 770–771, 2010.

[11] S. Takaishi, T. Okumura, S. Tu et al., "Identification of gastric cancer stem cells using the cell surface marker CD44," *Stem Cells*, vol. 27, no. 5, pp. 1006–1020, 2009.

[12] L. Yang, Y. F. Ping, X. Yu et al., "Gastric cancer stem-like cells possess higher capability of invasion and metastasis in association with a mesenchymal transition phenotype," *Cancer Letters*, vol. 310, no. 1, pp. 46–52, 2011.

[13] H. J. Lee, Y. S. Choi, S. J. Kim, and H. J. Moon, "CD44 and CD133 as cancer stem cell markers for gastric cancer," *Journal of Gastric Cancer*, vol. 10, no. 3, pp. 99–105, 2010.

[14] Z. Xue, H. Yan, J. Li et al., "Identification of cancer stem cells in vincristine preconditioned SGC7901 gastric cancer cell line," *Journal of Cellular Biochemistry*, vol. 113, no. 1, pp. 302–312, 2012.

[15] Y. Saikawa, K. Fukuda, T. Takahashi, R. Nakamura, H. Takeuchi, and Y. Kitagawa, "Gastric carcinogenesis and the cancer stem cell hypothesis," *Gastric Cancer*, vol. 13, no. 1, pp. 11–24, 2010.

[16] J. E. Visvader and G. J. Lindeman, "Cancer stem cells in solid tumours: accumulating evidence and unresolved questions," *Nature Reviews Cancer*, vol. 8, no. 10, pp. 755–768, 2008.

[17] A. B. Alvero, R. Chen, H. H. Fu et al., "Molecular phenotyping of human ovarian cancer stem cells unravel the mechanisms for repair and chemo-resistance," *Cell Cycle*, vol. 8, no. 1, pp. 158–166, 2009.

[18] N. Takebe, P. J. Harris, R. Q. Warren, and S. P. Ivy, "Targeting cancer stem cells by inhibiting Wnt, Notch, and Hedgehog pathways," *Nature Reviews Clinical Oncology*, vol. 8, no. 2, pp. 97–106, 2011.

[19] K. Garber, "Notch emerges as new cancer drug target," *Journal of the National Cancer Institute*, vol. 99, no. 17, pp. 1284–1285, 2007.

[20] H. T. Jun, J. Stevens, and P. Kaplan-Lefko, "Top NOTCH targets: Notch signaling in cancer," *Drug Development Research*, vol. 69, no. 6, pp. 319–328, 2008.

[21] J. Dufraine, Y. Funahashi, and J. Kitajewski, "Notch signaling regulates tumor angiogenesis by diverse mechanisms," *Oncogene*, vol. 27, no. 38, pp. 5132–5137, 2008.

[22] T. S. Yeh, C. N. Wu, K. W. Hsu et al., "The activated Notch1 signal pathway is associated with gastric cancer progression through cyclooxygenase-2," *Cancer Research*, vol. 69, no. 12, pp. 5039–5048, 2009.

[23] D. W. Li, Q. Wu, Z. H. Peng, Z. R. Yang, and Y. Wang, "Expression and significance of Notch1 and PTEN in gastric cancer," *Ai Zheng*, vol. 26, no. 11, pp. 1183–1187, 2007.

[24] V. Bolós, M. Blanco, V. Medina, G. Aparicio, S. Díaz-Prado, and E. Grande, "Notch signalling in cancer stem cells," *Clinical and Translational Oncology*, vol. 11, no. 1, pp. 11–19, 2009.

[25] Y. H. Zhan, J. Liu, X. J. Qu et al., "β-Elemene induces apoptosis in human renal-cell carcinoma 786-0 cells through inhibition of MAPK/ERK and PI3K/Akt/mTOR signalling pathways," *Asian Pacific Journal of Cancer Prevention*, vol. 312, no. 13, pp. 2739–2744, 2012.

[26] P. Zhao, Y. Li, and Y. Lu, "Aberrant expression of CD133 protein correlates with Ki-67 expression and is a prognostic marker in gastric adenocarcinoma," *BMC Cancer*, vol. 10, p. 218, 2010.

[27] S. J. Shin, H. C. Jeung, J. B. Ahn et al., "Mobilized CD34+ cells as a biomarker candidate for the efficacy of combined maximal tolerance dose and continuous infusional chemotherapy and G-CSF surge in gastric cancer," *Cancer Letters*, vol. 270, no. 2, pp. 269–276, 2008.

[28] W. Gong, L. Wang, J. C. Yao et al., "Expression of activated signal transducer and activator of transcription 3 predicts expression of vascular endothelial growth factor in and angiogenic phenotype of human gastric cancer," *Clinical Cancer Research*, vol. 11, no. 4, pp. 1386–1393, 2005.

[29] H. G. Yu, J. Y. Li, Y. N. Yang et al., "Increased abundance of cyclooxygenase-2 correlates with vascular endothelial growth factor-A abundance and tumor angiogenesis in gastric cancer," *Cancer Letters*, vol. 195, no. 1, pp. 43–51, 2003.

[30] Y. E. Joo, J. S. Rew, Y. H. Seo et al., "Cyclooxygenase-2 overexpression correlates with vascular endothelial growth factor expression and tumor angiogenesis in gastric cancer," *Journal of Clinical Gastroenterology*, vol. 37, no. 1, pp. 28–33, 2003.

[31] O. Vidal, A. Soriano-Izquierdo, M. Pera et al., "Positive VEGF immunostaining independently predicts poor prognosis in curatively resected gastric cancer patients: results of a study assessing a panel of angiogenic markers," *Journal of Gastrointestinal Surgery*, vol. 12, no. 6, pp. 1005–1014, 2008.

[32] P. E. Vermeulen, G. Gasparini, S. B. Fox et al., "Quantification of angiogenesis in solid human tumours: an international consensus on the methodology and criteria of evaluation," *European Journal of Cancer Part A*, vol. 32, no. 14, pp. 2474–2484, 1996.

[33] O. H. Lowry, N. J. Rosebrough, A. L. Farr, and R. J. Randall, "Protein measurement with the Folin phenol reagent," *The Journal of Biological Chemistry*, vol. 193, no. 1, pp. 265–275, 1951.

[34] N. A. Lobo, Y. Shimono, D. Qian, and M. F. Clarke, "The biology of cancer stem cells," *Annual Review of Cell and Developmental Biology*, vol. 23, pp. 675–699, 2007.

[35] Z. Wang, Y. Zhang, Y. Li, S. Banerjee, J. Liao, and F. H. Sarkar, "Down-regulation of Notch-1 contributes to cell growth inhibition and apoptosis in pancreatic cancer cells," *Molecular Cancer Therapeutics*, vol. 5, no. 3, pp. 483–493, 2006.

[36] Z. Wang, Y. Zhang, S. Banerjee, Y. Li, and F. H. Sarkar, "Notch-1 down-regulation by curcumin is associated with the inhibition of cell growth and the induction of apoptosis in pancreatic cancer cells," *Cancer*, vol. 106, no. 11, pp. 2503–2513, 2006.

[37] M. L. Deftos, E. Huang, E. W. Ojala, K. A. Forbush, and M. J. Bevan, "Notch1 signaling promotes the maturation of CD4 and CD8 SP thymocytes," *Immunity*, vol. 13, no. 1, pp. 73–84, 2000.

[38] A. Fischer, N. Schumacher, M. Maier, M. Sendtner, and M. Gessler, "The Notch target genes Hey1 and Hey2 are required for embryonic vascular development," *Genes and Development*, vol. 18, no. 8, pp. 901–911, 2004.

[39] W. Hu, C. Lu, H. H. Dong et al., "Biological roles of the Delta family notch ligand Dll4 in tumor and endothelial cells in ovarian cancer," *Cancer Research*, vol. 71, no. 18, pp. 6030–6039, 2011.

[40] G. Thurston and J. Kitajewski, "VEGF and Delta-Notch: interacting signalling pathways in tumour angiogenesis," *British Journal of Cancer*, vol. 99, no. 8, pp. 1204–1209, 2008.

[41] Z. Wang, Y. Li, and F. H. Sarkar, "Notch signaling proteins: legitimate targets for cancer therapy," *Current Protein and Peptide Science*, vol. 11, no. 6, pp. 398–408, 2010.

[42] T. Kawahara, N. Kawaguchi-Ihara, Y. Okuhashi, M. Itoh, N. Nara, and S. Tohda, "Cyclopamine and quercetin suppress the growth of leukemia and lymphoma cells," *Anticancer Research*, vol. 29, no. 11, pp. 4629–4632, 2009.

[43] L. Lin, Y. Liu, H. Li et al., "Targeting colon cancer stem cells using a new curcumin analogue, GO-Y030," *British Journal of Cancer*, vol. 105, no. 2, pp. 212–220, 2011.

[44] B. Bao, S. Ali, D. Kong et al., "Anti-tumor activity of a novel compound-CDF is mediated by regulating miR-21, miR-200, and pten in pancreatic cancer," *PLoS ONE*, vol. 6, no. 3, Article ID e17850, 2011.

[45] Y. Zhen, S. Zhao, Q. Li, Y. Li, and K. Kawamoto, "Arsenic trioxide-mediated Notch pathway inhibition depletes the cancer stem-like cell population in gliomas," *Cancer Letters*, vol. 292, no. 1, pp. 64–72, 2010.

[46] H. Sun and S. Zhang, "Arsenic trioxide regulates the apoptosis of glioma cell and glioma stem cell via down-regulation of stem cell marker Sox2," *Biochemical and Biophysical Research Communications*, vol. 410, no. 3, pp. 692–697, 2011.

[47] A. Shiras, S. Chettiar T, V. Shepal, G. Rajendran, G. Rajendra Prasad, and P. Shastry, "Spontaneous transformation of human adult nontumorigenic stem cells to cancer stem cells is driven by genomic instability in a human model of glioblastoma," *Stem Cells*, vol. 25, no. 6, pp. 1478–1489, 2007.

[48] M. Kondratyev, A. Kreso, R. M. Hallett et al., "Gamma-secretase inhibitors target tumor-initiating cells in a mouse model of ERBB2 breast cancer," *Oncogene*, vol. 31, no. 1, pp. 93–103, 2011.

[49] A. Sharma, A. N. Paranjape, A. Rangarajan, and R. R. Dighe, "A monoclonal antibody against human Notch1 ligand-binding domain depletes subpopulation of putative breast cancer stem-like cells," *Molecular Cancer Therapeutics*, vol. 11, no. 1, pp. 77–86, 2012.

[50] R. C. A. Sainson and A. L. Harris, "Anti-Dll4 therapy: can we block tumour growth by increasing angiogenesis?" *Trends in Molecular Medicine*, vol. 13, no. 9, pp. 389–395, 2007.

[51] I. Noguera-Troise, C. Daly, N. J. Papadopoulos et al., "Blockade of Dll4 inhibits tumour growth by promoting non-productive angiogenesis," *Nature*, vol. 444, no. 7122, pp. 1032–1037, 2006.

[52] J. L. Li, R. C. A. Sainson, W. Shi et al., "Delta-like 4 Notch ligand regulates tumor angiogenesis, improves tumor vascular function, and promotes tumor growth *in vivo*," *Cancer Research*, vol. 67, no. 23, pp. 11244–11253, 2007.

[53] L. Xu, S. Tao, X. Wang et al., "The synthesis and anti-proliferative effects of β-elemene derivatives with mTOR inhibition activity," *Bioorganic and Medicinal Chemistry*, vol. 14, no. 15, pp. 5351–5356, 2006.

[54] Y. Q. Yao, X. Ding, Y. C. Jia, C. X. Huang, Y. Z. Wang, and Y. H. Xu, "Anti-tumor effect of β-elemene in glioblastoma cells depends on p38 MAPK activation," *Cancer Letters*, vol. 264, no. 1, pp. 127–134, 2008.

[55] G. Li, B. Xie, X. Li et al., "Down-regulation of survivin and hypoxia-inducible factor-1α by β-elemene enhances the radiosensitivity of lung adenocarcinoma xenograft," *Cancer Biotherapy and Radiopharmaceuticals*, vol. 27, no. 1, pp. 56–64, 2012.

[56] G. Wang, X. Li, F. Huang et al., "Antitumor effect of β-elemene in non-small-cell lung cancer cells is mediated via induction of cell cycle arrest and apoptotic cell death," *Cellular and Molecular Life Sciences*, vol. 62, no. 7-8, pp. 881–893, 2005.

[57] X. Li, G. Wang, J. Zhao et al., "Antiproliferative effect of β-elemene in chemoresistant ovarian carcinoma cells is mediated through arrest of the cell cycle at the G2-M phase," *Cellular and Molecular Life Sciences*, vol. 62, no. 7-8, pp. 894–904, 2005.

[58] Z. Yu, R. Wang, L. Xu, S. Xie, J. Dong, and Y. Jing, "β-Elemene piperazine derivatives induce apoptosis in human leukemia cells through downregulation of c-FLIP and Generation of ROS," *PLoS ONE*, vol. 6, no. 1, Article ID e15843, 2011.

[59] Z. Yu, R. Wang, L. Xu, J. Dong, and Y. Jing, "N-(β-Elemene-13-yl)tryptophan methyl ester induces apoptosis in human leukemia cells and synergizes with arsenic trioxide through a hydrogen peroxide dependent pathway," *Cancer Letters*, vol. 269, no. 1, pp. 165–173, 2008.

[60] J. E. Nör, J. Christensen, D. J. Mooney, and P. J. Polverini, "Vascular endothelial growth factor (VEGF)-mediated angiogenesis is associated with enhanced endothelial cell survival and induction of Bcl-2 expression," *American Journal of Pathology*, vol. 154, no. 2, pp. 375–384, 1999.

[61] A. Iervolino, D. Trisciuoglio, D. Ribatti et al., "Bcl-2 overexpression in human melanoma cells increases angiogenesis through VEGF mRNA stabilization and HIF-1-mediated transcriptional activity," *The FASEB Journal*, vol. 16, no. 11, pp. 1453–1455, 2002.

[62] I. S. Song, A. G. Wang, Y. Y. Sun et al., "Regulation of glucose metabolism-related genes and VEGF by HIF-1α and HIF-1β, but not HIF-2α, in gastric cancer," *Experimental and Molecular Medicine*, vol. 41, no. 1, pp. 51–58, 2009.

[63] Y. Yoshino, M. Aoyagi, M. Tamaki, L. Duan, T. Morimoto, and K. Ohno, "Activation of p38 MAPK and/or JNK contributes to increased levels of VEGF secretion in human malignant glioma cells," *International Journal of Oncology*, vol. 29, no. 4, pp. 981–987, 2006.

[64] R. Qi, H. An, Y. Yu et al., "Notch1 signaling inhibits growth of human hepatocellular carcinoma through induction of cell cycle arrest and apoptosis," *Cancer Research*, vol. 63, no. 23, pp. 8323–8329, 2003.

[65] Y. Chen, D. Li, H. Liu et al., "Notch-1 signaling facilitates survivin expression in human non-small cell lung cancer cells," *Cancer Biology and Therapy*, vol. 11, no. 1, pp. 14–21, 2011.

Hindawi Publishing Corporation
Evidence-Based Complementary and Alternative Medicine
Volume 2013, Article ID 170261, 14 pages
http://dx.doi.org/10.1155/2013/170261

Research Article

Cyclohexylmethyl Flavonoids Suppress Propagation of Breast Cancer Stem Cells via Downregulation of NANOG

Wen-Ying Liao,[1,2] Chih-Chuang Liaw,[2,3,4] Yuan-Chao Huang,[2] Hsin-Ying Han,[1] Hung-Wei Hsu,[5] Shiaw-Min Hwang,[6] Sheng-Chu Kuo,[2,7] and Chia-Ning Shen[1,5,7,8]

[1] *Stem Cell Program, Genomics Research Center, Academia Sinica, Nangang, Taipei 115, Taiwan*
[2] *Graduate Institute of Pharmaceutical Chemistry, China Medical University, Taichung 402, Taiwan*
[3] *Department of Marine Biotechnology and Resources, National Sun Yat-sen University, Kaohsiung 804, Taiwan*
[4] *Asia-Pacific Ocean Research Center, National Sun Yat-sen University, Kaohsiung 804, Taiwan*
[5] *Department of Biotechnology and Laboratory Science in Medicine, National Yang-Ming University, Taipei 112, Taiwan*
[6] *Bioresource Collection and Research Center, Food Industry Research and Development Institute, Hsinchu 300, Taiwan*
[7] *The Ph.D. Program for Cancer Biology and Drug Discovery, China Medical University, Taichung 402, Taiwan*
[8] *Graduate Institute of Clinical Medicine, Taipei Medical University, Sinyi District, Taipei 110, Taiwan*

Correspondence should be addressed to Chia-Ning Shen; cnshen@gate.sinica.edu.tw

Received 7 February 2013; Accepted 2 March 2013

Academic Editor: Hui-Fen Liao

Breast cancer stem cells (CSCs) are highly tumorigenic and possess the capacity to self-renew. Recent studies indicated that pluripotent gene *NANOG* involves in regulating self-renewal of breast CSCs, and expression of NANOG is correlated with aggressiveness of poorly differentiated breast cancer. We initially confirmed that breast cancer MCF-7 cells expressed NANOG, and overexpression of NANOG enhanced the tumorigenicity of MCF-7 cells and promoted the self-renewal expansion of $CD24^{-/low}CD44^{+}$ CSC subpopulation. In contrast, knockdown of NANOG significantly affected the growth of breast CSCs. Utilizing flow cytometry, we identified five cyclohexylmethyl flavonoids that can inhibit propagation of NANOG-positive cells in both breast cancer MCF-7 and MDA-MB231 cells. Among these flavonoids, ugonins J and K were found to be able to induce apoptosis in non-CSC populations and to reduce self-renewal growth of $CD24^{-/low}CD44^{+}$ CSC population. Treatment with ugonin J significantly reduced the tumorigenicity of MCF-7 cells and efficiently suppressed formation of mammospheres. This suppression was possibly due to p53 activation and NANOG reduction as either addition of p53 inhibitor or overexpression of NANOG can counteract the suppressive effect of ugonin J. We therefore conclude that cyclohexylmethyl flavonoids can possibly be utilized to suppress the propagation of breast CSCs via reduction of NANOG.

1. Introduction

Breast cancer is a leading cause of cancer death among women, as cancer recurrence and metastasis occur frequently in breast cancer patients [1, 2]. Accumulating evidence indicates that $CD24^{-/low}CD44^{+}$ breast cancer cells, also referred to as "tumorigenic breast cancer cells" [3, 4], "breast cancer stem cells (CSCs)" [5], and "stem-like breast cancer cells" [6], possess stem cell characteristics, display resistance to conventional therapies, and have high tumor-initiating and metastatic ability [3, 4, 7–9]. Therefore, the presence of breast CSCs has been suggested to be the underlying cause of breast cancer recurrence and metastasis [2, 8, 9]. In order to improve breast cancer therapeutics, efforts are now being directed towards identifying strategies that target breast CSCs [2, 9].

Accumulating evidence supports that self-renewal regulators of normal stem cells may govern clinical behavior of human cancer [10, 11]. For example, embryonic stem cell (ESC) signature is associated with poor clinical outcome in patient of breast cancer patients [12]. Among the regulatory genes involved in pluripotent maintenance of ESCs, NANOG was found to express a NANOGP8 retrogene

locus in a wide variety of somatic and cancer cells [13–15]. Recent work has shown that NANOG was functionally involved in human tumor development and in regulating cancer stemness [15, 16]. Knockdown of NANOG significantly reduced the tumorigenic potentials of various cancer cells including breast cancer [17]. NANOG has also been identified in breast cancer cells and was found to mediate multidrug resistance via activation of STAT3 signaling [18] suggesting that NANOG is a potential target for breast cancer therapeutics.

Herbal medicine has been proposed for utilizing a complementary approach for control of breast cancer recurrence and metastasis [19, 20]. However, whether the activity of breast CSCs can be suppressed by treatment of herbal medicine has never been addressed. In Chinese traditional medicine, the roots of the fern *Helminthostachys zeylanica* (L.) Hook. (Ophioglossaceae), known as "Ding-Di-U-Gon", is used as antipyretic and antiphlogistic agent to treat inflammatory diseases, various hepatic disorders, and possibly malignancy in pancreas [21–23]. The rhizome of this medicinal fern is also named as "tunjuk langit" in India which has been used as a folk medicine to treat pulmonary disease and even to cure impotency by the tribal people [24]. In Malaysia, the rhizome is used as an antidiarrheal agent and chewed with areca for whooping cough relief [25]. However, efforts to evaluate the efficacy of such treatment on CSCs and to identify responsible principles of its effect on cancer were scarce.

In the present study, a group of natural cyclohexylmethyl flavonoids isolated from the rhizomes of *H. zeylanica* had been examined. Utilizing flow cytometry, we identified five members of natural cyclohexylmethyl flavonoids that can inhibit expansion of $NANOG^+$ cells. Among these cyclohexylmethyl flavonoids, ugonins J and K, which were the main components of the ethyl acetate-soluble extract of the rhizomes of *H. zeylanica*, were able to suppress propagation of $CD24^{-/low}CD44^+$ breast cancer stem cells both *in vitro* and *in vivo*.

2. Materials and Methods

2.1. Cell Culture. Both human breast cancer cell lines MCF-7 and MDA-MB231 were obtained from Bioresource Collection and Research Center (Hsin-Chu, Taiwan) and maintained in either α-Minimum Essential Medium (α-MEM) or L-15 medium (Invitrogen) supplemented with 2 mM L-glutamine (Sigma), 1.5 g/L sodium bicarbonate, 0.1 mM nonessential amino acids (Invitrogen), 1.0 mM sodium pyruvate (Invitrogen), and 10% fetal bovine serum (FBS) (Invitrogen). Human foreskin fibroblast HFF-1 cells were imported from ATCC and were maintained in ATCC-formulated Dulbecco's modified Eagle's medium supplemented with 15% FBS (Invitrogen).

2.2. Chemicals. Doxorubicin (Dox) was obtained from Sigma. Ugonins (J-S) were isolated and purified from the rhizomes of *Helminthostachys zeylanica* [21]. All of the ugonins used in the experiments were repurified by reversed-phase HPLC to ensure the purity >99%.

2.3. Formation of Mammospheres. MCF-7 cells (1×10^4 cells) were grown in suspension culture in serum-free Dulbecco's Modified Eagle Medium (DMEM) supplemented with 2 mM-L-glutamine, 0.1 mM nonessential amino acids, 20 ng/mL human epidermal growth factor (R&D), 20 ng/mL basic fibroblast growth factor (Millipore), 4 μg/mL heparin, and 5 μg/mL insulin (Sigma) and 1x B27 supplement (Invitrogen).

2.4. Flow Cytometric Analysis. Cells were trypsinized and washed three times with PBS before resuspension in Hanks' Balanced Salt Solution (HBSS; Invitrogen) containing 2% FBS and 10 mM HEPES (Invitrogen). The cell density was adjusted to $10^6/100\ \mu$L in staining buffer before being stained with antibodies FITC-conjugated anti-CD24 (BD Biosciences) and APC-conjugated anti-CD44 (BD Biosciences) for 30 minutes. In some experiments, MCF-7 cells were stained with anti-NANOG antibodies (Cell Signaling) followed by staining with FITC-conjugated goat anti-rabbit IgG (BD Biosciences). Stained cells were analyzed utilizing FACSCalibur flow cytometry (BD Biosciences) after the addition of propidium iodide (2 μg/mL) to exclude dead cells.

2.5. Immunofluorescent Staining. MCF-7 cells (5×10^4 cell/well) were seeded in the 24-well plate and cultured overnight. After cells were treated with different compounds for different time course, cells were fixed by 4% PFA (Sigma) for 30 minutes at room temperature and permeabilized at room temperature in 0.1% Triton X-100 for 30 minutes. After blocking with 2% Roche blocking reagent, the cells were incubated with primary antibody overnight at 4°C and with secondary antibody for 2 hours at room temperature. The primary antibodies were used at the following dilutions: rabbit anti-NANOG 1 : 100 (Cosmo Bio USA, Inc) and rabbit antiphospho-$p53^{S15}$ 1 : 400 (Cell Signaling). Cells were counter-stained with Hoechst dye (Sigma) to visualize the cell nuclei. Images of the immunostaining were obtained using a fluorescence microscopy (Leica Microsystems Inc).

2.6. Establishment of NANOG-Overexpressing and p53-Overexpressing Cells. The lentiviral construct-pSin-EF2-NANOG-Pur was obtained from Addgene (plasmid 16578) [26]. In order to produce NANOG lentivirus, the day prior to transfection, 293T cells were seeded at 2.4×10^6 cells per 10-cm dish. Each 10-cm dish was transfected with 7.5 μg pSin-EF2-Nanog-Pur 6.75 μg pCMV-Δ8.91 packaging plasmid, and 0.75 μg pMD.G envelope plasmid using Genejuice transfection reagent (Novagen). Virus-containing supernatant was collected and filtered through 0.45 μm pore filters and stored at 4°C. Virus was further concentrated by ultracentrifugation for 2.5 hours at 26000 rpm in a Beckman SW 28.1 rotor (Beckman Coulter), and the resulting virus pellet was resuspended in PBS (pH 7.4) containing 1% BSA at 4°C overnight before being aliquoted and stored at −80°C. MCF-7 cells were first infected with NANOG lentivirus and then NANOG-overexpressing cells were selected in α-MEM containing 1 μg/mL puromycin. The GFP-p53 plasmid was obtained from Addgene (plasmid 12091) [27]. MCF-7 cells (5×10^4 cell/well in 24-well plate) were seeded on coverslips

and transfected with 0.25 μg of GFP-p53 plasmid using GeneJuice reagent (Merck Millipore).

2.7. Establishment of NANOG-Knockdown Cells. The lentiviral shNANOG construct (TRCN0000004884) was obtained from the National RNAi Core Facility (Institute of Molecular Biology/Genomic Research Center, Academia Sinica), and the lentivirus was generated as described in the previous section. MCF-7 cells were infected with shNANOG lentivirus, and then NANOG-knockdown cells were selected in α-MEM containing 1 μg/mL puromycin.

2.8. Western Blotting Analysis. Whole-cell extracts were prepared using RIPA buffer containing 150 mM NaCl, 50 mM Tris HCl (pH 8), 1% NP-40, 0.5% sodium deoxycholate, 0.1% SDS, and protease inhibitors and phosphatase inhibitors cocktails (Sigma). Whole-cell extracts of MCF-7 cells were separated by 10% SDS-PAGE and subsequently transferred to PVDF membrane (Millipore). Samples were incubated in blocking buffer (0.1% Tween 20, 5% nonfat milk powder in TBS) for 1 hour at room temperature. Afterwards, the membrane was incubated with primary antibody in blocking buffer overnight at 4°C before being washed twice with TBST (0.1% Tween in TBS) and incubated with the appropriate secondary antibody in blocking buffer for 1 hour at room temperature. The blot was developed using ECL western blotting substrate (Millipore) and analyzed using the luminescent image analyzer, LAS-4000mini (Fujifilm). The primary antibodies were used at the following dilutions: rabbit anti-NANOG, 1 : 1000 (Cell Signaling); rabbit anti-p53, 1 : 1000 (Cell Signaling); rabbit anti-p53-Ser15p, 1 : 1000 (Cell Signaling); rabbit anti-p53-Ser392p, 1 : 1000 (Cell Signaling); rat anti-ABCG2, 1 : 100 (Abcam); rabbit anti-Stat3, 1 : 2000 (Cell Signaling); rabbit antiphospho-Stat3^{Y705}, 1 : 1000 (Cell Signaling); rabbit antiphospho-Stat3^{S727}, 1 : 1000 (Cell Signaling); rabbit anticleaved PARP, 1 : 1000 (Cell Signaling); rabbit anticleaved Caspase9, 1 : 1000 (Cell Signaling); and mouse anti-β-actin, 1 : 10000 (Sigma). The secondary antibodies used were anti-rabbit HRP (1 : 1000, Santa Cruz) or anti-mouse HRP (1 : 1000, Santa Cruz).

2.9. Analysis of the Promoter and p53-Binding Site of NANOG and NANOGP8. To analyze the elements upstream of NANOG and NANOGP8, the 5-kb upstream sequences of the translation start sites of NANOG and NANOGP8 were retrieved from the human RefSeq files (NC_000012 and NC_000015, resp.). The *p53MH* program (PMID: 12077306) was employed to detect possible P53-binding site within the 5-kb sequence. The top 100 possible p53-binding sites were extracted. For the identification of the most likely binding site, the threshold of the percentage of maximum possible score was set as 80%. The prediction of the promoter region was carried out with *CoreBoost_HM* (PMID: 18997002). The score of 0.7 was set as a cutoff value for the plausible promoter region.

2.10. Establishment of Orthotropic Tumor Xenografts in SCID Mice. All animal experiments were approved by the Academia Sinica Institutional Animal Care and Utilization Committee. Four-week-old female SCID mice purchased from BioLASCO were used to carry out MCF-7 xenograft experiments. For tumorigenicity assay, eighteen mice were divided into three groups (6 mice/group) and were injected in the mammary fat pad with Control, NANOG-overexpressing, or NANOG-knockdown MCF-7 cells (1×10^6 cells/60 μL). To determine if ugonin J can suppress tumor growth, eighteen mice were divided into three groups (6 mice/group) and were injected in the mammary fat pad with MCF-7 cells (2×10^5 cells/60 μL). When the tumor volume reached 50 mm^3 (set as Day 0), the tumor-bearing mice were then administered a weekly dose of doxorubicin (12 mg/kg, dissolved in 100 μL of DMSO) or ugonin J (50 mg/kg, dissolved in 100 μL of DMSO) interperitoneally for a total of 4 doses. Body weight of mice and tumor size were measured weekly.

2.11. Histology and Immunohistochemistry. Tumor tissues were fixed overnight at room temperature with 3.5% formaldehyde solution containing 68.6% EtOH and 4.8% acetic acid (FAA fixative) prior to being processed and embedded in paraffin. 4 μm thick sections were cut and mounted on Superfrost plus slides (Thermo Scientific). For immunohistochemical staining, sections were subjected to antigen retrieval in Citric-acid based buffer (Vector Laboratories) at 95°C for 20 minutes. The sections were then permeabilized with 0.1% (v/v) Triton X-100 in PBS for 30 min and incubated in 2% blocking buffer (Roche) before being incubated sequentially with primary, HRP-conjugated secondary antibodies. Super Sensitive Polymer HRP IHC Detection System (Biogenex Laboratories) was used to visualize the positive cells. Sections were counterstained with hematoxylin and mounted with Entellan Neu (Merck). The primary antibodies were used at the following dilutions: rabbit anti-Nanog 1 : 150 (Cosmo Bio), mouse anti-MUC 1 1 : 100 (Abcam), and mouse anti-HCAM/CD44 1 : 100 (SantaCruz).

2.12. Invasion Assay. 1×10^4 of MCF-7 cells suspended in serum-free medium with or without ugonins J or K was seeded into the top chamber of the matrigel-coated insert (Millicell, 24-well plate, 8 μm, Millipore) in 100 μL serum-free medium. In the lower chamber, the well was filled with serum-containing medium which was used as a chemoattractant. After 24-hour incubation, cells that did not invade through the pores were removed by a cotton swab. Cells on the lower surface of the membrane were fixed with methanol and stained with Giemsa solution (Merck). The number of invasive cells/each well was counted under a light microscope. Data are representative of three independent experiments. $^{***}P < 0.001$, $^{**}P < 0.01$ versus compared control.

2.13. Statistical Analysis. Experiments were repeated at least three times with consistent results. Statistical differences between groups were determined by unpaired Student's t test. The statistical significance was set at $^{*}P < 0.05$, $^{**}P < 0.01$, $^{***}P < 0.001$. FACS data were analyzed by FlowJo software (Ashland, OR, USA). The statistical analysis

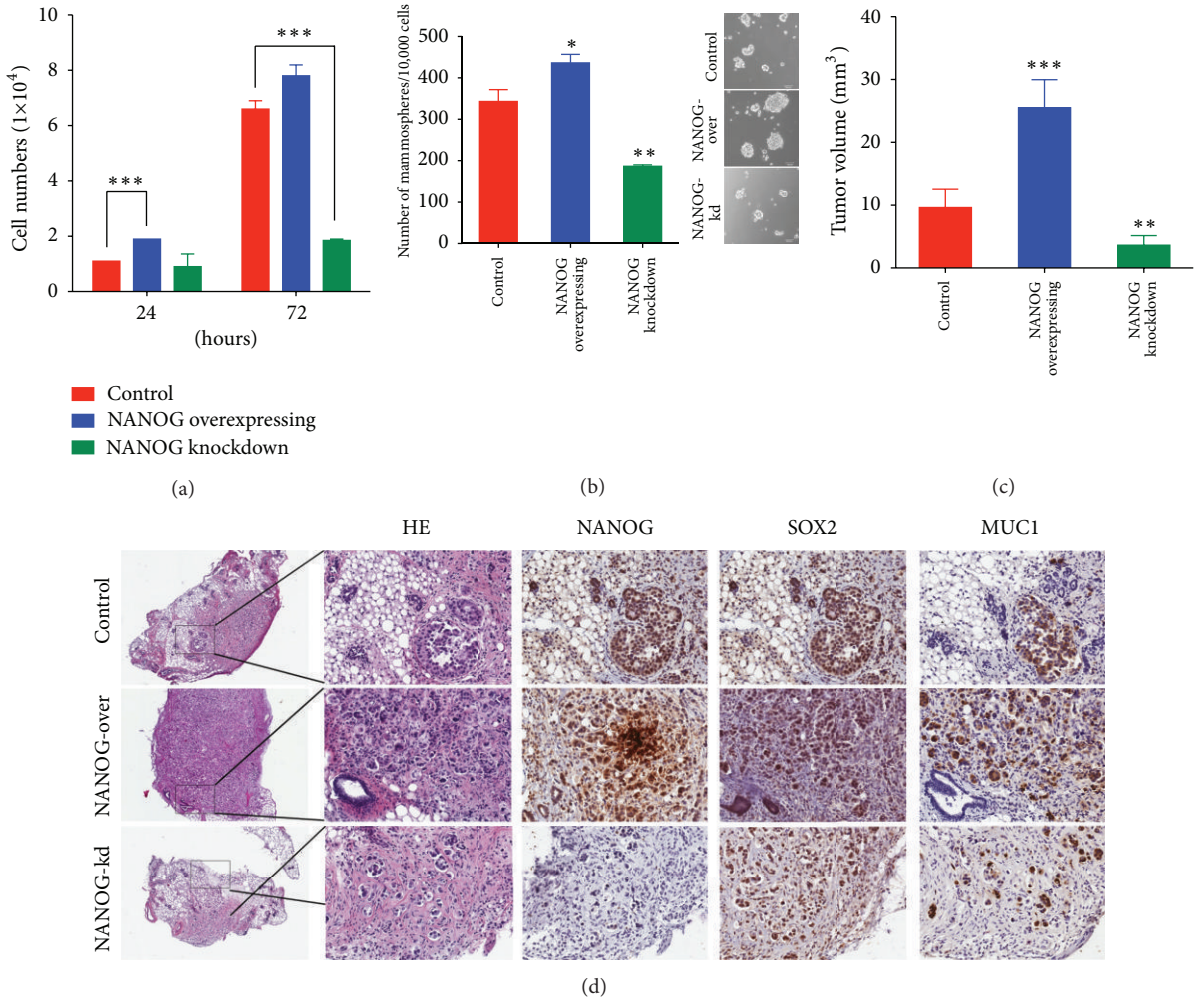

FIGURE 1: NANOG expression plays an important role in cell proliferation and tumorigenesis. (a) Total cell number of MCF-7, NANOG-overexpressing MCF-7, and NANOG-knockdown MCF-7 cells (0.9×10^5 cells in 12-well plates) were counted after 24, 72 hours of culture ($n = 3$). (b) Mammosphere formation in sphere-forming medium for 28 days. Total mammospheres were counted under a microscope at days 28. Mean of three independent experiments ± SEM. $^{**}P < 0.01$, $^{*}P < 0.05$ versus control mammospheres. (c) Eighteen SCID mice were divided into three groups (6 mice/group). The MCF-7 orthotopic tumors in SCID mice were formed with vector control, NANOG-overexpressing, and NANOG-knockdown MCF-7 cells (1×10^6). The tumor volumes of SCID mice were measured weekly. The average tumor volume of MCF-7 tumors was removed from SCID after 4 weeks. $^{***}P < 0.001$, $^{**}P < 0.01$ versus vector control (d) NANOG overexpression enhanced expression of the cancer stem cell marker SOX2 and MUC1 in tumor xenografts. Hematoxylin-Eosin stain and Immunohistochemical detection (x200) for NANOG, SOX2 and MUC1 on vector control, NANOG-overexpressing and NANOG-knockdown tumor xenografts.

for fluorescent staining used MetaMorph imaging analytical software (Molecular Devices).

3. Results

3.1. A Critical Role of NANOG in Modulating Proliferation and Tumorigenicity of Breast Cancer Cells. We initially investigated whether expression of NANOG plays an important role in breast cancer growth. To address this question, we generated NANOG-overexpressing and NANOG-knockdown MCF-7 cell lines. As shown in Figure 1(a), RNA interference-mediated NANOG knockdown reduced breast cancer. And overexpression of NANOG slightly increased the overall growth rate. To further determine if NANOG is the key component modulating self-renewal capability and tumorigenicity of the tumorigenic breast cancer cells, we carried out the mammosphere-forming assay and orthotropic tumor xenografts experiments in female SCID mice. As shown in Figures 1(b) and 1(c), NANOG-overexpressing cells formed 20% more of mammospheres and generated twofold larger tumor xengrafts than control MCF-7 cells. In contrast, knockdown of NANOG not only significantly reduced the ability to form mammospheres, but also dramatically reduced the tumorigenicity of MCF-7 cells. Immunohistochemical analysis of tumor xengrafts (Figure 1(d)) further confirmed that NANOG overexpression enhanced tumor development and increased expressions of cancer stemness protein-SOX2 and MUC1 in tumor xengrafts. Oppositely, NANOG-knockdown

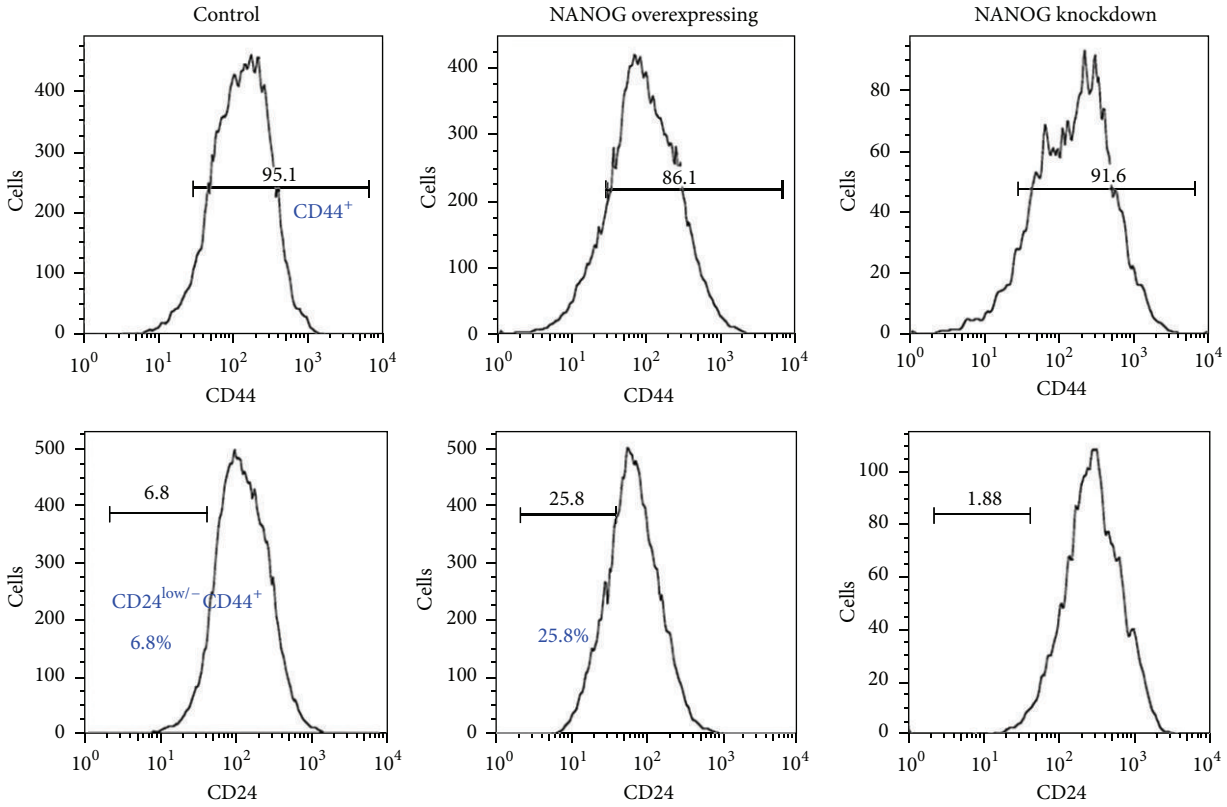

Figure 2: NANOG overexpression enhanced propagation of cancer stem cells. Control, NANOG-overexpressing and NANOG-knockdown MCF-7 cells were double-stained with anti-CD24 and anti-CD44 antibodies followed by FACS analysis ($n > 3$). $CD44^+$ cell population (top panel) and $CD24^-$/low in $CD44^+$ cell population (bottom panel) were analyzed.

cells generated tiny tumor nodules with lower levels of SOX2 and MUC1.

Since NANOG knockdown suppressed mammosphere formation and reduced levels of SOX2 and MUC1 in tumor xengrafts, we next tried to determine if propagation of $CD24^{-/low}CD44^+$ breast CSC subpopulation in MCF-7 cells is also regulated by NANOG [3, 4]. As shown in Figure 2, we found that overexpression of NANOG increased the proportion of $CD24^{-/low}CD44^+$ CSC subpopulation in MCF-7 cells from 6.8% to 25.8%. In contrast, NANOG knockdown reduced the proportion of $CD24^{-/low}CD44^+$ CSC subpopulation in MCF-7 cells from 6.8% to 1.88%. These data indicated that NANOG played an important role in modulating self-renewal and tumorigenicity of breast CSC subpopulations.

3.2. Identification of Bioactive Cyclohexylmethyl Flavonoids Targeting $NANOG^+$ Breast Cancer Cells. We have explored that NANOG possibly played a critical role in modulating self-renewal expansion and tumorigenicity of breast CSCs. We therefore then assume identification of bioactive natural components from herb medicine that can suppress that NANOG would be beneficial for developing a complementary approach for control of breast CSC-driven recurrence and metastasis. Since the dietary flavonoids were reported to possess the ability to suppress the prostate CSCs via inhibiting NANOG [28], a group of natural cyclohexylmethyl flavonoids isolated from the rhizomes of *H. zeylanica* that had been examined. Initially, an MTT colorimetric assay was used to determine cytotoxicity of cyclohexylmethyl flavonoids to two breast cancer cell lines (MCF-7 and MDA-MB231) (Table 1). Among these flavonoids, ugonins J and K were found to display cytotoxicity ($IC_{50} < 25\ \mu M$) to breast cancer cells. In contrast, these two ugonins were less cytotoxic to normal foreskin fibroblasts (HFF). Utilizing flow cytometry, we identified five members of natural cyclohexylmethyl flavonoids that inhibited expansion of $NANOG^+$ population in both MCF-7 and MDA-MB 231 cells (Figures 3(a) and 3(b)). Among these natural cyclohexylmethyl flavonoids, based on using immune-fluorescent staining, we validated that either treatment of ugonins J or K, both compounds were the main component of the ethyl acetate-soluble extract of the rhizomes of *H. zeylanica*, significantly reduced the expression level of NANOG and MUC1 in MCF-7 cells (Figure 3(c)).

3.3. Downregulation of NANOG Mediates the Suppressive Effect of Ugonin J on Propagation of Breast Cancer Stem Cells. The ability of formation of mammospheres is known as one of self-renewal characteristics of breast CSCs; we then determined if treatment of ugonin J can suppress mammosphere-forming ability. In comparing with NANOG overexpression increased mammosphere formation, pre-treatment with ugonin J completely inhibited formation of

Table 1: Structures and activities of ugonins.

Compound name	Chemical structure	IC50 (μM)		
		HFF-1 cells[a]	MCF-7 cells[b]	MDA-MB231 cells[b]
Ugonin J	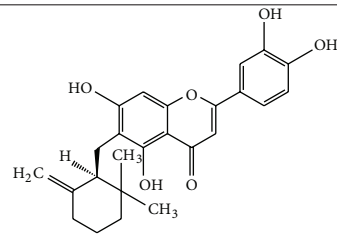	42.1	15.1	22.5
Ugonin K	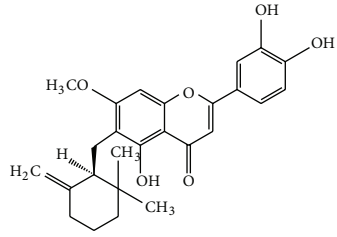	41.0	15.7	22.9
Ugonin L	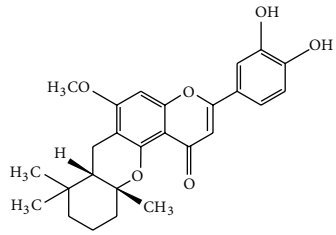	ND*	33.9	54.1
Ugonin P	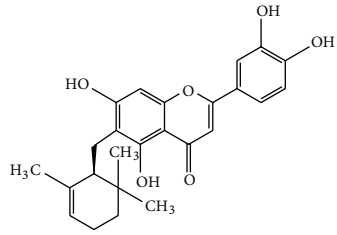	>100	63.1	>100
Ugonin Q	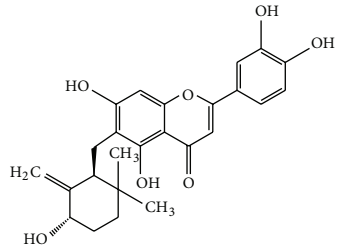	100	>100	67.7
Ugonin R	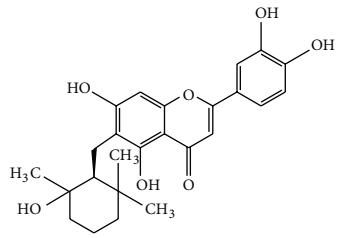	ND	58.8	48.9

Table 1: Continued.

Compound name	Chemical structure	IC50 (μM) HFF-1 cells[a]	MCF-7 cells[b]	MDA-MB231 cells[b]
Ugonin S	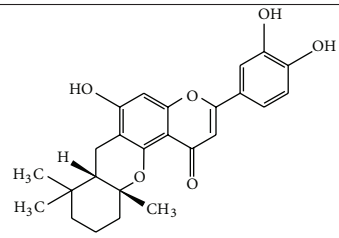	ND	65.9	83.8
Ugonin M	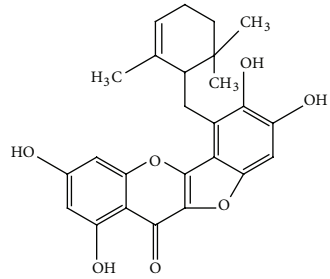	>100	>100	>100
Ugonin N	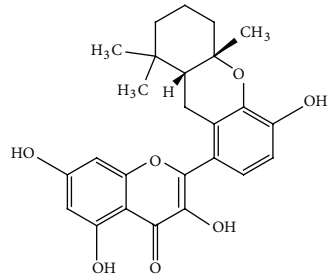	100	65.5	67.2
Ugonin O	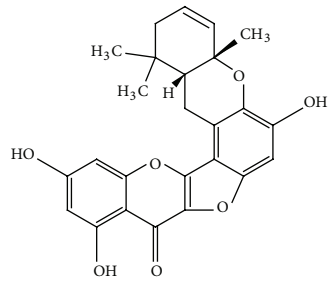	>100	>100	>100

*ND: not determined. [a]HFF-1: human foreskin fibroblasts and [b]MCF-7/MDA-MB-231: human breast adenocarcinoma cell lines.

mammospheres in control MCF-7 cells (Figure 4(a)). In contrast, NANOG overexpression partially counteracted the suppressive effect of ugonin J on mammosphere formation. We then determined if ugonin J can reduce the malignant features of MCF-7 cells including invasion ability, and IL-6 secretion led to STAT3 phosphorylation in mammospheres (Figure 4(b)) [29]. Treatment with ugonin J or K for 24 hours significantly suppressed invasion ability of MCF-7 cells. Moreover, treatment of 28-day mammospheres with ugonin J for 24 hours significantly reduced IL-6 secretion and STAT3 phosphorylation in both control mammospheres and NANOG-overexpressing mammospheres (Figures 4(c) and 4(d)). These results suggest that ugonin J-mediated downregulation of NANOG may be a key event affecting the propagation of breast CSCs.

3.4. P53-Dependent Pathway Mediates Downregulation of NANOG by Ugonin J Treatment. NANOG is a pluripotent regulator of embryonic stem cells, and previous studies have shown that p53 binds to the promoter of *NANOG* and suppresses *NANOG* expression after DNA damage [30, 31]. However, it has recently been shown that there are 11 *NANOG* pseudogenes [32]. *NANOGP8* has been recognized as a retrogene and was recently found to be expressed in various cancer tissues and several cancer cell lines including breast cancer MCF-7 cells. We therefore determined if *NANOGP8* can also be regulated by p53. The *p53MH* program was employed to detect possible P53-binding site within the 5-kb sequence in the *NANOG* and *NANOGP8* promoter regions. As shown in Figure 5, both *NANOG* and *NANOGP8* promoter regions contained several potential binding site for p53.

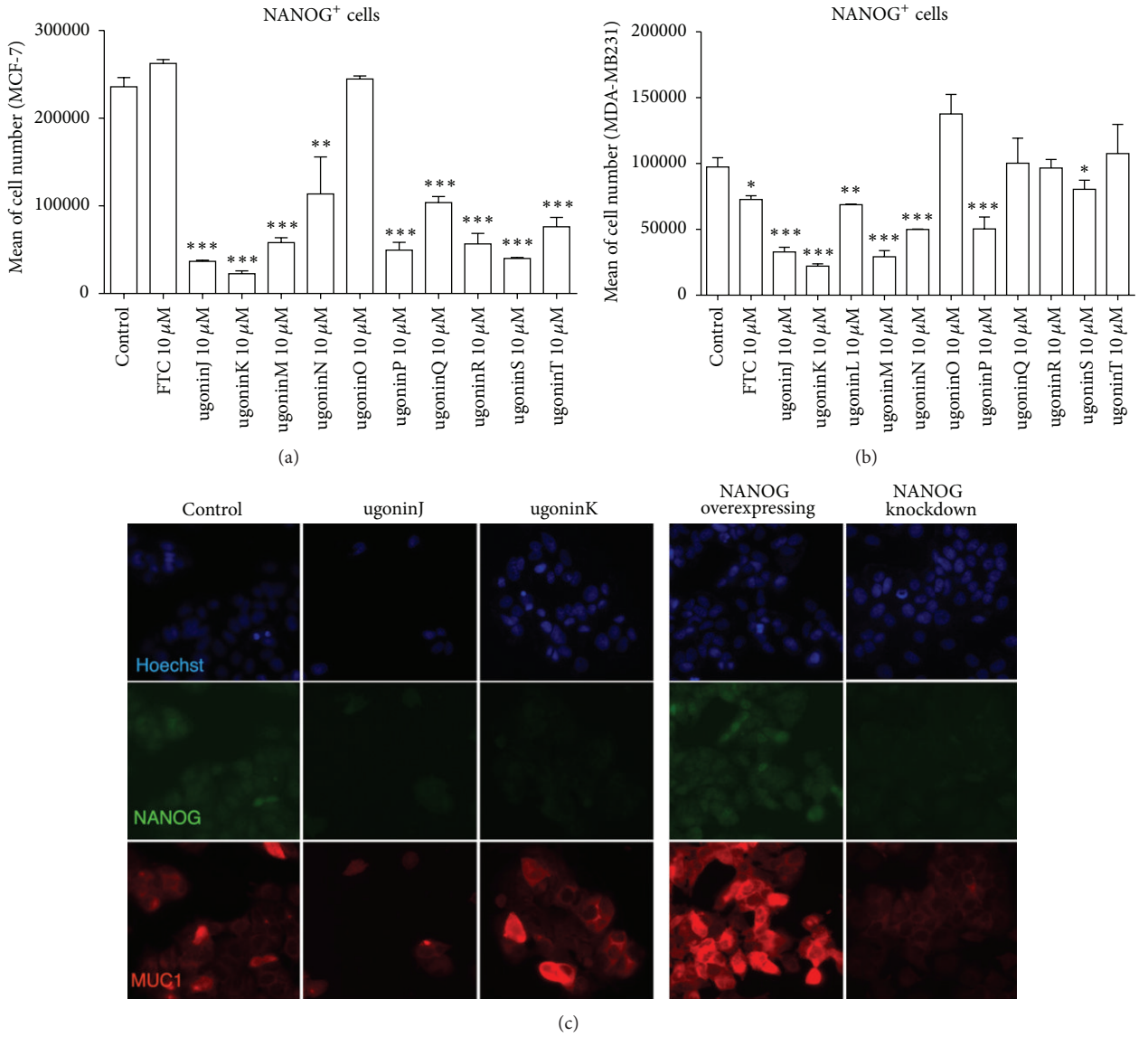

Figure 3: Natural product screening to reduce NANOG$^+$ subpopulation of MCF-7 cells. ((a) and (b)) Screening for natural products by reducing NANOG$^+$ population assay. MCF-7 cells and MDA-MB231 cells (9×10^4 cells in 12-well plates) were treated with natural products for 72 hours before NANOG levels were measured. Total NANOG$^+$ cells were calculated and data were shown as mean ± SEM from 3 independent experiments. $^{***}P < 0.001$ or $^{**}P < 0.01$ versus control cells. (c) Immunofluorescent staining of NANOG (green) and MUC1 (red) on control, treated with ugonins (J, K), NANOG-overexpressing, and NANOG-knockdown MCF-7 cells.

To further determine if p53 pathway can be activated by ugonin J treatment. Time-course experiments were performed and showed that treatment of ugonin J (Figure 6(a)) did in fact increase phosphorylation of p53 at ser15 and ser392 and also activated the apoptotic pathway, as evidenced by cleaved forms of Poly (ADP-ribose) polymerase (PARP) and caspase 9 in western blot analysis. In order to determine whether the downregulation of NANOG in MCF-7 cells with ugonin J treatment was directly mediated by p53, we generated p53-overexpressing MCF-7 cells. A 60% reduction of NANOG$^+$ cells was found in p53-overexpressing MCF-7 cells, combined treatment with ugonin J further reduced 90% of NANOG$^+$ cells. In contrast, treatment of pifithrin-α (p53 inhibitor) rescued the reduction of NANOG induced by ugonin J (Figures 6(b) and 6(c)). The results suggested that activation of p53 pathway mediated the effect of ugonin J on suppression of the NANOG expression.

3.5. Ugonin J Could Suppress Propagation of Breast Cancer Stem Cells In Vivo. To further determine whether ugonin J can suppress the propagation of tumorigenic breast CSCs *in vivo,* MCF-7 cells (2×10^5 cells) were injected into the mammary fat pads of female SCID mice. When the tumor volume reached 50 mm^3 (Day 0), the tumor-bearing animals were administered 4 doses of doxorubicin (12 mg/kg) or ugonin J (50 mg/kg). As shown in Figures 7(a) and 7(b), ugonin J treatment significantly inhibited tumor propagation. Immunohistochemical analysis of tumor xengrafts further

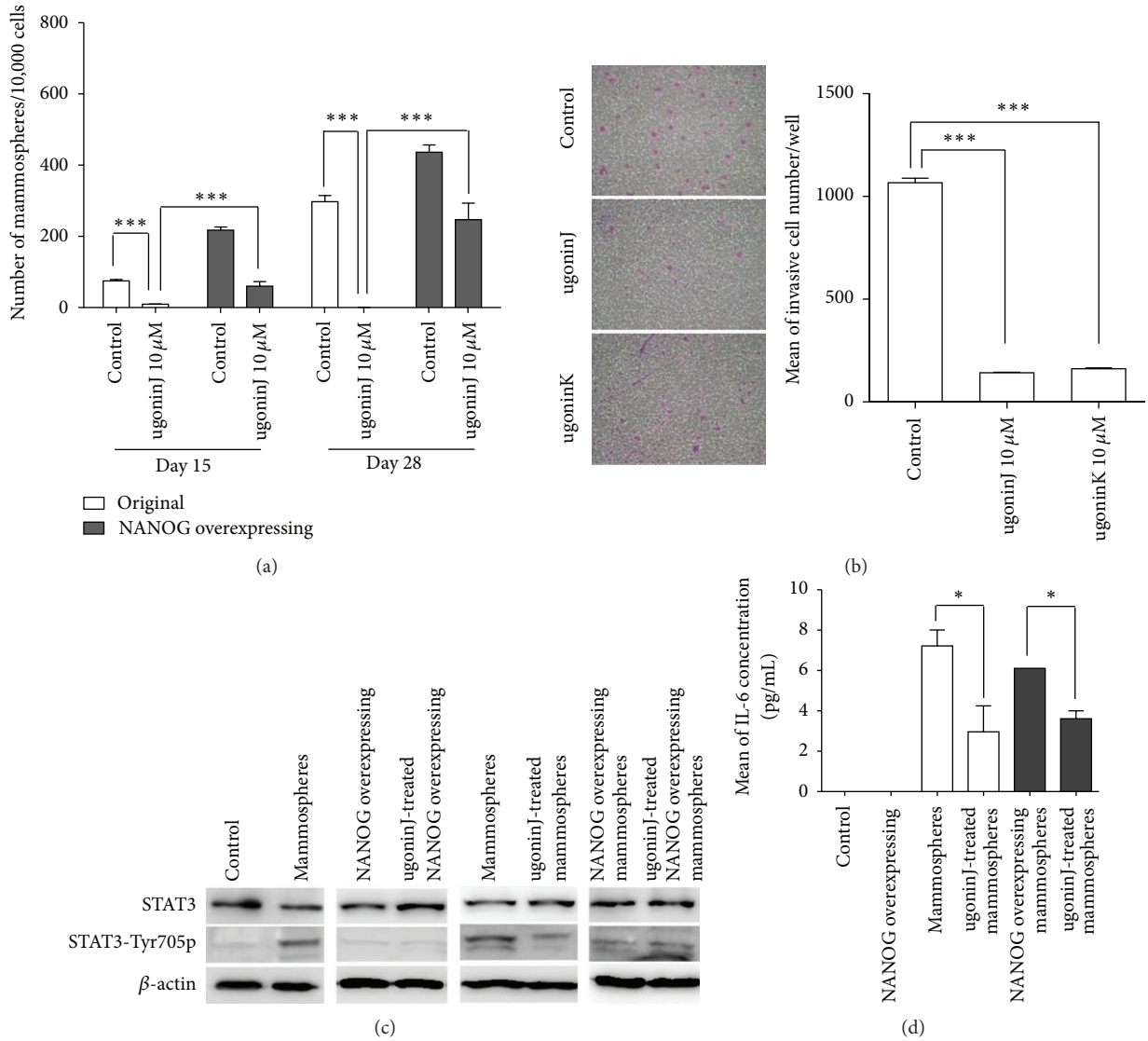

Figure 4: NANOG overexpression counteracts the suppressive effect of ugonin J on propagation of breast cancer stem cells. (a) Control and NANOG-overexpressing MCF-7 cells (1×10^4 cells in 24-well plates) were treated with ugonin J for 3 days prior to mammosphere formation in mammosphere forming medium for 28 days. Total mammospheres were counted under a microscope at days 15 and 28. Mean of three independent experiments ± SEM. $^{***}P < 0.001$ versus control mammospheres. (b) Invasion assay of MCF-7 was performed on matrigel with or without ugonins J or K treatment. Data was shown as mean ± SEM from three independent experiments. $^{***}P < 0.001$, $^{**}P < 0.01$ versus control. (c) Control, NANOG-overexpressing cells (4×10^5 cells in 6-well plates), mammospheres, and NANOG-overexpressing mammospheres (1000 spheres in 6-well plates) were treated with ugonin J for 24 hours before protein extraction. Western blot probed for STAT3 and phospho-STAT3 Tyr705. Equal amounts of protein were used (40 μg per lane). (d) Mammospheres were formed for 15 days from control and NANOG-overexpressing mammospheres (20 spheres in 96 plates) before treatment with or without 10 μM ugonin J for 24 hours. Medium was collected and analyzed by ELISA to determine the production of IL-6 ($n = 3$). Data was shown as mean ± SEM. $^{*}P < 0.05$ versus control.

confirmed that treatment with ugonin J suppressed NANOG expression. In contrast, some Dox-treated cancer cells still expressed NANOG (Figure 7(c)) which can explain how tumors can still be slightly propagated (Figure 7(a)). These results suggest that ugonin J can suppress the propagation of breast CSCs *in vivo* via reduction of NANOG.

4. Discussion

NANOG is a transcriptional factor that plays key roles in the self-renewal and maintenance of pluripotency in embryonic stem cells [31]. There are 11 NANOG pseudogenes [32]. *NANOGP8* has been recognized as a retrogene and was recently found to be expressed in various cancer tissues and several cancer cell lines including the MCF-7 cells used in the current study. We have previously shown that activation of p53 by disrupting porphyrin homeostasis in embryonic stem cells resulted in suppression of NANOG expression [33]. In the current work, we observed a similar phenotype, where treatment of MCF-7 cells with cyclohexylmethyl flavonoids induced activation of p53, which in turn led to the reduction

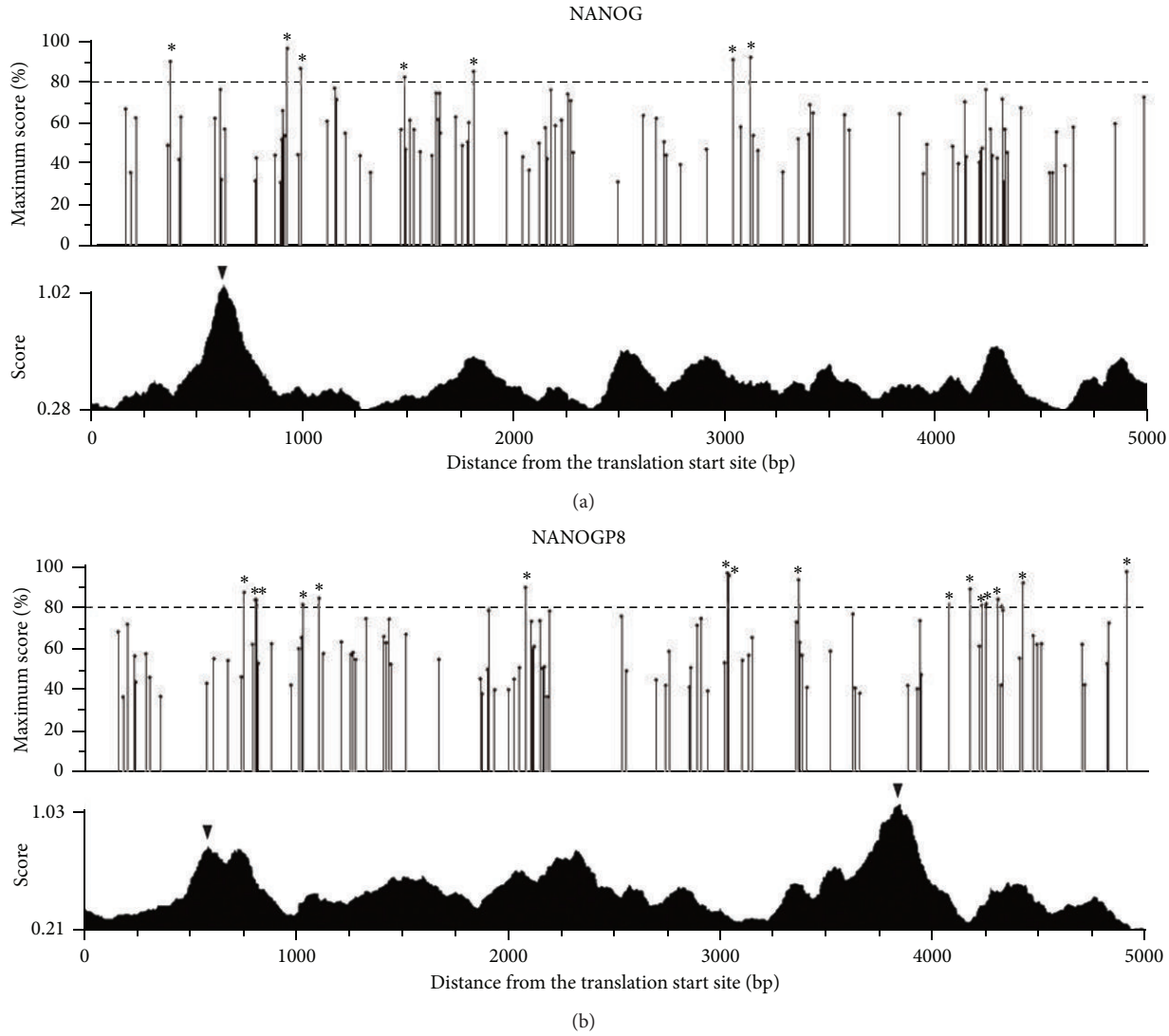

Figure 5: P53-binding site existed in the regulatory region of *NANOG* and *NANOGP8*. The upper panel presents the detection of the p53-binding site in the 5-kb upstream sequence of the translation start site of a gene. The percentage of maximum possible score stands for the possibility of being a p53-binding site. The cutoff value was set as 80% to unveil the p53-binding site candidates. The most likely p53-binding site is indicated by asterisk. The lower panel exhibits the prediction of the promoter region. The triangle indicates the possible promoter region with the score of more than 0.7. $^{*}P < 0.05$ or $^{**}P < 0.01$.

of NANOG expression. This suggests that NANOG expression is regulated by a similar mechanism in both breast CSCs and embryonic stem cells. Recent work further indicates that NANOG could be upregulated by beta-catenin through interaction with Oct3/4 [34]. We have evaluated the possibility by immunohistochemical analysis and Top/Fop flash assay (data not shown) and found that ugonin J treatment decreased the level of beta-catenin in tumor xengraft. However, the activity of beta-catenin was extremely low in both MCF-7 and MDA-MB231 cells. We therefore proposed that it is possible that Ugonin J treatment causes concomitant downregulation of beta-catenin and NANOG in breast cancer, but, in absence of wnt/beta-catenin, ugonin J is capable to downregulate NANOG expression through p53 activation. P53, a well-known tumor suppressor protein, involves regulating cell cycle, senescence, and apoptosis responses against the cell suffering from stress such as hypoxia or DNA damage. In most cancers, p53 is either lost or mutated to allow cancer cells to expand and progress [35]. Recent reports raised the possibility to suppress tumor growth by restoring wild-type p53 to cancer cells [36]. Our current work further highlights the importance of restoring the function of p53 in CSCs.

Recent work has further demonstrated that NANOG transcribed from the NANOGP8 locus is important in tumorigenesis [16]. RNA interference-mediated NANOG knockdown inhibited tumor development in xenograft animals and decreased long-term clonal and clonogenic growth of cancer cells [16, 17]. These results are consistent with our findings that overexpression of NANOG enhances the overall growth rate of MCF-7 cells and downregulation of NANOG

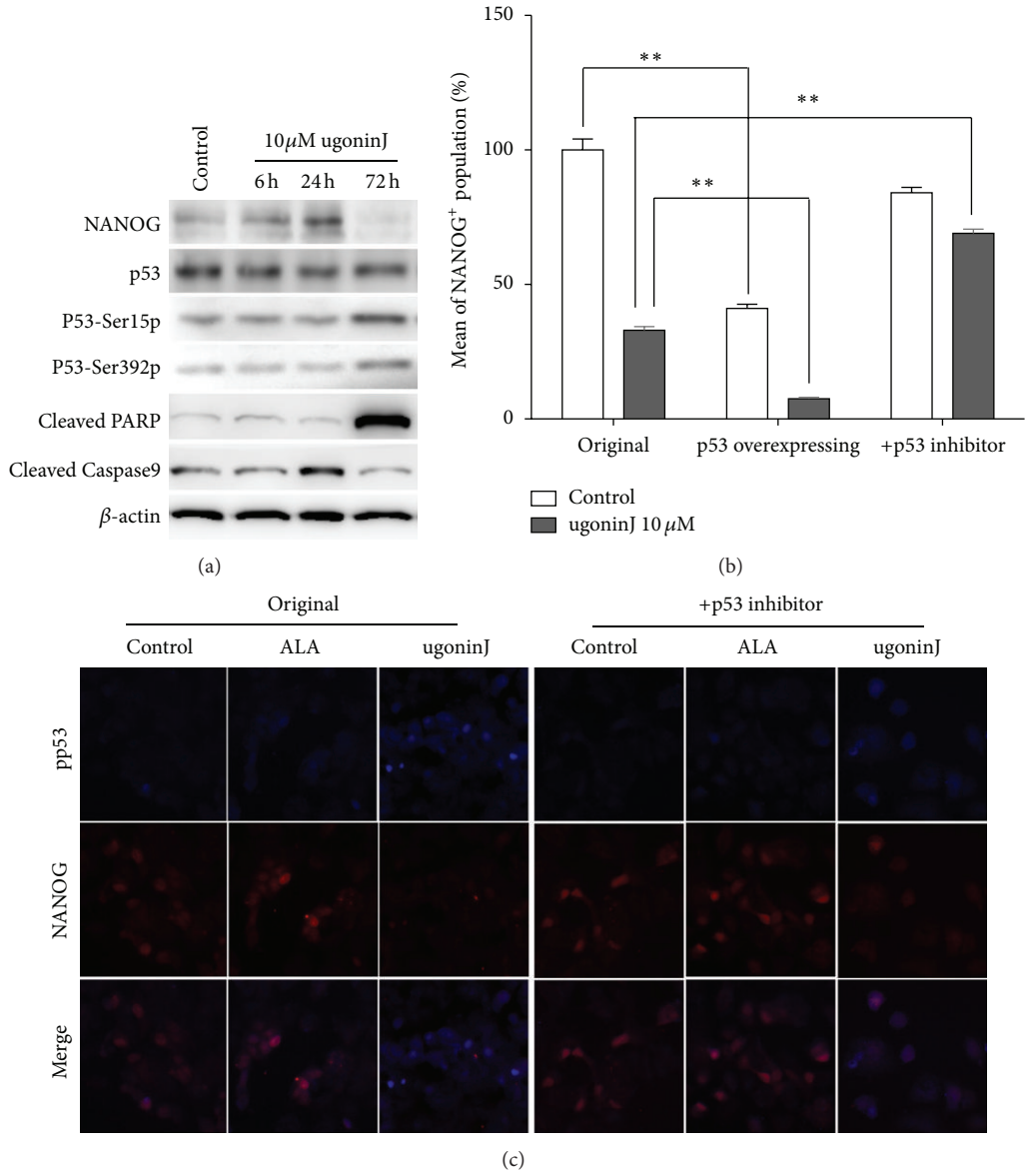

Figure 6: P53-dependent pathway mediates the downregulation of NANOG by ugonin J treatment in MCF-7 cells. (a) MCF-7 cells were treated with 10 μM ugonin J for 6, 24, and 72 hours before protein extraction. Western blot probed for anti-ABCG2, NANOG, p53, phospho-p53 Ser15 and 392, and cleaved PARP and caspase 9 antibodies. Equal amounts of protein were used (40 μg per lane). (b) Relative percentage of NANOG$^+$ population in MCF-7, p53-overexpressing MCF-7, and pifithrin-α (p53 inhibitor)-treated MCF-7 (0.9×10^5 cells in 12-well plates) were treated with 10 μM ugonin J and counted after 48 hours of culture ($n = 3$). $^{**}P < 0.01$ versus J-treated control. (c) Pifithrin-α treatment rescued the reductive effect of Nanog. MCF-7 cells were treated with ALA and ugonin J for 72 hours. Nanog (red) and phospho-p53^{ser15} (blue) expression was analyzed by immunofluorescent staining.

by ugonin J treatment suppresses propagation of breast CSCs. However, the mechanisms, involved in regulating transcription of NANOG from the NANOGP8 locus during breast carcinogenesis, remain to be determined.

We have tried to determine the structure-activity relationship (SAR) of several cyclohexylmethyl flavonoids with high potency to suppress NANOG that may possess the specific structural features. We proposed that 6, 6-dimethyl-2-methylene-cyclohexylmethyl groups on the C-6 position are important for the potency of ugonins J and K to suppress propagation of breast CSCs. In contrast, the bulky isoprenyl group attached to position 2 of the B ring (found in ugonins M, N and O) may reduce the potency. In addition, the free rotation of the bulky isoprenyl moiety (ugonins J and K) may contribute more stereohindrance and lipophilic properties compared with the cyclized moiety with C-4 by ether-linkage (ugonins L and S), as the double bond in the cyclohexane (ugonin P) disrupts the chair form of the cyclohexane moiety and reduces its lipophilicity. And one hydroxyl group attached to the cyclohexyl ring (ugonins Q and R) might

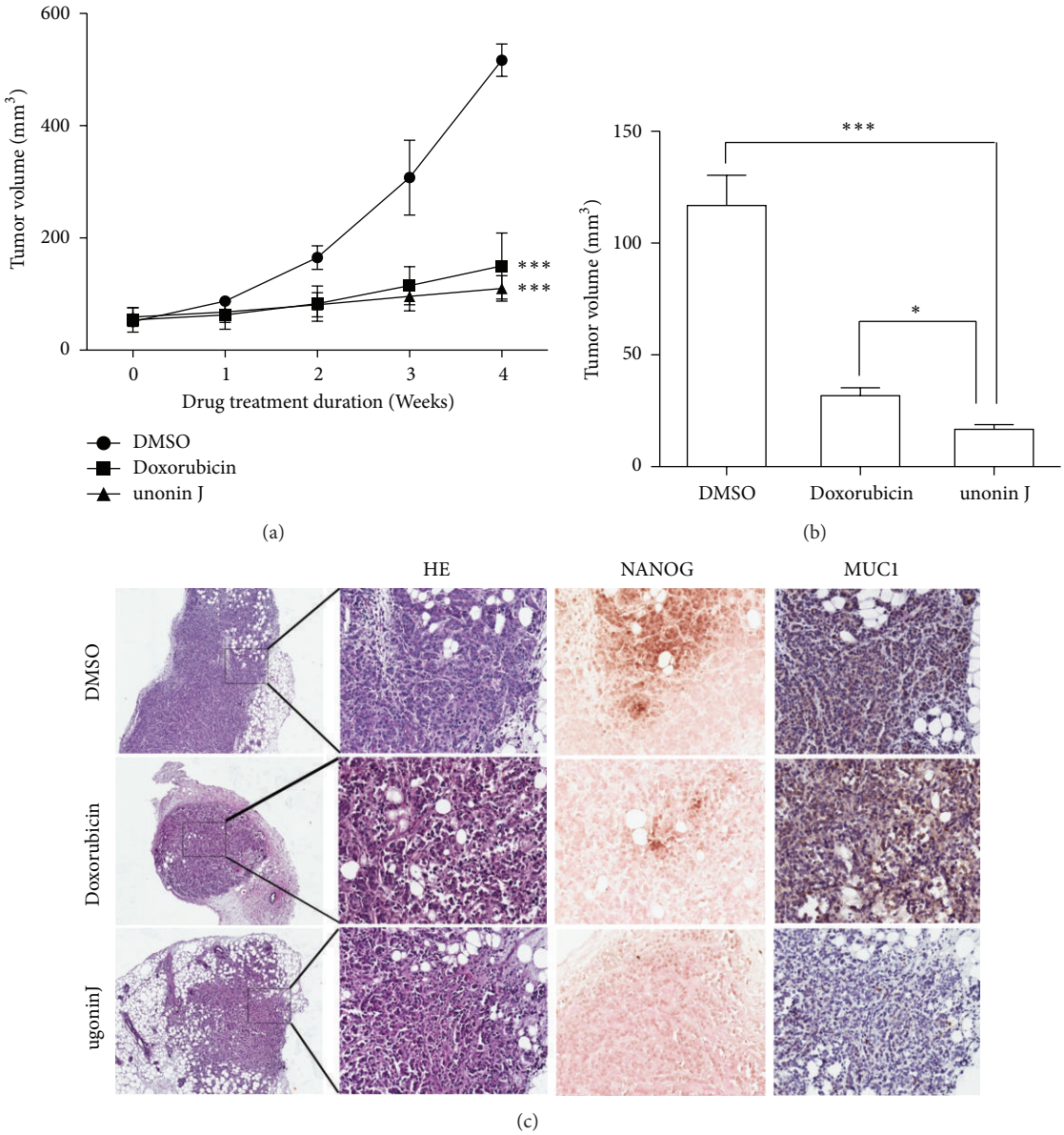

Figure 7: Effect of ugonin J on the growth of MCF-7 orthotopic tumor model. (a) SCID mice bearing MCF-7 orthotopic tumor were administrated weekly once with Doxorubicin (12 mg/kg) or ugonin J (50 mg/kg). Each group used 6 mice. The tumor volumes of SCID mice were measured weekly when the treatment began. (b) The average tumor volume of MCF-7 tumors was removed from SCID after 4 weeks. $^{***}P < 0.001$, $^{**}P < 0.01$ versus DMSO control or Doxorubicin. (c) Hematoxylin-Eosin stain and immunohistochemical detection (×200) for NANOG and MUC1 on control, doxorubicin-treated, and ugonin J-treated tumor xenografts.

increase the hydrophilicity, which would also reduce the potency. It has been reported that derivatives of ambrein and agelasine that possessed cyclohexylmethyl groups are capable to suppress the expansion of multiple cancer cell lines [37, 38]. This may explain why ugonins J and K exhibited relatively high potency to suppress propagation of breast CSCs.

$CD24^{-/low}CD44^{+}$ breast CSCs have been suggested to be the underlying cause of breast cancer recurrence and are a critical target for breast cancer therapies. *H. zeylanica* have been used in Chinese traditional medicine for treating inflammatory diseases and various hepatic disorders. In the present study, we have identified two cyclohexylmethyl flavonoids, ugonins J and K, which were the main components of the rhizomes of *H. zeylanica* and were able to suppress propagation of breast CSCs in mammosphere cultures and in tumor xengrafts. The current work also found that the suppressive effect of ugonin J on propagation of breast CSCs was mediated by activation of p53 which in turn led to reduction of NANOG. Overexpression of NANOG counteracted the suppressive effect of ugonin J. The current findings suggest that the rhizomes of *H. zeylanica* can possibly be used as complementary medicine for reducing CSC-mediated breast cancer recurrence.

Authors' Contribution

W. Y. Liao, S. C. Kuo, C. C. Liaw, and C. N. Shen designed research; W. Y. Liao, C. C. Liaw, H. Y. Han, and Y. C. Huang performed research; S. M. Hwang, H. W. Hsu contribute to analytic tools; W. Y. Liao, S. C. Kuo, C. C. Liaw, and C. N. Shen analyzed data; W. Y. Liao, C. C. Liaw, and C. N. Shen wrote the paper. W. Y. Liao and C. C. Liaw contribute equally to the paper.

Conflict of Interests

The authors indicate no potential conflict of interests.

Acknowledgments

The authors greatly appreciate the excellent technical assistance on flow cytometric analysis provided by the FACS core facility of Genomics Research Center, Ms. Wen-Wen Chen and Ms. Wan-Yu Mao. The authors would like to acknowledge Dr. Chi-Hung Huang and Mr. Yu-Hsing Lin (Genomics Research Center, Academia Sinica) for excellent assistance on tumor xenograft experiments and western blotting. Special thanks are to Dr. James Thomson (Stem Cell and Regenerative Medicine Center, University of Wisconsin) and Dr. Tyler Jacks (MIT Center for Cancer Research, Massachusetts Institute of Technology) for providing the NANOG and GFP-p53 constructs. They also appreciate Dr. Liang-Jie Wang for proofreading. The authors thank the National RNAi Core Facility (NSC 97-3112-B-001-016) for providing lentiviral shNANOG clones. This work was supported in part by Intramural Grant of Academia Sinica and the National Science Council Grants 98-3111-B-001-005 to CNS. Wen-Ying Liao and Chih-Chuang Liaw contributed equally to the paper.

References

[1] E. Amir, O. C. Freedman, B. Seruga, and D. G. Evans, "Assessing women at high risk of breast cancer: a review of risk assessment models," *Journal of Natinoal Cancer Institue*, vol. 102, no. 10, pp. 680–691, 2010.

[2] M. A. Velasco-Velázquez, V. M. Popov, M. P. Lisanti, and R. G. Pestell, "The role of breast cancer stem cells in metastasis and therapeutic implication," *The American Journal of Pathology*, vol. 179, no. 1, pp. 2–11, 2011.

[3] M. Al-Hajj, M. S. Wicha, A. Benito-Hernandez, S. J. Morrison, and M. F. Clarke, "Prospective identification of tumorigenic breast cancer cells," *Proceedings of the National Academy of Sciences*, vol. 100, no. 7, pp. 3983–2988, 2003.

[4] R. Liu, X. Wang, G. Y. Chen et al., "The prognostic role of a gene signature from tumorigenic breast-cancer cells," *The New England Journal of Medicine*, vol. 356, no. 3, pp. 217–226, 2007.

[5] J. E. Dick, "Breast cancer stem cells revealed," *Proceedings of the National Academy of Sciences*, vol. 100, no. 7, pp. 3547–3549, 2003.

[6] L. Patrawala, T. Calhoun, R. Schneider-Broussard, J. Zhou, K. Claypool, and D. G. Tang, "Side population is enriched in tumorigenic, stem-like cancer cells, whereas ABCG2$^+$ and ABCG2$^-$ cancer cells are similarly tumorigenic," *Cancer Research*, vol. 65, no. 14, pp. 6207–6219, 2005.

[7] X. Li, M. T. Lewis, J. Huang et al., "Intrinsic resistance of tumorigenic breast cancer cells to chemotherapy," *Journal of the National Cancer Institute*, vol. 100, no. 9, pp. 672–679, 2008.

[8] F, Al-Ejeh, C. E. Smart et al., "Breast cancer stem cells: treatment resistance and therapeutic opportunities," *Carcinogenesis*, vol. 32, no. 5, pp. 650–658, 2011.

[9] S. Liu and M. S. Wicha, "Targeting breast cancer stem cells," *Journal of Clinical Oncology*, vol. 28, no. 25, pp. 4006–4012, 2010.

[10] P. A. Beachy, S. S. Karhadkar, and D. M. Berman, "Tissue repair and stem cell renewal in carcinogenesis," *Nature*, vol. 432, no. 7015, pp. 324–331, 2004.

[11] G. V. Glinsky, "Stemness genomics law governs clinical behavior of human cancer: implications for decision making in disease management," *Journal of Clinical Oncology*, vol. 26, no. 17, pp. 2846–2853, 2008.

[12] I. Ben-Porath, M. W. Thomson, V. J. Carey et al., "An embryonic stem cell-like gene expression signature in poorly differentiated aggressive human tumors," *Nature Genetics*, vol. 40, no. 5, pp. 499–507, 2008.

[13] J. Zhang, X. Wang, M. Li et al., "NANOGP8 is a retrogene expressed in cancers," *FEBS Journal*, vol. 273, no. 8, pp. 1723–1730, 2006.

[14] S. Ambady, C. Malcuit, O. Kashpur et al., "Expression of NANOG and NANOGP8 in a variety of undifferentiated and differentiated human cells," *The International of Developmental Biology*, vol. 54, pp. 1743–1754, 2010.

[15] C. R. Jeter, M. Badeaux, G. Choy et al., "Functional evidence that the self-renewal gene NANOG regulates human tumor development," *Stem Cells*, vol. 27, no. 5, pp. 993–1005, 2009.

[16] C. R. Jeter, B. Liu, X. Liu et al., "NANOG promotes cancer stem cell characteristics and prostate cancer resistance to androgen deprivation," *Oncogene*, vol. 30, no. 36, pp. 3833–3845, 2011.

[17] J. Han, F. Zhang, M. Yu et al., "RNA interference-mediated silencing of NANOG reduces cell proliferation and induces G0/G1 cell cycle arrest in breast cancer cells," *Cancer Letters*, vol. 321, no. 1, pp. 80–88, 2012.

[18] L. Y. W. Bourguignon, K. Peyrollier, W. Xia, and E. Gilad, "Hyaluronan-CD44 interaction activates stem cell marker Nanog, Stat-3-mediated MDR1 gene expression, and ankyrin-regulated multidrug efflux in breast and ovarian tumor cells," *Journal of Biological Chemistry*, vol. 283, no. 25, pp. 17635–17651, 2008.

[19] I. Cohen, M. Tagliaferri, and D. Tripathy, "Traditional Chinese medicine in the treatment of breast cancer," *Seminars in Oncology*, vol. 29, no. 6, pp. 563–574, 2002.

[20] Y. He, X. Zheng, C. Sit et al., "Using association rules mining to explore pattern of Chinese medicinal formulae (prescription) in treating and preventing breast cancer recurrence and metastasis," *Journal of Translational Medicine*, vol. 10, supplement 1, article S12, 2012.

[21] Y. C. Huang, T. L. Hwang, C. S. Chang et al., "Anti-inflammatory flavonoids from the rhizomes of Helminthostachys zeylanica," *Journal of Natural Products*, vol. 72, no. 7, pp. 1273–1278, 2009.

[22] Y. C. Huang, T. L. Hwang, Y. L. Yang et al., "Acetogenin and prenylated flavonoids from helminthostachys zeylanica with inhibitory activity on superoxide generation and elastase release by neutrophils," *Planta Medica*, vol. 76, no. 5, pp. 447–453, 2010.

[23] S. R. Suja, P. G. Latha, P. Pushpangadan, and S. Rajasekharan, "Evaluation of hepatoprotective effects of *Helminthostachys zeylanica* (L.) Hook against carbon tetrachloride-induced liver damage in Wistar rats," *Journal of Ethnopharmacology*, vol. 92, no. 1, pp. 61–66, 2004.

[24] V. Singh, Z. A. Ali, S. T. H. Zaidi, and M. K. Siddqui, *Fitoterapia*, Department of Botany, Aligarh Muslim Universities, Aligarh, India, 1996.

[25] J. Jalil, A. A. Bidin, and T. S. Chye, "Phytochemical study of ophyoglosaceae family species," in *Proceedings of the Malays Biochemistry Society Conference*, vol. 12, pp. 160–164, Fakultas Sains Hayati Universitas Kebangsaan, Bangi, Malaysia, 1986.

[26] J. Yu, M. A. Vodyanik, K. Smuga-Otto et al., "Induced pluripotent stem cell lines derived from human somatic cells," *Science*, vol. 318, no. 5858, pp. 1917–1920, 2007.

[27] S. D. Boyd, K. Y. Tsai, and T. Jacks, "An intact HDM2 RING-finger domain is required for nuclear exclusion of p53," *Nature Cell Biology*, vol. 2, no. 9, pp. 563–568, 2000.

[28] S. N. Tang, C. Singh, D. Nall, D. Meeker, S. Shankar, and R. K. Srivastava, "The dietary bioflavonoid quercetin synergizes with epigallocathechin gallate (EGCG) to inhibit prostate cancer stem cell characteristics, invasion, migration and epithelial-mesenchymal transition," *Journal of Molecular Signaling*, vol. 5, article no. 14, 2010.

[29] P. Sansone, G. Storci, S. Tavolari et al., "IL-6 triggers malignant features in mammospheres from human ductal breast carcinoma and normal mammary gland," *Journal of Clinical Investigation*, vol. 117, no. 12, pp. 3988–4002, 2007.

[30] T. Lin, C. Chao, S. Saito et al., "p53 induces differentiation of mouse embryonic stem cells by suppressing Nanog expression," *Nature Cell Biology*, vol. 7, no. 2, pp. 165–171, 2005.

[31] I. Chambers, D. Colby, M. Robertson et al., "Functional expression cloning of Nanog, a pluripotency sustaining factor in embryonic stem cells," *Cell*, vol. 113, no. 5, pp. 643–655, 2003.

[32] J. Zhang, X. Wang, M. Li et al., "NANOGP8 is a retrogene expressed in cancers," *FEBS Journal*, vol. 273, no. 8, pp. 1723–1730, 2006.

[33] J. Susanto, Y. H. Lin, Y. N. Chen et al., "Porphyrin homeostasis maintained by ABCG2 regulates self-renewal of embryonic stem cells," *PLoS One*, vol. 3, no. 12, Article ID e4023, 2008.

[34] Y. Takao, T. Yokota, and H. Koide, "β-Catenin up-regulates Nanog expression through interaction with Oct-3/4 in embryonic stem cells," *Biochemical and Biophysical Research Communications*, vol. 353, no. 3, pp. 699–705, 2007.

[35] C. Ginestier, E. Charafe-Jauffret, and D. Birnbaum, "p53 and cancer stem cells: the mevalonate connexion," *Cell Cycle*, vol. 11, no. 14, pp. 2583–2584, 2012.

[36] V. V. Prabhu, J. E. Allen, B. Hong, S. Zhang, H. Cheng, and W. S. El-Deiry, "Therapeutic targeting of the p53 pathway in cancer stem cells," *Expert Opinion on Therapeutic Targets*, vol. 16, no. 12, pp. 1161–1174, 2012.

[37] A. K. Bakkestuen and L. L. Gundersen, "Synthesis of (+)-trixagol and its enantiomer, the terpenoid side chain of (-)-agelasine E," *Tetrahedron*, vol. 59, no. 1, pp. 115–121, 2003.

[38] Y. C. Shen, S. Y. Cheng, Y. H. Kuo, T. L. Hwang, M. Y. Chiang, and A. T. Khalil, "Chemical transformation and biological activities of ambrein, a major product of ambergris from *Physeter macrocephalus* (Sperm Whale)," *Journal of Natural Products*, vol. 70, no. 2, pp. 147–153, 2007.

Hindawi Publishing Corporation
Evidence-Based Complementary and Alternative Medicine
Volume 2013, Article ID 569737, 8 pages
http://dx.doi.org/10.1155/2013/569737

Research Article

Medicinal Fungus *Antrodia cinnamomea* Inhibits Growth and Cancer Stem Cell Characteristics of Hepatocellular Carcinoma

Yu-Ming Liu,[1,2] Yu-Kuo Liu,[3] Keng-Li Lan,[1] Yu-Wei Lee,[3] Tung-Hu Tsai,[2,4] and Yu-Jen Chen[2,5]

[1] *Cancer Center, Taipei Veterans General Hospital, Taipei 11217, Taiwan*
[2] *Institute of Traditional Medicine, School of Medicine, National Yang Ming University, Taipei 11221, Taiwan*
[3] *Department of Chemical and Material Engineering, Chang Gung University, Kwei-Shan, Tao-Yuan 333, Taiwan*
[4] *Department of Education and Research, Taipei City Hospital, Taipei 10341, Taiwan*
[5] *Department of Radiation Oncology, Mackay Memorial Hospital, Taipei 10449, Taiwan*

Correspondence should be addressed to Tung-Hu Tsai; thtsai@ym.edu.tw and Yu-Jen Chen; chenmdphd@gmail.com

Received 1 January 2013; Accepted 16 January 2013

Academic Editor: Hui-Fen Liao

Background. *Antrodia cinnamomea* is an edible fungus commonly used in Asia as a well-known medicinal herb capable of treating drug intoxication and liver cancer. *Methods*. This study evaluated the anticancer activity of its biotechnological product, mycelial fermentation broth (*AC*-MFB) on hepatocellular carcinoma (HCC) by tetrazolium-based colorimetric assay *in vitro* and syngeneic Balb/c 1MEA.7R.1 tumor implantation model *in vivo*. Given that cancer stem cell characteristics, such as angiogenesis, invasiveness, and migration, are known to cause recurrence, we further evaluated the effect of *AC*-MFB on cellular viability inhibition of HCC cells, angiogenic activity and migration of endothelial cells, and the release of proangiogenic factors from HCC cells. *Results*. We found that *AC*-MFB markedly inhibited the growth of HCC without hepatic enzyme abnormality. This anti-HCC activity was validated by growth-inhibitory effects on both cultured murine 1MEA.7R.1 and human HA22T/VGH HCC cells. For cancer stem cell characteristics, *AC*-MFB inhibited the cellular viability, migration, and tube formation activity of EA. hy926 and SVEC4-10 endothelial cells. Production of extracellular vascular endothelial growth factor and intracellular hypoxia-inducible factor-1 alpha from HCC cells was suppressed by *AC*-MFB. *Conclusion*. *Antrodia cinnamomea* could inhibit the growth and cancer stem cell characteristics of HCC cells.

1. Background

Antrodia cinnamomea, also known as niu-chang-chih, *Taiwanofungus camphorate* or *Antrodia camphorata*, is a fungus indigenous to Taiwan which grows on decayed *Cinnamomum kanehirae* [1–3]. In folk medicine, it is well known for its antidotal and antitumoral functions as it has been traditionally used to treat toxicities caused by food, alcohol, and drugs as well as diarrhea, abdominal pain, hypertension, itchy skin, and tumors [4, 5].

A. cinnamomea has been shown to exhibit anticancer properties [6–9] with many studies aimed at exploring the exact bioactive compounds [10–14]. For example, Chen et al. reported that the oral administration of *A. cinnamomea* fruiting bodies significantly increased the life span of ATCC BNL IMEA.7R.1 hepatoma-bearing mice [15]. It has also been reported that polysaccharides from *A. cinnamomea* mycelial extract could inhibit angiogenic activities in endothelial cells (ECs) [16–18].

To avoid contamination in the wild source and to expand the production of this fungus for food use, *A. cinnamomea* mycelial fermentation broth (*AC*-MFB) produced using biotechnology has been developed by our group and others. Although *AC*-MFB is not used as natural form, it could be regarded as a modern formulation of this herbal drug. However, the anticancer activity and safety of these biotechnological products have not been extensively examined.

We previously purified a series of compounds from the fruiting body of *A. cinnamomea,* including 24-methylenelanosta-7,9(11)-diene-3b,15adiol-21-oic acid (designated

herein as MMH01), which possesses cytotoxicity against human leukemia and pancreatic cancer cells [19]. In the present study, we investigated the anticancer effect and safety of *AC*-MFB with a syngeneic hepatocellular carcinoma (HCC) implantation model. The effect of *AC*-MFB against cancer stem cell characteristics in HCC and endothelial cells was also evaluated.

2. Methods

2.1. Plants Materials, Fermentation, and Characterization. *A. cinnamomea*, strain B137, identified by fungi specialist Dr. T. T. Chang (Taiwan Forestry Research Institute, Taipei, Taiwan), was maintained on potato dextrose agar pasteurized Petri dishes and transferred to a fresh medium at 1-month intervals. Mycelial agar discs (8 pieces, 0.5 cm each) were obtained by a sterilized tip and used as the inoculum in a shake flask preculture. The preculture medium (LM-B) consisted of the following components (mg/mL): glucose 30, sucrose 20, yeast extract 15, peptone 13, $MgSO_4$ 0.3, KH_2PO_4 0.3, and K_2HPO_4 0.3 with an initial condition of pH 4.0. For the preculture, a 200 mL medium was prepared in a 500 mL flask and inoculated, followed by a 7-day incubation at 28°C on a rotary shaker (100 rpm). For a series of experiments, a 100 mL medium (LM-B) was prepared in a 500 mL flask and inoculated with mycelium suspension (6%) from the preculture broth, followed by a 14-day incubation at 28°C on a rotary shaker (100 rpm). The fermentation product was then harvested and poured through a nonwoven fabric on a 20-mesh sieve to separate the deep-red fermented culture broth and the mycelia, followed by centrifugation at 3000 g for 10 min and then by passage through a filter of 0.22 μm pore size. The culture broth (1.0 L) was then concentrated into a colloid (47.6 mg) under vacuum and stored at −30°C before the analysis. The *AC*-MFB colloid was redissolved and directly taken into the study without further extraction. The polysaccharide components in *AC*-MFB were used in quantity analysis for standardization in this study. The phenol-sulfuric acid assay, a colorimetric method, was employed to determine the total concentration of carbohydrates present in *AC*-MFB [20].

2.2. In Vivo Tumorigenesis and Hepatic Toxicity Assay in Mice. A subcutaneous allogenic mice animal model was used for tumorigenesis assay. Specific pathogen-free male BALB/c mice (4 weeks old, 25–28 gm) were obtained from the National Laboratory Animal Center (Taipei, Taiwan) and were maintained in pathogen-free conditions. They were kept in our animal facility for at least two weeks before use. All of the mice were used at the age of 6–8 weeks. All animals were cared for following the *Guide for the Care and Use of Laboratory Animals* (NIH publication no. 85-23, revised in 1985). The mice were subcutaneously injected with 1×10^5 1MEA.7R.1 HCC cells over the flank. The mice were fed orally either with 50 mg/mL *AC*-MFB 200 μL or with a vehicle of normal saline 200 μL ($N = 6$ for each group) for 28 days. The tumor size of each mouse was measured by a caliper and calculated by the formula: $L \times W^2/2$, where W was the shortest dimension and L was the longest dimension in centimeters. The tumor size was estimated every 2 to 3 days after the tumor size increased to 0.1 mL in size. Tumor growth curves were plotted as the mean tumor volume relative to the treatment group.

Table 1: Effect of *AC*-MFB on ALT levels in mice.

Treatment group	Dose (g/Kg BW)	Day 0	Day 3	Day 28
Normal saline 200 μL	0.0	75 ± 20	96 ± 62	60 ± 2
50 mg/mL 200 μL	0.4	49 ± 12	48 ± 11	44 ± 4
100 mg/mL 200 μL	0.8	111 ± 52	60 ± 12	126 ± 42
250 mg/mL 200 μL	2.0	78 ± 42	44 ± 10	44 ± 2
500 mg/mL 200 μL	4.0	73 ± 36	93 ± 42	77 ± 22
500 mg/mL 300 μL	6.0	130 ± 95	56 ± 15	160 ± 79

All values represent mean ± SD. Normal value of mouse ALT: 28–132 U/L. $N = 6$ for each group.

Hepatic enzyme alanine aminotransferase (ALT) is found primarily in the cytoplasm of hepatic cells which catalyses gluconeogenesis from noncarbohydrate sources and is an important marker for liver injury [21, 22]. Elevation of the serum concentrations of this marker implied disruption of plasma membrane integrity, which eventually led to leakage of the enzymes into the blood circulation [23]. ALT was used as a biochemical marker for hepatic damage assay in this study. Animals were fed with different doses of *AC*-MFB by gastric tube for each condition for 28 days (Table 1); each group had 6 mice. Blood samples were collected for the assays of ALT on the first day as a control and on the third day and the 28th day for acute and chronic hepatic toxicity assays, respectively. Serum activities of ALT were determined using the colorimetric method [24].

The protocol used in this study was approved by the Institutional Animal Care and Use Committee, Chang Gung University, Taiwan (IACUC approval no. CGU10-143).

2.3. In Vitro Cytotoxicity Assays. The *in vitro* cytotoxicities of the *AC*-MFB on both HCC cells and ECs were examined using a modified MTT assay [25]. The human ECs EA. hy926 (a gift from Dr. Cora-Jean S. Edgell, Pathology Department, University of North Carolina), human HCC cell HA22T/VGH [26], and the BALB/c murine BNL 1MEA.7R.1 (BNL) HCC cells were grown in DMEM, containing 584 mg/mL L-glutamine and 10% FBS. The murine SV40-transformed mouse ECs (SVEC4-10, ATCC no. CRL-2181) were maintained in DMEM with 10% FBS.

2.4. In Vitro Antiangiogenic Assays. The antiangiogenic activity was investigated by the capability of endothelial cell migration and tube formation on Matrigel *in vitro*.

Endothelial cell migration was determined by means of a wound-healing assay. ECs were seeded into 6-well tissue culture dishes and cultured in medium containing 10% FBS to confluent cell monolayers, which were then carefully wounded using sterile 200 μL pipette tips with all cell debris removed by phosphate buffered saline (PBS). The cells were

then incubated for another 24 h in medium with or without *AC*-MFB treatment. The cells that had migrated across the edge of the wound were photo recorded under an inverted phase-contrast microscope (Nikon, Tokyo, Japan), and the cellular migration was determined by measuring the widths of the wounds. The differences in the width of the wounds were measured with Adobe Photoshop version 5.5 (Adobe Systems Incorporated, USA). Each data point was compared with its own control present in the control dish at 24 h and interpreted as a percentage of wound migration inhibition.

Matrigel (BD BioCoat Angiogenesis System, Franklin Lakes, NJ, USA) was employed to promote the differentiation of ECs into capillary tube-like structures. A total of 75 μL of thawed Matrigel was added to 96-well tissue culture plates, followed by incubation for 60 min at 37°C to allow polymerization. Then, 4×10^4 quiescent ECs were seeded on the gels in medium supplemented without FBS in the presence or absence of *AC*-MFB, followed by incubation at 37°C in 5% CO_2 for 12 h. Tube formation was examined by an inverted phase-contrast microscope (Nikon, Tokyo, Japan). The number of the tubes was counted with Adobe Photoshop version 5.5 (Adobe Systems Incorporated, USA). Each data point was compared with its own control (without *AC*-MFB) at 12 h and interpreted as a percentage of tube formation inhibition.

2.5. Inhibition of Proangiogenic Factors from Hepatic Cancer Cells. Secretion of VEGF and HIF-1α by HCCs was stimulated by 2 h incubation with 200 μM desferrioxamine (DFO) (Sigma, St. Louis, MO, USA) to mimic hypoxia. VEGF levels of HA22T and 1MEA.7R.1 HCCs were measured by Human VEGF ELISA kit no. DY293B and Mouse VEGF ELISA no. DY493, respectively. The HIF-1α was measured using a solid-phase enzyme immunoassay ("sandwich ELISA," NOVUS and NeoMarkers, Inc.). Each measurement was done in triplicate, and the data were calculated and normalized to total protein in the culture media.

2.6. Statistical Analysis. Data from three separate experiments were expressed as a mean ± standard deviation (SD). Statistical comparisons of the results were made using analysis of variance [27] as indicated. Significant differences ($P < 0.05$) between the means of the two test groups were analyzed by Tukey's test.

3. Results

3.1. Characterization and Stability of AC-MFB. Although the bioactive ingredients of *AC*-MFB remain to be determined, the amount of polysaccharides in a concentrated *AC*-MFB colloid was used as the standard of quality control to characterize each batch of product. The phenol-sulfuric acid method showed that there were 0.341 mg polysaccharides in 47.6 mg *AC*-MFB colloid from 1.0 L fermentation broth. The polysaccharides shared 0.7% weight in the concentrated cultured broth colloid. There was no significant change in the amount of polysaccharides in *AC*-MFB throughout the 12 months of storage, indicating it is a product with long-term stability.

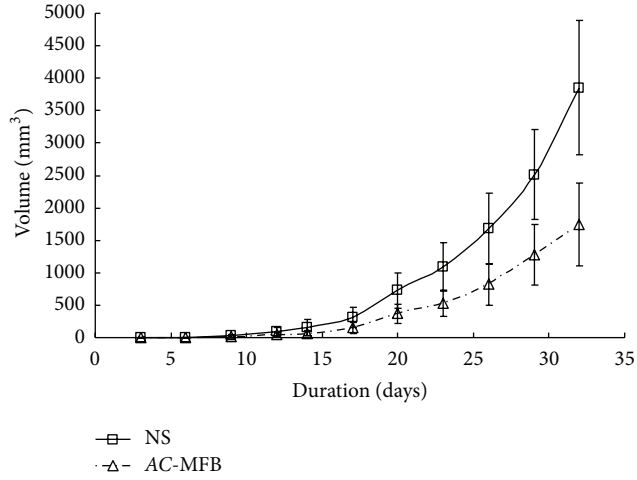

Figure 1: Antitumor effect of *AC*-MFB on BALB/c liver cancer. Effect of *AC*-MFB on growth of 1MEA.7R.1 liver cancer cells in BALB/c mice. Mice were treated with oral *AC*-MFB (50 mg/mL) or normal saline for 28 days. $^*P < 0.05$.

3.2. AC-MFB Inhibited Tumor Growth in Mice without Hepatic Enzyme Abnormality. In BALB/c mice bearing 1MEA.7R.1 liver cancer cells, oral intake of 200 μL *AC*-MFB (50 mg/mL) for 28 days significantly inhibited the tumor growth in comparison with the vehicle control ($P < 0.05$) (Figure 1).

Mice serum ALT levels at 3 days and 28 days after treatment were examined for estimation of liver toxicity. As shown in Table 1, there was no statistically significant difference between serum ALT levels of *AC*-MFB and control groups after 3 days and 28 days of *AC*-MFB oral intake.

3.3. AC-MFB Inhibited Cellular Viability of HCC Cells and ECs. As shown in Figures 2 and 3, *AC*-MFB inhibited the viability of HCC cells (human HA22T/VGH, murine 1MEA.7R.1) and ECs (EA. hy926, SVEC4-10) in both dose-dependent and time-dependent parameters.

3.4. AC-MFB Inhibited Endothelial Cell Migration and Tube Formation Activity. The migration and tube formation activity of ECs are important *in vitro* endpoints for angiogenesis. As demonstrated in Figure 4, *AC*-MFB profoundly inhibited the migration of EA. hy926 and SVEC4-10 cells in a concentration-dependent manner. The IC_{50} values of migration inhibition of EA. hy926 and SVEC4-10 were 8.8 ± 1.6 mg/mL and 3.0 ± 0.3 mg/mL, respectively. The tube formation activity in these two endothelial cell lines was also inhibited by treatment using *AC*-MFB with IC_{50} ranging from 1.4 to 3.1 mg/mL (Figure 5).

3.5. AC-MFB Suppressed Production of VEGF and Down-regulated Intracellular HIF-1α Levels in HA22T/VGH and 1MEA.7R.1 Cell Lines. Given that VEGF plays a critical role

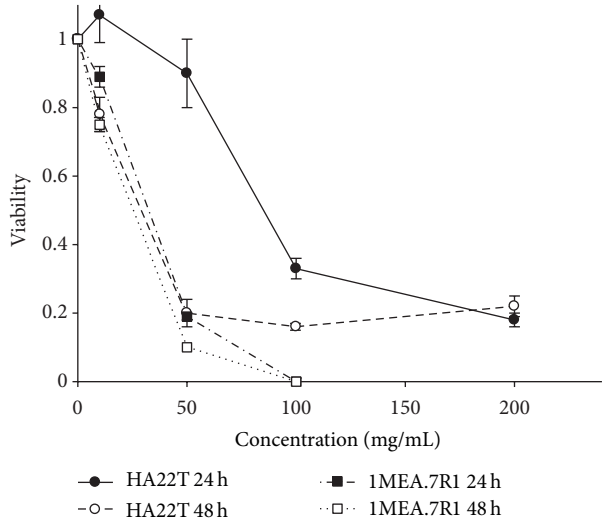

Figure 2: Cytotoxicity of *AC*-MFB on hepatocellular carcinoma cell. Effect of *AC*-MFB on cellular viability of HA22T and 1MEA.7R.1 HCC cells by MTT assay. Data from three separate experiments were expressed as percentages of untreated cells after 24 and 48 h.

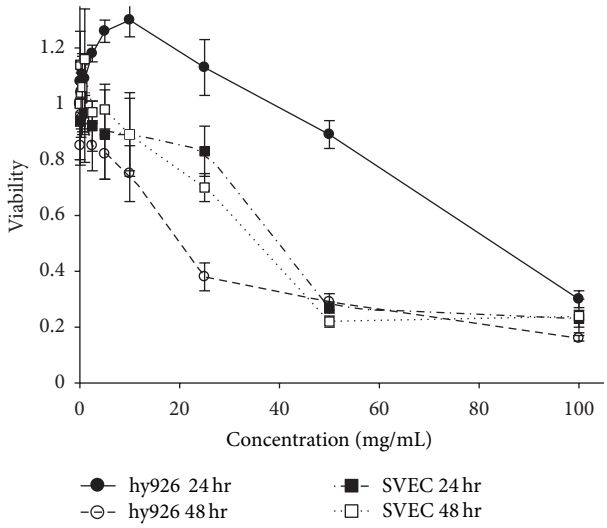

Figure 3: Cytotoxicity of *AC*-MFB on endothelial cell. Effect of *AC*-MFB on cellular viability of EA. hy926 and SVEC4-10 ECs by MTT assay. Data from three separate experiments were expressed as percentages of untreated cells after 24 and 48 h.

in angiogenesis, we investigated whether *AC*-MFB could modulate the secretion of VEGF from HCC cells. As shown in Figure 6, *AC*-MFB treatment suppressed the DFO-stimulated VEGF secretion in both HCC cell lines, but only the difference in HA22T/VGH cells reached statistical significance ($P < 0.05$).

Hypoxia-inducible factor-1α (HIF-1α) is a protein that regulates gene transcription through binding to hypoxia response elements, resulting in upregulation of VEGF and thereby enhancing angiogenesis. *AC*-MFB treatment significantly downregulated the DFO-stimulated intracellular HIF-1α levels in both HCC cell lines ($P < 0.05$) (Figure 7).

4. Discussion

In this study, we examined the *in vivo* activity of *AC*-MFB first. Since the animal model showed it was effective without major toxicity, we next evaluated the *in vitro* effect of *AC*-MFB on both HCC cells and endothelial cells to explore possible targets. Based on the antiangiogenesis activity of *AC*-MFB, we further assessed the modulation of angiogenic factors by *AC*-MFB.

The results showed that *AC*-MFB could inhibit the viability of HCC cells (human HA22T/VGH, murine 1MEA.7R.1) and ECs (EA. hy926, SVEC4-10) in both dose-dependent and time-dependent parameters *in vitro* (Figures 1 and 2). The *AC*-MFB could also inhibit the migration and tube formation activities in both ECs (Figures 4 and 5). *In vivo*, oral intake of *AC*-MFB inhibited the tumor growth in BALB/c mice bearing 1MEA.7R.1 liver cancer cells without hepatic enzyme abnormality (Figure 3, Table 1). In bimolecular activity, *AC*-MFB could suppress the secretion of VEGF and downregulate the HIF-1α level (Figures 6 and 7).

The *A. cinnamomea* mycelial fermentation broth, a biotechnological product serving as a medicinal herb, could inhibit the growth of hepatocellular carcinoma *in vivo* without liver toxicity. Further investigation to clarify the antitumoral mechanisms revealed an inhibitory activity on angiogenesis and the release of related proangiogenic factors VEGF and HIF-1α, indicative of inhibitory activity related to cancer stem cell characters.

Natural *A. cinnamomea* is very rare and slowly growing. Moreover, the host wood, *Cinnamomum kanehirae,* is a local species that is getting scarce and difficult to find in the forest. Therefore, the extracts of the fruiting body are difficult to obtain for use as a medicinal herb. Through biotechnological production in a fermentation broth and the examination of its bioactivity against HCC, a scientific basis for *AC*-MFB to serve as a medicinal herb in adjunct cancer treatment was found.

Hepatocellular carcinoma is one of the most frequently occurring malignancies with poor prognosis in Taiwan [28]. *A. cinnamomea* has attracted great attention due to its hepatoprotective effect and antitumoral activity against HCC [4, 7, 9]. Experimental and clinical data had indicated that HCC tumor progression is associated with angiogenesis and that an increase in microvascular density is associated with a poor prognosis [29]. Given that HCC is characterized by hypervascularity [30], antiangiogenesis might be one of the primary treatment approaches [31].

Our study showed that not only did *AC*-MFB have antitumoral activity against HCC cells *in vitro*, it also delayed 1MEA.7R.1 HCC growth without hepatic enzyme abnormality *in vivo*. In other words, *AC*-MFB might be a potential therapeutic agent or an adjuvant regimen for treatment of HCC.

Furthermore, *AC*-MFB inhibited the cellular events related to cancer stem cells, such as angiogenesis, migration, and HIF-α expression. For antiangiogenesis, our study also showed that *AC*-MFB could inhibit the cellular viability, migration, and tube formation of ECs and decreased both the extracellular VEGF and the intracellular HIF-1α levels

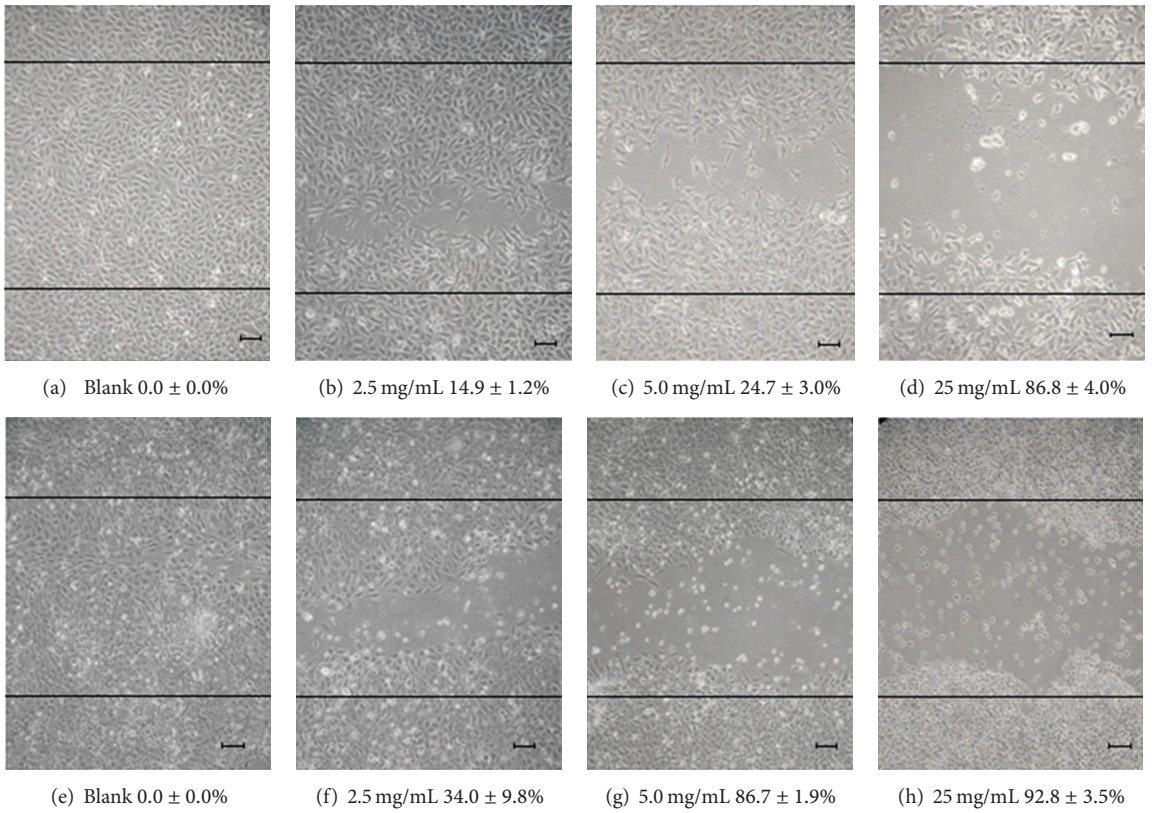

(a) Blank 0.0 ± 0.0% (b) 2.5 mg/mL 14.9 ± 1.2% (c) 5.0 mg/mL 24.7 ± 3.0% (d) 25 mg/mL 86.8 ± 4.0%

(e) Blank 0.0 ± 0.0% (f) 2.5 mg/mL 34.0 ± 9.8% (g) 5.0 mg/mL 86.7 ± 1.9% (h) 25 mg/mL 92.8 ± 3.5%

Figure 4: Migration inhibition of *AC*-MFB on endothelial cell. Effect of *AC*-MFB on migration of EA. hy926 ((a)–(d)) and SVEC4-10 ((e)–(h)) ECs by *in vitro* wound-healing migration assay. Data from three separate experiments were expressed as mean inhibition percentages compared with untreated cells after 24 h treatment.

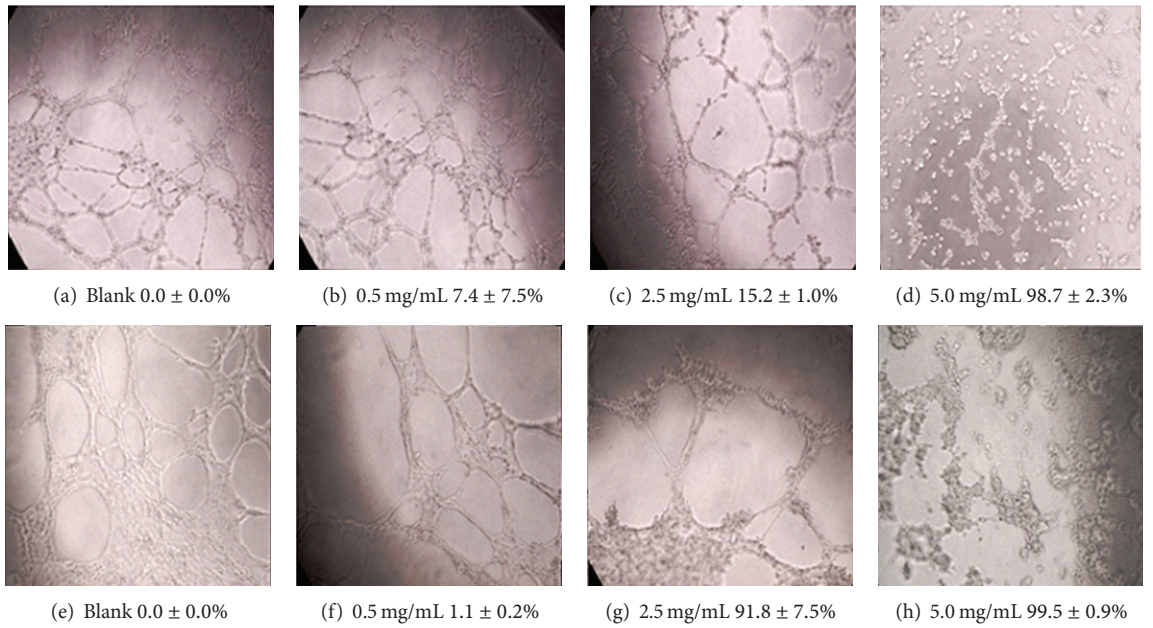

(a) Blank 0.0 ± 0.0% (b) 0.5 mg/mL 7.4 ± 7.5% (c) 2.5 mg/mL 15.2 ± 1.0% (d) 5.0 mg/mL 98.7 ± 2.3%

(e) Blank 0.0 ± 0.0% (f) 0.5 mg/mL 1.1 ± 0.2% (g) 2.5 mg/mL 91.8 ± 7.5% (h) 5.0 mg/mL 99.5 ± 0.9%

Figure 5: Tube formation inhibition of *AC*-MFB on endothelial cell. Effect of *AC*-MFB on tube formation activity of EA. hy926 ((a)–(d)) and SVEC4-10 ((e)–(h)) ECs. Data from three separate experiments were expressed as mean inhibition percentages compared with untreated cells after 12 h treatment.

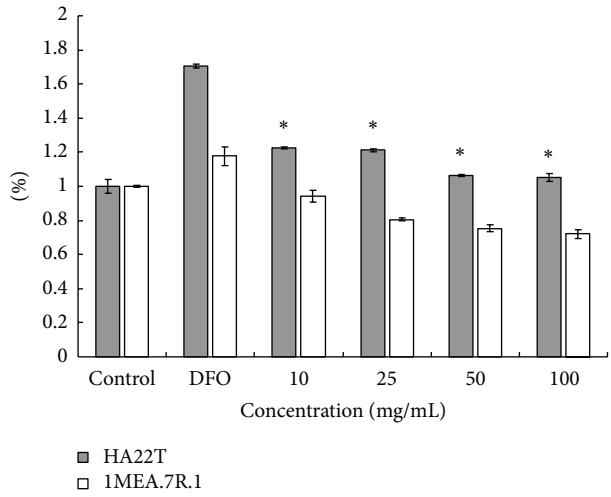

Figure 6: *AC*-MFB inhibits VEGF from hepatocellular cancer cell. Effect of various concentrations of *AC*-MFB on extracellular VEGF levels in culture of HA22T and 1MEA.7R.1 HCC cells. Cells were pretreated with 200 μM DFO for 2 h followed by *AC*-MFB for 6 h. All the data are normalized to the control group (*AC*-MFB 0.0 mg/mL). Data from three independent experiments in triplicate were expressed as mean ± standard error of mean; $^*P < 0.05$ versus 200 μM DFO.

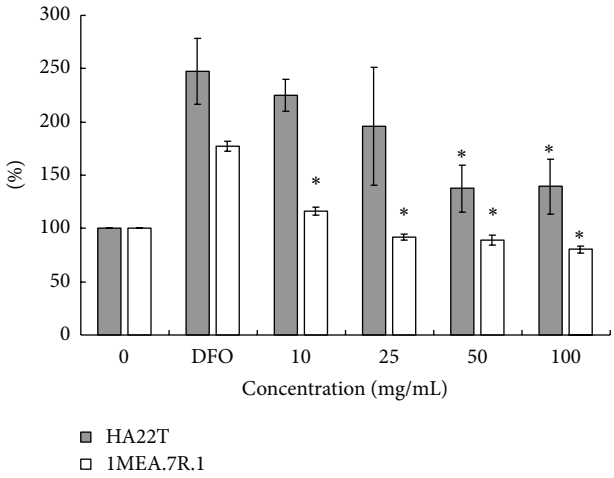

Figure 7: *AC*-MFB inhibits HIF-1α from hepatocellular cancer cell. Effect of various concentrations of *AC*-MFB on intracellular HIF-1α levels in culture of HA22T and 1MEA.7R.1 HCC cells. Cells were pretreated with 200 μM DFO for 2 h followed by *AC*-MFB for 2 h. All the data were normalized to the control group (*AC*-MFB 0 mg/mL). Data from three independent experiments in triplicate were expressed as mean ± standard error of mean; $^*P < 0.05$ versus 200 μM DFO.

of HCC cells under hypoxia. These findings suggest that the antiangiogenic activity of *AC*-MFB might involve inhibition of HIF-1α transcription and downregulation of VEGF expression in HCC cells. Such claims could be supported by previous investigations. For example, Yang reported that fractionated polysaccharides from *A. cinnamomea* mycelia, with molecular weight (MW) > 100 kDa, are antiangiogenic *in vitro* and *ex vivo*, and the effects are likely through immunomodulation [17]. Cheng et al. not only reported that polysaccharides extracted from fermented *A. cinnamomea* mycelia could inhibit VEGF receptor phosphorylation and angiopoietin-2 protein expression but also found the chemical structure of the polysaccharide [16, 18]. Shih et al. also reported that extracted polysaccharides from the fruiting body of *A. cinnamomea* with a molecular weight between 2693 and 2876 kDa had a critical inhibitory effect on tube formation without cytotoxicity [32]. Polysaccharides were also proved to elicit an antitumoral effect by promoting a Th1-dominant state and killer activities [6]. The polysaccharides only shared 0.7% weight of our concentrated cultured broth colloid; soother lanostane-type components like MMH01 isolated from *A. cinnamomea* could have anticancer activity [33]. Taken together, polysaccharides may not be the major bioactive component in *AC*-MFB. Instead, the amount of exopolysaccharide could serve as a good standardization index for each batch of fermented products.

Our study is the first one demonstrating the antiangiogenic activity of *A. cinnamomea* mycelial fermentation broth, not from extracts of fruiting body. It indicates that medicinal herbal products of *A. cinnamomea* may possess the original bioactivity against HCC and angiogenesis.

5. Conclusion

The *A. cinnamomea* mycelial fermentation broth, a biotechnological product serving as a medicinal herb, could inhibit growth of hepatocellular carcinoma *in vivo*. Furthermore, *AC*-MFB could inhibit the cellular events related to cancer stem cells, such as angiogenesis, migration, and HIF-α expression in HCC.

Abbreviations

AC-MFB: *Antrodia cinnamomea* mycelial fermentation broth
HCC: Hepatocellular carcinoma
ECs: Endothelial cells
MTT: Modified tetrazolium-based colorimetric assay (3-(4,5-dimethylthiazol)-2,5-diphenyl tetrazolium bromide assay
VEGF: Vascular endothelial growth factor
HIF-1α: Hypoxia-inducible factor-1α
ALT: Alanine aminotransferase.

Authors' Contribution

Y.-M. Liu and Y.-K. Liu contributed to this work equally.

Conflict of Interests

The authors declare that they have no competing interests in the publication of the paper.

Acknowledgments

The authors thank the great help from Ms. S. L. Chou and Dr. P. I. Huang from Cancer Center of Taipei Veterans General Hospital, Taipei, Taiwan, for their great assistance in this study.

References

[1] S. H. Wu, L. Ryvarden, and T. T. Chang, "Antrodia cinnamomea ("niu-chang-chih"), new combination of a medicinal fungus in Taiwan," *Botanical Bulletin of Academia Sinica*, vol. 38, pp. 273–275, 1997.

[2] T. T. Chang and W. N. Chou, "*Antrodia cinnamomea* sp. nov. on *Cinnamomum kanehirai* in Taiwan," *Mycological Research*, vol. 99, no. 6, pp. 756–758, 1995.

[3] M. Zang and C. H. Su, "*Ganoderma comphoratum*, a new taxon in genus *Ganoderma* from Taiwan," *China Acta Botanica Yunnanica*, vol. 12, pp. 395–396, 1990.

[4] Z. T. Tsai and S. L. Liaw, Eds., *The Use and the Effect of Ganoderma*, Sheng-Yun Publisher, Taichung, Taiwan, 1982.

[5] B. C. Wang and R. C. Huang, "The development and marketing of *Ganoderma lucidum* and *Antrodia camphorata*," *Food Industry*, vol. 34, no. 5, pp. 3–14, 2002.

[6] J. J. Liu, T. S. Huang, M. L. Hsu et al., "Antitumor effects of the partially purified polysaccharides from *Antrodia camphorata* and the mechanism of its action," *Toxicology and Applied Pharmacology*, vol. 201, no. 2, pp. 186–193, 2004.

[7] Y. L. Hsu, Y. C. Kuo, P. L. Kuo, L. T. Ng, Y. H. Kuo, and C. C. Lin, "Apoptotic effects of extract from *Antrodia camphorata* fruiting bodies in human hepatocellular carcinoma cell lines," *Cancer Letters*, vol. 221, no. 1, pp. 77–89, 2005.

[8] Y. C. Hseu, H. L. Yang, Y. C. Lai, J. G. Lin, G. W. Chen, and Y. H. Chang, "Induction of apoptosis by *Antrodia camphorata* in human premyelocytic leukemia HL-60 cells," *Nutrition and Cancer*, vol. 48, no. 2, pp. 189–197, 2004.

[9] Y. L. Hsu, P. L. Kuo, C. Y. Cho et al., "*Antrodia cinnamomea* fruiting bodies extract suppresses the invasive potential of human liver cancer cell line PLC/PRF/5 through inhibition of nuclear factor κB pathway," *Food and Chemical Toxicology*, vol. 45, no. 7, pp. 1249–1257, 2007.

[10] S. W. Yang, Y. C. Shen, and C. H. Chen, "Steroids and triterpenoids of *Antrodia cinnamomea*—a fungus parasitic on *Cinnamomum micranthum*," *Phytochemistry*, vol. 41, no. 5, pp. 1389–1392, 1996.

[11] Y. C. Shen, S. W. Yang, C. S. Lin, C. H. Chen, Y. H. Kuo, and C. F. Chen, "Zhankuic acid F: a new metabolite from a formosan fungus *Antrodia cinnamomea*," *Planta Medica*, vol. 63, no. 1, pp. 86–88, 1997.

[12] Y. C. Hseu, W. C. Chang, Y. T. Hseu et al., "Protection of oxidative damage by aqueous extract from *Antrodia camphorata* mycelia in normal human erythrocytes," *Life Sciences*, vol. 71, no. 4, pp. 469–482, 2002.

[13] G. Hsiao, M. Y. Shen, K. H. Lin et al., "Antioxidative and hepatoprotective effects of *Antrodia camphorata* extract," *Journal of Agricultural and Food Chemistry*, vol. 51, no. 11, pp. 3302–3308, 2003.

[14] M. T. Geethangili and Y. M. Tzeng, "Review of pharmacological effects of *Antrodia camphorata* and its bioactive compounds," *Evidence-Based Complementary and Alternative Medicine*, vol. 2011, Article ID 212641, 17 pages, 2011.

[15] Y. Y. Chen, H. H. Chang, H. Y. Lee, and F. Sheu, "Immunomodulatory and anti-tumor effects of oral administration with *Antrodia cinnamomea* fruiting bodies in BALB/c mice," *Taiwanese Journal of Agricultural Chemistry and Food Science*, vol. 46, no. 2, pp. 87–95, 2008.

[16] J. J. Cheng, N. K. Huang, T. T. Chang, D. L. Wang, and M. K. Lu, "Study for anti-angiogenic activities of polysaccharides isolated from *Antrodia cinnamomea* in endothelial cells," *Life Sciences*, vol. 76, no. 26, pp. 3029–3042, 2005.

[17] C. M. Yang, Y. J. Zhou, R. J. Wang, and M. L. Hu, "Anti-angiogenic effecct and mecchanisms of polysaccharides from *Antrodia cinnamomea* wiith different molecular weights," *Journal of Ethnopharmacology*, vol. 123, no. 3, pp. 407–412, 2009.

[18] J. J. Cheng, M. K. Lu, C. Y. Lin, and C. C. Chang, "Characterization and functional elucidation of a fucosylated 1,6-α-d-mannogalactan polysaccharide from *Antrodia cinnamomea*," *Carbohydrate Polymers*, vol. 83, no. 2, pp. 545–553, 2011.

[19] Y. J. Chen, C. J. Chou, and T. T. Chang, "Compound MMH01 possesses toxicity against human leukemia and pancreatic cancer cells," *Toxicology In Vitro*, vol. 23, no. 3, pp. 418–424, 2009.

[20] M. Dubois, K. A. Gilles, J. K. Hamilton, P. A. Rebers, and F. Smith, "Colorimetric method for determination of sugars and related substances," *Analytical Chemistry*, vol. 28, no. 3, pp. 350–356, 1956.

[21] U. S. Satyapal, V. J. Kadam, and R. Ghosh, "Hepatoprotective activity of livobond a polyherbal formulation against CCl_4 induced hepatotoxicity in rats," *International Journal of Pharmacology*, vol. 4, no. 6, pp. 472–476, 2008.

[22] J. K. Limdi and G. M. Hyde, "Evaluation of abnormal liver function tests," *Postgraduate Medical Journal*, vol. 79, no. 932, pp. 307–312, 2003.

[23] D. E. Johnston, "Special considerations in interpreting liver function tests," *The American Family Physician*, vol. 59, no. 8, pp. 2223–2230, 1999.

[24] S. Reitman and S. Frankel, "A colorimetric method for the determination of serum GOT and GPT," *American Journal of Clinical Pathology*, vol. 28, pp. 57–60, 1957.

[25] J. A. Plumb, R. Milroy, and S. B. Kaye, "Effects of the pH dependence of 3-(4,5-dimethylthiazol-2-yl)-2,5-diphenyltetrazolium bromide-formazan absorption on chemosensitivity determined by a novel tetrazolium-based assay," *Cancer Research*, vol. 49, no. 16, pp. 4435–4440, 1989.

[26] Y. M. Lin, C. P. Hu, C. K. Chou et al., "A new human hepatoma cell line: establishment and characterization," *Chinese Journal of Microbiology and Immunology*, vol. 15, no. 3, pp. 193–201, 1982.

[27] S. El Bahi, E. Caliot, M. Bens et al., "Lymphoepithelial interactions trigger specific regulation of gene expression in the M cell-containing follicle-associated epithelium of Peyer's patches," *The Journal of Immunology*, vol. 168, no. 8, pp. 3713–3720, 2002.

[28] E. K. Teo and K. M. Fock, "Hepatocellular carcinoma: an Asian perspective," *Digestive Diseases*, vol. 19, no. 4, pp. 263–268, 2001.

[29] J. Folkman, "Tumor angiogenesis: therapeutic implications," *The New England Journal of Medicine*, vol. 285, no. 21, pp. 1182–1186, 1971.

[30] R. S. . Mc Cuskey, Ed., *The Hepatic Microvascular System*, Raven Press, New York, NY, USA, 1994.

[31] D. Ribatti, A. Vacca, B. Nico, D. Sansonno, and F. Dammacco, "Angiogenesis and anti-angiogenesis in hepatocellular carcinoma," *Cancer Treatment Reviews*, vol. 32, no. 6, pp. 437–444, 2006.

[32] C. C. Shih, M. K. Lu, J. J. Cheng, and L. W. Danny, "Antiangiogenic activities of polysaccharides isolated from medicinal fungi," *FEMS Microbiology Letters*, vol. 249, no. 2, pp. 247–254, 2005.

[33] C. C. Shen, Y. C. Kuo, R. Y. Huang, L. C. Lin, and C. J. Chou, "New ergostane and lanostane from *Antrodia camphorata*," *The Journal of Chinese Medicine*, vol. 14, pp. 247–258, 2003.

Hindawi Publishing Corporation
Evidence-Based Complementary and Alternative Medicine
Volume 2013, Article ID 547430, 11 pages
http://dx.doi.org/10.1155/2013/547430

Research Article

Resveratrol Downregulates Interleukin-6-Stimulated Sonic Hedgehog Signaling in Human Acute Myeloid Leukemia

Yu-Chieh Su,[1,2] Szu-Chin Li,[2] Yin-Chi Wu,[3] Li-Min Wang,[3] K. S. Clifford Chao,[4] and Hui-Fen Liao[3,5]

[1] *Department of Medicine, College of Medicine, Tzu Chi University, Hualien 97004, Taiwan*
[2] *Division of Hematology and Oncology, Department of Internal Medicine, Buddhist Dalin Tzu Chi General Hospital, Chiayi 62247, Taiwan*
[3] *Department of Biochemical Science and Technology, National Chiayi University, Chiayi 60004, Taiwan*
[4] *Department of Radiation Oncology, Columbia University, New York, NY 10027, USA*
[5] *Institute of Traditional Medicine, National Yang-Ming University, Taipei 11221, Taiwan*

Correspondence should be addressed to K. S. Clifford Chao; ksc2119@columbia.edu and Hui-Fen Liao; liao.huifen@gmail.com

Received 15 December 2012; Accepted 15 January 2013

Academic Editor: Yu-Jen Chen

IL-6 and sonic hedgehog (Shh) signaling molecules are considered to maintain the growth of cancer stem cells (CSCs). Resveratrol, an important integrant in traditional Chinese medicine, possesses certain antitumor effects. However, the mechanisms on regulating acute myeloid leukemia (AML) are unclear. This study first used human subjects to demonstrate that the plasma levels of IL-6 and IL-1β in AML patients were higher and lower, respectively, than healthy donors. The expression of Shh preproproteins, and C- and N-terminal Shh peptides increased in bone marrow and peripheral blood mononuclear cells isolated from AML patients, and the plasma N-Shh secretion was greater. To further clarify the effect of IL-6 and resveratrol in Shh signaling, human AML HL-60 cells were tested. IL-6 upregulated Shh and Gli-1 expression and was accompanied by an increase of cell viability. Resveratrol significantly decreased CSC-related Shh expression, Gli-1 nuclear translocation, and cell viability in IL-6-treated HL-60 cells and had synergistic effect with Shh inhibitor cyclopamine on inhibiting cell growth. *Conclusions*. IL-6 stimulated the growth of AML cells through Shh signaling, and this effect might be blocked by resveratrol. Further investigations of Shh as a prognostic marker and resveratrol as a therapeutic drug target to CSCs in AML are surely warranted.

1. Introduction

Recent investigation support the existence of cancer stem cells (CSCs) in human cancers, suggesting that CSCs may arise from mutated progenitor cells and then develop the capacity of unregulated self-renewal [1, 2]. Therefore, CSCs are a small number of self-renewing tumor cells that undergo multilineage differentiation and survive in supportive microenvironments [3, 4]. The first study of leukemia stem cells (LSCs) demonstrated that a subpopulation of acute myeloid leukemia (AML) cells, defined as $CD34^+$ $CD38^-$ and shared similar cell surface marker expression patterns with normal hematopoietic progenitor cells, may cause the malignancies continue to relapse as a consequence of resistance to chemotherapies [5, 6].

The intercellular signaling mechanisms for CSC maintenance may involve Wnt/β-catenin, Hedgehog (Hh) pathway, as well as epigenetic, metabolic, and molecular chaperone pathways [7]. Among these, the Hh signaling pathway is a crucial regulator of embryogenesis and development in adult hematopoietic, neural, skin and hair follicle stem cells [8, 9]. The Hh signaling pathway, initiated through the binding of secreted Hh ligands (Sonic, Indian, and Desert) to the membrane receptor patched (PTCH), results

in nuclear translocation and activation of the transcription factors of the Gli family [10]. In leukemia, Hh signaling is also important in the maintenance of neoplastic stem cells in the haematopoietic system, raising the possibility of drug resistance and disease recurrence [11]. The inhibition of sonic hedgehog (Shh) signaling downregulates the expression of the ATP-binding cassette transporter multidrug resistant (MDR) proteins, and thus may be a target for overcoming drug resistance and increasing the likelihood of response to chemotherapy [12]. Our previous study demonstrated that Shh signaling molecules expressed in human chronic myeloid leukemia (CML) cells may regulate Bcr-Abl activation [13]. In addition, a research indicated that thalidomide reduces vascular endothelial growth factor (VEGF) and interleukin (IL)-6 expression in the tumor microenvironment accounts, as well as attenuates Hh signaling activity in advanced prostate cancers [14].

Growth factors and cytokines released in the bone marrow (BM), thymus, and other immune tissue microenvironments provide the paracrine and autocrine effects for long-term hematopoietic regulation of stem cells [15]. Such microenvironment-derived cytokines also play a key role in maintaining the growth of tumors [16]. For example, upregulating IL-8 in the marrow microenvironment and CXCL12/CXCR4 axis may control the pathogenesis of T-cell acute lymphoblastic leukemia [16]. Peroxisome proliferator-activated receptor gamma (PPARgamma) negatively controls multiple myeloma growth, in part through the inhibition of IL-6 production by marrow stromal cells [17]. In CML K562 cells, treatment with BM stromal-derived conditioned medium caused the cells' resistance to the therapeutic drug imatinib mesylate (IM, also named STI571), an effect which correlated with increased IL-6-related phospho-Stat3 expression [15].

Resveratrol (3,5,4′-trans-trihydroxystilbene) is a phytochemical that widely found in plants (such as grape skin, red wine, cranberries, blueberries, and peanuts) and in traditional Chinese medicines (TCMs, such as *Rheum officinale* Baill. and *Polygonum cuspidatum*) [18, 19]. Resveratrol possesses cytotoxic and apoptotic controlling on various types of cancer and normal cells [20]. Our previous study reported that resveratrol regulates the apoptosis induction and erythrocytic differentiation through the modulation of nuclear factor-kappaB in human leukemia cells [21]. In CML, resveratrol acts as a Bcr-Abl inhibitor and suppresses Shh signaling in both IM-sensitive and IM-resistant cells [13]. Resveratrol also reverses doxorubicin-mediated resistance in AML cells via the downregulation of multidrug resistant protein (MRP)-1 expression [22]. However, little is known of resveratrol on regulation of CSCs in AML.

Cancer cells secrete various cytokines to maintain their microenvironment, stimulate certain signal pathways in CSCs, thereby increase their survival rate and resistance to chemotherapy [23]. However, the regulatory effects of cytokines on Hh-related molecules in the setting of AML are unclear. In this study, we first brought in human subjects, including control donors and patients with AML, to examine the expression of Shh signaling molecules and cytokines in BM cells and peripheral blood. We subsequently performed an *in vitro* assay to clarify the effect of IL-6 on regulating Shh signaling and assess the possibility of resveratrol used as a potent Shh inhibitor in AML.

2. Materials and Methods

2.1. Subjects and Isolation of Mononuclear Cells (MNCs) from Bone Marrow (BM) and Peripheral Blood (PB). Twenty-six healthy volunteers (six for BM and twenty for PB collection) and twenty-six patients with AML (M3 type excluded, six for BM and twenty for PB collection) with ages ranging from 21–88 years were recruited. All patients had either newly diagnosed or recently relapsed AML before anticancer chemotherapeutic treatment. Characteristics of AML patients were listed in Table 2. Our study design was approved by the Institutional Review Board (IRB) of Buddhist Dalin Tzu Chi General Hospital, Taiwan (No. B09703022). All control donors and patients provided written informed consent prior to any testing. Patients' information was not revealed in this study, and the data were analyzed anonymously. Mononuclear cells (MNCs) were separated from BM or PB on a density gradient (Histopaque, 1.077 g/mL, Sigma, St. Louis, MO) followed by centrifugation at 2,000 rpm for 15 min. The plasma samples isolated from PB were collected for cytokine detection and Shh expression.

2.2. Measurement of Cytokine Levels in Plasma. Plasma levels of cytokines, including GM-CSF, IL-1β, TNF-α, and IL-6 from the control donors and AML patients, were assayed using a BioSource Multiplex Bead Immunoassay kit (BioSource International, Inc., Camarillo, CA) with the Luminex xMAP (Luminex Corp., Austin, TX) instrument and software program for data analysis. The assay method was performed according to the manufacturer's protocol.

2.3. Western Blot Analysis. To measure Shh expression, total proteins isolated from BM cells, PB-MNCs, and plasma from human subjects, as well as human leukemia HL-60 cell line. The concentrations of the collected proteins were quantified using a bicinchoninic acid (BCA) protein assay kit (Bio-Rad). The same amount of protein (100 μg per well) was disrupted with 2x concentrated electrophoresis sample buffer (1 M Tris, pH 6.8, 5% SDS, 40% glycerol, 0.005% bromophenol blue, 8% β-mercaptoethanol) and subjected to 10% SDS-polyacrylamide gel electrophoresis. The protein gel was transferred to a PVDF membrane, blotted with primary antibodies, including anti-Shh (1 : 200, Santa Cruz), anti-Smo (1 : 200, Santa Cruz), anti-Gli-1 (1 : 200, Santa Cruz), anti-β-actin (1 : 1000, Santa Cruz), and anti-glyceraldehyde-3-phosphate dehydrogenase (GAPDH, 1 : 1000, Santa Cruz), and then incubated at 4°C for overnight. The membrane was further hybridized with horseradish peroxidase (HRP)-conjugated secondary antibody (1 : 1000, Santa Cruz) for 1.5 h followed by exposing with enhanced chemiluminescence (Perkin Elmer, Waltham, MA). Relative protein levels were determined by densitometry using ImageJ software (Version 1.36b, NIH, Bethesda, MD). Relative values were normalized to the internal control.

2.4. AML Cell Line and Cell Culture. To clarify the possible roles of IL-6 and Shh signaling in AML, a human AML HL-60 cell line was used for *in vitro* assay. HL-60 cells were obtained from American Type Culture Collection (ATCC, Manassas, VA) and maintained in RPMI 1640 medium (Gibco Products, Carlsbad, CA) containing 10% (v/v) fetal bovine serum (FBS) (Gibco) and 2 mM L-glutamine (Sigma) in a 37°C incubator. For the *in vitro* assay, cells (2×10^5 cells/mL) were treated with recombinant human IL-6 (0–10 ng/mL; Cytolab Ltd., Rehovot, Israel), cyclopamine (2 μM, Sigma), humanized anti-human IL-6 receptor antibody (MRA, 100 nM, Chugai Pharmaceutical Co., Ltd.), and/or various concentrations of resveratrol (0–50 μM, Sigma) for 24 h. For the analysis of Shh/Gli-1 expression, total RNA and proteins were extracted from the cells and then adjusted for reverse transcription-polymerase chain reaction (RT-PCR) and Western blot analysis. Viable cells were counted using a trypan blue dye exclusion test. The translocation of Gli-1 was also assayed using immunofluorescence staining and Western blotting of the nucleic and cytosolic Gli-1 levels.

2.5. RT-PCR Assay of Shh and Gli-1 Expression. AML HL-60 cells were treated with IL-6 (0–10 ng/mL) in the addition with or without MRA (100 nM) for 24 h; then, total RNAs were isolated from the cells using TRIzol reagent (Life Technologies, Gaithersburg, MD) and reverse transcribed to cDNA by reaction in a PCR thermal cycler (Bio-Rad, Hercules, CA) for 10 min at 25°C, 70 min at 37°C, 10 min at 72°C and stored at 4°C. Shh, Gli-1, and GAPDH genes were amplified by PCR using specific primers (Mission Biotech., Taipei, Taiwan) and PCR thermal cycle profiles as listed in Table 1. PCR products were assayed by electrophoresis in a 1% agarose gel in Tris-acetate/EDTA buffer and visualized by ethidium bromide (0.01%) staining. GAPDH was used for internal control.

2.6. Preparation of Nuclear and Cytosolic Extracts from Cells. To prepare the cytosolic and nucleic proteins, the cell nuclei were first separated from the cytosol using the nuclear extraction buffer (500 mM NaCl, 1.5 mM $MgCl_2$, 0.2 mM EDTA, 1 mM DTT, 20% Glycerol, 0.1% Triton X-100, and 20 mM HEPES, pH 7.4). Then, the nuclei were resuspended in lysis buffer (150 mM NaCl, 0.1% SDS, 1% Triton X-100, and 100 mM Tris, pH 8.0) and centrifuged at 400 g for 10 min. The nuclear proteins were collected and stored at −80°C. The protein concentrations were determined using a BCA protein assay kit (Bio-Rad), and the levels of cytosolic and nucleic Gli-1 were assayed by Western blotting.

2.7. Immunofluorescence Staining of Gli-1. The treated cells were collected and reacted with anti-Gli-1 primary antibody (1 : 200, Santa Cruz Biotechnology, Inc., Heidelberg, Germany) and immunofluorescence PE-conjugated anti-IgG-TR antibody (1 : 500, Santa Cruz) in order to determine the distribution of Gli-1 expression in cells. Hoechst 33342 fluorescence dye was also used to stain the location of the nucleus. The cells were then photographed under a fluorescence microscope at a magnification of 400x.

2.8. Statistical Analysis. Data were obtained from at least three independent experiments and expressed as the mean ± standard error (SE). Student's *t*-test or analysis of variance was applied to compare the results for the AML patients and control donors, as well as the results from the *in vitro* studies. Differences were considered significant at $P < 0.05$. All statistical analyses were carried out using SigmaStat and SigmaPlot software (Jandel Scientific, San Rafael, CA).

3. Results

3.1. Plasma Cytokine Production in Control Donors and AML Patients. Characteristics of AML patients were listed in Table 2. Among the AML patients, 9 patients died from cancer within 3 months of blood sample collection. There was no significant difference in age and gender between living AML patients and those who died from cancer. In Figure 1, peripheral blood collected from the AML patients showed that the AML patient group ($n = 20$) had a markedly decreased plasma IL-1β level (10.0-fold) and an increased plasma IL-6 level (72.6-fold) as compared to the healthy volunteers ($n = 20$). The plasma levels of GM-CSF and TNF-α were not different between the control and AML patients. Moreover, 9 of the 20 patients with AML, who showed poor prognosis (such as poor quality of life, resistants to chemotherapy, and higher risk of life threat) and died from cancer, had higher levels of IL-6 and N-Shh than the patients who were alive at the same time point (Table 2). The average age and IL-6 value of normal control were 45.5 ± 8.5 yr old and 0.8 ± 0.1 pg/mL, respectively.

3.2. Effect of Shh Expression in BM Cells, PB-MNCs, and Plasma between Control Volunteers and AML Patients. In Figure 2(a), the expressions of Shh preproproteins (Pre-Shh, 45 kDa), C-terminal (C-Shh, 25 kDa), and N-terminal (N-Shh, 20 kDa) peptides were all markedly increased in the BM cells of the AML patients. There was a similar result in the PB-MNCs from the AML patients, showing greater expression of Pre-Shh (1.5-fold), C-Shh (1.6-fold), and N-Shh (1.4-fold) than the cells from the control donors (Figure 2(b)). However, the expression of smoothened (Smo) did not significantly differ among these two groups. Western blot analysis (Figure 2(c)) showed that the soluble Shh secreted into plasma was significantly increased, along with the active N-Shh levels, in the AML patient group. Additionally, 9 of 20 patients with AML showed poor prognosis and died from cancer within 3 months of the blood collection, and they had higher plasma IL-6 levels and N-Shh expression on testing than the AML patients who were alive at that point (Table 2).

3.3. Effect of IL-6 on Shh Signaling in Human AML HL-60 Cells. To clarify the possible regulation of IL-6 and Shh signaling in AML, a human AML HL-60 cell line was used for further assay. The mRNA expression of Shh and Gli-1 was estimated with RT-PCR assay (for primers, see Table 1). Treatment with IL-6 at 5 and 10 ng/mL significantly increased the mRNA expression of both Shh and Gli-1 in HL-60 cells (Figure 3(a)). The stimulatory effect of IL-6 was also

Table 1: Primer sequences used for RT-PCR analysis.

Genes	Sequences	Annealing temp.[a]	Products (bp)
Shh:		33.8	477
Forward	5′-CGCACGGGGACAGCTCGGAAGT-3′		
Reverse	5′-CTGCGCGGCCCTCGTAGTGC-3′		
Gli-1:		49	185
Forward	5′-TTCCTACCAGAGTCCCAAGT-3′		
Reverse	5′-CCCTATGTGAAGCCCTATTT-3′		
GAPDH:		55	574
Forward	5′-CCACCCATGGCAAATTCCATGGCT-3′		
Reverse	5′-TCTAGACGGCAGGTCAGGTCCACC-3′		

[a]The PCR thermal cycle profile consisted of 1 cycle of denaturation for 5 min at 95°C; 30 cycles of denaturation for 30 sec at 95°C, annealing of primers for 45 sec at different temperatures as shown in this Table, and extension for 50 sec at 72°C; and 1 cycle of a final extension step at 72°C for 10 min.

Table 2: Characteristics of AML patients (M3 excluded) collected in this study.

Patient number	BM or PB collection	Alive or died	New diagnose or relapse	Type	Gender	Age (yr)	Average values[a]
1	BM	Alive	New diagnose	M1	F	58	Age: 46.8 ± 6.5 yr old
2	BM	Alive	New diagnose	M2	M	30	
3	BM	Alive	New diagnose	M0	M	53	
4	BM	Alive	New diagnose	M2	M	36	
5	BM	Alive	New diagnose	M2	F	34	
6	BM	Alive	New diagnose	M1	M	70	
7	PB	Alive	New diagnose	M2	M	30	Age: 55.5 ± 7.6 yr old IL-6: 10.1 ± 6.3 pg/mL N-Shh: 1.7 ± 0.2 fold
8	PB	Alive	New diagnose	M1	M	52	
9	PB	Alive	New diagnose	M4	F	84	
10	PB	Alive	New diagnose	M1	M	75	
11	PB	Alive	New diagnose	M2	M	88	
12	PB	Alive	New diagnose	M1	F	60	
13	PB	Alive	New diagnose	M2	M	84	
14	PB	Alive	New diagnose	M2	M	59	
15	PB	Alive	Relapse	M1	F	29	
16	PB	Alive	Relapse	M2	M	21	
17	PB	Alive	Relapse	M2	M	29	
18	PB	Died	New diagnose	M2	M	51	Age: 69.6 ± 2.8 yr old IL-6: 116.6 ± 54.9 pg/mL* N-Shh: 2.4 ± 0.2 fold*
19	PB	Died	New diagnose	M1	M	80	
20	PB	Died	New diagnose	M0	M	71	
21	PB	Died	New diagnose	M1	F	69	
22	PB	Died	New diagnose	M2	M	78	
23	PB	Died	New diagnose	M2	F	75	
24	PB	Died	Relapse	M4	M	66	
25	PB	Died	Relapse	M2	F	68	
26	PB	Died	Relapse	M1	F	68	

[a]The average age and IL-6 value of normal control were 45.5 ± 8.5 yr old and 0.8 ± 0.1 pg/mL, respectively. The relative fold of N-Shh in AML was normalized to the normal control, and the data were expressed as mean ± SE.

*$P < 0.05$ as compared to the living AML patients. The results were calculated from at least three independent experiments and expressed as mean ± standard error (SE).

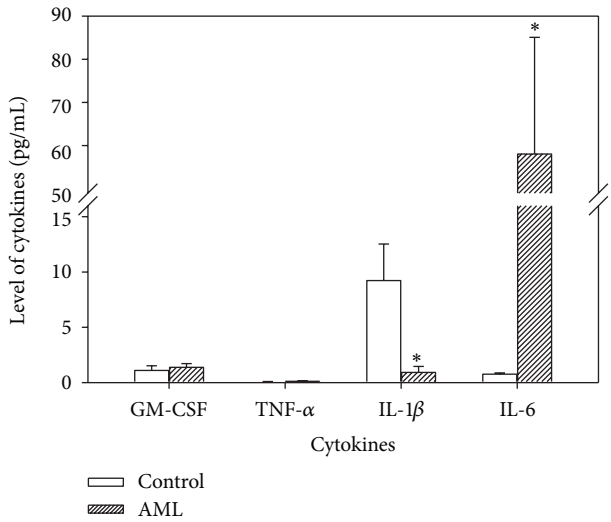

Figure 1: Plasma levels of GM-CSF, TNF-α, IL-1β, and IL-6 in donors of normal control ($n = 20$) and AML patients ($n = 20$) that analyzed by using a BioSource Multiplex Bead Immunoassay kit. $^*P < 0.05$ as compared to the control group. The results were calculated from three independent experiments and expressed as mean ± standard error (SE).

accompanied with the increased expression of Shh proteins, including Pre-Shh, C-Shh, and N-Shh (Figure 3(b)). Such stimulatory effect of IL-6 would be blocked in the addition of MRA (100 nM) in IL-6-treated HL-60 cells (Figure 3(b)). Moreover, resveratrol effectively decreased the expression of Pre-Shh, C-Shh, and N-Shh in IL-6-treated HL-60 cells (Figure 3(c)).

3.4. Viability of Resveratrol and Cyclopamine in IL-6-Induced HL-60 Cells. In Figure 4(a), IL-6 (10 ng/mL) significantly increased the viability of HL-60 cells. Resveratrol inhibited the IL-6-induced cell viability in a dose-dependent manner. To clarify the roles of IL-6 and Shh signaling in AML, HL-60 cells were treated with IL-6, Shh inhibitor cyclopamine, and/or resveratrol for cell viability assay. In Figure 4(b), cyclopamine significantly decrease the cell viability, as well as the viability that had been augmented by IL-6. Additionally, resveratrol enhanced the activity of cyclopamine in HL-60 cells with and without IL-6 treatment (Figure 4(b)). As summarized in Figures 3 and 4, IL-6 might stimulate downstream Shh/Gli-1 signaling that cause the growth of AML HL-60 cells. Resveratrol has the potential to block this effect and also has synergistic effect to enhance the inhibitory effects that induced by cyclopamine.

3.5. Effect of Resveratrol on IL-6-Mediated Gli-1 Nuclear Translocation in HL-60 Cells. In Figure 5(a), Western blot analysis of the nucleic and cytosolic Gli-1 expression demonstrated that IL-6 significantly increased the nucleic Gli-1 expression in the HL-60 cells. Cyclopamine and resveratrol significantly prohibited the nucleic translocation of Gli-1 in IL-6-stimulated HL-60 cells (Figure 5(a)). Moreover, immunofluorescence staining of these treated cells also showed that IL-6 markedly induced Gli-1 expression in nucleus of HL-60 cells, while cyclopamine and resveratrol obviously decreased both the Gli-1 level and Gli translocation to nuclei (Figure 5(b)). Therefore, it was suggested that resveratrol, like cyclopamine, has potential effect on inhibition of IL-6-mediated Shh signaling and Gli-1 nuclear translocation in AML HL-60 cells.

4. Discussion

Leukemia is a common cancer worldwide. Developments of potential drugs targeted to CSC inhibition that enhance efficacy and prevent drug resistance are currently the most principal treatment of leukemia [24]. In CML, IM is designed to treat patients with Bcr/Abl-containing leukemic cells [14]. Our previous study reported that Shh signaling might upregulate Bcr-Abl overexpression and caused the cells more resistant to IM treatment, while resveratrol acted as a Shh inhibitor and reversed such resistant effect [13]. In AML, the present study also demonstrated that the level of IL-6 and Shh were higher in AML patients than normal donors, and even higher IL-6 and Shh levels in patients who showed poor prognosis (such as poor quality of life, resistant to chemotherapy, and higher risk on life threat) and died from cancer. This study excluded AML-M3 patient, because of a notable difference between M3 and other AMLs involved the common occurrence of life-threatening consumptive coagulopathies in M3 patients that dramatically affected patient outcomes [25].

Both IL-6 and Shh are important in the maintenance of CSCs in the neoplastic microenvironment, limiting the access of therapeutics to the tumor, alter drug metabolism, and contribute to the development of drug resistance and disease recurrence [11, 14, 26]. Kobune et al. indicated that aberrant Hh pathway activation is a feature of some $CD34^+$ myeloid leukemic cells, and Hh inhibitors may have a therapeutic role in the treatment of AML [27]. Here, we studied the correlation between Shh signaling and IL-6 regulation in myeloid leukemia. AML HL-60 cells were treated with IL-6 and subsequently assayed for the expression of Shh and Gli-1 genes. IL-6 significantly increased the expression of both Shh and Gli-1, as well as cell viability, demonstrating that upstream regulation of IL-6 may initiate cellular Shh/Gli-1 signaling pathways and cause growth in the AML cells. Such effect was confirmed by the treatment of MRA, a humanized anti-human IL-6 receptor antibody, with blocking activity on IL-6-mediated Shh signaling. In addition, the Shh inhibitor cyclopamine significantly decreased the viability and Gli-1 translocation of IL-6-treated HL-60 cells, hinting that blocking the Shh pathway may be a potential strategy for AML treatment. An article reported that up to 40% of hepatocellular carcinomas are potentially arising from stem cells and increased activation of multiple pathways including IL-6/STAT3, WNT, CDK4, and the Hh signaling pathway [28]. In gastric cancer patients, chronic *Helicobacter pylori* infection elevated IL-1β, IL-6, IL-8, TNF-α, and IFN-γ in the gastric mucosa, as well as activating the stem

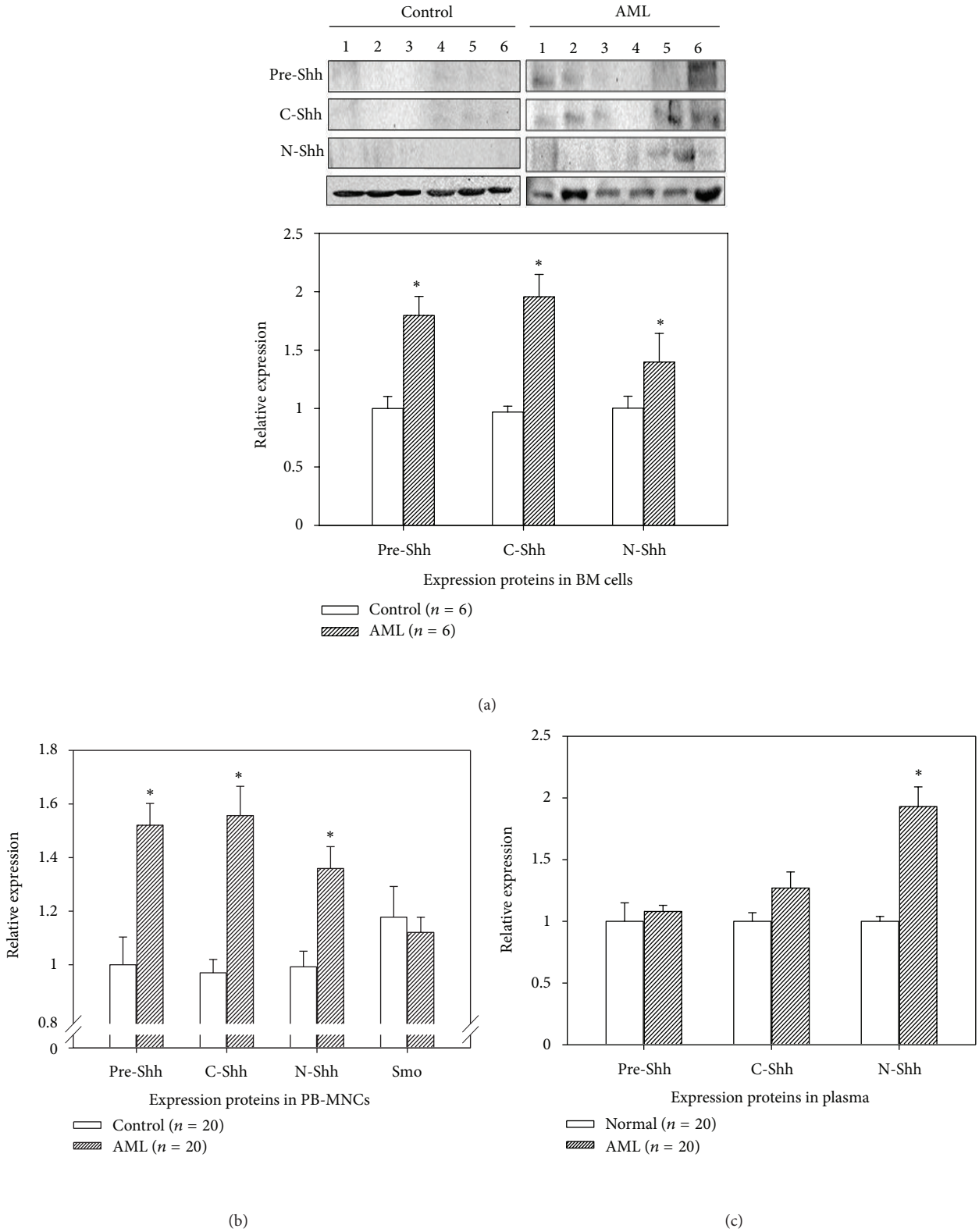

Figure 2: Expression of Shh preproprotein (pre-Shh), C-terminal (C-Shh), and N-terminal (N-Shh) in (a) bone marrow (BM) cells, (b) peripheral blood mononuclear cells (PB-MNCs), and (c) plasma collected from the normal control donors and the AML patients using a Western blot analysis. The relative values were normalized to the internal control β-actin, and the data were expressed as mean ± SE. $^{*}P < 0.05$ as compared to the control group.

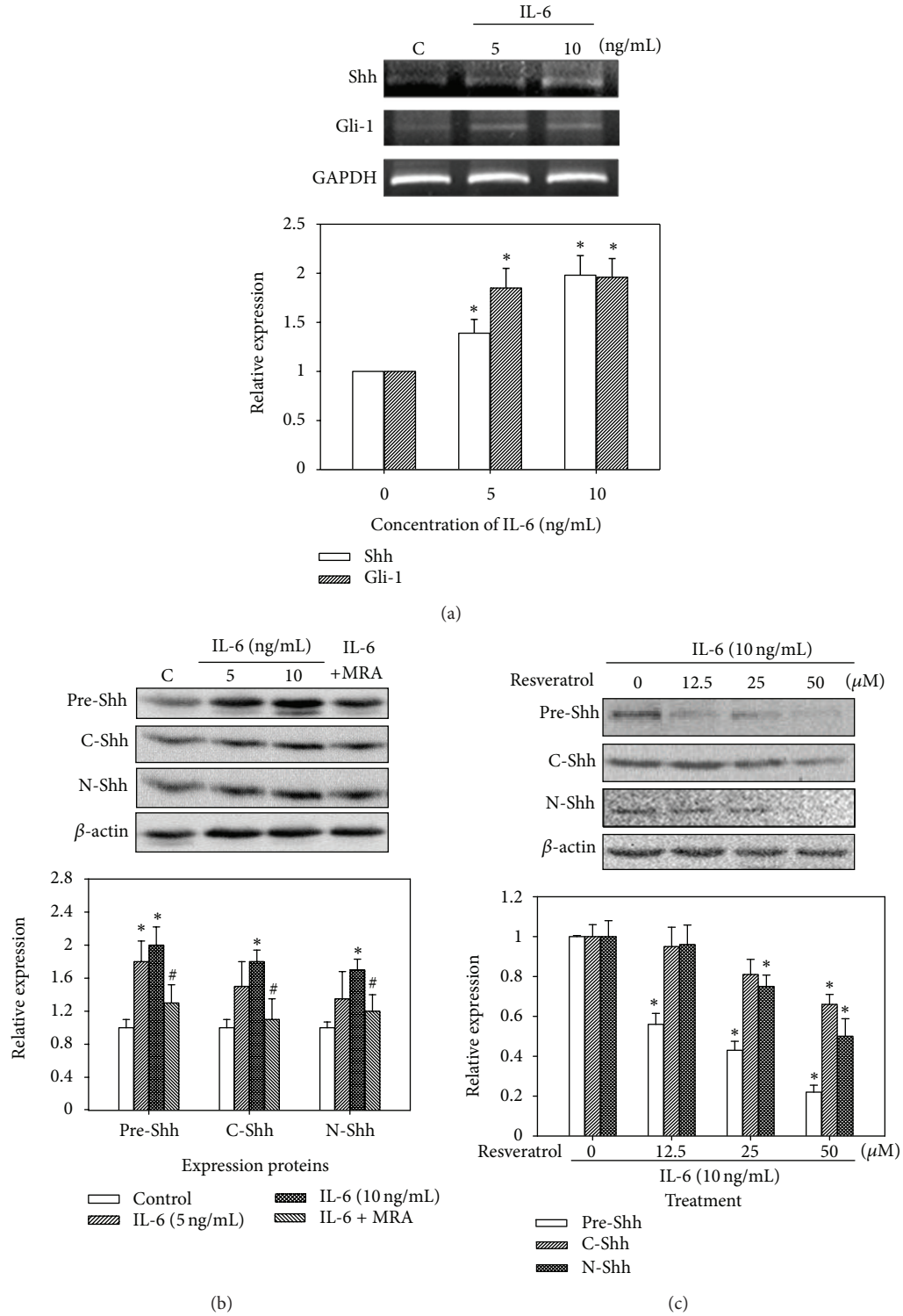

Figure 3: Regulation of IL-6 and resveratrol in Shh signaling in AML HL-60 cells. (a) RT-PCR assay of Shh and Gli-1 expressed in HL-60 cells with the treatment of IL-6 (5 and 10 ng/mL) for 24 h. (b) Western blot analysis of Shh preproproteins (Pre-Shh, 45 kDa), C-terminal (C-Shh, 25 kDa), and N-terminal (N-Shh, 20 kDa) peptides in IL-6-treated HL-60 cells with or without MRA (100 nM) treatment. (c) Effect of resveratrol on Shh expression in IL-6-treated HL-60 cells. The relative values were normalized to the internal control, were calculated from three independent experiments, and were expressed as mean ± SE. $^{*}P < 0.05$ as compared to the control group. $^{\#}P < 0.05$ as compared to the IL-6 alone group.

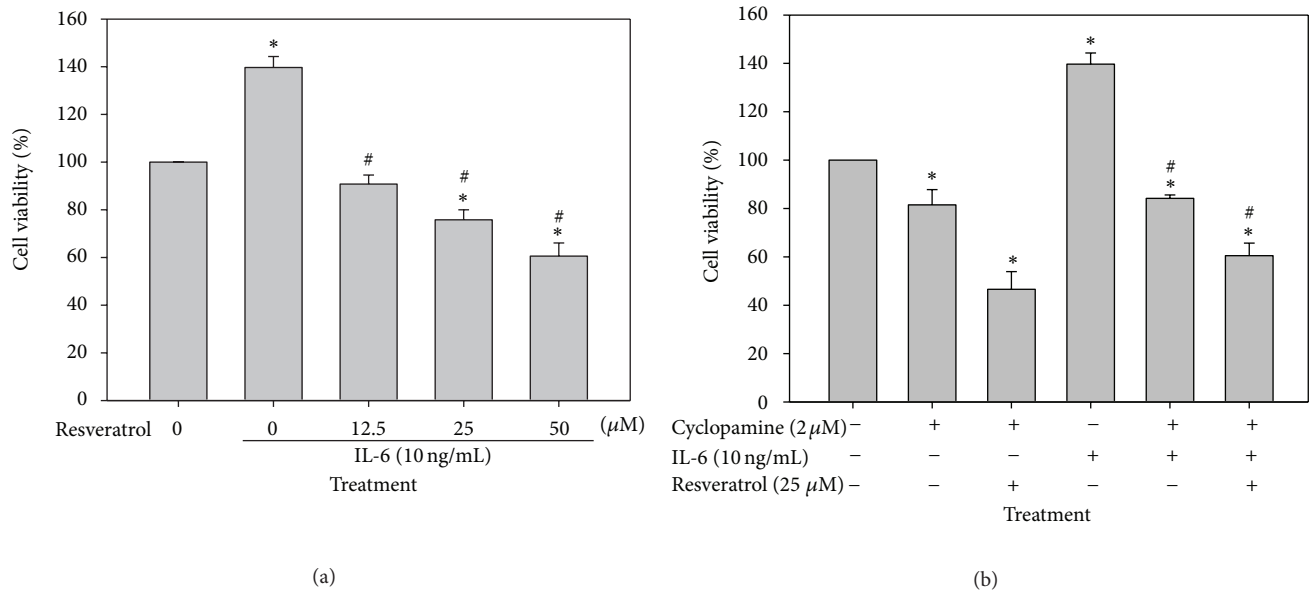

Figure 4: Viability of IL-6, cyclopamine, and resveratrol in HL-60 cells that assayed by using a trypan blue dye exclusion test. (a) Viability of resveratrol in IL-6-treated HL-60 cells. (b) Cell viability assay of IL-6 (10 ng/mL), cyclopamine (2 μM), and resveratrol (25 μM). The results were calculated from three independent experiments and were expressed as mean ± SE. $^{*}P < 0.05$ as compared to the control group. $^{\#}P < 0.05$ as compared to the IL-6 alone group.

cell signaling network, consisting of the WNT, Notch, FGF, Hh, and BMP signaling pathways [29]. Our study is the first to demonstrate that IL-6 production in AML would stimulate the downstream Shh signaling pathway and induce the growth of leukemia cells. Modulating Shh molecules with their antagonists, such as cyclopamine, may prove to be a strong therapeutic option for AML patients.

More and more chemopreventive natural products (such as soy, genistein, resveratrol, catechin, and curcumin) are suggested for the reversal of adverse epigenetic marks in cancer cells and CSCs to attenuate tumorigenesis progression, prevent metastasis, or sensitize for drug sensitivity [30]. Resveratrol, a natural phytoalexin widely presented in foods and TCMs [18, 19], has multiple biological functions that affect cell growth, anti-inflammation, apoptosis, angiogenesis, and metastasis [31]. Herbal medicines with resveratrol-containing, such as *Rheum officinale* Baill. and *Polygonum cuspidatum*, have been widely used in TCM for eliminating inflammatory response and reducing tumor growth [32, 33]. It was suggested that these TCMs may have certain capacity to regulate tumor microenvironment and inhibit CSC characteristics. An article reported that treatment of resveratrol effectively inhibited the cancer stem-like cell properties and radioresistance of $CD133^{+}$-glioblastoma multiforme (GBM) cells [34]. Resveratrol inhibits pancreatic CSC characteristics in human and Kras(G12D) transgenic mice by inhibiting pluripotency maintaining factors and epithelial-mesenchymal transition [35]. In this study, resveratrol decreased the cell viability that augmented by CSC-related factor IL-6 and decreased the expression of CSC-specific Shh signaling in IL-6-treated HL-60 cells. Like Shh inhibitor cyclopamine, resveratrol significantly prohibited the Gli-1 expression and nucleic translocation in IL-6-stimulated HL-60 cells. Similar researches of resveratrol on CSC effect also reported that resveratrol and several dietary compounds that possess potential effect against CSCs through the regulation of self-renewal pathways, including Wnt/β-catenin, Hh, and Notch pathways [36, 37]. Therefore, it was suggested that resveratrol might have potential inhibitory properties of CSC-related IL-6 and Shh molecule expression in AML cells.

5. Conclusions

The present study is the first to discover that AML patients were associated with elevated expression of CSC-related IL-6 and Shh molecules in marrow and/or blood compared with the control donors. We found in subsequent experiments that IL-6 stimulated downstream Shh/Gli-1 signaling and caused an increase in cell viability in AML cells. The TCM component resveratrol, like the Shh inhibitor cyclopamine, effectively prohibited the IL-6-mediated cell growth and Shh signaling in AML. The increased production of IL-6 in patients with AML may stimulate the Shh signaling pathway and increase the risk of unfavorable prognosis, implying that further investigation of new drugs (such as resveratrol) targeted to block Shh may prove to be beneficial for patients with AML.

Conflict of Interests

The authors declare that they have no conflict of interests.

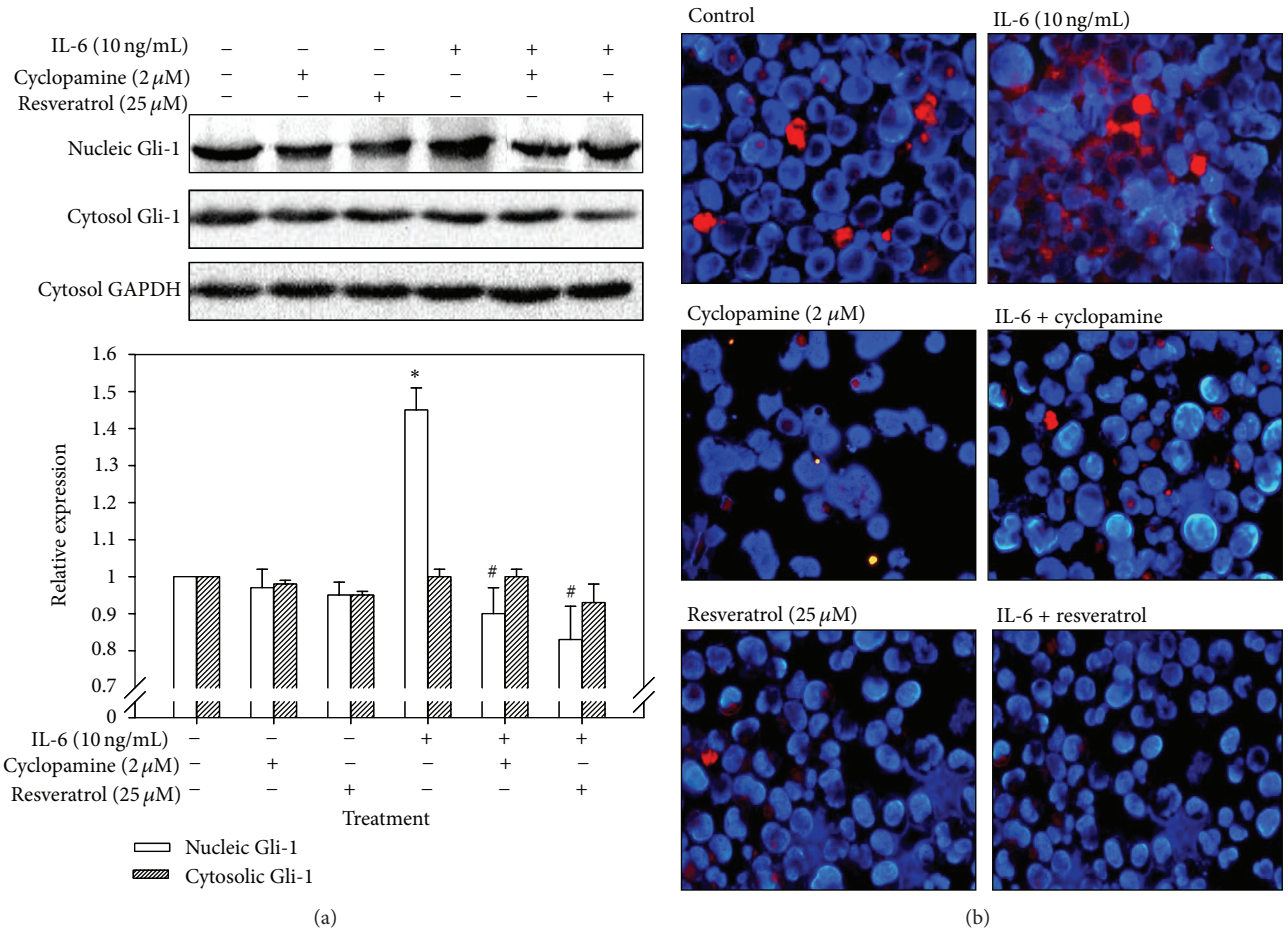

FIGURE 5: Effect of cyclopamine and resveratrol on Gli-1 nuclear translocation in HL-60 cells with or without IL-6 treatment. (a) Expression of nucleic and cytosolic Gli-1 using a Western blot analysis. The relative values were normalized to the internal control, were calculated from three independent experiments, and were expressed as mean ± SE. (b) Immunofluorescence staining of Gli-1. These cells were double stained with PE-conjugated anti-Gli-1 antibody (red) and Hoechst 33342 fluorescence dye (blue, nucleus). $^{*}P < 0.05$ as compared to the control group. $^{\#}P < 0.05$ as compared to the IL-6 alone group.

Acknowledgments

This human subject research was approved by the IRB of Buddhist Dalin Tzu Chi General Hospital, Taiwan (no. B09703022). The authors thank Miss Ya-Ting Tung and Chia-Yun Lee for blood sample collection. This study was supported by Grants NSC 99-2313-B-415-002-MY3 and NSC 101-2321-B-415-001 from the National Science Council of the Republic of China, Taipei, Taiwan, and Grant DTCRD 98-20 from Buddhist Dalin Tzu Chi General Hospital, Chiayi, Taiwan. This paper has been edited by a native English speaker prior to submission. Proofreading certificate is available upon request.

References

[1] B. J. P. Huntly, H. Shigematsu, K. Deguchi et al., "MOZ-TIF2, but not BCR-ABL, confers properties of leukemic stem cells to committed murine hematopoietic progenitors," *Cancer Cell*, vol. 6, no. 6, pp. 587–596, 2004.

[2] C. H. M. Jamieson, L. E. Ailles, S. J. Dylla et al., "Granulocyte-macrophage progenitors as candidate leukemic stem cells in blast-crisis CML," *New England Journal of Medicine*, vol. 351, no. 7, pp. 657–667, 2004.

[3] M. T. Mueller, P. C. Hermann, J. Witthauer et al., "Combined targeted treatment to eliminate tumorigenic cancer stem cells in human pancreatic cancer," *Gastroenterology*, vol. 137, no. 3, pp. 1102–1113, 2009.

[4] C. Tang, B. T. Ang, and S. Pervaiz, "Cancer stem cell: target for anticancer therapy," *The FASEB Journal*, vol. 21, no. 14, pp. 3777–3785, 2007.

[5] D. Bonnet and J. E. Dick, "Human acute myeloid leukemia is organized as a hierarchy that originates from a primitive hematopoietic cell," *Nature Medicine*, vol. 3, no. 7, pp. 730–737, 1997.

[6] J. M. Gerber, B. D. Smith, B. Ngwang et al., "A clinically relevant population of leukemic $CD34^{+}$ $CD38^{-}$ cells in acute myeloid leukemia," *Blood*, vol. 119, no. 15, pp. 3571–3517, 2012.

[7] Y. Chen, C. Peng, C. Sullivan, D. Li, and S. Li, "Critical molecular pathways in cancer stem cells of chronic myeloid leukemia," *Leukemia*, vol. 24, no. 9, pp. 1545–1554, 2010.

[8] J. J. Trowbridge, M. P. Scott, and M. Bhatia, "Hedgehog modulates cell cycle regulators in stem cells to control hematopoietic regeneration," *Proceedings of the National Academy of Sciences of the United States of American*, vol. 103, no. 38, pp. 14134–14139, 2006.

[9] L. A. Crews and C. H. Jamieson, "Selective elimination of leukemia stem cells: hitting a moving target," *Cancer Letters*, 2012.

[10] N. T. Nguyen, D. P. Lin, S. Y. Yen et al., "Sonic hedgehog promotes porcine oocyte maturation and early embryo development," *Reproduction, Fertility, and Development*, vol. 21, no. 6, pp. 805–815, 2009.

[11] C. Zhao, A. Chen, C. H. Hamieson et al., "Hedgehog signalling is essential for maintenance of cancer stem stem cells in myeloid leukaemia," *Nature*, vol. 458, no. 7239, pp. 776–780, 2009.

[12] J. Sims-Mourtada, J. G. Izzo, J. Ajani, and K. S. C. Chao, "Sonic Hedgehog promotes multiple drug resistance by regulation of drug transport," *Oncogene*, vol. 26, no. 38, pp. 5674–5679, 2007.

[13] H. F. Liao, Y. C. Su, Z. Y. Zheng et al., "Sonic hedgehog signaling regulates Bcr-Abl expression in human chronic myeloid leukemia cells," *Biomedicine & Pharmacotherapy*, vol. 66, no. 5, pp. 378–383, 2012.

[14] E. Efstathiou, P. Troncoso, S. Wen et al., "Initial modulation of the tumor microenvironment accounts for thalidomide activity in prostate cancer," *Clinical Cancer Research*, vol. 13, no. 4, pp. 1224–1231, 2007.

[15] N. N. Bewry, R. R. Nair, M. F. Emmons, D. Boulware, J. Pinilla-Ibarz, and L. A. Hazlehurst, "Stat3 contributes to resistance toward BCR-ABL inhibitors in a bone marrow microenvironment model of drug resistance," *Molecular Cancer Therapeutics*, vol. 7, no. 10, pp. 3169–3175, 2008.

[16] M. T. Scupoli, M. Donadelli, F. Cioffi et al., "Bone marrow stromal cells and the upregulation of interleukin-8 production in human T-cell acute lymphoblastic leukemia through the CXCL12/CXCR4 axis and the NF-κB and JNK/AP-1 pathways," *Haematologica*, vol. 93, no. 4, pp. 524–532, 2008.

[17] T. M. Garcia-Bates, S. H. Bernstein, and R. P. Phipps, "Peroxisome proliferator-activated receptor γ overexpression suppresses growth and induces apoptosis in human multiple myeloma cells," *Clinical Cancer Research*, vol. 14, no. 20, pp. 6414–6425, 2008.

[18] S. K. Lee, W. Zhang, and B. J. S. Sanderson, "Selective growth inhibition of human leukemia and human lymphoblastoid cells by resveratrol via cell cycle arrest and apoptosis induction," *Journal of Agricultural and Food Chemistry*, vol. 56, no. 16, pp. 7572–7577, 2008.

[19] B. Y. Chen, C. H. Kuo, Y. C. Liu, L. Y. Ye, J. H. Chen, and C. J. Shieh, "Ultrasonic-assisted extraction of the botanical dietary supplement resveratrol and other constituents of *Polygonum cuspidatum*," *Journal of Natural Products*, vol. 75, no. 10, pp. 1810–1813, 2012.

[20] Z. Cakir, G. Saydam, F. Sahin, and Y. Baran, "The roles of bioactive sphingolipids in resveratrol-induced apoptosis in HL60 acute myeloid leukemia cells," *Journal of Cancer Research and Clinical Oncology*, vol. 137, no. 2, pp. 279–286, 2011.

[21] H. F. Liao, A. J. Cheng, H. T. Huang, M. L. Shen, T. K. Hei, and Y. J. Chen, "Nuclear factor-kappaB as a switch in regulation of resveratrol-mediated apoptosis and erythrocytic differentiation in human leukemia cells," *Food Chemistry*, vol. 132, no. 4, pp. 2094–2101, 2012.

[22] S. H. Kweon, J. H. Song, and T. S. Kim, "Resveratrol-mediated reversal of doxorubicin resistance in acute myeloid leukemia cells via downregulation of MRP1 expression," *Biochemical and Biophysical Research Communications*, vol. 395, no. 1, pp. 104–110, 2010.

[23] G. Lorusso and C. Rüegg, "The tumor microenvironment and its contribution to tumor evolution toward metastasis," *Histochemistry and Cell Biology*, vol. 130, no. 6, pp. 1091–1103, 2008.

[24] Z. Trnková, R. Bedrlíková, J. Marková, K. Michalová, P. Stöckbauer, and J. Schwarz, "Semiquantitative RT-PCR evaluation of the MDR1 gene expression in patients with acute myeloid leukemia," *Neoplasma*, vol. 54, no. 5, pp. 383–390, 2007.

[25] T. R. Randolph, "Acute promyelocytic leukemia (AML-M3)—part 1: pathophysiology, clinical diagnosis, and differentiation therapy," *Clinical Laboratory Science*, vol. 13, no. 2, pp. 98–105, 2000.

[26] M. B. Meads, R. A. Gatenby, and W. S. Dalton, "Environment-mediated drug resistance: a major contributor to minimal residual disease," *Nature Reviews Cancer*, vol. 9, no. 9, pp. 665–674, 2009.

[27] M. Kobune, R. Takimoto, K. Murase et al., "Drug resistance is dramatically restored by hedgehog inhibitors in $CD34^+$ leukemic cells," *Cancer Science*, vol. 100, no. 5, pp. 948–955, 2009.

[28] R. Amin and L. Mishra, "Liver stem cells and TGF-Beta in hepatic carcinogenesis," *Gastrointestinal Cancer Research*, vol. 2, supplement 4, pp. S27–S30, 2008.

[29] M. Katoh, "Dysregulation of stem cell signaling network due to germline mutation, SNP, *Helicobacter pylori* infection, epigenetic change and genetic alteration in gastric cancer," *Cancer Biology and Therapy*, vol. 6, no. 6, pp. 832–839, 2007.

[30] W. Vanden Berghe, "Epigenetic impact of dietary polyphenols in cancer chemoprevention: lifelong remodeling of our epigenomes," *Pharmacological Research*, vol. 65, no. 6, pp. 565–576, 2012.

[31] M. Athar, J. H. Back, L. Kopelovich, D. R. Bickers, and A. L. Kim, "Multiple molecular targets of resveratrol: anti-carcinogenic mechanisms," *Archives of Biochemistry and Biophysics*, vol. 486, no. 2, pp. 95–102, 2009.

[32] X. Chu, M. Wei, X. Yang et al., "Effects of an anthraquinone derivative from Rheum officinale Baill, emodin, on airway responses in a murine model of asthma," *Food and Chemical Toxicology*, vol. 50, no. 7, pp. 2368–2375, 2012.

[33] B. Hu, H. M. An, K. P. Shen, H. Y. Song, and S. Deng, "Polygonum cuspidatum extract induces anoikis in hepatocarcinoma cells associated with generation of reactive oxygen species and downregulation of focal adhesion kinase," *Evidence-Based Complementary and Alternative Medicine*, vol. 2012, Article ID 607675, 9 pages, 2012.

[34] Y. P. Yang, Y. L. Chang, P. I. Huang et al., "Resveratrol suppresses tumorigenicity and enhances radiosensitivity in primary glioblastoma tumor initiating cells by inhibiting the STAT3 axis," *Journal of Cellular Physiology*, vol. 227, no. 3, pp. 976–993, 2012.

[35] Y. Li, M. S. Wicha, S. J. Schwartz, and D. Sun, "Implications of cancer stem cell theory for cancer chemoprevention by natural dietary compounds," *Journal of Nutritional Biochemistry*, vol. 22, no. 9, pp. 799–806, 2011.

[36] S. Shankar, D. Nall, S. N. Tang et al., "Resveratrol inhibits pancreatic cancer stem cell characteristics in human and KrasG12D transgenic mice by inhibiting pluripotency maintaining factors and epithelial-mesenchymal transition," *PLoS ONE*, vol. 6, no. 1, Article ID e16530, 2011.

[37] F. H. Sarkar, Y. Li, Z. Wang, and D. Kong, "The role of nutraceuticals in the regulation of Wnt and Hedgehog signaling in cancer," *Cancer and Metastasis Reviews*, vol. 29, no. 3, pp. 383–394, 2010.

Hindawi Publishing Corporation
Evidence-Based Complementary and Alternative Medicine
Volume 2012, Article ID 908601, 12 pages
doi:10.1155/2012/908601

Research Article

Herbal Compound "Songyou Yin" Renders Hepatocellular Carcinoma Sensitive to Oxaliplatin through Inhibition of Stemness

Qing-An Jia,[1] Zheng-Gang Ren,[1] Yang Bu,[1,2] Zhi-Ming Wang,[1] Qiang-Bo Zhang,[1] Lei Liang,[1] Xue-Mei Jiang,[1] Quan-Bao Zhang,[1] and Zhao-You Tang[1]

[1] *Liver Cancer Institute, Zhongshan Hospital, Fudan University and Key Laboratory of Carcinogenesis and Cancer Invasion, Ministry of Education, 180 Fenglin Road, Shanghai 200032, China*
[2] *Institutes of Biomedical Sciences, Fudan University, Shanghai 200032, China*

Correspondence should be addressed to Zhao-You Tang, zytang88@163.com

Received 12 October 2012; Accepted 12 November 2012

Academic Editor: Hui-Fen Liao

We investigated the effect of Chinese herbal compound Song-you Yin on HCC stemness. MHCC97H and Hep3B cell lines were pretreated with SYY for 4 weeks, and their chemosensitivity to oxaliplatin was evaluated. The expression of CSC-related markers, cell invasion and migration, and colony formation were also examined. SYY-treated orthotopic nude mouse models of human HCC were developed to explore the effect of oxaliplatin on tumor growth, metastasis, and survival. The CSC-related molecular changes *in vivo* were also evaluated. The result showed that MHCC97H and Hep3B cells pretreated with SYY showed significantly increased chemosensitivity to oxaliplatin and the downregulation of CSC-related markers CD90, CD24, and EPCAM. SYY also attenuated cell motility, invasion, and colony formation in MHCC97H and Hep3B cell lines. The reduced tumorigenicity and pulmonary metastasis were observed in SYY-pretreated cell lines. Combination treatment with oxaliplatin and SYY significantly reduced tumor volume and pulmonary metastasis and prolonged survival compared with oxaliplatin treatment alone. Immunohistochemical analysis showed reduced expression of CD90, ABCG2, ALDH, CD44, EPCAM, vimentin, and MMP-9 and increased the expression of E-cadherin, in HCC cells following combination treatment. These data clearly demonstrate that SYY renders hepatocellular carcinoma sensitive to oxaliplatin through the inhibition of stemness.

1. Introduction

Liver cancer, most commonly hepatocellular carcinoma (HCC), is the fifth most frequently diagnosed cancer in men worldwide, but the second most frequent cause of cancer death [1]. In clinical practice, fewer than 30% of patients with HCC have the chance to be treated with curative options such as liver transplantation, surgical resection, and ablation therapy because HCC is typically confirmed at an advanced stage at diagnosis [2]. As a result, transcatheter hepatic arterial chemoembolization (TACE) and systemic chemotherapy are frequently used [3, 4] although unfortunately the overall response rate to such treatments is poor [5, 6].

Recently, biological deterioration of tumor cells after chemotherapy has been reported. *In vitro* exposure to chemotherapeutic agents enhanced metastatic potential in colorectal, pancreatic, breast, and ovarian carcinoma cells [7–10]. Yamauchi et al. similarly reported the so-called "opposite effect," an increased metastatic ability in cyclophosphamide-pretreated fibrosarcoma cells [11]. Recent evidence suggests that a certain type of HCC is hierarchically organized by a wide variety of cancer cells including a subset of cells with stem cell features [12–15]. These cancer stem cells (CSCs) are resistant to conventional chemotherapy due to cellular characteristics such as high expression of drug transporters, relative cell cycle quiescence, high levels of DNA repair, and resistance to apoptosis [16, 17]. Costello et al. found that $CD34^+CD38^-$ CSCs in AML patients exhibited decreased daunorubicin sensitivity compared with $CD34^+CD38^+$ cells, which correlated with high expression levels of the drug resistance-related genes *LRP* and *MRP* [18]. Similarly, Liu et al. reported that $CD133^+$ glioblastoma

cells exhibited less cell death than their $CD133^-$ counterparts when treated with multiple chemotherapeutic agents as a result of overexpression of genes that inhibit apoptosis, including *FLIP*, *Bcl-2*, and *Bcl-XL* [19]. The emergence of the CSC theory provides insight into why treatment of tumors with chemotherapy often appears to show an initial response but ultimately results in treatment failure.

Our previous study demonstrated that Songyou Yin (SYY, a traditional Chinese medicine containing five herbal compounds) inhibits molecular changes consistent with the epithelial-mesenchymal transition (EMT) in oxaliplatin-treated tumor tissues and cell lines [20]. There is accumulating evidence that the EMT and CSCs form a coalition against cancer therapy [21–24]. Thus, the objective of this study was to investigate whether SYY directly downregulates the proportion of CSCs and inhibits stemness of HCC cells in tumor tissues and HCC cell lines, thus resulting in the sensitization of HCC to oxaliplatin. To date, there is no apparent consensus on the best marker by which to identify CSCs in any particular cancer. Widely used CSC-related markers include CD133, CD90, CD44, CD24, OV6, EPCAM, and staining of side population cells by Hoechst dye [25]. However, defined expression patterns of CSC markers in specific cell lines remain controversial. To select suitable cell lines to explore the effect of SYY on HCC, we first examined the expression of CSC-related markers in a variety of HCC cell lines with high and low metastatic potential. We next investigated changes in CSC proportion and stemness characteristics such as invasion, motility, colony formation, tumorigenesis, and pulmonary metastasis in SYY-treated cell lines and evaluated their changes in chemosensitivity which were also reconfirmed *in vivo*.

2. Materials and Methods

2.1. Cell Lines and Animals. The human HCC cell lines with high metastatic potential used in this study were MHCC97H and HCCLM3, which originated from MHCC97 and were established in the authors' institution [26, 27]. The human HCC cell lines with low metastatic potential were SMMC-7721 (established at second military medical university) and Huh7, Hep3B, and HepG2 (obtained from American Type Culture Collection). MHCC97H and Hep3B cells cultured with 2 mg/mL SYY for 4 weeks were termed MHCC97H-SYY and Hep3B-SYY, respectively. The MHCC97H-RFP (red fluorescent protein) cell line established in the authors' institute [28] was also cultured with 2 mg/mL SYY (MHCC97H-RFP-SYY). Male BALB/c nu/nu mice (aged 4–6 weeks and weighing approximately 20 g) were obtained from the Chinese Academy of Science and maintained under standard pathogen-free conditions. The experimental protocol was approved by the Shanghai Medical Experimental Animal Care Commission.

2.2. Regents and Antibodies. Oxaliplatin was purchased from Sigma Chemical Co. Monoclonal antibodies used in flow cytometric analysis were mouse anti-human monoclonal antibodies CD90-PE, EPCAM-APC, CD24-FITC, CD133-APC, CD44-PE, IgG-PE isotype, IgG-APC isotype, and IgG-FITC isotype (all purchased from Miltenyi Biotec). Antibodies used for immunofluorescence, immunoblotting and/or, immunohistochemistry were as follows: mouse anti-human monoclonal CD90 (Abcam), rabbit anti-human polyclonal CD133 (Abnova), mouse anti-human monoclonal EPCAM (Millipore), mouse anti-human monoclonal CD44 (Cell Signaling Technologies), rabbit anti-human polyclonal CD24 (Epitomics), mouse anti-human monoclonal MMP-9 (Abcam), mouse anti-human monoclonal E-cadherin (Abcam), mouse anti-human monoclonal Vimentin (Abcam), mouse anti-human monoclonal actin (Beyotime), mouse anti-human monoclonal ABCG2(Millipore), and rabbit anti-human monoclonal ALDH1(ABGENT).

2.3. Characterization and Preparation of Herbal Extracts. The Chinese herbal medicine formula SYY, a dietary component authorized by the Chinese State Food and Drug Administration (Grant no. G20070160), includes five Chinese medicinal herbal extracts whose proportions, fingerprint, and protocol of preparation have previously been reported [29]. The SYY used *in vitro* and *in vivo* in this study was from the same batch number 20110401 and was produced by Shanghai Fang Xin Pharmaceutical Technology Co., Ltd. Shanghai, China. A 800 mg/mL solution of SYY was sterilized twice by 0.22-μm filtration (Millipore) for further use *in vitro*.

2.4. LDH Cytotoxicity Assay. The cytotoxicity detection kit^{plus} (Roche) is a precise and fast colorimetric assay for the quantitative determination of cytotoxicity by measuring release of lactate dehydrogenase (LDH) activity from damaged cells. MHCC97H cells were cultured to 80% confluence. After trypsin digestion, the cells were counted and pipetted into 96-well plates at a density of 2000 cells/well. Background control (medium only), low controls (spontaneous LDH release), high controls (maximum LDH release), and experimental substance (2 mg/mL and 4 mg/mL SYY) were prepared on the same plate according to the manufacturer's instructions. The 96-well plates were incubated in a humidified incubator at 37°C in 5% CO_2 for 4, 8, 12, 24, 48, and 72 h. Results were expressed as the absorbance of each well at 492 nm (OD492). Cytotoxicity (%) was calculated using the equation: (experimental value − low control)/(high control − low control) × 100%.

2.5. Flow Cytometric Analysis. The expression level of CSC-related markers was determined by flow cytometry. Briefly, MHCC97H, HCCLM3, SMMC-7721, Hep3B, Huh7, and HepG2 cells were grown to 80% confluence. After trypsin digestion, the cells were resuspended in medium at a concentration of 1×10^6 cells/mL and incubated with primary antibodies against CD90, CD133, CD24, EPCAM, and CD44 (diluted 1 : 11) at 4°C for 15 min. After washing three times with PBS, the cells were analyzed using a FACSC Flow Cytometer (BD Biosciences). The biomarkers CD90/EPCAM in MHCC97H-SYY and CD24/EPCAM in Hep3B-SYY were also examined for comparison with their parental cell lines.

2.6. Immunofluorescence and Western Blot Analysis. The expression of CSC-related markers was also determined by immunofluorescence. Cells were grown on glass cover slips to 40%–50% confluence and then fixed, permeabilized, blocked, and incubated with primary monoclonal antibodies overnight at 4°C. Slides were washed and incubated with anti-mouse or anti-rabbit Cy3-conjugated secondary antibody (Jackson). Cells were counterstained with 4′-6-diamidino-2-phenylindole to visualize cell nuclei and detected by fluorescence microscopy (Olympus).

Western blot analysis of protein expression of CD90, CD24, EPCAM, E-cadherin, and vimentin in MHCC97H-SYY, Hep3B-SYY, and their parental cell lines was performed according to the manufacturer's instructions. The concentration of protein extracted from MHCC97H-SYY, Hep3B-SYY, and parental cell lines was determined using the BCA Protein Assay Kit (Beyotime).

2.7. Quantitative Real-Time PCR Analysis. Total RNA was extracted from MHCC97H-SYY, Hep3B-SYY, and their parental cell lines using Trizol Reagent (Invitrogen). Total RNA was reversely transcribed using a Prime Script RT reagents kit (TaKaRa). Messenger RNA expression was determined by real-time PCR using SYBR Premix Ex Taq II (TaKaRa). The primers used for the amplification of human genes were as follows: CD90 forward primer 5′-CAGCATTCTCAGCCACAA C-3′ and reverse primer 5′-TTACCTCCT TCTCCAACCCT-3′; CD24 forward primer 5′-TCGGGTGTGCTATGGATG-3′ and reverse primer 5′-AGA GGG GGTCTGTTGAAG AT-3′; EPCAM forward primer 5′-CAGTGTACTTCAGTTGGTG-3′ and reverse primer 5′-TCAGGTTTTGCTCTTC TC-3′.

2.8. Cell Migration and Invasion Assays. Cell migration and invasion of MHCC97H and Hep3B cell lines were assessed by transwell assays (Boyden chambers; Corning). Briefly, 6×10^4 cells in serum-free Dulbecco's modified Eagle medium (DMEM) were seeded into the upper chamber of each well of 24-well plates containing 8.0-μm pore size membranes. DMEM containing 10% fetal bovine serum (FBS) was added to the lower chamber of each well. After 48 h, cells that had reached the underside of the membrane were stained with Giemsa (Sigma), counted at ×100, and photographed at ×200 magnification. The cell invasion assay was carried out similarly, except that 80 μL matrigel (BD Biosciences) was added to each well 6 h before cells were seeded on the membrane.

2.9. Cell Proliferation and Colony Formation Assay. MHCC97H and Hep3B cell lines were pretreated with SYY for 4 weeks and then plated in 96-well plates (3×10^3 cells/well) and exposed to oxaliplatin at increasing concentrations for 24, 48, 72, and 96 h. Cell proliferation assays were carried out with the Cell Counting Kit 8 (CCK8; Dojindo). Results were expressed as the absorbance of each well at 450 nm (OD450).

For colony formation assays, 1×10^3 cells were plated in 6-well plates (Corning) and cultured with 1% FBS DMEM with or without SYY (2 mg/mL). Culture medium was replaced every 3 days, and the colonies were fixed with ice-cold 4% paraformaldehyde 14 days after the initiation of treatment. Cells were stained with Giemsa (Sigma) and photographed at ×5 magnification.

2.10. Animal Model and Treatment Procedures. Twenty-four nude mice bearing orthotopic xenografts were randomly divided into control group, SYY group, oxaliplatin+SYY group, and oxaliplatin only group. Seven days after orthotopic implantation the mice were treated as follows: SYY group mice were treated intraperitoneally (i.p.) with 0.1 mL 5% glucose solution (GS) once a week and orally with SYY (4 g/kg/d) every day; control group mice were treated with 5% GS and distilled water in the same way as the SYY group; oxaliplatin group mice were treated with oxaliplatin (10 mg/kg) i.p. and 0.1 mL distilled water orally; oxaliplatin+SYY group mice were treated with 0.1 mL oxaliplatin (10 mg/kg) i.p. and 0.1 mL SYY (4 g/kg/d) orally. Tumor weight and lung metastasis were evaluated 4 weeks after the initiation of treatment. Using another 12 nude mice bearing orthotopic xenografts, survival time of an oxaliplatin+SYY group and oxaliplatin only group was determined as the interval between the day of inoculation and the day of death.

To evaluate the growth and metastasis potential of SYY-treated HCC cells *in vivo*, another 24 male BALB/c nu/nu mice were divided into four groups. Group I mice were subcutaneously injected with 5×10^6 MHCC97H-SYY cells and group II mice were injected with the same number of MHCC97H cells. Tumor weight was measured 4 weeks after injection. Group III mice were injected with 1×10^5 MHCC97H-RFP-SYY cells through the tail vein, and group IV mice were injected with the same number of MHCC97H-RFP cells. Six weeks later, lung metastases were evaluated by fluorescence microscopy and confirmed by microscopic examination of serial sections of every lung tissue block.

2.11. Immunohistochemistry. Tumor tissue was fixed, embedded, and sliced into 5 μm thick sections. Immunohistochemical staining of CD90, ABCG2, ALDH, CD44, EPCAM, E-cadherin, vimentin, and MMP-9 was carried out using a standard protocol [30].

2.12. Statistical Analysis. *In vitro* LDH cytotoxicity assay data, the proportion of CSC cells, cell migration, invasion, and proliferation assays were compared by Student's *t*-test. Tumor weight was compared by analysis of variance (ANOVA), the lung metastasis assay was analyzed using Fisher's exact test, and survival was compared with Kaplan-Meier method with a log-rank test. Statistical analysis was performed with SPSS 15.0 for Windows (SPSS Inc. Chicago, IL, USA). $P < 0.05$ was considered statistically significant.

3. Results

3.1. Expression of CSC-Related Markers in HCC Cell Lines. The expression of CSC-related markers in the cell lines HCCLM3, MHCC97H, HepG2, SMMC7721, Hep3B, and

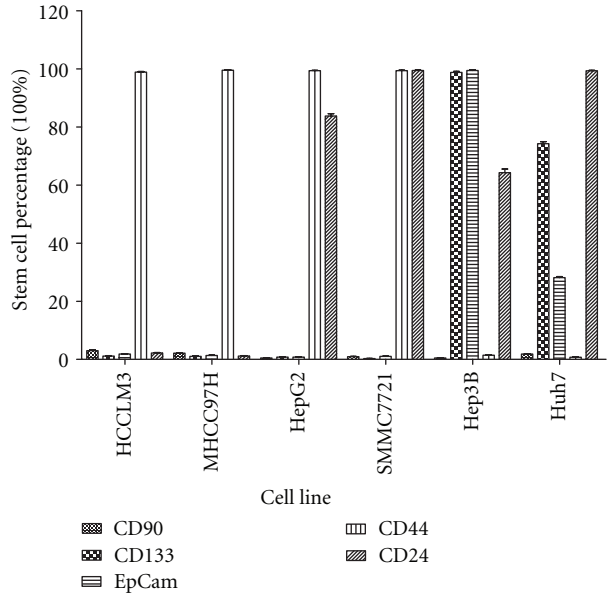

Figure 1: The expression of the CSC-related markers in HCCLM3, MHCC97H, HepG2, SMMC7721, Hep3B and Huh7 HCC cell cultures.

Huh7 was examined by flow cytometry and immunofluorescence (Additional file 1 (see Supplementary Material available online at doi:10.1155/2012/908601)). The proportion of CSCs in each cell line is presented in Figure 1. The expression of CD90/EpCAM in MHCC97H was 2.13 ± 0.37% and 1.35 ± 0.24%. The expression of CD24/EpCAM in Hep3B was 99.48 ± 3.87% and 64.30 ± 3.09%, all of which were consistent with reports in the literature. Moreover, these CSC-related markers were previously used to study CSCs [12–14]. Therefore, MHCC97H and Hep3B were selected for further study.

3.2. SYY Exhibited No Significant Cytotoxicity in HCC Cell Lines but Increased Their Sensitivity to Oxaliplatin. MHCC97H cells that were treated with SYY (2 mg/mL and 4 mg/mL) for 4, 8, 12, 24, 48, and 72 h demonstrated no significant increase in release of lactate dehydrogenase (LDH) compared with the control group. When LDH release of the control group was set at 100%, the relative emission of LDH at 4, 8, 12, 24, 48, and 72 h was 98.91 ± 3.09%, 97.84 ± 2.17%, 96.50 ± 4.72%, 98.75 ± 3.00%, 101.58 ± 3.86%, and 101.75 ± 4.81% in cells treated with 2 mg/mL SYY and 98.84 ± 3.19%, 99.00 ± 2.43%, 99.58 ± 2.72%, 101.58 ± 3.86%, 101.75 ± 4.81%, and 100.41 ± 3.47% in cells treated with 4 mg/mL SYY. There was no statistically significant difference between the control and experimental groups (Figure 2(a)), indicating that SYY did not exhibit acute cytotoxicity to MHCC97H cells.

The IC_{50} of oxaliplatin was lower in SYY-treated MHCC97H cells (MHCC97H-SYY) and Hep3B cells (Hep3B-SYY) compared with the corresponding parental cell lines MHCC97H and Hep3B. The CCK8 assay showed that the IC_{50} of oxaliplatin in Hep3B-SYY was 0.41 ± 0.16 μmol/L, compared with 1.38 ± 0.28 μmol/L for Hep3B ($P = 0.0376$). The IC_{50} of oxaliplatin against MHCC97H-SYY was also lower than that for MHCC97H (12.15 ± 1.64 μmol/L versus 28.93 ± 2.18 μmol/L; $P = 0.0011$; Figure 2(b)).

3.3. SYY Reduced Expression of CSC-Related Markers and Inhibited the Stemness of HCC Cell Lines. We further explored the underlying mechanism of the chemosensitization to oxaliplatin by SYY and found that the expression of the CSC-related marker CD90 in MHCC97H and MHCC97H-SYY cells was 1.83% ± 0.42% and 0.61% ± 0.19% ($P < 0.01$), respectively, and the expression of EpCAM was 1.37% ± 0.35% and 0.50% ± 0.19% ($P < 0.01$), respectively. Similarly, the expression of CD24 in Hep3B and Hep3B-SYY was 62.74% ± 4.45% and 7.75% ± 2.00% ($P < 0.01$), respectively, and the expression of EPCAM was 99.28% ± 0.50% and 92.71% ± 2.30% ($P < 0.01$), respectively (Figure 3(a), Additional file 2). Reverse transcription-polymerase chain reaction (RT-PCR) and Western blot analyses gave similar results, confirming the downregulation of CSC-related markers in SYY-treated cells. The upregulation of E-cadherin and the downregulation of vimentin were also observed in SYY-treated cell lines (Figure 3(b)).

The transwell assay for cell migration and invasiveness demonstrated that MHCC97H-SYY and Hep3B-SYY cells passed through the basement membrane less efficiently than the parental cell lines MHCC97H and Hep3B ($P < 0.01$). The number of cells crossing the basement membrane was lower in MHCC97H-SYY than in MHCC97H in both the cell migration assay (149.50 ± 18.13 versus 44.36 ± 8.15; $P = 0.0005$) and invasion assay (127.83 ± 18.01 versus 38.66 ± 5.57; $P = 0.002$). Similarly, the passage of Hep3B-SYY cells through the basement membrane was lower than that of Hep3B for cell migration (95.66.50 ± 14.12 versus 48.02 ± 25.51; $P = 0.0083$) and invasion (88.33 ± 7.74 versus 41.51 ± 5.57; $P = 0.0001$) (Figure 3(c), Additional file 3).

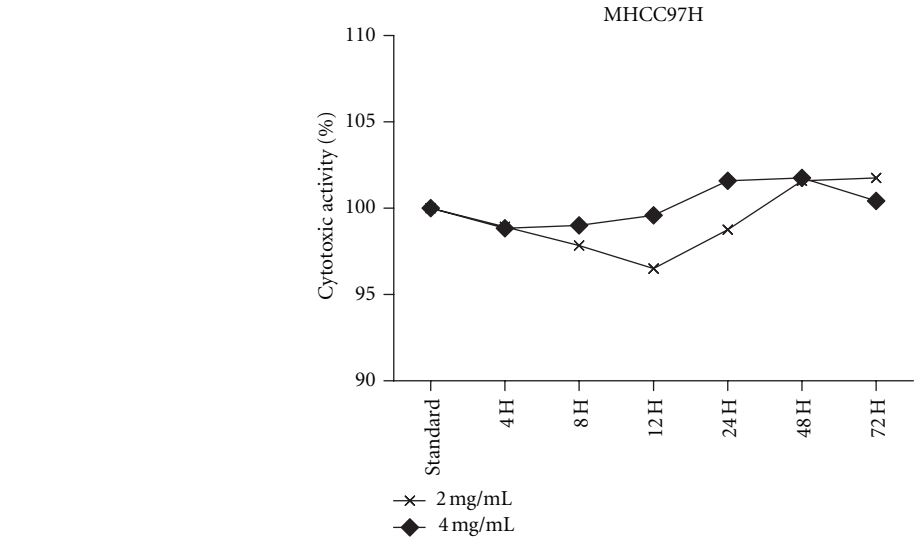

(a)

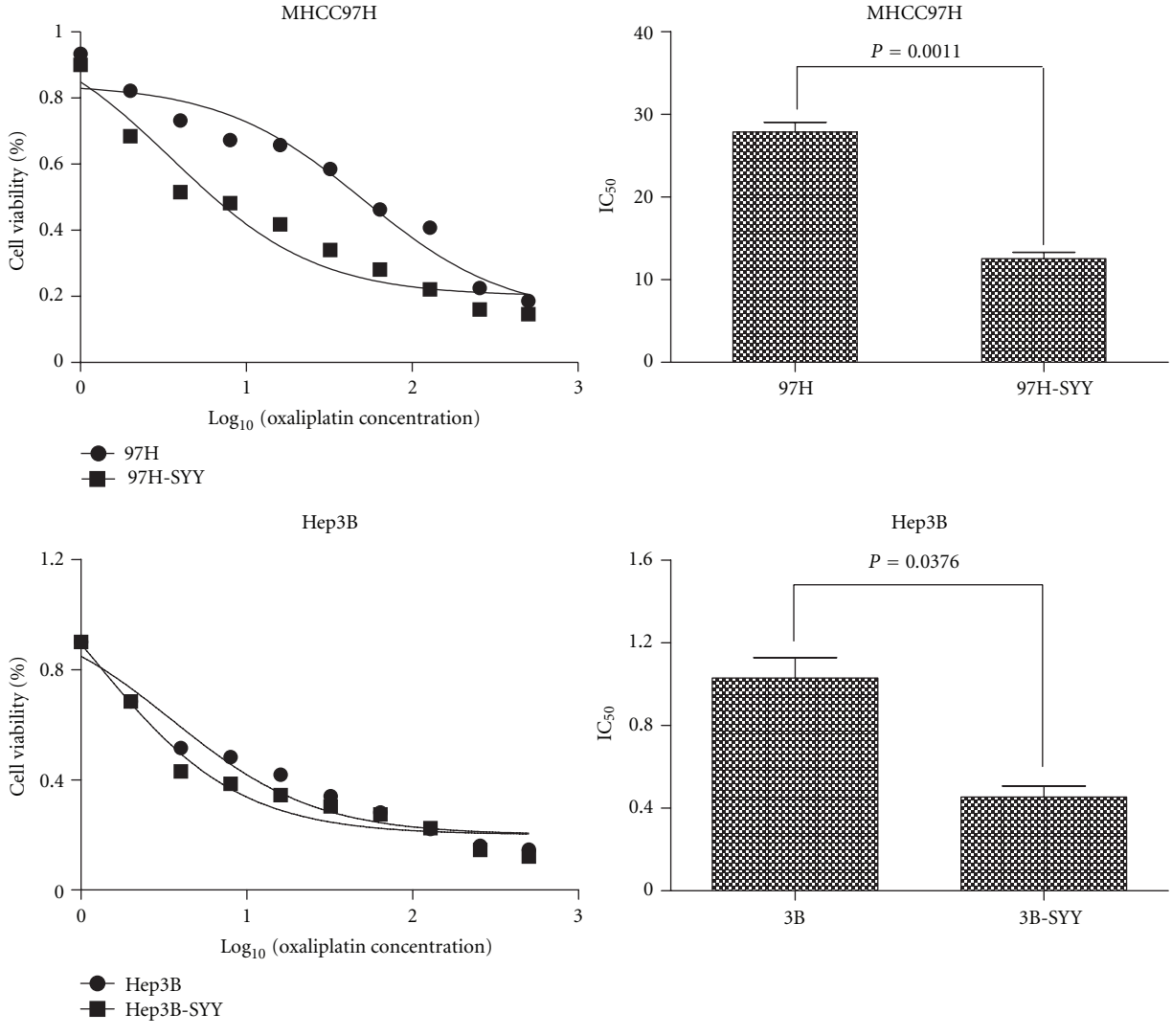

(b)

Figure 2: SYY exhibited no significant cytotoxicity in HCC cell lines but increased their sensitivity to oxaliplatin: (a) MHCC97H cells treated with 2 mg/mL and 4 mg/mL SYY demonstrated no increase in LDH release indicating no acute cytotoxicity and (b) MHCC97H and Hep3B cell lines treated with 2 mg/mL SYY for 4 weeks showed increased chemosensitivity to oxaliplatin compared with parental cell lines.

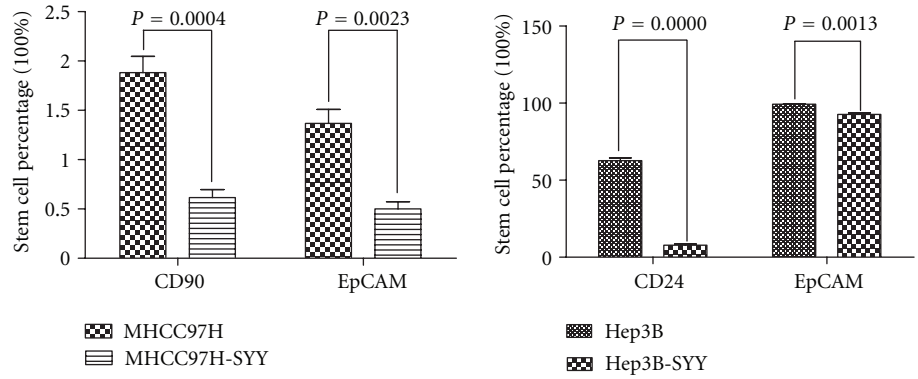

(a)

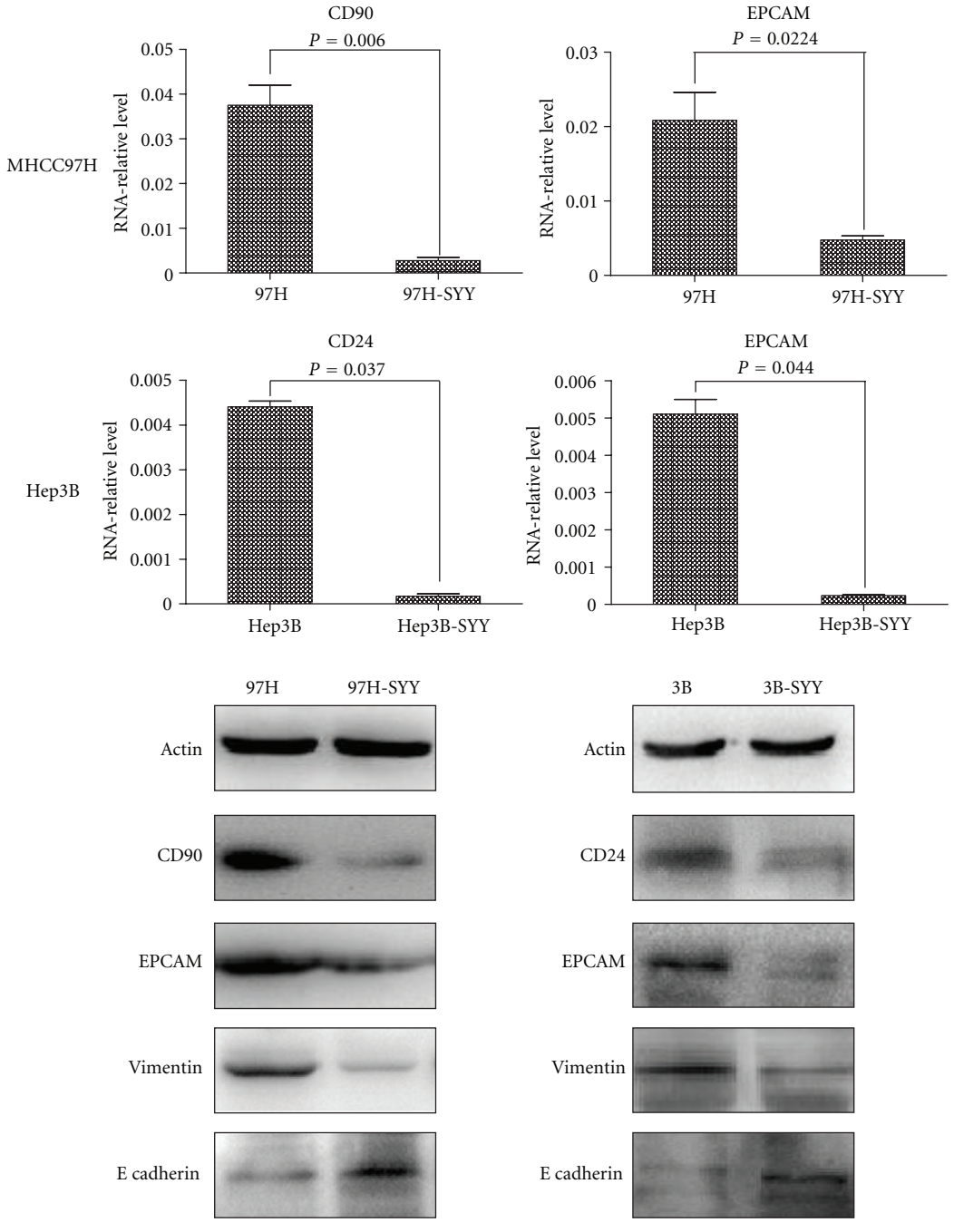

(b)

Figure 3: Continued.

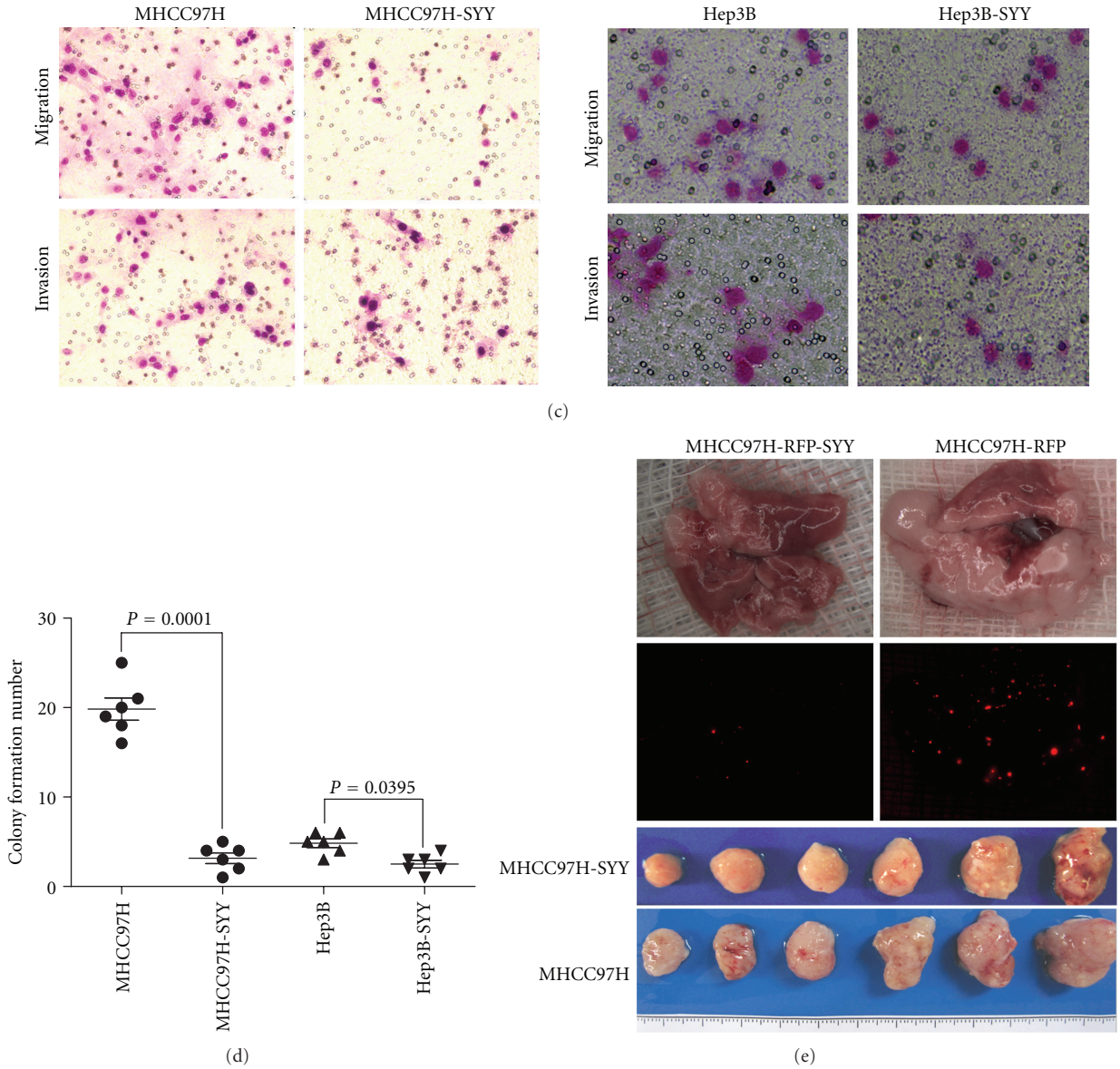

Figure 3: Hepatoma cell lines MHCC97H and Hep3B treated with SYY (2 mg/mL) for 4 weeks exhibited decreased stemness. (a) Tumor cells that were treated with SYY for 4 weeks showed reduced expression of CSC-related markers compared with their parental cell lines by flow cytometry. (b) RT-PCR and Western blot analyses confirmed the decreased expression of CSC-related markers in SYY-treated cell lines. (c) The transwell assay demonstrated that MHCC97H-SYY and Hep3B-SYY cells migrated through the basement membrane less efficiently than the parental cell lines MHCC97H and Hep3B. (d) Colony formation assay demonstrated that MHCC97H-SYY and Hep3B-SYY had a significantly lower proliferation rate and colony-forming ability than untreated parental cells. (e) MHCC97H-SYY cell lines also showed diminished subcutaneous tumor growth capacity and pulmonary metastasis compared with parental cells in nude mouse models.

In colony formation assays, MHCC97H-SYY and Hep3B-SYY exhibited a significantly lower proliferation rate and colony-forming ability than their parental cells. The number of colonies formed was lower in MHCC97H-SYY than in the parental cells (19.83 ± 3.43 versus 4.67 ± 1.63; $P < 0.001$) and in Hep3B-SYY compared with Hep3B (3.85 ± 1.43 versus 3.13 ± 1.03; $P = 0.0395$; Figure 3(d), Additional file 4).

MHCC97H-SYY cell lines also showed diminished subcutaneous tumor growth capacity compared with parental cells in nude mouse models. Four weeks after implantation, the tumor weight was 2.46 ± 0.59 g and 1.89 ± 0.86 g in MHCC97H and MHCC97H-SYY groups, respectively, ($P = 0.0038$). Six weeks after tail vein injection, the mean number of lung metastatic nodules in the MHCC97H-RFP group and MHCC97H-RFP-SYY group was 13.66 ± 6.35 and 4.83 ± 4.87, respectively, ($P = 0.048$; Figure 3(e), Additional file 5).

3.4. Oxaliplatin and SYY Combination Treatment Resulted in Enhanced Inhibition of Tumor Growth and Reduced Pulmonary Metastasis. First, we evaluated the effect of SYY alone on tumor growth and pulmonary metastasis in nude mice using MHCC97H-RFP cells. Treatment with a low

dose of SYY (2 g/kg) did not significantly inhibit tumor growth (2.31 ± 1.15 g versus 2.40 ± 1.21 g; $P > 0.05$) or the number of pulmonary metastasis nodules (15.00 ± 8.41 versus 25.83 ± 5.25 $P = 0.0526$) compared with the control group. Similarly, a medium dose of SYY (4 g/kg) did not decrease tumor growth (2.22 ± 0.31 g versus 2.40 ± 1.21 g; $P > 0.05$) although there was a significant decrease in the number of pulmonary metastasis nodules compared with the control group (7.00 ± 6.71 versus 25.83 ± 5.25; $P = 0.0009$). However, treatment with the high dose of SYY (8 g/kg) significantly inhibited tumor growth (1.32 ± 0.64 g versus 2.40 ± 1.21 g; $P = 0.0466$) and the number of pulmonary metastasis nodules (0.67 ± 1.63 versus 25.83 ± 5.25; $P < 0.0001$) compared with the control group (Figure 4(a)).

SYY (4 g/kg) enhanced the antitumor effect of oxaliplatin. The tumor weight was lower in the SYY+OXA group than in the OXA alone group (0.83 ± 0.20 g versus 1.92 ± 0.79 g; $P = 0.0069$), and a lower number of pulmonary metastasis nodules were observed compared with oxaliplatin treatment alone (22.34 ± 9.06 versus 44.50 ± 7.34; $P = 0.0143$). Combination treatment with oxaliplatin and SYY also prolonged survival compared with oxaliplatin treatment alone (58.17 ± 9.22 days versus 46.33 ± 5.96 days; $P = 0.0005$; Figure 4(b)).

3.5. Combination Treatment with Oxaliplatin and SYY Showed Decreased the Expression of CSC-Related Markers and Reversed EMT. To investigate the role of SYY in modulating the proportion of CSCs *in vivo*, we examined tumor tissues by immunohistochemistry and observed a decreased proportion of ABCG2-, CD44-, ALDH1-, EpCAM-, and CD90-positive CSCs after cotreatment with SYY and oxaliplatin compared with oxaliplatin treatment alone. A significant decrease in the expression of matrix metalloproteinase 9 (MMP-9), which is involved in the breakdown of extracellular matrix during tumor metastasis, was also observed after cotreatment with oxaliplatin and SYY. In addition, the typical membranous E-cadherin expression was significantly upregulated in tumors treated with SYY and oxaliplatin (Figure 5).

4. Discussion

For HCC patients with advanced stage disease, TACE and systemic chemotherapy are usually the treatment of choice. However, these therapies often transiently shrink tumors by targeting the tumor bulk but fail to kill CSCs, leading to eventual treatment failure and tumor relapse. In the present study, we found that the Chinese herbal medicine SYY renders HCC cells sensitive to oxaliplatin. CSCs possess certain characteristics that make them difficult to kill: they have the property of self-protection through increased activity of multiple drug resistance transporters such as ABCB1 and/or ABCG2 [31–33]; they divide much more slowly than other cells, allowing them to evade traditional chemotherapies that hit rapidly multiplying cells [34], and they overexpress antiapoptotic proteins such as BCL-2 and survivin and have a high capacity for DNA repair, leading to resistance to apoptosis and anticancer drugs [35, 36]. The discovery of CSCs not only explained why treatment with chemotherapy often seems to be initially successful but ultimately fails to eradicate the tumor, but also had a profound impact on our current perception of cancer diagnosis, management, and treatment options [37].

The most critical issue in the field of CSCs is to develop phenotypic assays that can be used to reliably identify CSCs [38]. Currently, the most widely used method to identify these cells is through their expression of markers such as CD133, CD90, CD24, CD44, OV6, and EpCAM and through staining of side population cells by Hoechst dye [25]. However the identification of specific CSC markers in a defined cell line remains controversial. In the current study, the expression of CD90/EpCAM in MHCC97H cells and CD24/EpCAM in Hep3B cells was consistent with reports in the literature and their previous use as CSC-related markers to study hepatoma CSCs [12–14]. MHCC97H and Hep3B cells that were pretreated with SYY (2 mg/mL) for 4 weeks showed increased sensitivity to chemotherapy compared with their parental cell lines. One of the typical feature of CSCs is resistance to chemotherapy [39]. In the present study, we found that the expression of CSC-related markers in MHCC97H-SYY (CD90/EpCAM) and Hep3B-SYY (CD24/EpCAM) cells was significantly lower than in their parental cell lines.

Traits such as invasiveness, motility, colony-forming ability, tumorigenicity, and lung metastasis have been attributed to the existence of CSCs and are considered characteristics associated with the stemness of cancer [40]. Therefore, we explored changes in the stemness characteristics of SYY-treated cell lines and tissues that reflect changes in CSCs. SYY-treated MHCC97H-SYY and Hep3B-SYY cells showed lower motility, invasiveness, and colony-forming ability *in vitro*. We injected the tail vein of BALB/c nu/nu mice with MHCC97H-RFP-SYY cells and found a reduced incidence of lung metastasis compared with mice injected with MHCC97H. In the nude mice models, MHCC97H-SYY also showed diminished subcutaneous tumor growth capacity compared with the parental cells. Cotreatment of nude mice with oxaliplatin and SYY resulted in smaller tumor volume and a lower percentage of pulmonary metastasis than oxaliplatin treatment alone. Consistent with these findings, we found that oxaliplatin and SYY cotreatment decreased the expression of CSC-related markers and reversed EMT compared with oxaliplatin treatment alone. Together, these findings indicate that SYY suppresses the stemness of HCC by decreasing expression of CSC-related markers in tumor tissues and cell lines.

SYY is a Chinese herbal medicine formula consisting of five herbs. Some components of SYY have demonstrated value in the treatment of malignancies [41, 42]. In our previous study, we reported that SYY effectively inhibited tumor growth and metastasis, and increased survival in a HCC nude mouse model bearing a MHCC97H xenograft [29]. Xiong et al. reported that SYY inhibits molecular changes consistent with EMT in oxaliplatin-treated tumor tissues and cell lines [20]. We suggest that the downregulation of CSC-related markers in the current study was responsible for the increased chemosensitivity of SYY-treated tissues and

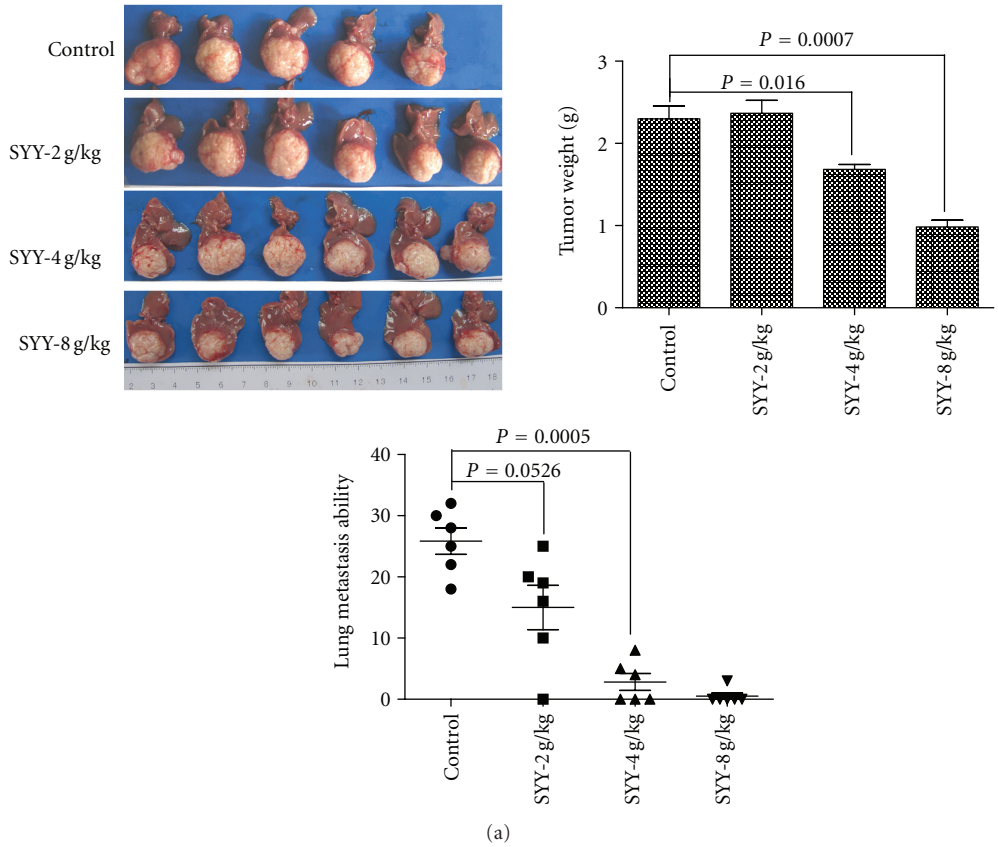

(a)

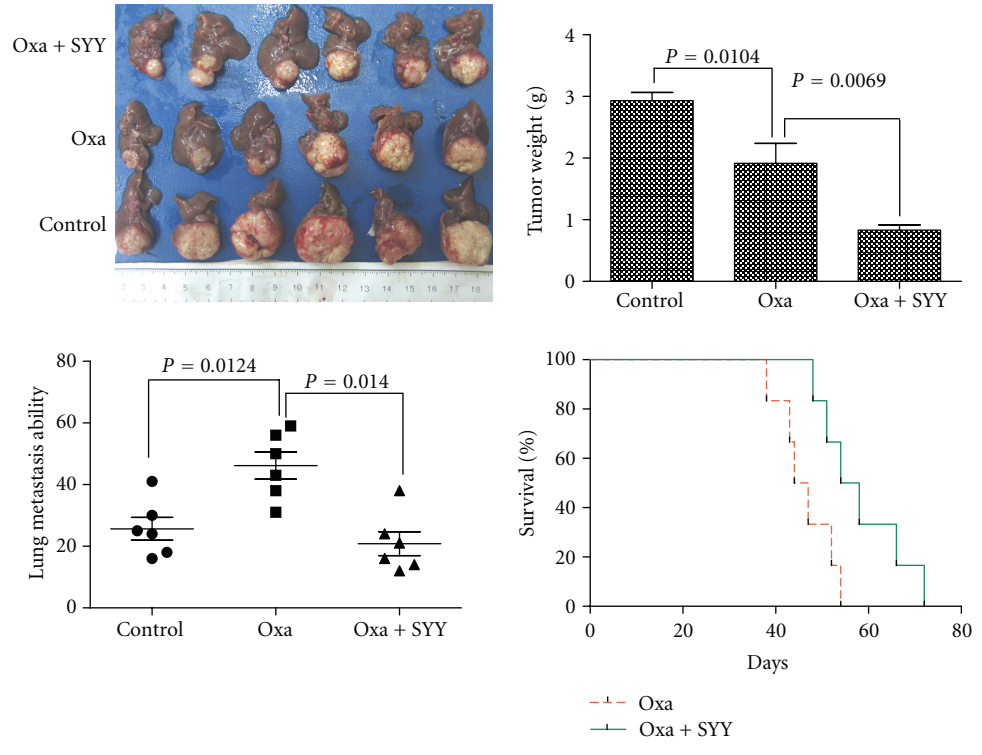

(b)

Figure 4: Oxaliplatin and SYY cotreatment resulted in a smaller tumor volume and a lower percentage of pulmonary metastasis than oxaliplatin treatment alone. (a) Treatment with low-dose SYY (2 g/kg) did not significantly inhibit tumor growth or decrease the incidence of pulmonary metastasis. Treatment with 4 g/kg SYY decreased the number of pulmonary metastasis nodules but did not inhibit tumor growth. In contrast, high-dose SYY (8 g/kg) treatment significantly inhibited tumor growth and pulmonary metastasis. (b) Cotreatment with oxaliplatin and SYY (4 g/kg) reduced tumor volume, decreased the percentage of pulmonary metastasis, and prolonged survival compared with oxaliplatin treatment alone.

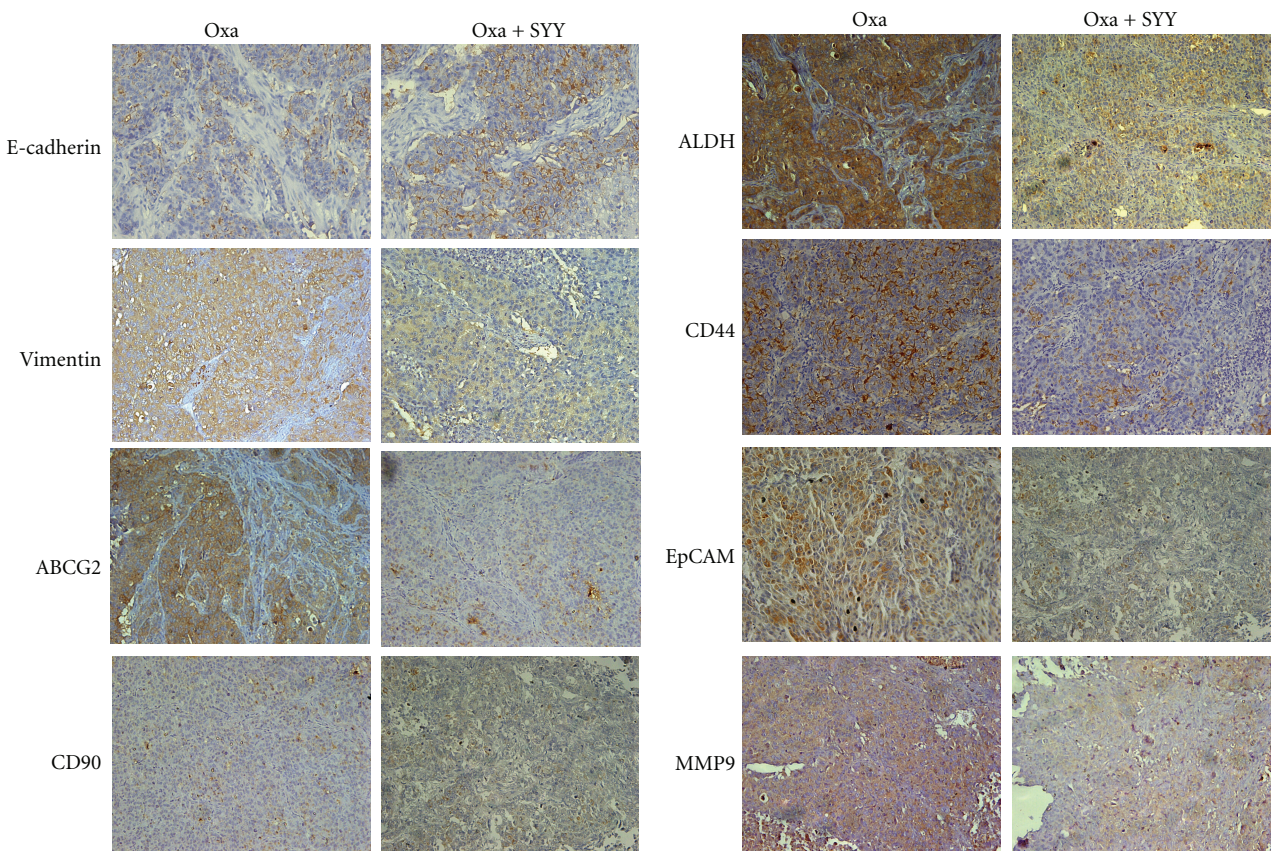

Figure 5: Oxaliplatin and SYY cotreatment reduced the proportion of CSCs, decreased the expression of MMP-9, and reversed EMT with increased expression of E-cadherin compared with oxaliplatin treatment alone.

cell lines and the repression of stemness. There are two ways to decrease the proportion of CSCs: induction of CSC differentiation or direct elimination of CSCs. The efficacy of retinoic acid-induced differentiation to target the stem-like tumor cells in glioma has recently been demonstrated [43]. Elimination therapy is antigen-based therapy that targets different aspects of CSCs, and can either take the form of vaccines or monoclonal antibody therapy or be based on the spontaneous response of the immune system to cancer [44]. At present it is not clear whether SYY targets CSC through the induction of CSC differentiation or direct elimination of CSCs. This question will be investigated in further studies using isolated CSCs.

5. Conclusions

SYY can render hepatocellular carcinoma sensitive to oxaliplatin through the inhibition of stemness.

Abbreviations

CSCs: Cancer stem cells
EMT: Epithelial-mesenchymal transition
HCC: Hepatocellular carcinoma
LDH: Lactate dehydrogenase
TACE: Transcatheter hepatic arterial chemoembolization
SYY: Songyou Yin
GS: Glucose solution.

Conflict of Interests

The authors declare that they have no competing interests.

Authors' Contribution

Q.-A. Jia, Z.-Y. Tang, Z.-G. Ren, Y. Bo, Z.-M. Wang, Q.-B. Zhang (SD), X.-M. Jiang, L. Liang, and Q.-B. Zhang (GS) contributed to the study design, analysis, and interpretation of data. Z.-Y. Tang and Z.-G. Ren conceived the study. Q.-A. Jia performed the experiments. Z.-M. Wang, Y. Bo, Q.-B. Zhang, and X.-M. Jiang participated in the establishment of the nude mouse model. L. Liang and Q.-B. Zhang (GS) participated in statistical analysis. Q.-A. Jia and Z.-G. Ren drafted the manuscript. Z.-Y. Tang carried out revisions and provided important suggestions. All authors approved the final manuscript.

Acknowledgments

This research project was supported by grants from the Foundation of China National "211" Project for Higher Education (no. 2007-353); the National Key Science, Technology

Specific project (2008ZX10002-019); the National Natural Science Foundation of China (81172275); the National Basic Research Program of China (973 Program, 2009CB521700).

References

[1] A. Jemal, F. Bray, M. M. Center, J. Ferlay, E. Ward, and D. Forman, "Global cancer statistics," *CA Cancer Journal for Clinicians*, vol. 61, no. 2, pp. 69–90, 2011.

[2] S. L. Ye, T. Takayama, J. Geschwind, J. A. Marrero, and J. P. Bronowicki, "Current approaches to the treatment of early hepatocellular carcinoma," *The Oncologist*, vol. 15, supplement 4, pp. 34–41, 2010.

[3] J. Bruix, M. Sala, and J. M. Llovet, "Chemoembolization for hepatocellular carcinoma," *Gastroenterology*, vol. 127, pp. S179–S188, 2004.

[4] H. B. El-Serag, "Hepatocellular carcinoma," *New England Journal of Medicine*, vol. 365, pp. 1118–1127, 2011.

[5] B. I. Carr, "Hepatocellular carcinoma: current management and future trends," *Gastroenterology*, vol. 127, no. 5, supplement 1, pp. S218–S224, 2004.

[6] A. Aguayo and Y. Z. Patt, "Nonsurgical treatment of hepatocellular carcinoma," *Seminars in Oncology*, vol. 28, no. 5, pp. 503–513, 2001.

[7] A. D. Yang, F. Fan, E. R. Camp et al., "Chronic oxaliplatin resistance induces epithelial-to-mesenchymal transition in colorectal cancer cell lines," *Clinical Cancer Research*, vol. 12, no. 14, pp. 4147–4153, 2006.

[8] A. N. Shah, J. M. Summy, J. Zhang, S. I. Park, N. U. Parikh, and G. E. Gallick, "Development and characterization of gemcitabine-resistant pancreatic tumor cells," *Annals of Surgical Oncology*, vol. 14, no. 12, pp. 3629–3637, 2007.

[9] J. E. De Larco, B. R. K. Wuertz, J. C. Manivel, and L. T. Furcht, "Progression and enhancement of metastatic potential after exposure of tumor cells to chemotherapeutic agents," *Cancer Research*, vol. 61, no. 7, pp. 2857–2861, 2001.

[10] H. Kajiyama, K. Shibata, M. Terauchi et al., "Chemoresistance to paclitaxel induces epithelial-mesenchymal transition and enhances metastatic potential for epithelial ovarian carcinoma cells," *International Journal of Oncology*, vol. 31, no. 2, pp. 277–283, 2007.

[11] K. Yamauchi, M. Yang, K. Hayashi et al., "Induction of cancer metastasis by cyclophosphamide pretreatment of host mice: an opposite effect of chemotherapy," *Cancer Research*, vol. 68, no. 2, pp. 516–520, 2008.

[12] T. Yamashita, J. Ji, A. Budhu et al., "EpCAM-positive hepatocellular carcinoma cells are tumor-initiating cells with stem/progenitor cell features," *Gastroenterology*, vol. 136, no. 3, pp. 1012–e4, 2009.

[13] T. K. W. Lee, A. Castilho, V. C. H. Cheung, K. H. Tang, S. Ma, and I. O. L. Ng, "CD24+ liver tumor-initiating cells drive self-renewal and tumor initiation through STAT3-mediated NANOG regulation," *Cell Stem Cell*, vol. 9, no. 1, pp. 50–63, 2011.

[14] Z. F. Yang, D. W. Ho, M. N. Ng et al., "Significance of CD90+ cancer stem cells in human liver cancer," *Cancer Cell*, vol. 13, no. 2, pp. 153–166, 2008.

[15] L. L. Liu, D. Fu, Y. Ma, and X. Z. Shen, "The power and the promise of liver cancer stem cell markers," *Stem Cells and Development*, vol. 20, no. 12, pp. 2023–2030, 2011.

[16] M. Dean, T. Fojo, and S. Bates, "Tumour stem cells and drug resistance," *Nature Reviews Cancer*, vol. 5, no. 4, pp. 275–284, 2005.

[17] C. T. Jordan and M. L. Guzman, "Mechanisms controlling pathogenesis and survival of leukemic stem cells," *Oncogene*, vol. 23, no. 43, pp. 7178–7187, 2004.

[18] R. T. Costello, F. Mallet, B. Gaugler et al., "Human acute myeloid leukemia CD34+/CD38- progenitor cells have decreased sensitivity to chemotherapy and Fas-induced apoptosis, reduced immunogenicity, and impaired dendritic cell transformation capacities," *Cancer Research*, vol. 60, no. 16, pp. 4403–4411, 2000.

[19] G. Liu, X. Yuan, Z. Zeng et al., "Analysis of gene expression and chemoresistance of CD133+ cancer stem cells in glioblastoma," *Molecular Cancer*, vol. 5, p. 67, 2006.

[20] W. Xiong, Z. G. Ren, S. J. Qiu et al., "Residual hepatocellular carcinoma after oxaliplatin treatment has increased metastatic potential in a nude mouse model and is attenuated by Songyou Yin," *BMC Cancer*, vol. 10, p. 219, 2010.

[21] B. G. Hollier, K. Evans, and S. A. Mani, "The epithelial-to-mesenchymal transition and cancer stem cells: a coalition against cancer therapies," *Journal of Mammary Gland Biology and Neoplasia*, vol. 14, no. 1, pp. 29–43, 2009.

[22] S. A. Mani, W. Guo, M. J. Liao et al., "The epithelial-mesenchymal transition generates cells with properties of stem cells," *Cell*, vol. 133, no. 4, pp. 704–715, 2008.

[23] M. E. Peter, "Let-7 and miR-200 microRNAs: guardians against pluripotency and cancer progression," *Cell Cycle*, vol. 8, no. 6, pp. 843–852, 2009.

[24] M. Santisteban, J. M. Reiman, M. K. Asiedu et al., "Immune-induced epithelial to mesenchymal transition *in vivo* generates breast cancer stem cells," *Cancer Research*, vol. 69, pp. 2887–2895, 2009.

[25] C. M. Tong, S. Ma, and X. Y. Guan, "Biology of hepatic cancer stem cells," *Journal of Gastroenterology and Hepatology*, vol. 26, no. 8, pp. 1229–1237, 2011.

[26] J. Tian, Z. Y. Tang, S. L. Ye et al., "New human hepatocellular carcinoma (HCC) cell line with highly metastatic potential (MHCC97) and its expressions of the factors associated with metastasis," *British Journal of Cancer*, vol. 81, no. 5, pp. 814–821, 1999.

[27] Y. Li, Z. Y. Tang, S. L. Ye et al., "Establishment of cell clones with different metastatic potential from the metastatic hepatocellular carcinoma cell line MHCC97," *World Journal of Gastroenterology*, vol. 7, no. 5, pp. 630–636, 2001.

[28] B. W. Yang, Y. Liang, J. L. Xia et al., "Biological characteristics of fluorescent protein-expressing human hepatocellular carcinoma xenograft model in nude mice," *European Journal of Gastroenterology and Hepatology*, vol. 20, no. 11, pp. 1077–1084, 2008.

[29] X. Y. Huang, L. Wang, Z. L. Huang, Q. Zheng, Q. S. Li, and Z. Y. Tang, "Herbal extract Songyou Yin inhibits tumor growth and prolongs survival in nude mice bearing human hepatocellular carcinoma xenograft with high metastatic potential," *Journal of Cancer Research and Clinical Oncology*, vol. 135, no. 9, pp. 1245–1255, 2009.

[30] Q. Gao, S. J. Qiu, J. Fan et al., "Intratumoral balance of regulatory and cytotoxic T cells is associated with prognosis of hepatocellular carcinoma after resection," *Journal of Clinical Oncology*, vol. 25, no. 18, pp. 2586–2593, 2007.

[31] M. M. Gottesman, T. Fojo, and S. E. Bates, "Multidrug resistance in cancer: role of ATP-dependent transporters," *Nature Reviews Cancer*, vol. 2, no. 1, pp. 48–58, 2002.

[32] Y. Huang, P. Anderle, K. J. Bussey et al., "Membrane transporters and channels: role of the transportome in cancer chemosensitivity and chemoresistance," *Cancer Research*, vol. 64, no. 12, pp. 4294–4301, 2004.

[33] A. Elliot, J. Adams, and M. Al-Hajj, "The ABCs of cancer stem cell drug resistance," *IDrugs*, vol. 13, no. 9, pp. 632–635, 2010.
[34] J. Gil, A. Stembalska, K. A. Pesz, and M. M. Sasiadek, "Cancer stem cells: the theory and perspectives in cancer therapy," *Journal of Applied Genetics*, vol. 49, no. 2, pp. 193–199, 2008.
[35] S. Bao, Q. Wu, R. E. McLendon et al., "Glioma stem cells promote radioresistance by preferential activation of the DNA damage response," *Nature*, vol. 444, no. 7120, pp. 756–760, 2006.
[36] M. Diehn, R. W. Cho, N. A. Lobo et al., "Association of reactive oxygen species levels and radioresistance in cancer stem cells," *Nature*, vol. 458, no. 7239, pp. 780–783, 2009.
[37] T. Reya, S. J. Morrison, M. F. Clarke, and I. L. Weissman, "Stem cells, cancer, and cancer stem cells," *Nature*, vol. 414, no. 6859, pp. 105–111, 2001.
[38] R. C. Zhao, Y. S. Zhu, and Y. Shi, "New hope for cancer treatment: exploring the distinction between normal adult stem cells and cancer stem cells," *Pharmacology and Therapeutics*, vol. 119, no. 1, pp. 74–82, 2008.
[39] M. R. Alison, W. R. Lin, S. M. Lim, and L. J. Nicholson, "Cancer stem cells: in the line of fire," *Cancer Treatment Reviews*, vol. 38, no. 6, pp. 589–598, 2012.
[40] V. Tirino, V. Desiderio, F. Paino, G. Papaccio, and M. De Rosa, "Methods for cancer stem cell detection and isolation," *Methods in Molecular Biology*, vol. 879, pp. 513–529, 2012.
[41] S. L. Yuan, R. M. Huang, X. J. Wang, Y. Song, and G. Q. Huang, "Reversing effect of Tanshinone on malignant phenotypes of human hepatocarcinoma cell line," *World Journal of Gastroenterology*, vol. 4, no. 1–6, pp. 317–319, 1998.
[42] M. M. Y. Tin, C. H. Cho, K. Chan, A. E. James, and J. K. S. Ko, "Astragalus saponins induce growth inhibition and apoptosis in human colon cancer cells and tumor xenograft," *Carcinogenesis*, vol. 28, no. 6, pp. 1347–1355, 2007.
[43] B. Campos, F. Wan, M. Farhadi et al., "Differentiation therapy exerts antitumor effects on stem-like glioma cells," *Clinical Cancer Research*, vol. 16, no. 10, pp. 2715–2728, 2010.
[44] P. Rajan and R. Srinivasan, "Targeting cancer stem cells in cancer prevention and therapy," *Stem Cell Reviews*, vol. 4, no. 3, pp. 211–216, 2008.